HWVP NCAW Melter Feed Rheology FY 1993 Testing and Analyses: Letter Report

P. A. Smith

March 1996

Pacific Northwest National Laboratory
Operated for the U.S. Department of Energy
by Battelle Memorial Institute

⚙ Battelle

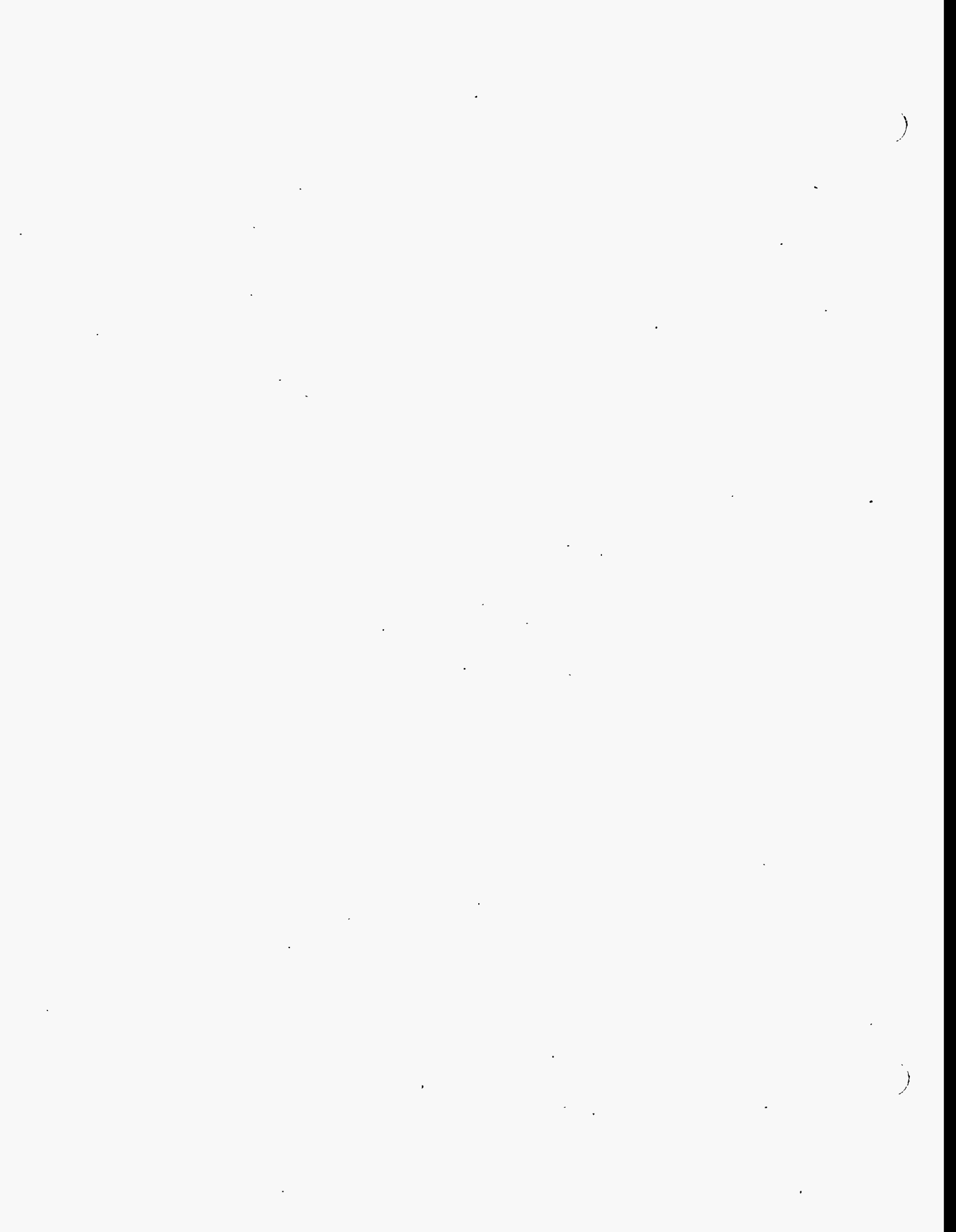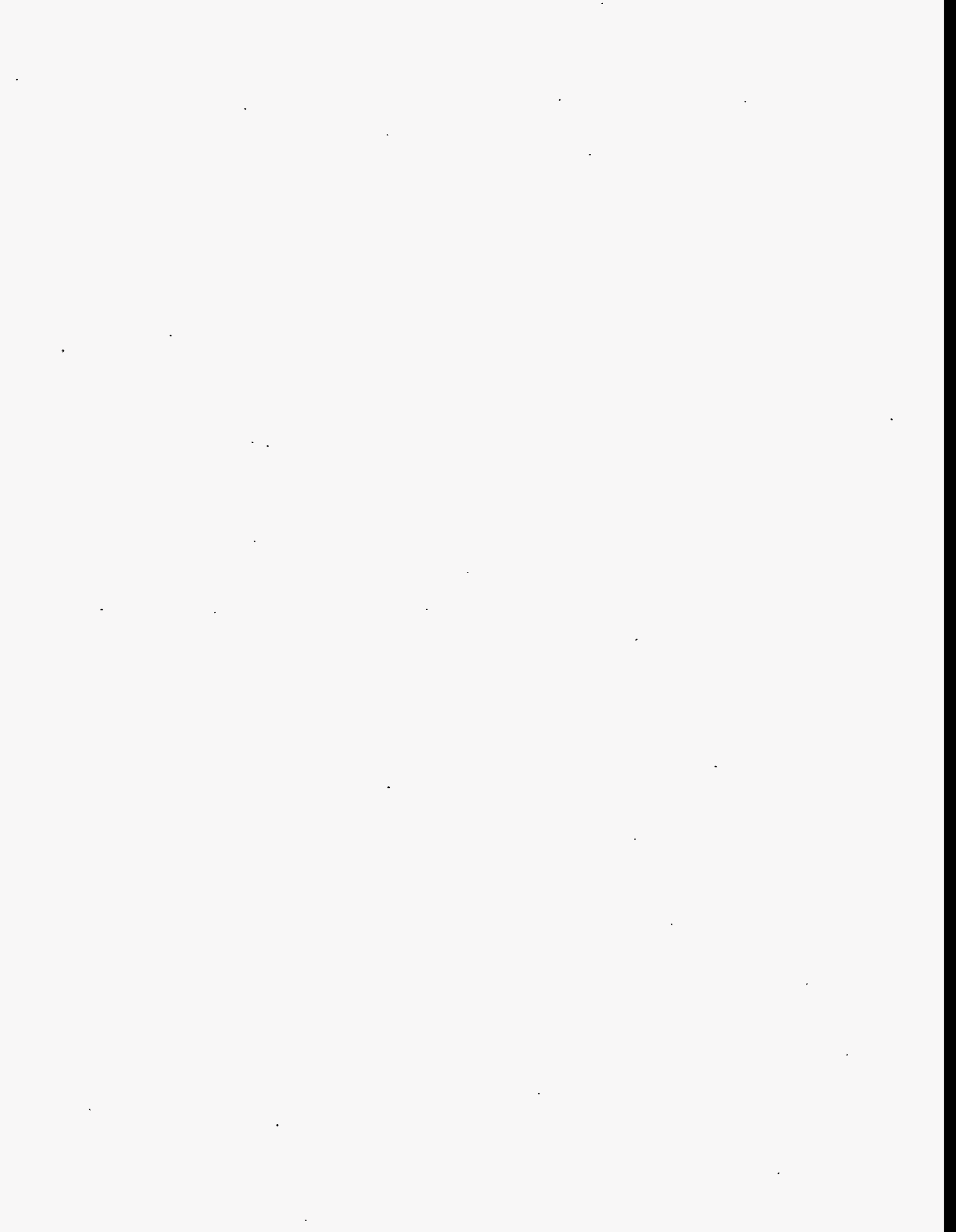# HWVP NCAW Melter Feed Rheology FY 1993 Testing and Analyses: Letter Report

P. A. Smith

March 1996

Prepared for
the U.S. Department of Energy
under Contract DE-AC06-76RLO 1830

Pacific Northwest National Laboratory
Richland, Washington 99352
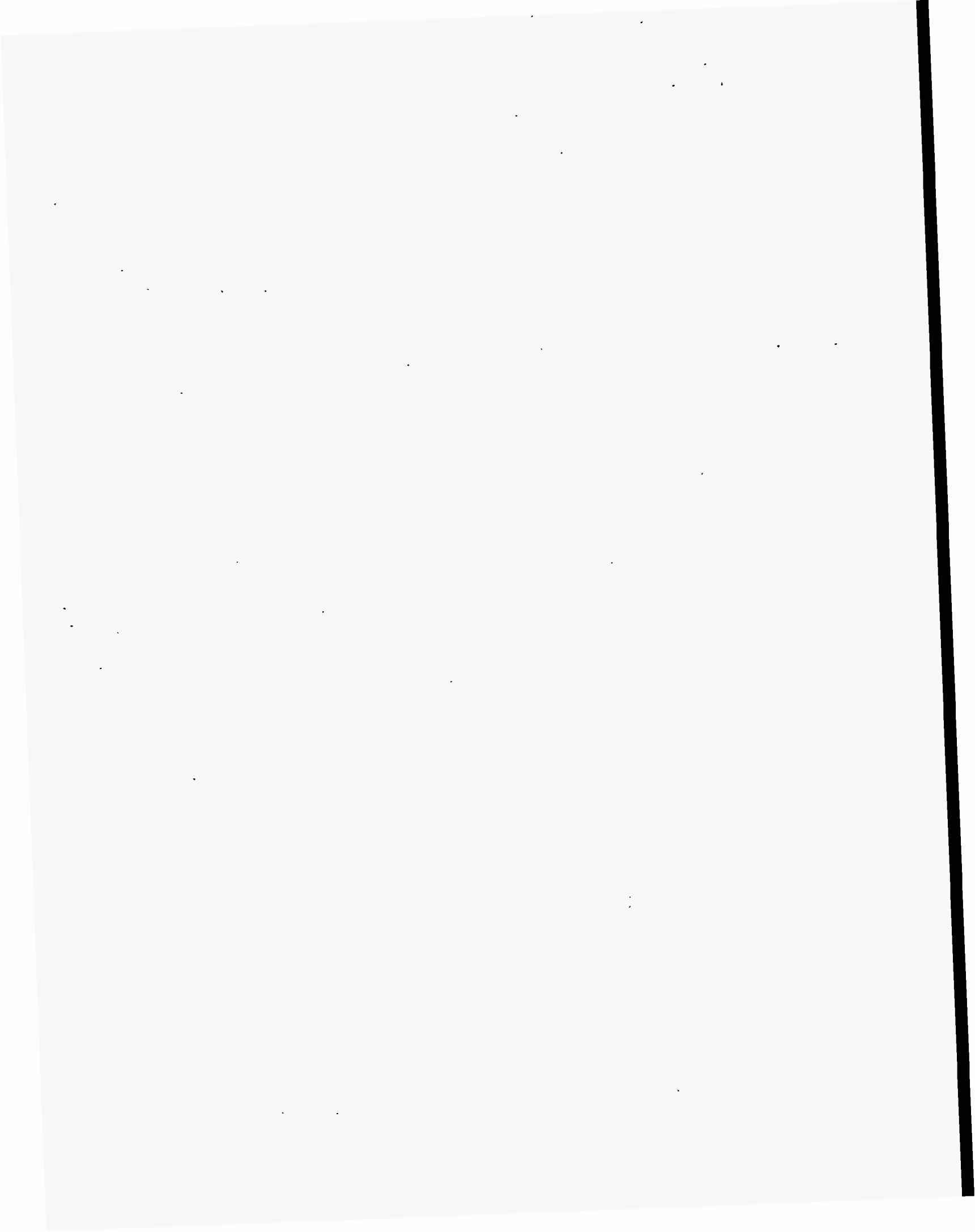
Summary

The rheology of melter feed is crucial to the Hanford Waste Vitrification Plant (HWVP) since the waste must be transported to the liquid fed ceramic melter (LFCM). The examined melter feed consists of simulated neutralized current acid waste (NCAW), recycle, and frit. The rheology of the melter feed was examined for three frits (202, HW-39, and FY 91) in a variety of process conditions. The compositions of these frits were (in wt%)

Frit Type	SiO_2	B_2O_3	Li_2O	Na_2O	MgO	CaO
202	77	8	7	6	2	—
HW-39	70	14	5	9	1	1
FY 91	72.3	20.4	7.3	—	—	—

To simulate anticipated HWVP process times and temperatures, the rheology was examined over a 4-week period at 50°C. The pH of the suspensions was monitored throughout the experiment. Typically, no effort was made to alter the pH. The tests were conducted under the following process conditions:

- The 202 and FY 91 frits were compared on the basis of boiling times: 0, 2, 8, and 24 h at 500 g TO/L.

- The three frits were compared for 2-h boiling time, at a waste loading of 500 g TO/L.

- The 202 and FY 91 frits were compared at 600 g TO/L with a 2-h boiling time.

- The three frits were compared in a concentration cycling experiment and the boiling time was 2 h. The samples were aged for 10 days at 500 g TO/L, concentrated to 600 g TO/L and held for an additional 10 days, and subsequently returned to 500 g TO/L for 15 days of further aging.

- The 202 and FY 91 frits were examined with noble metal containing waste at 500 g TO/L, uncontrolled pH, and boiling time of 2 h.

- The 202 and FY 91 frits were also compared in pH <5 environments. The sample concentrations were 500 g TO/L, and boiling time was 2 h. After the 2-h boiling time, the samples were titrated and maintained at pH <5 with 6 M HNO_3.

To analyze the experimental results, slurry rheology, particle size, x-ray diffraction, weight percent solids chemical analysis, and acoustophoresis measurements were used. The results of these tests showed:

- Large- and laboratory-scale rheology data did not produce similar yield stress increases with aging.

- FY 91 frit leaches more readily than the HW-39 and 202 frits, as indicated by chemical analysis of the frit components in the melter feed supernatant liquid. Also, pH measurements indicated leaching behavior.

- The effect of aging on the rheology of melter feed suspensions was not significant. However, aging was correlated with pH changes and frit leaching.

- Boiling time did not significantly affect the rheology of the melter feed.

- Increased solids loading caused yield stress increases. Reducing the solids loading by dilution did not show a hysteresis in yield stress. Therefore, dilution is a method to control rheology.

- Noble metals content did not affect the 202 and FY 91 melter feed rheology.

- The rheology of the pH < 5 was not significantly different for the 202 and FY 91 frits. However, the FY 91 consumed an order of magnitude more nitric acid to maintain the specified pH.

Acknowledgments
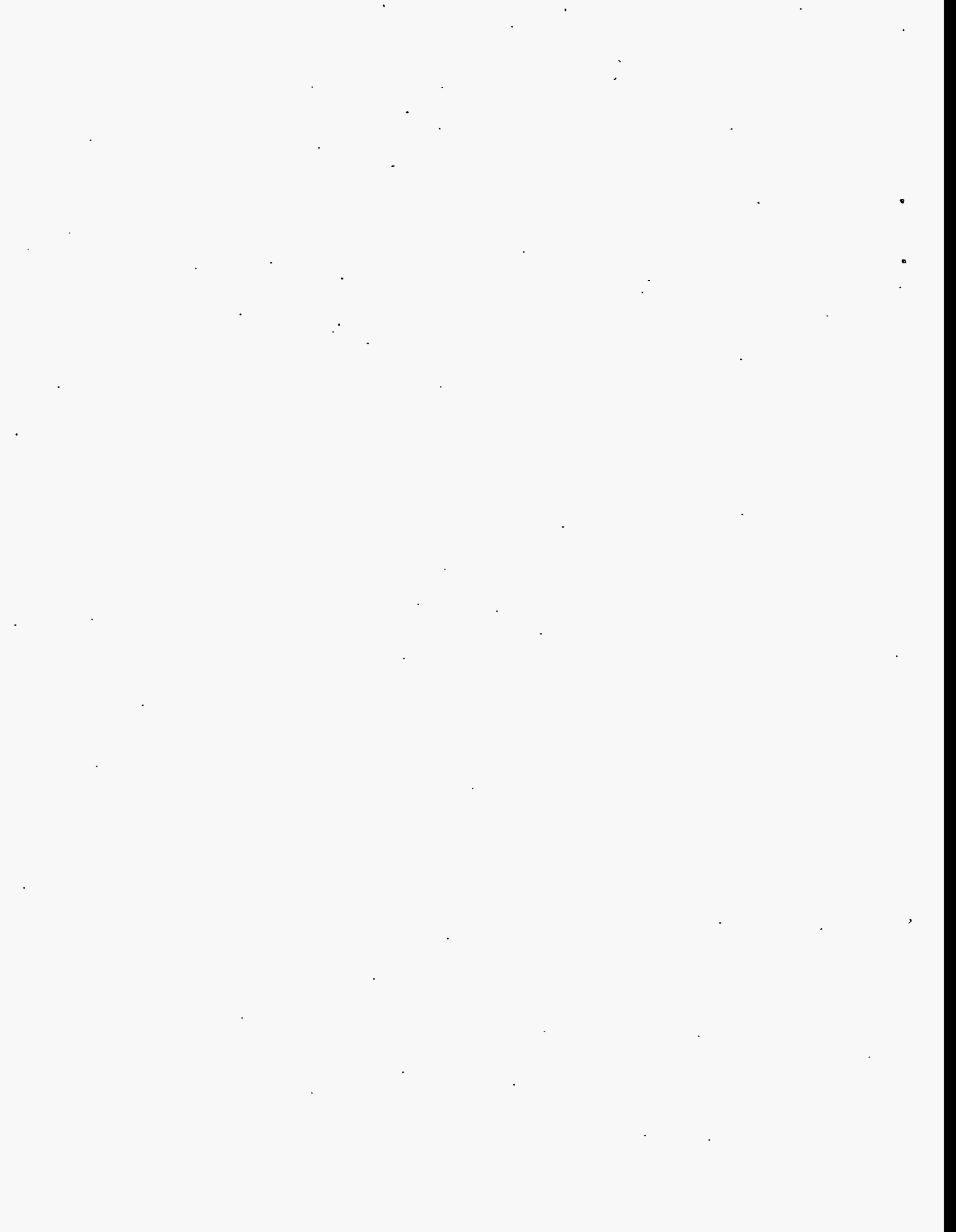
Acronyms

DWPF	Defense Waste Processing Facility
ESA	electrokinetic sonic amplitude
ESM	engineering-scale melter
FY	fiscal year
HWVP	Hanford Waste Vitrification Plant
IC	ion chromatography
ICP	inductively coupled argon plasma
IDMS	Integrated DWPF Melter System
iep	isoelectric point
INE	Institut fur Nukleare Entsorgungstechnik
KfK	Kernforschungszentrum Karlsruhe
LFCM	liquid fed ceramic melter
MFT	melter feed tank
NCAW	neutralized current acid waste
PHTD	PNL HWVP Technology Development
RSM	research-scale melter
RWS	recycle waste stream
SIPT	slurry integrated performance test
SRAT	slurry receipt and adjustment tank
TEM	transmission electron microscopy

TO/L total oxides/liter

WO/L waste oxides/liter

XRD x-ray diffraction

Contents

Figures

Tables

1.0 Introduction

The Hanford Waste Vitrification Plant (HWVP) program has been established to immobilize selected Hanford nuclear wastes before shipment to a geologic repository. The HWVP program is directed by the U.S. Department of Energy (DOE). The Pacific Northwest Laboratory (PNL)[a] provides waste processing and vitrification technology to assist the design effort. The focus of this letter report is melter feed rheology, Process/Product Development, which is part of the Task in the PNL HWVP Technology Development (PHTD) Project. Specifically, the melter feed must be transported to the liquid fed ceramic melter (LFCM) to ensure HWVP operability and the manufacture of an immobilized waste form. The objective of the PHTD Project slurry flow technology development is to understand and correlate dilute and concentrated waste, formated waste, waste with recycle addition, and melter feed transport properties.

The objectives of the work described in this document were to examine frit effects and several processing conditions[b] on melter feed rheology. The investigated conditions included boiling time, pH, noble metal containing melter feed, solids loading, and aging time. The results of these experiments contribute to the understanding of melter feed rheology.

This document is organized in eight sections. This section provides the introductory remarks, followed by Section 2.0 that contains conclusions and recommendations. Section 3.0 reviews the scientific principles, and Section 4.0 details the experimental methods. The results and discussion and the review of related rheology data are in Sections 5.0 and 6.0, respectively. Section 7.0, an analysis of NCAW melter feed rheology data, provides an overall review of melter feed with FY 91 frit. References are included in Section 8.0. This letter report satisfies contractor milestone PHTD C93-03.02E, as described in the FY 1993 Pacific Northwest Hanford Laboratory Waste Plant Technology Development (PHTD) Project Work Plan.[b]

(a) Pacific Northwest Laboratory is operated by Battelle Memorial Institute for the U.S. Department of Energy under Contract DE-AC06-76RLO 1830.

(b) FY 1993 Pacific Northwest Laboratory Hanford Waste Vitrification Plant Technology Development (PHTD) Project Work Plan. Draft. December 1992. PHTD-93-002-Rev 2. Change Request 0962. Reference internal memos, J. M. Creer to R. A. Smith, "PHTD Input to HWVP CR 0962 Revision 1," dated June 3, 1993, PNL-93-156; and R. A. Smith to J. M. Creer, "Approved Change Request HWVP-0962 R1," dated July 6, 1993, 9355537.
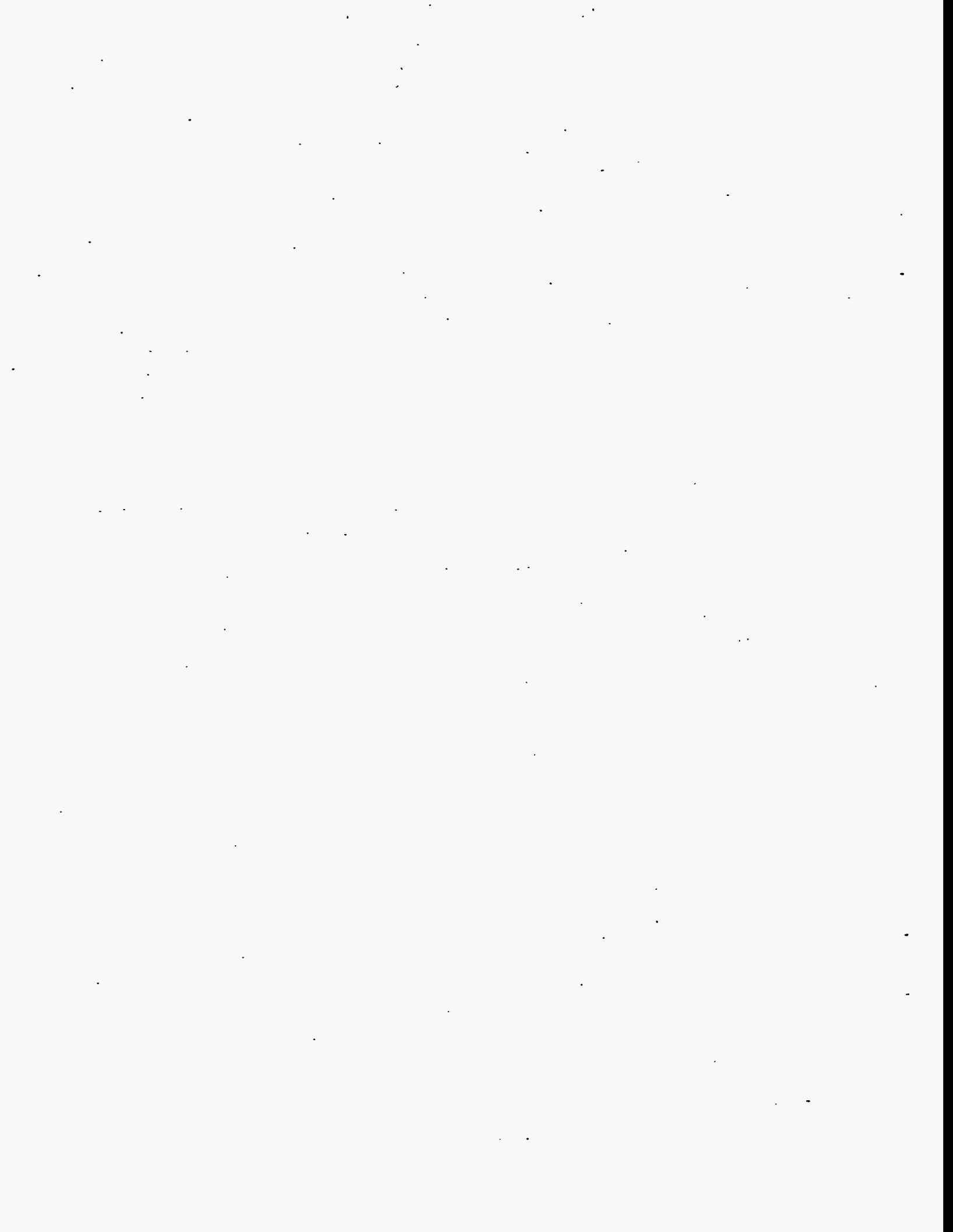
2.0 Conclusions and Recommendations

Based on the results of the boiling time experiments for FY 91 and 202 frits, there was no significant difference in the rheology of the melter feed for the different boiling times. The absence of boiling slowed the leaching process for the FY 91 melter feed as observed by pH measurement.

A comparison of the three frits, FY 91, 202, and HW-39, according to yield stress and viscosity showed no significant differences. Significant changes in melter feed rheology observed in large-scale testing were not duplicated. However, the supernatant liquid chemical analysis and pH measurements showed the FY 91 frit leached more readily and to a greater extent compared to the HW-39 and 202 frits. This behavior provides the opportunity for condensation reactions to occur that could increase yield stress in large-scale testing.

The effect of aging melter feed was shown to be rheologically insignificant; however, aging contributed to the leaching of the frits, which was measured by changes in pH. The influence of aging on frit leaching was also shown in the chemical analysis of the supernatant liquid.

The results of the pH < 5 experiment did not show any significant rheological differences between the FY 91 and 202 frits. However, the amount of HNO_3 required to maintain pH 5 was an order of magnitude higher for the FY 91 melter feed. The chemical analysis showed that the frits were leached a similar amount compared to the analogous pH 8-10 samples. However, these experiments (pH < 5) were performed with an initial boiling during which the pH drifted upward and leaching occurred. To properly understand the influence of pH control, the melter feed should be maintained at the desired pH before the frit addition and throughout the aging period.

A solids loading increase to 600 g TO/L from 500 g TO/L caused increased viscosity and yield stress for the FY 91 and 202 melter feeds. Surprisingly, aging of the 600 g TO/L melter feeds decreased viscosity and yield stress. This result is not fully understood. Concentration cycling of the three melter feeds did not cause a hysteresis in viscosity or yield stress. This result suggests that irreversible bonds were not produced when concentration increased.

Noble metals content were shown to have an insignificant effect on the 202 and FY 91 melter feed rheology.

Currently, rheology data are gathered by a shear strain rate sweep of 0 to 451 s^{-1} over a 2-min time period. Many of the pumping concerns are predicated on the yield stress. The measurement of the yield stress must be scrutinized. Is the methodology for rheological characterization sufficient? In addition, to understand the influence of frit in the melter feed, this methodology must be improved. Alternative rheological measurements for understanding frit influences would include measurements of the elastic and loss moduli, stress growth, and stress relaxation experiments.

Melter feed falls into the category of concentrated suspensions. These suspensions are susceptible to a phenomenon known as wall slip. This phenomenon could have a significant impact on slurry transport and should be examined as a function of processing conditions.

Melter feed rheology can be controlled by manipulating the solids loading. Dilution of the melter feed with water from 600 g TO/L to 500 g TO/L showed a significant decrease in yield stress. Similar behavior was observed in large-scale testing. It would be useful to construct more detailed plots of viscosity and yield stress versus solids loading for HWVP melter feeds.

3.0 Scientific Principles

The rheology of melter feed is influenced by colloidal properties of the waste and frit-water interactions. A brief review of colloidal chemistry principles is given in Section 3.1, and the silica chemistry is discussed in Section 3.2 to provide background for frit-water interactions. A relevant rheology background is described in Section 3.3. Since an acoustophoresis experiment was performed during the course of the work, the principles of this measurement are given in Section 3.4.

3.1 Colloidal Chemistry Principles

Several factors that affect melter feed rheology have been identified[a] including:

- total solids

- method of dewatering

- pH and salt content

- frit particle size.

These factors influence structure development in the melter feed suspension. The underlying colloidal, rheological, and chemical principles will be discussed to further the understanding of the melter feed flow behavior.

Suspension stability results from maintaining a dispersed solid phase. Electrostatic forces are present in a suspension and influence stability. A suspension can be termed stable when the van der Waals attractive forces are overcome by the repulsive forces (Sebera 1964).

A methodology has been developed that establishes the magnitude of the attractive forces between two spheres of size a, separated by a distance, H (Van Megan and Snook 1984). Hamaker (1937) showed an expression for the attractive energy, V_A:

$$V_A = -Aa/12H \qquad (3.1)$$

(a) Memo to R. B. Ferguson from J. R. Fowler, June 29, 1982. *Rheology of Synthetic Feed for the Slurry Fed Melter.* DP51-81-491, Savannah River Laboratory, Aiken, South Carolina.

The Hamaker constant, A, describes a material's attractive behavior.

To produce a stable suspension, the previously described attractive energy must be overcome. When a particle is placed in an aqueous medium, it becomes charged. Hunter (1981) quotes four mechanisms for charge development:

1. electron affinity differences of the two phases

2. different affinities of the two phases for ions

3. surface group ionization

4. entrapment of nonmobile charge in a phase, i.e., isomorphic substitution in clays.

The charge that develops on a particle surface must be equal and opposite to the charges present in the surrounding medium so that electrical neutrality is maintained. Ions of unlike charge (counterions) are attracted to the particle surface, while ions of like charge (co-ions) are repelled from the particle. The repulsive energy, V_R, can be described simply (Hogg et al. 1956) as:

$$V_R = 2\pi\epsilon a\Psi_d^2 \exp[-\kappa H] \qquad (3.2)$$

where $\epsilon =$ the dielectric constant,

   $\Psi_d =$ the particle's surface potential,

   $\kappa =$ the Debye parameter.

The total potential energy, V_T, of an electrostatic system is obtained by summing:

$$V_T = V_A + V_R \qquad (3.3)$$

Restating, a stable suspension is produced when the attractive energy is overcome by the repulsive term; this is often accomplished by controlling pH and is represented graphically by a plot of zeta potential versus pH. The zeta potential provides a measure of a particle's surface potential. As the magnitude of the zeta potential increases, the viscosity is reduced.

Generally, the isoelectric point (iep) is found at the pH where the zeta potential is equivalent to zero. This corresponds to a particle surface with equal numbers of positive and negative charges.

Rheologically, the iep corresponds to a maximum in viscosity. To produce a stable suspension, it is best to process at pH values far from the iep. This is highlighted in the Nerst equation that shows the dependence of surface potential, Ψ_0, on pH:

$$\Psi_0 = kT/2.303e \ (pH_{iep} - pH_{process})\tag{3.4}$$

where K is Boltzmann's constant and T is temperature.

Rheologically, at pH values far from the iep, the particles build up repulsive charge, and viscosity is reduced. At the iep, viscosity reaches a maximum corresponding to the absence of a net repulsive term.

Particles in an aqueous suspension orient surrounding molecules (Horn 1990). This creates a third type of force, hydration, that can influence suspension behavior. The strength and range of hydration increases with the number and degree of the bound ions on a particle's surface (Israelchvili and Adams 1978). For a coagulated suspension, the expected rheology would be Bingham yield, pseudoplastic or yield pseudoplastic. If the particles of this suspension type became highly hydrated, liquid-like rheology would be observed due to the repulsive hydration layer present on the particle surfaces (Chang et al. 1991).

3.2 Silica Chemistry

The fact that silica dissolves in aqueous media has been widely reported in the literature. Further, a thorough treatment of the phenomenon is found in the work of Iler (1979). A summary of important concepts of silica chemistry applicable to the melter feed will follow.

Since glass frits anticipated in the melter feed may be phase separated and highly leachable, and the three-component frit leaches rapidly, microporous amorphous silica will be considered to provide insight for the frit's influence as melter feed chemistry and rheology. In microporous systems, a large quantity of surface area is available for interaction with the aqueous medium, which implies that equilibrium will be reached rapidly. For silica systems that are not microporous, the time required for equilibrium may be on the order of 15 days. This would be the expected behavior for more durable frits.

The work of Baumann (1955) was summarized by Iler (1979). A comparison of amorphous silica and the path to equilibrium was discussed. Baumann compared equilibrium attainment for initial aqueous pH < 7 and pH > 7. Below pH 7, the concentration of soluble silica increases for several

days and approaches the final solubility value asymptotically. Above pH 7, the silica concentration rises rapidly to form a supersaturated solution of Si, leading to an oversupply of low molecular weight silica, the excess of which polymerizes to form colloidal particles.

The solubility rate has also been the subject of significant discussion. The solubility of Si is a function of pH. Iler plotted the literature data from pH > 2 to pH < 11. The solubility of Si was shown to be between 100 and 150 ppm for 2 < pH < 8. At pH > 8, the solubility of Si markedly increased. At 9 < pH < 10.7, the solubility increase was attributed to the formation of silicate ion in addition to the monomer that is in equilibrium with the solid phase. The equilibrium reactions were described:

$$(SiO_2)_x + 2H_2O = Si(OH)_4 + (SiO_2)_{x-1} \tag{3.5}$$

$$Si(OH)_4 + OH^- = Si(OH)_5^- \ (or \ HSiO_3^-) \tag{3.6}$$
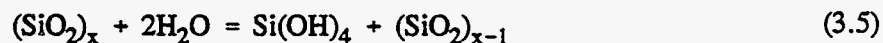
At pH ≥ 10.7, the amorphous silica is completely soluble.

The solubility in HNO_3 should be mentioned since HNO_3 has been used to mitigate rheological problems. Elmer and Nordberg (1958) have furnished data on the solubility of porous vitreous silica. The solubility of Si is vastly reduced in HNO_3 over temperatures ranging from 36° to 95°C. Hence, the HNO_3 mitigation is effective in two areas. The first is the reduction of pH which lessens the solubility of Si, and secondly, Si is not as soluble in HNO_3 compared to an aqueous environment.

Since the solubility of Si has been established, its behavior in solution must be discussed. This requires a treatment of sol-gel principles. There are two distinct areas of sol-gel processes: metal alkoxide precursors and particulate sols. Since frit particles are on the order of 75 μm, the pertinent discussion is related to the particulate sols. Iler showed the polymerization and growth behavior of silica. Figure 3.1 is a reproduction of Iler's conception after particle formation. The portion most applicable to the melter feed is pH 7 to 10, with salts present. Therefore, it is observed that three-dimensional gel networks are possible; however, the length scale must be emphasized. Because the frit particles are on the order of 75 μm, the viability of three-dimensional gel creation must be questioned.

To impart some clarity to the melter feed suspension, it is instructive to review Bunker et al. (1984). The development of gel structures was examined for $Na_2O \bullet 3SiO_2$ and $K_2O \bullet SiO_2$ glasses. Both glasses are subject to leaching and allow an analogy for the three-component frit. The leaching in water causes depletion of the alkali cations, and a silica gel layer results. The gel layer is heterogeneous and consists of voids and/or particles. In addition, Bunker et al. (1984) used transmission electron microscopy (TEM) to examine gel structure. The gel structure was consistent with structures that

3.4
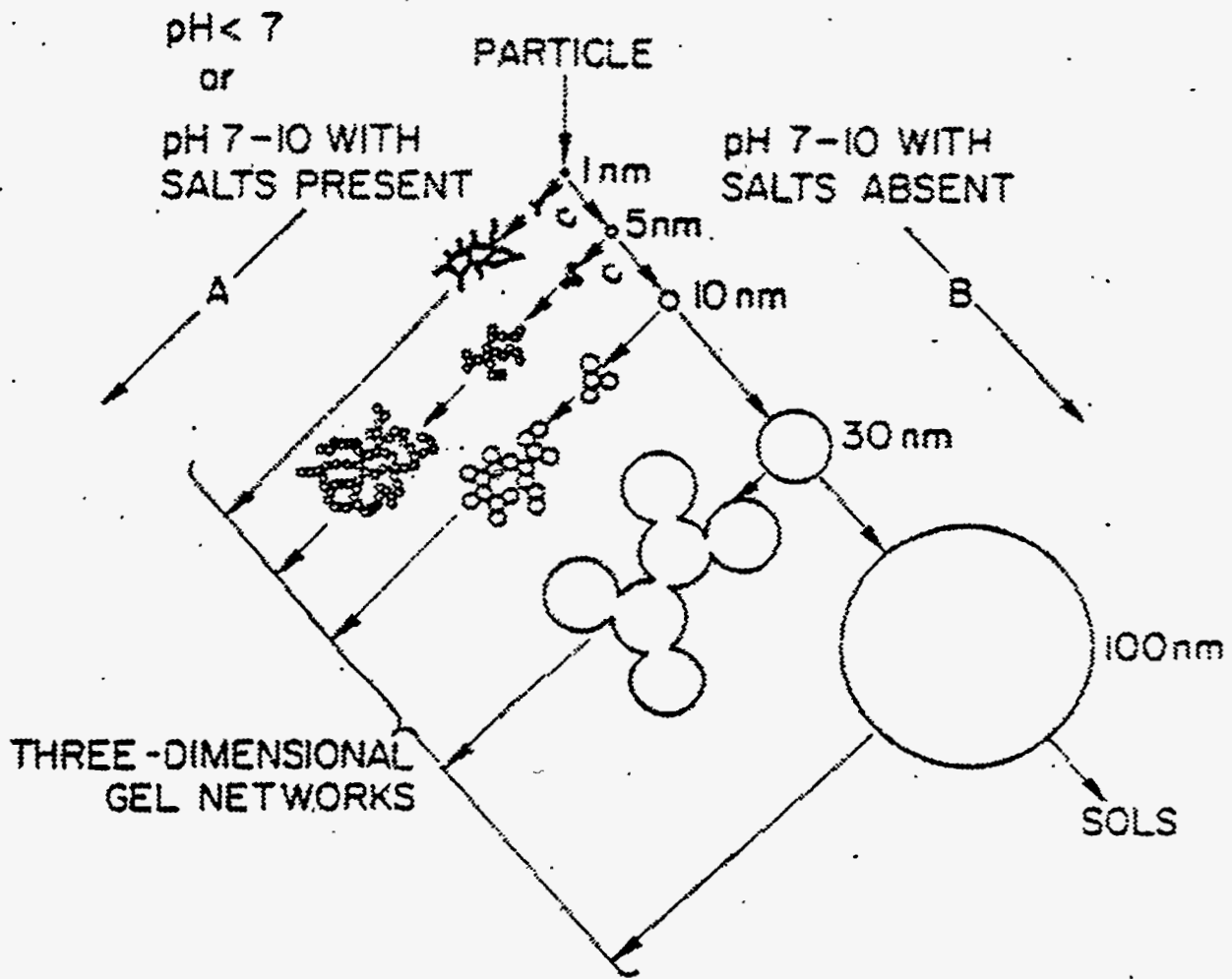
Figure 3.1. Polymerization Behavior of Silica. In basic solution (B), particles in sol grow in size with a decrease in numbers. In acid solution or in presence of flocculating salts (A), particles aggregate into three-dimensional networks and form gels. Reproduced from Iler (1979). (Copyright © 1979. Reprinted by permission of John Wiley and Sons, Inc.)

develop from pH 9 to 11 regardless of the pH of the surrounding solution. This is the gel structure predicted by the figure for systems with pH 7 to 10 in the absence of salts. The scale of the gel layer was approximately 200 μm.

As time passes, the aqueous phase within the assemblage becomes interconnected, silica clusters grow, and ultimately a resemblance to colloidal silica particles is attained (Bunker et al. 1984). For example, consider amorphous silica in water. Silica sol particle surfaces are strongly hydrated (Allen and Matijevic 1969) and are represented as:

$$\equiv Si - OH \text{ or } Si <^{OH}_{OH} \qquad (3.7)$$

The interior of a silica particle consists of hydrophobic siloxane bonds (Si - O - Si). Consider the phase-separated system (Bunker et al. 1984): as repolymerization of the silicate network proceeds, silicate clusters are produced in which all silanol groups and the associated water molecules occupy the cluster surface, while the hydrophobic siloxane bridges reside in the cluster interior creating a highly cross-linked network containing few silanol groups or entrapped water.

Consider the 75-μm frit particles. This length scale is quite different from the sol particles described above. The increased length scale requires a longer period of time for equilibrium. Essentially, the frit particle is not homogeneous and may be described as a gradient with respect to composition. The particle contains a diffuse microporous region and a core particle. The length of each of these depends on the degree and rate of phase separation of the frit particle in an aqueous environment. The behavior of this assemblage could be divided into two mechanisms. The particle core likely behaves as a hard amorphous silica particle. Time-related changes follow the path of Ostwald ripening. This effect could likely be ignored for anticipated frit particles. The diffuse or microporous region likely behaves as a hydrolyzed precursor molecule or a cross-linked network. Recall Bunker's discussion: as clusters grow H_2O is expelled, and the network contains little entrapped water. If Bunker's argument were to apply for the frit, rheological problems would not be anticipated. However, the length scales are quite different, and the attainment of equilibrium requires longer time. So, if a condensation reaction (Brinker and Scherer 1990)

$$SiO^- + Si(OH)_4 \rightleftharpoons Si-O-Si + OH^- + H_2O \qquad (3.8)$$
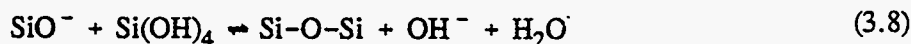
were driven by some external catalyst, the pore structure could entrap water. This would increase yield stress and viscosity. Hence, a delicate balance is required to maintain a stable melter feed.

3.3 Rheology

Rheology is the science of flow and deformation of matter. Particle movement within a given body causes flow and deformation (Reiner 1960). Rheology is pertinent to melter feed suspensions in probing the arrangement and interaction of the particulate phase in suspension.

The rheological behavior of ceramic suspensions is chiefly influenced by the nature of the liquid, the concentration of the dispersed phase, the particle size and particle size distribution, as well as the presence of dispersant and/or coagulants that contribute to the degree of flocculation (Smith 1972). These factors contour the suspension behavior.

The inherent rheology of time independent systems falls into two categories: Newtonian and non-Newtonian (see Figure 3.2). A Newtonian fluid is characterized by shear insensitivity. That is, there is no change in viscosity with increasing shear rates. Non-Newtonian systems are subdivided into two basic categories: pseudoplastic and dilatant, both possess shear dependence. Pseudoplastic behavior is often referred to as shear thinning, which stems from the fact that the shear stress breaks down the structure of the suspension (Quemada 1978). The viscosity decreases with increasing rates of shear. Dilatant flow can be termed shear thickening. The shear stress increases more rapidly than the shear rate (Andrade and Fox 1949). This behavior has been attributed to a volume expansion of a suspension as well as mechanical interlocking of the particulate phase of the suspension (Green 1949). Lastly, these two non-Newtonian flows are often quoted as antonyms. While the measured rheograms are quite opposite, the physical principles of cause are unrelated.

Having discussed the rheological behaviors typically encountered in suspensions, the following discussion focuses on the parameters that influence these types of flow. There have been numerous attempts to document the volume loading (Saunders 1961; Einstein 1909) of a suspension as it applies to viscosity. Mooney (1951) extended the work of Einstein to address the flow of concentrated suspensions related to solids content. The approach was initially described for monosize systems, but subsequent treatment of the polydisperse case was incorporated. The monodisperse equation that was described:

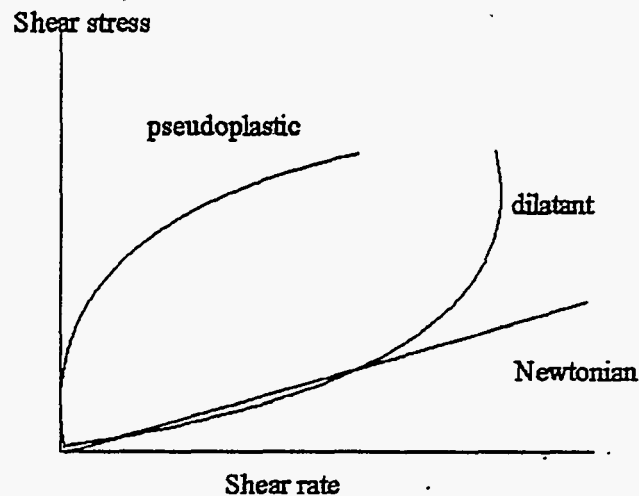$$\eta_r = \exp\left[\frac{2.5\Phi}{1-k\Phi}\right] \qquad (3.9)$$

Figure 3.2. Typical Rheological Behavior for Ceramic Suspensions Under the Influence of Shear

relates relative viscosity, η_r, directly to volume fraction of solids Φ, and k is a constant. Figure 3.3 illustrates the relationship. Other researchers (Michaels 1958; Chaffey and Wagstaff 1977; Russel 1987) addressed flow and concentration in empirical as well as phenomenalogical approaches. Based on these investigations, it was observed that increases in solids content increase viscosity. This approach was shown to be applicable to ceramic suspensions by Chou's incorporation of the work of Thomas (1965) for SiO_2 and Al_2O_3 suspensions (Chou and Senna 1987).

Particle size of the solute phase and its distribution breadth have a major influence on viscosity. The behavior of suspensions changes markedly as the particle size transgresses 1 μm. Particles < 1 μm in size typically exhibit pseudoplastic behavior. Submicron particles are highly translational owing to Brownian motion and are subjected to many more particle-particle interactions than coarser particles. This motion eventually can lead to the formation of a three-dimensional network. Suspensions of this type show structure breakdown under the influence of shear and pseudoplasticity (Wagstaff and Chaffey 1977). Closer inspection reveals that van der Waals attractive forces are prevalent, which leads to the creation of the structural assemblages within the suspension (Knickerbocker 1976). Furthermore, as the particle size is decreased to smaller sizes in the submicron regime, van der Waals forces dominate, which adds to the likelihood of agglomeration; ultimately, higher viscosities are measured (Collins, Hoffman, and Soni 1979).

Dilatant behavior is often observed in highly concentrated ceramic suspensions that possess suspended phases consisting of particles > 1 μm (Phelps et al. 1983). For dilatant behavior to occur, the suspension must be dispersed. Dispersion is readily accomplished for ceramic particles > 1 μm
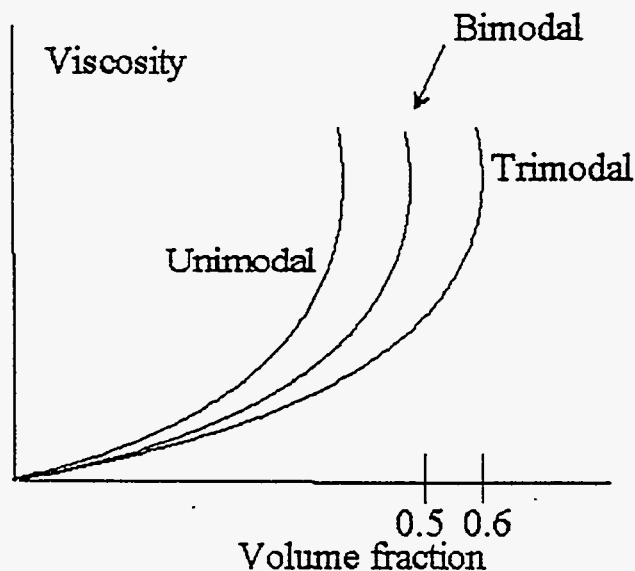

Figure 3.3. Viscosity as a Function of Volume Fraction and Particle Composition

3.8

because of diminished surface area. In response to an applied shear, the voids between the particles enlarge and the liquid phase no longer provides sufficient lubrication. Hence, dilatant behavior is observed.

The models for rheological behavior, concentration dependence, and size assume that the solid phase consists of spheres. When nonspherical particles are subjected to shear, the body orients along its major axis in the direction of the applied force (Smith 1972). Deviations from sphericity may cause higher than expected viscosities. Furthermore, depending on particle size, pseudoplasticity or dilatancy can become more severe owing to the greater number of contact points.

3.4 Acoustophoresis

O'Brien (1988) showed that the physical properties of a suspension could be characterized using acoustophoresis. Acoustophoresis relies on the electroacoustic effect that describes the propagation of sound waves in colloid suspensions. For the first measurement of this effect, dilute suspensions of spherical particles were considered under the influence of an applied alternating electric field. When an alternating electric field is applied to a suspension, the particle velocity and the applied field are out of phase. The phase difference is attributed strictly to the inertia of the field and the particles and is commonly referred to as the electrokinetic sonic amplitude (ESA). The phase difference will increase with the frequency of the applied field. By accounting for this phase difference, the ESA signal can be related to the physical properties of the sample.

Typically, a suspension is circulated through a narrow opening containing two opposing electrodes that apply an alternating electric field. This causes the particles to undergo an oscillatory acceleration that generates an acoustic wave. This ESA signal can be described as a function of operating conditions:

$$\text{ESA}(W) = P/E = c \, \Delta\rho \, \phi \, G_f \, u_d \, (w) \tag{3.10}$$

where w = angular frequency
P = pressure amplitude
E = amplitude of the applied field
c = velocity of the sound wave
$\Delta\rho$ = density difference
ϕ = volume fraction
G_f = geometry factor
$u_d(w)$ = dynamic mobility.

3.9

Since the ESA signal is proportional to volume loading and dynamic mobility, the technique is adaptable to the characterization of the dispersability of NCAW as a function of pH.

4.0 Experimental Methods

4.1 Test Objectives

Melter feed rheology affects melter feed mixing and transport and may impact plant operations. The conditions and mechanisms that control HWVP feed rheology must be understood. Therefore, the objective of this experiment was to establish the correlation of process conditions, frit type, and melter feed rheology behavior.

4.2 Test Matrix

A variety of testing conditions were used to represent conditions that the melter feed may encounter in plant operation. The test matrix is provided in this section (Table 4.1) in the relative order of performance. Three frit types (202, FY 91, and HW-39) were compared during testing (see Table 4.2). The NCAW simulant target composition[a] is provided in Table 4.3. The melter feed was formated and consisted of 28 wt% waste oxides, 3.4 wt% recycle, and 68.6 wt% frit.

For the tests, the melter feed was aged for 4 weeks to represent a bounding case period of time in the HWVP melter feed tanks. The first of five tests was a boiling-time comparison using 202 and FY 91 frits. The objective was to establish the effect of boiling time on melter feed rheology. At 500 g TO/L loading, the test was conducted without holding the constant pH and without noble metals; temperature was maintained at 50°C during the aging period. Boiling times of 2, 8, and 24 h were examined, along with a "no boil" period. A condenser was attached to the apparatus to avoid evaporation during boiling. The 2-h boiling time tests were repeated for both frits.

A second test was designed to examine the influence of HNO_3 on melter feed rheology at pH < 5; this test used the 202 and FY 91 frits. Noble metals were not present. The loading was 500 g TO/L, and the holding temperature was 50°C. Boiling at 105°C proceeded for 2 h. These experiments were performed because Kernforschungszentrum Karlsruhe (KfK) testing showed that mitigation with HNO_3 (a pH reduction) improved melter feed rheology.

The third test examined separate melter feeds containing 202 and FY 91 at a loading of 600 g TO/L. The pH was not held constant, the holding temperature was 50°C, and noble metals were absent. Boiling at 105°C proceeded for 2 h. It is well known that increases in volume loading cause an exponential increase in viscosity. It was necessary to examine the rheological response of the melter

---

(a) Smith, R. A. 1991. Revision of Pretreated Neutralized Current Acid Waste Composition for FY 1991 Pilot Testing–Errata Correction. Letter to J. M. Creer #915051.

Table 4.1. Test Matrix for FY 1993 Testing

Frit	Boiling Time, h	Concentration, g TO/L	pH Control[a]	Noble Metals Concentration[b]
202	None	500		
	2	500		
	8	500		
	24	500		
FY 91	None	500		
	2	500		
	8	500		
	24	500		
HW-39	2	500		
202	2	500	<5	
FY 91	2	500	<5	
202	2	600		
FY 91	2	600		
202	2	500		Yes
FY 91	2	500		Yes
202	2	500		
FY 91	2	500		
HW-39	2	500		
202	2	500 - 600 - 500		
FY 91	2	500 - 600 - 500		
HW-39	2	500 - 600 - 500		

(a) None unless noted.

(b) Absent unless noted.

Table 4.2. Frit Compositions (wt%)

Frit Type	SiO_2	B_2O_3	Li_2O	Na_2O	MgO	CaO
202	77	8	7	6	2	
FY 91	72.3	20.4	7.3			
HW-39	70	14	5	9	1	1

Table 4.3. FY 1991 Neutralized Current Acid Waste (NCAW) Reference[a] and Simulant Target Compositions

	FY 1991 Reference NCAW Composition			FY 1991 NCAW Simulant Target Composition[b]	
Component	Component (wt%)	Moles element/ L feed (125 g WO/L)	Substitution/ Deletion	Component (wt%)	Moles element/ L feed (125 g WO/L)
Ag_2O	1.20E-01	1.29E-03		1.22E-01	1.32E-03
Al_2O_3	9.04E+00	2.22E-01		9.25E+00	2.27E-01
Am_2O_3	7.22E-02	5.38E-07	DEL	--	--
As_2O_3	4.25E-05	3.41E-04	DEL	--	--
B_2O_3	5.75E-03	2.06E-04		5.86E-03	2.10E-04
BaO	1.76E-01	1.43E-03		1.79E-01	1.46E-03
BeO	1.01E-01	5.04E-03	SUB Mg	--	--
Br	--	--	N/A	--	--
CaO	7.91E-01	1.76E-02		8.06E-01	1.80E-02
CdO	3.02E+00	2.94E-02		3.08E+00	3.00E-02
CeO_2	6.05E-01	4.39E-03		6.56E-01	4.77E-03
Co_2O_3	--	--		--	--
Cr_2O_3	2.62E-01	4.30E-03		2.67E-01	4.39E-03
Cs_2O	6.05E-01	5.32E-03		6.12E-01	5.43E-03
CuO	2.45E-01	3.85E-03		2.50E-01	3.93E-03
Dy_2O_3	1.04E-04	6.98E-07	SUB Nd	--	--
Er_2O_3	3.08E-06	2.02E-08	SUB Nd	--	--
Eu_2O_3	2.02E-02	1.42E-04	SUB Nd	--	--
F	9.70E-02	6.38E-03		9.90E-02	6.52E-03
Fe_2O_3	2.82E+01	4.42E-01		2.88E+01	4.51E-01
Gd_2O_3	3.70E-03	2.57E-05	SUB Nd	--	--
GeO_2	1.57E-04	1.82E-06		1.56E-04	1.86E-06
HgO	--	--	N/A	--	--
Ho_2O_3	5.32E-06	3.52E-08	SUB Nd	--	--
I	4.50E-06	4.36E-08		4.60E-06	4.53E-08
In_2O_3	--	--	N/A	--	--
K_2O	1.96E-01	5.21E-03		2.00E-01	5.32E-03
La_2O_3	6.53E-01	5.01E-03		6.67E-01	5.12E-03
Li_2O	1.84E-04	5.92E-06		7.23E-05	6.05E-06
MgO	2.02E-01	6.25E-03		3.72E-01	1.15E-02
MnO_2	2.14E+00	3.08E-02		2.19E+00	3.15E-02
MoO_3	5.59E-01	4.85E-03		5.70E-01	4.95E-03
Na_2O	2.14E+01	8.64E-01		2.19E+01	8.82E-01
Nb_2O_3	1.01E-02	1.08E-04		1.03E-02	1.10E-04
Nd_2O_3	5.78E-01	4.29E-03		3.56E+00	2.64E-02
NiO	2.30E+00	3.85E-02		2.35E+00	3.93E-02
NpO_2	--	--		--	--

4.3

Table 4.3. (contd)

	FY 1991 Reference NCAW Composition			FY 1991 NCAW Simulant Target Composition[b]	
Component	Component (wt%)	Moles element/ L feed (125 g WO/L)	Substitution/ Deletion	Component (wt%)	Moles element/ L feed (125 g WO/L)
P_2O_5	8.72E-01	1.53E-02		8.87E-01	1.56E-02
PbO_2	7.00E-01	3.66E-03		7.15E-01	3.74E-03
PdO	1.20E-01	1.23E-03		1.23E-01	1.26E-03
Pm_2O_3	4.60E-02	3.32E-04	SUB Nd	--	--
Pr_2O_3	1.53E-01	1.16E-03		1.56E-01	1.18E-03
PuO_2	6.00E-02	2.77E-04	SUB Ce	--	--
Rb_2O_3	5.75E-02	6.56E-04		5.87E-02	6.70E-04
Re_2O_7	--	--		--	--
Rh_2O_3	1.04E-01	1.02E-03		1.06E-01	1.04E-03
Ru_2O_3	3.80E-01	3.77E-03		3.87E-01	3.85E-03
SO_3	6.55E-01	1.02E-02		6.69E-01	1.04E-02
Sb_2O_3	5.88E-03	5.00E-05		5.95E-03	5.11E-05
SeO_2	1.59E-02	1.78E-04		1.61E-02	1.82E-04
SiO_2	4.03E+00	8.38E-02		4.11E+00	8.56E-02
Sm_2O_3	7.50E-02	5.42E-04		7.72E-02	5.54E-04
SnO	1.08E-02	9.78E-05		1.08E-02	9.99E-05
SrO	1.19E-01	1.43E-03		1.21E-01	1.46E-03
Ta_2O_5	3.33E-03	1.88E-05		3.39E-03	1.92E-05
Tb_2O_3	2.26E-04	1.54E-06	SUB Nd	--	--
Tc_2O_7	1.52E-01	1.23E-03		--	--
TeO_2	1.07E-01	7.77E-04		1.01E-01	7.94E-04
ThO_2	--	--	SUB Zr	--	--
TiO_2	6.52E-01	1.02E-02		6.66E-01	1.04E-02
Tm_2O_3	1.68E-10	1.09E-12	SUB Nd	--	--
U_3O_8	4.74E+00	2.11E-02	SUB Nd	--	--
Y_2O_3	7.99E-02	8.85E-04		8.17E-02	9.04E-04
ZnO	3.34E-01	5.13E-03		3.41E-01	5.24E-03
ZrO_2	1.51E+01	1.53E-01		1.54E+01	1.56E-01
Sum	1.00E+02	2.02E+00		1.00E+02	2.06E+00

(a) Smith, R. A. 1991. Revision of Pretreated Neutralized Current Acid Waste Composition for FY 1991 Pilot Testing—Errata Correction. Letter to J. M. Creer #915051.

(b) Actual test slurry composition with substitutions made.

feed as a function of loading. In addition, samples of FY 91, 202, and HW-39 frits were used in a concentration cycling experiment. For this experiment, the feed was maintained at 500 g TO/L for 10 days, concentrated and held for 10 days, and then returned to 500 g TO/L.

The fourth test focused on the role of noble metals in melter feed rheology. The feed was boiled for 2 h, the pH was not held constant, and the holding temperature was 50°C. The 202 and FY 91 frits were examined under these conditions.

The fifth test used the HW-39 frit. The objective was to compare this frit to the 202 and FY 91 frits. In the test, pH was not held constant, holding temperature was 50°C, noble metals were absent, and boiling time was 2 h.

4.3 Methods

The NCAW simulant (Table 4.3) was prepared according to the Slurry Integrated Performance Test (SIPT) Slurry Simulant Protocol.[a] Recycle was added to the simulant (Table 4.4). The noble metal concentrations are provided in Table 4.5. The WO loading of the resulting simulant was batched with an appropriate quantity of frit to obtain the following target composition: 28.0% waste, 68.6% frit, and 3.4% recycle.

The waste simulant containing recycle was transferred to the mixing vessel. The frit was added and boiling began. After the mixture was boiled for the prescribed period of time, samples were taken, and the aging process began. During the aging process, samples were typically taken at times 1 day, 1 week, 2 weeks, and 4 weeks. These samples were subjected to the following tests, though not all tests were performed on each sample:

- rheological characterization

- chemical analysis of the supernatant liquid

- weight percent solids of dry (105°C for 24 h) melter feed

- particle size distribution

(a) Smith, H. D., K. D. Wiemers, M. H. Langowski, M. R. Powell, and D. E. Larson. 1993. *Evaluation of HWVP Feed Preparation Chemistry for an NCAW Simulant - Fiscal Year 1993: Evaluation of Offgas Generation and Ammonia Formation.*

Table 4.4. Recycle Simulant Composition

Reference and Target Oxides in Recycle Simulant			Sources of Recycle Simulant for NCAW Slurry Simulant[a]		
				<—target value—>	
Oxide	Reference[b] g Recycle Oxide per g oxide in SRAT Slurry	Target Value[c] g Recycle Oxide per L of Recycle Simulant	Source	g Source per 1L of Recycle Simulant	g Source per 1L of NCAW Slurry#
CdO	0.004	2.01	CdO	2.01	0.50
MnO2	0.0012	0.60	KMnO4	1.10	0.27
Na2O	0.05	25.17	NaOH	24.50	6.08
P2O5	0.004	2.01	Na3PO4	4.65	1.15
NO3⁻	0.08	40.27	HNO3	40.92	10.16
Cl⁻	0.00008	0.04	NaCl	0.07	0.02
TOC	0.0027	1.36	Na2C2O4	7.59	1.88
Diatomaceous Earth	0.04	20.13	Diatomaceous Earth	20.13	5.00
Zeolite (IE-96)	0.02	10.07	Zeolite (IE-96)	10.07	2.50
Sum of nonvolatiles	0.1192	60	Sum	111.04	27.57

(a) Approximately 0.19 moles of HCOOH/L of recycle simulant was added to recycle simulant before it was added to the NCAW simulant. 1L of NCAW slurry is @ 125 g WO/L of NCAW slurry. The approximate amount of recycle simulant necessary for addition to 1L of NCAW simulant is 250 ml of recycle simulant @ 60 g recycle oxide/L of recycle simulant).
Note: The recycle slurry was added on the basis of the gram waste oxides present in the vessel at the end of digestion. The amount of gram waste oxides was determined by subtracting the waste oxides contained in slurry samples (which were removed during formic acid addition and digestion) from the initial gram waste oxides (initial gram waste oxides = 1.5 L of slurry • 125 g WO/L of slurry = 187.5 g WO).

(b) Smith, R. A. 1991. Revision of Pretreated Neutralized Current Acid Waste Composition for FY 1991 Pilot Testing–Errata Correction. Letter to J. M. Creer #915051.

(c) The target concentration for the recycle slurry is 60 g oxide/L of recycle; actual composition was not measured. To convert from column 2 to 3:
(g recycle oxide/(sum of nonvolatiles) • (60 g total recycle oxide/L of recycle).

Table 4.5. Noble Metal Concentrations[a]

Component	Nominal NCAW FY 1991 Simulant (125 g WO/L) mole Element/L	Simulant Target Values L3.1 (125 g WO/L) mole Element/L
Pd	1.26E-03	1.45E-03
Rh	1.04E-03	1.28E-03
Ru	3.85E-07	4.79E-03

(a) Smith, H. D., K. D. Wiemers, M. H. Langowski, M. R. Powell, and D. E. Larson. 1993. Evaluation of HWVP Feed Preparation Chemistry for an NCAW Simulant - Fiscal Year 1993: Evaluation of Offgas Generation and Ammonia Formation.

- pH

- phase determination on the dry solids by x-ray diffraction (XRD).

The rheological measurements were performed using the Haake M5 measuring system with the MV2 sensor. Rheograms were generated by increasing the applied shear from 0 to 451 s^{-1} during a 2-min interval. Subsequently, the shear was reduced from 451 to 0 s^{-1} in a 2-min interval. The samples for rheological measurement were taken from the mixing vessel and tested within 2 h so that the rheological measurement corresponds closely with the aging time.

The increasing shear rheology data was fit with the Bingham equation:

$$\tau = \tau_0 + \eta\dot{\gamma} \qquad (4.1)$$

where τ = shear stress
τ_0 = yield stress
$\dot{\gamma}$ = shear strain rate
η = viscosity.

The rheograms and R^2 values for the frits are provided in Appendix A.

The melter feed slurry supernatant liquid was chemically analyzed by ion chromatography (IC) and inductively coupled argon plasma (ICP) (see PNL documents PNL-ALO-212[a] and PNL-ALO-211,[b] respectively). The measured weight percent solids was recorded by drying melter feed sample slurry at 105°C for 24 h and comparing the dry weight and wet weight. The particle size distribution was measured with the Brinkmann Instrument Model PSA 2010 in accordance with procedure PNL 2·50·3.

Phase determination was accomplished on the dry solids by XRD according to procedure HTA-3-3-4.[c] The range of 2 theta was 5 to 80 degrees, with a counting time of 15 to 20-s and a step size of 0.02 degrees 2 theta.

The test vessel used for suspension aging is depicted in Figures 4.1a and b. The apparatus consisted of a Stedfast lab stirrer, a stainless steel shaft 3/8 in. x 24 in., a 3-in. blade propeller, a 2-in. blade propeller, a 500-mL Pyrex brand beaker and top (clamped together), 3 mixing baffles, either a rubber stopper or circular fitting for the mixing shaft. The heating mantle was equipped with a J type 6-in. thermocouple and digital microprocessor from Glas-Col.

Lastly, an acoustophoresis measurement was made on the NCAW simulant, with 125 g WO/L. The measurement was made by titrating the unformated NCAW simulant with 6 M HNO_3. The MATEC ESA 8000 was used; for operating instructions, consult the ESA 8000 System Operating Manual.

(a) PNL Technical Procedure. PNL-ALO-212, *Determination of Inorganic Anions by Ion Chromatography*. M. W. Urie, December 4, 1992.

(b) PNL Technical Procedure. PNL-ALO-211, *Determination of Elements by Inductively Coupled Argon Plasma*. J. Wagner.

(c) Procedure HTA-3-3, Rev. 4. *Solids Analysis; X-Ray Diffraction Analysis*. L. E. Thomas.
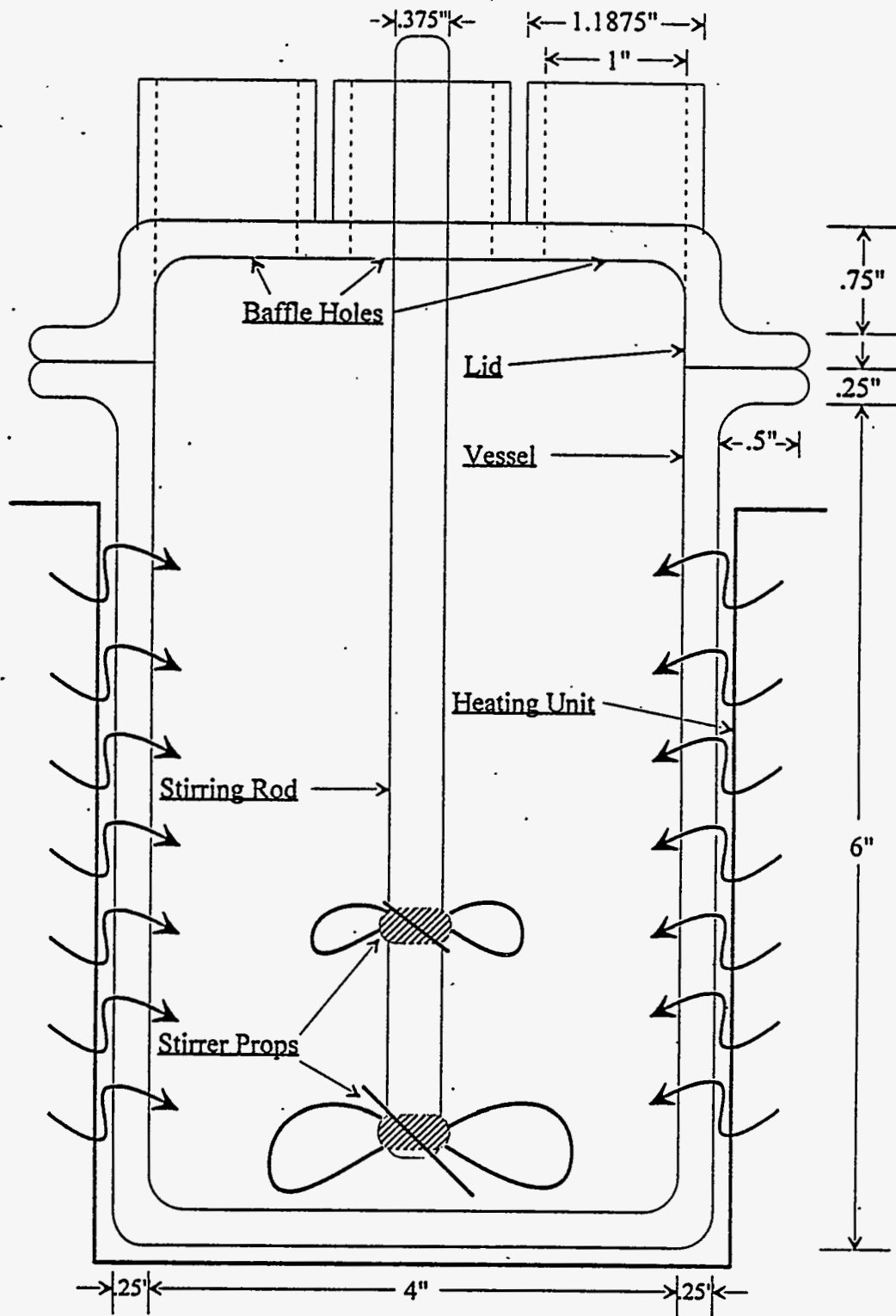
Figure 4.1a. Side View of Test Vessel

4.9
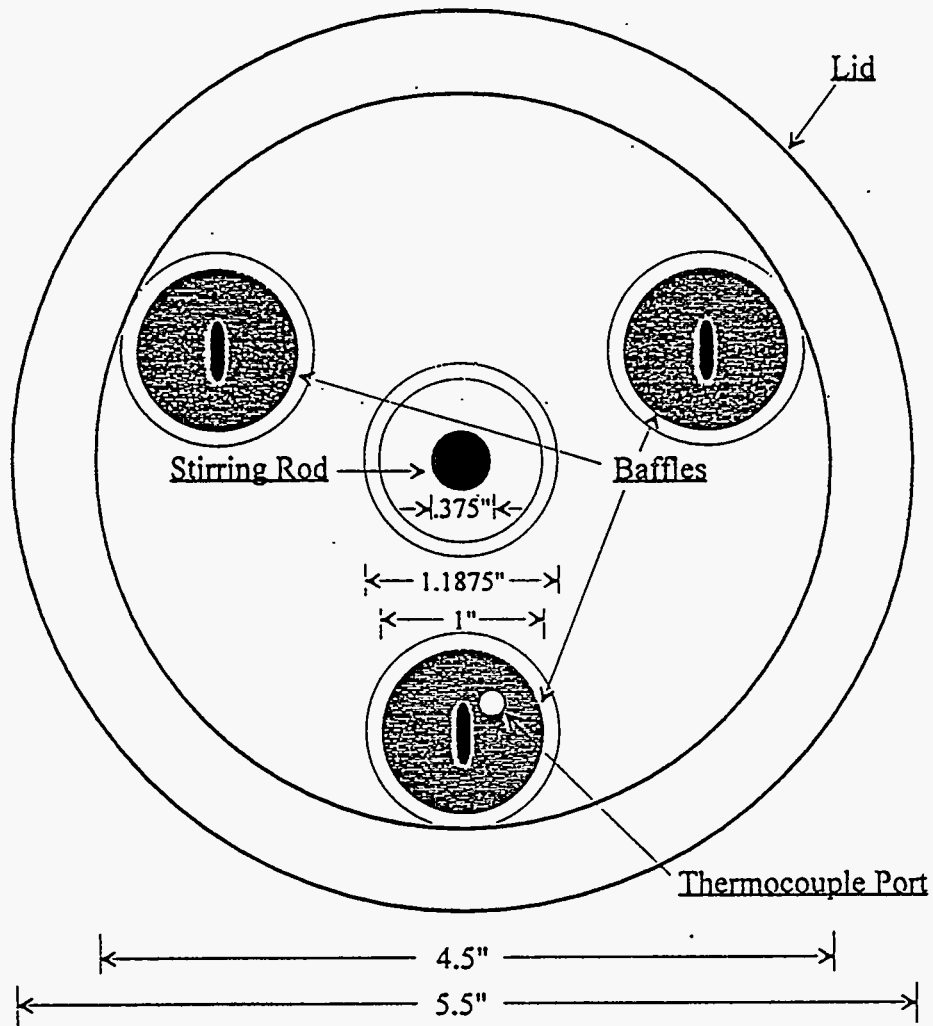
Figure 4.1b. Top View of Test Vessel

5.0 Results and Discussion

This section describes the results of the FY 1993 rheology testing. The order of the results should provide a basis for logical comparisons. Specifically, a boiling time comparison (Section 5.1) is initially described since the boiling time for the remaining experiments was chosen based in part on these results. A comparison of the frits is detailed in Section 5.2. These results are then used to compare the effect of pH on yield stress (Section 5.3). Section 5.4 shows the results of the pH controlled samples. Section 5.5 shows the influence of increased solids loading, and Section 5.6 completes the range of testing conditions by describing the influence of noble metals. A review of the FY 1992 results is given in Section 5.7. Sections 5.8, 5.9, and 5.10 discuss x-ray data, weight percent solids, and particle size data, respectively.

5.1 Boiling Time Comparison

Different boiling times were compared for their effects on the rheology of NCAW melter feed. Tests were conducted on the 202 and FY 91 frits at boiling times of 0, 2, 8, and 24 h. The viscosity data (see Figure 5.1) ranged from 5 to 18 centipoise (cp) after 4 weeks of aging at 0°C. The time 0 viscosities ranged from 4 to 21 cp. Figure 5.2 shows the corresponding yield stresses for the boiling-time investigation. The corresponding weight percent solids data are plotted in Figure 5.3. Weight percent solids data show significant variation. These values should be similar. A dilution of the 202 and FY 91 8-h samples must have occurred. This would explain the lower yield stress values omittted from Figure 5.2. In addition, the weight percent solids data reflect the dilution. However, the dilution effect was not as apparent in the viscosity data. These data are included for completeness; however, it is not appropriate to include these data in a rheological comparison.

Re-examining the valid yield stress data shows a range of data from 1 to 10 Pa for the period of aging. The viscosity data showed a range from 4 to 21 cp. For both rheological terms, viscosity and yield stress, the data are scattered. Therefore, a definitive statement on boiling time of first effects cannot be made in rheological terms.

The pH for each boiling time was examined during the aging period (see Figure 5.4). The FY 91 melter feed rose to approximately pH 9 immediately after boiling for the 2-, 8- and 24-h time periods. For the FY 91 melter feed that was not boiled, pH 9 was attained after 1 week. As aging progressed, the FY 91 melter feeds for the four boiling times showed a pH range of 9 to 9.7. Thus, the boiling time of the FY 91 melter feed showed no significant differences in pH. However, FY 91 melter feed that was not boiled required a longer time to reach the 9 to 9.7 range.

The pH data for the 202 melter feeds were not quite so clear. After 4 weeks of aging, pH ranged from 9.6 for the 202 melter feed that was not boiled to pH 7 for the 8-h boil. This range of pH values does not afford a specific conclusion for the effect of boiling time on 202 melter feed. However,
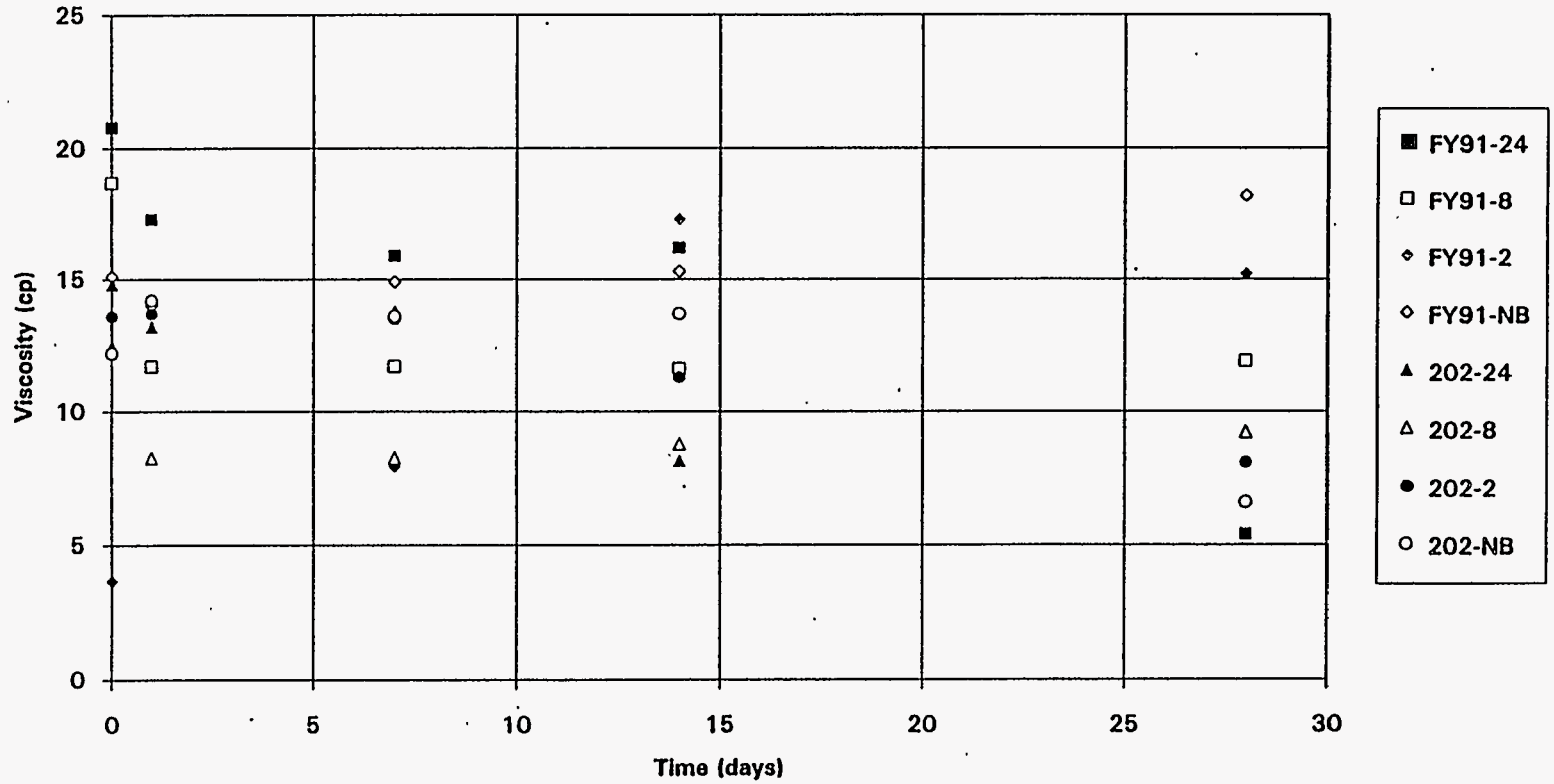
Figure 5.1. Viscosity Versus Age for the Boiling Time Experiments. (The first term indicates frit type. The second term indicates boiling time in hours, NB represents no boil.)
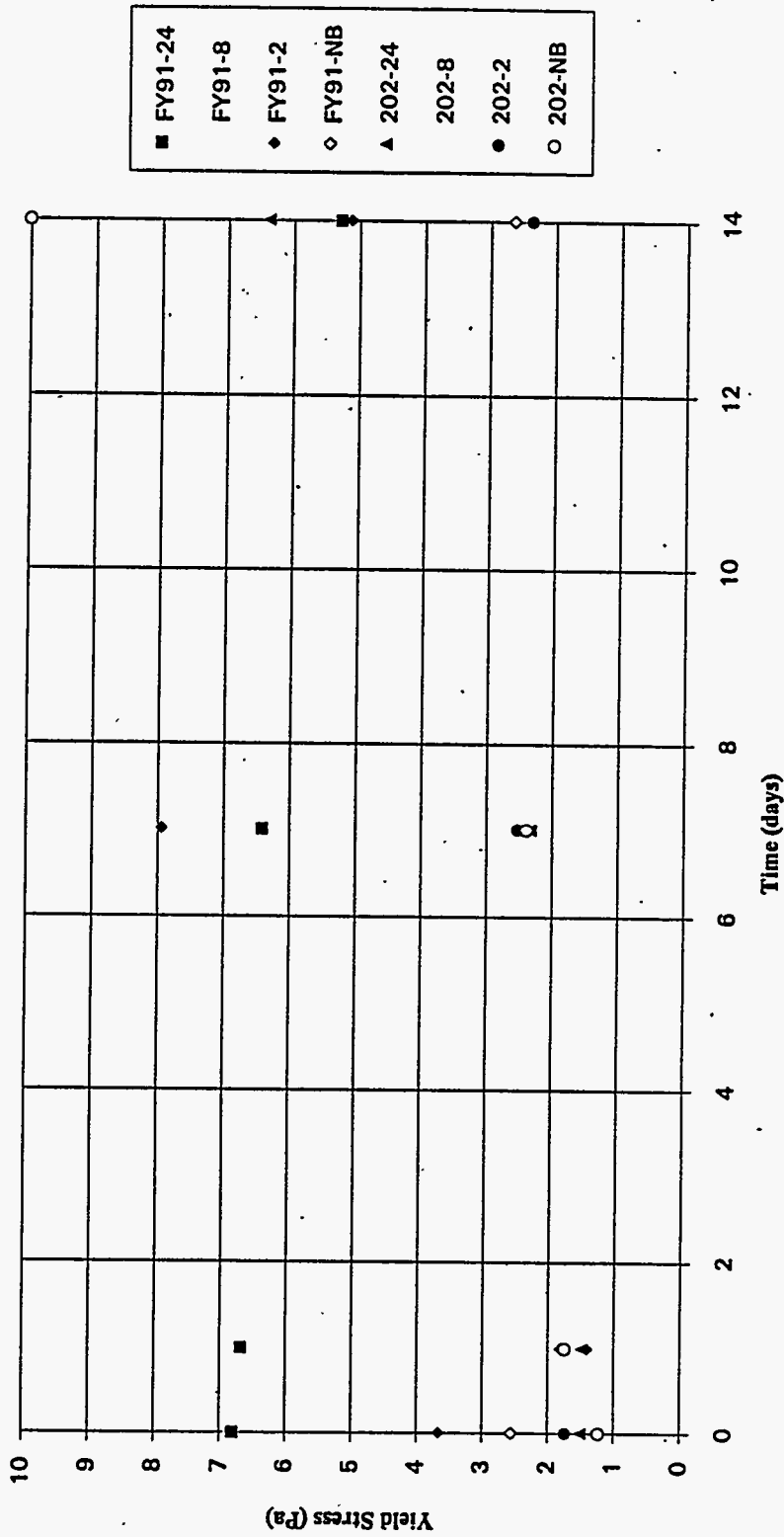
Figure 5.2. Yield Stress Versus Age for the Boiling Time Experiments
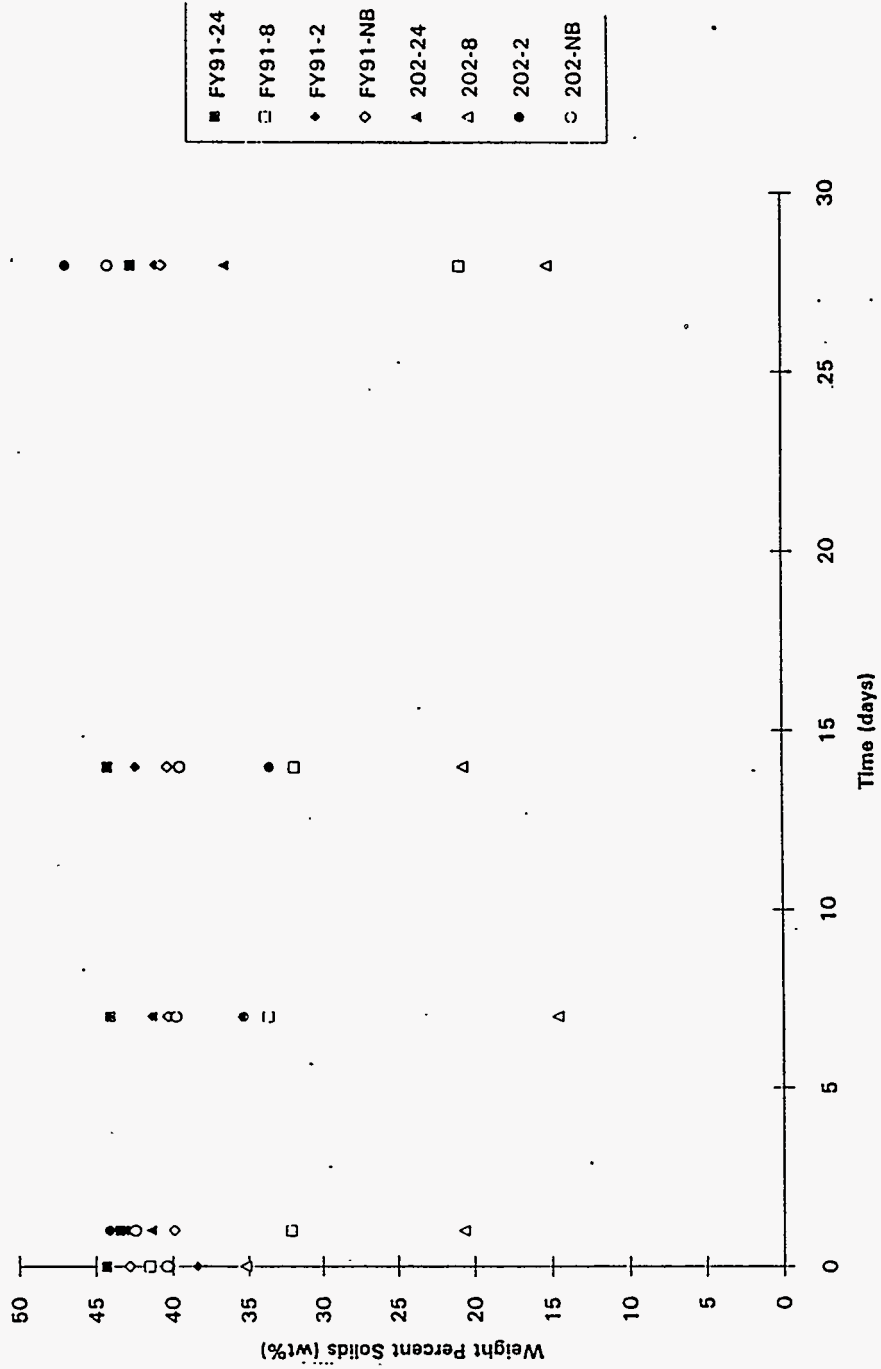
WT%BOIL.XLC

Legend:
- FY91-24 (filled square)
- FY91-8 (open square)
- FY91-2 (filled diamond)
- FY91-NB (open diamond)
- 202-24 (filled triangle)
- 202-8 (open triangle)
- 202-2 (filled circle)
- 202-NB (open circle)

Figure 5.3. Weight Percent Solids Versus Age for the Boiling Time Experiments

Y-axis: Weight Percent Solids (wt%) — 0, 5, 10, 15, 20, 25, 30, 35, 40, 45, 50

X-axis: Time (days) — 0, 5, 10, 15, 20, 25, 30

5.4
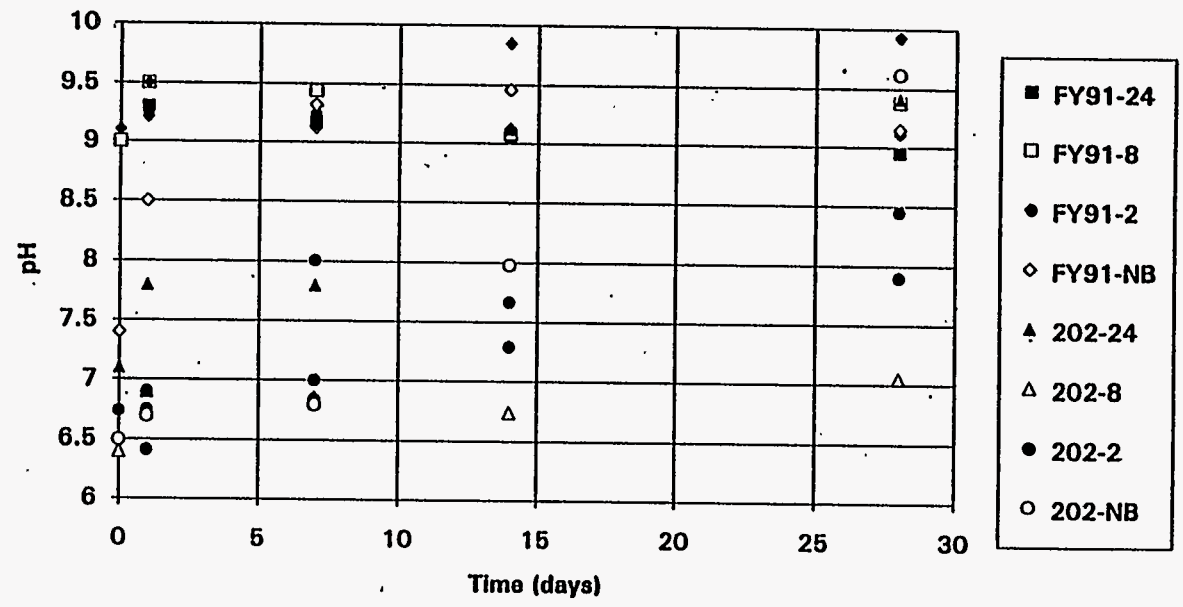
Figure 5.4. pH Versus Age for the Boiling Time Experiments

examining the data over the aging period shows that the pH increase was gradual and relatively continuous over the experimental time frame. This change in pH was observed for the four boiling times.

Chemical analysis was performed on the supernatant liquids of the FY 91 melter feed (Figure 5.5a) and the 202 melter feeds (Figure 5.5b) for the 2-week and 4-week aging times. The FY 91 melter feed supernatant liquid was analyzed for Li, B, and Si. For all the analyzed FY 91 melter feeds, the Si content was negligible or zero. The B content of the supernatant liquids, reported as fraction of frit in solution, ranged from 0.16 to 0.70.[a] Specific trends were not detected for B concentration as a function of aging time (2 versus 4 weeks) or boiling time. Examination showed the FY 91 is susceptible to considerable Li leaching. The Li concentration did not appear to be a function of boiling time. However, the 24-h boiling time showed the highest Li concentration. Also, the compared aging times do not show a distinct difference in Li concentration. Most importantly, the fraction of frit in solution ranged from 0.50 to 0.96 for the FY 91 frit based on the detected lithium.

The 202 melter feed showed significantly less leaching of the Li component compared to the FY 91 melter feed. Similar to the FY 91 melter feed, negligible or zero Si concentrations were detected. No correlation between aging or boiling time was made for the 202 melter feed based on the chemical analysis.

Based on these results, it was concluded that the melter feed behavior was not a primary function of boiling time. A 2-h boiling time was chosen to facilitate comparisons with previously obtained laboratory data. This choice allowed the HW-39 frit, which was boiled for 2 h under similar conditions as the 202 and FY 91 melter feeds, to be included in a direct comparison.

5.2 Comparison of Frits

The viscosities of HW-39, 202, and FY 91 melter feeds are shown (Figure 5.6) as a function of aging for nominal conditions. Nominal conditions are a 2-h boiling time, aging at 50°C, and a suspension concentration of 500 g WO/L. At time zero, the viscosity of the FY 91 melter feed is slightly higher than the viscosities of the HW-39 and 202 melter feeds. However, over the entire aging period, it is difficult to discern any significant differences in viscosities based on frit composition.

Examination of the yield stress (see Figure 5.7) for the three melter feeds generally showed a higher yield stress for the FY 91 melter feeds over the 4-week aging period.[b] However, this difference is on the order of 2 to 4 Pa. The HW-39 and 202 melter feeds showed similar yield stress values.

(a) These values are called fraction of frit in solution. These values are derived by assuming that the ion concentration of the supernatant liquid is solely and directly attributable to the frit. In addition, precipitation is not taken into account in this analysis.

(b) From this data, observe that the 202 samples aged 1 and 2 weeks were diluted and a lower yield stress was measured.
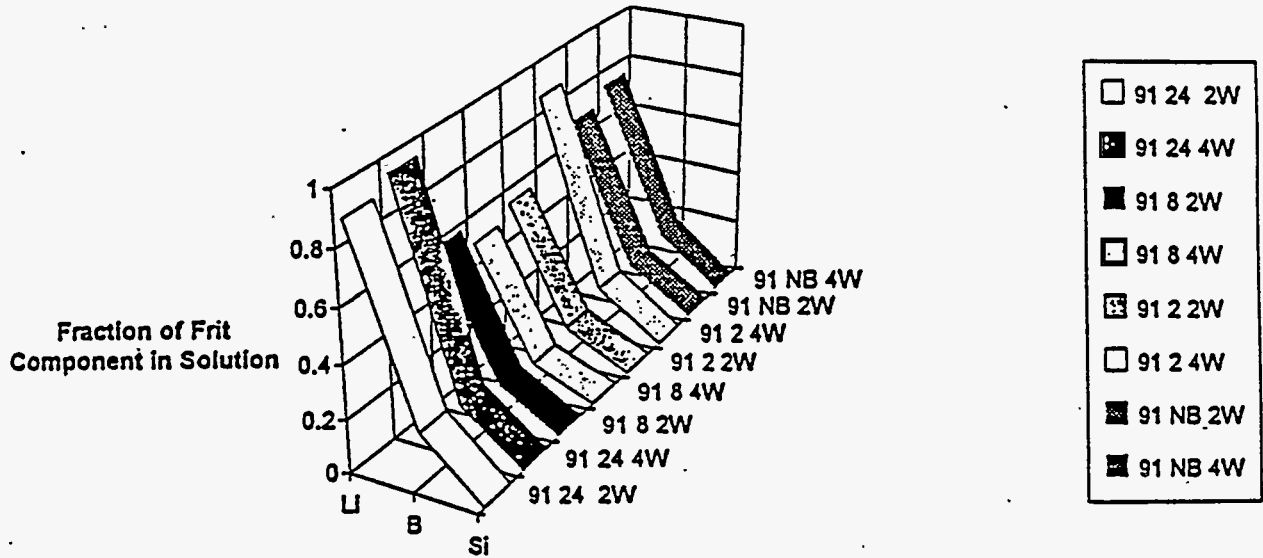
Figure 5.5a. FY 91 Melter Feed Supernatant Analysis as a Function of Boiling Time and Aging. (In the legend, 91 denotes FY 91 frit, the second term indicates boiling time, and the last term indicates age.
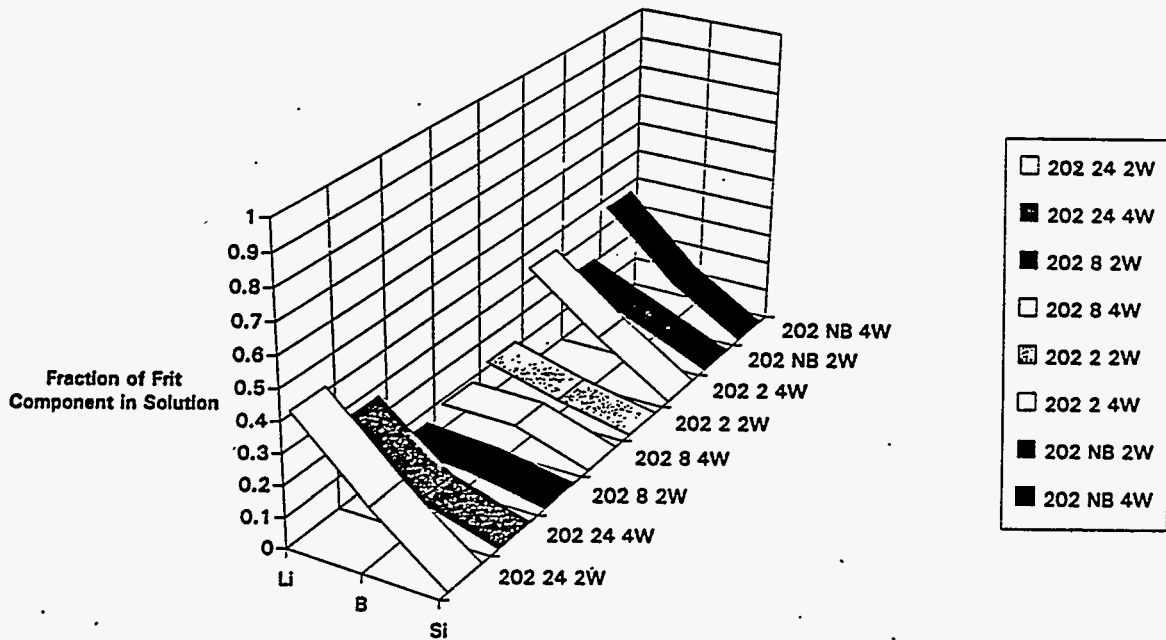
Figure 5.5b. 202 Melter Feed Supernatant Analysis as a Function of Boiling Time and Aging. In the legend, 202 denotes 202 frit, the second term indicates boiling time, and the last term indicates age.)
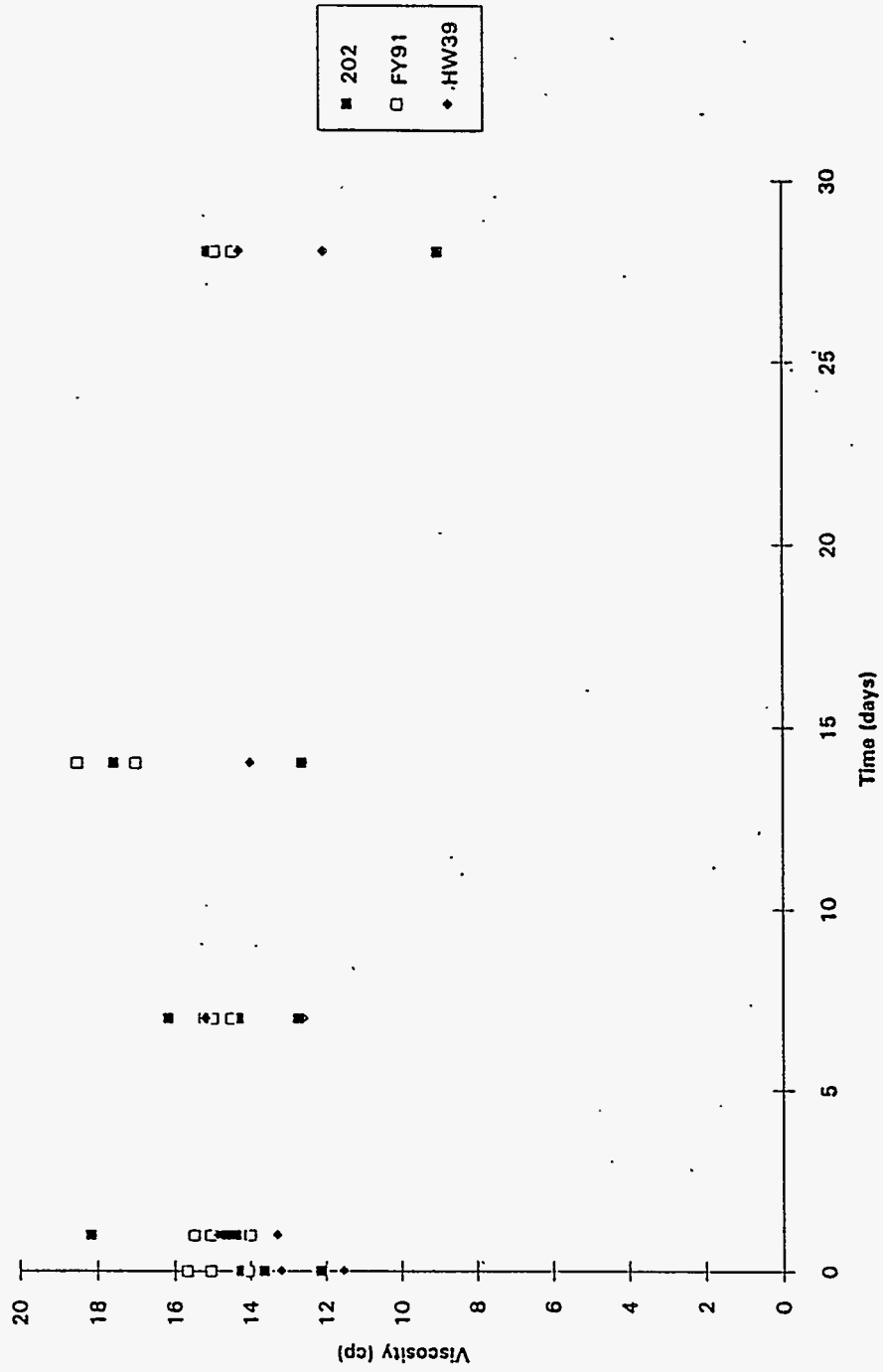
Figure 5.6. Viscosity Versus Age for the Frit Comparison. These samples were boiled for 2 h.

5.8
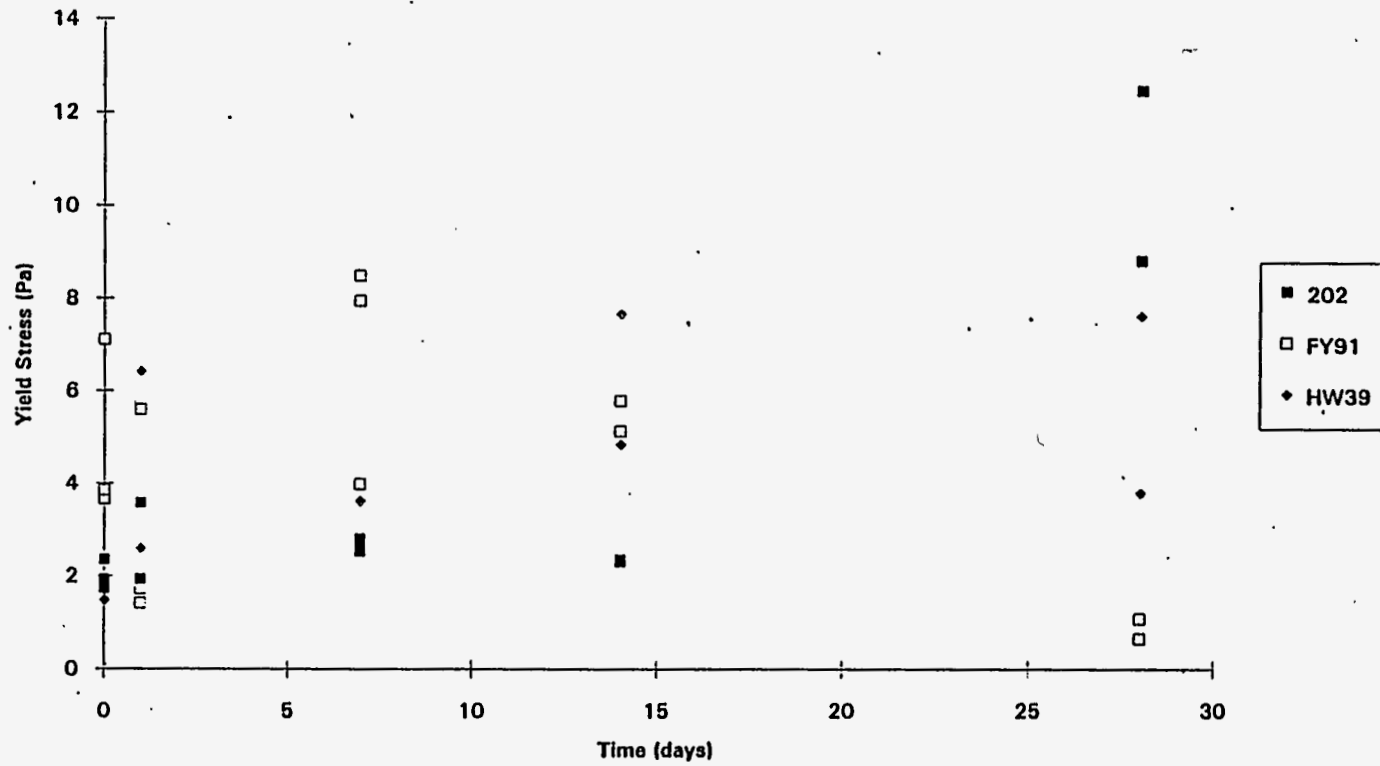
Figure 5.7. Yield Stress Versus Age for the Frit Comparison. These samples were boiled for 2 h.

The corresponding weight percent solids data are shown in Figure 5.8. The results of the large-scale testing (see Section 6.0) were not reproduced, based on the yield stress differences detected in the laboratory.

Figure 5.9 shows pH versus time for the three melter feeds under the same processing conditions. The trend for the FY 91 and 202 melter feeds pH is similar to the results shown for all of the boiling times in Figure 5.3. The pH of the FY 91 melter feed ranged between 9 and 9.7 for the entire aging period. The pH of the 202 melter feeds was approximately 8 after the aging period. The HW-39 melter feed was slightly higher in pH compared to the 202 melter feeds. Based on the observed pH changes, the FY 91 frit appeared to leach more than the HW-39 and 202 melter feeds.

The supernatant liquid for the three melter feeds was examined (Figures 5.10a-c). Note that these data correspond to the pH values shown in Figure 5.9. The frit components, Si, Li, and B for the 4-week aging period are described in terms of the fraction of the element detected in the supernatant liquid that originated from the frit particles. Hence, the fraction corresponds to the minimal amount of the component that has leached from the frit particle. For the three types of melter feeds, the Si concentration is zero or negligible. If a Si-based network was forming, some Si cations would likely be detected in the supernatant liquid.

The Li concentrations clearly depict the leaching for each frit in the melter feeds. Boron reflects the level of leaching to a lesser degree. The general time-based trend was that more Li leached as aging proceeded. Frit comparison showed that the HW-39 is least susceptible to Li release in the melter feed. The 202 frit showed slightly higher Li releases.

Lithium leaching of the melter feeds can be correlated with the change in pH. As Li is released, H satisfies the broken bond. Hence, the pH is increased and hydrated Si forms. The degree of hydration corresponds to the amount of leaching. The hydrated silica is susceptible to condensation reactions that would cause a gel network to form. Network formation could cause the yield stress of the suspension to increase and result in pumping difficulties. Based on these statements, a frit of lesser durability is more susceptible to network formation under similar conditions. However, to realize the gel network formation, a condensation reaction must occur. So, the frit durability illustrates the possibility of gel network formation but does not specify that the network will actually form. Thus, the formation of a gel network in the melter feed is more likely with the FY 91 frit compared to the 202 and HW-39 frits.

5.3 The Effect of pH on Yield Stress and the Electrokinetic Sonic Amplitude

In the previous section, pH was linked to an increase in the leaching of the frit in the melter feed. This leaching created the opportunity for a gel network to form. Macroscopically, this network may be characterized by the yield stress. For Figure 5.11, the yield stresses of the samples described in Sections 5.2 and 5.1 are plotted as a function of pH. There appears to be no specific correlation for
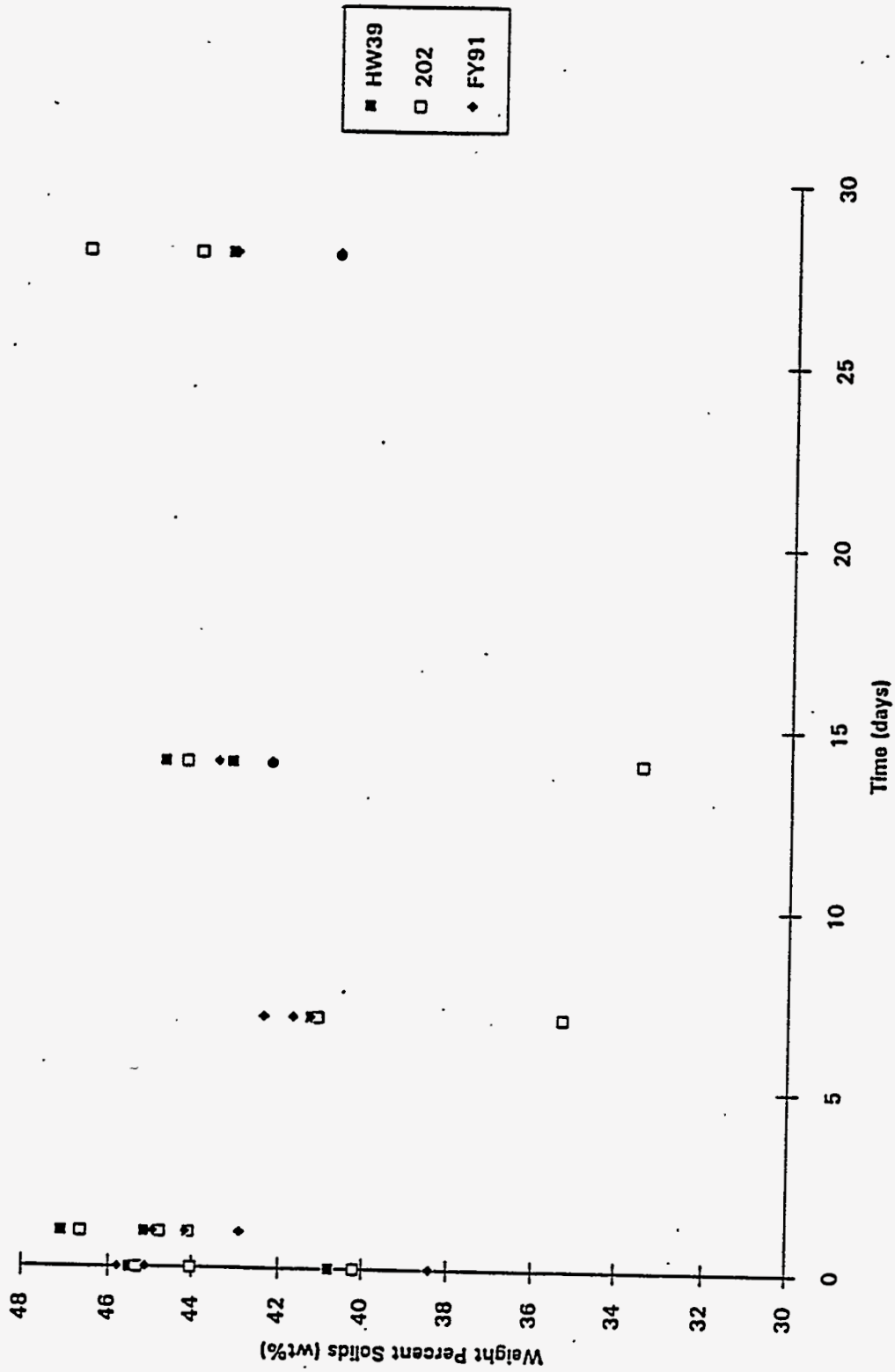
Figure 5.8. Weight Percent Solids Versus Age for the Frit Comparison. These samples were boiled for 2 h.

5.11
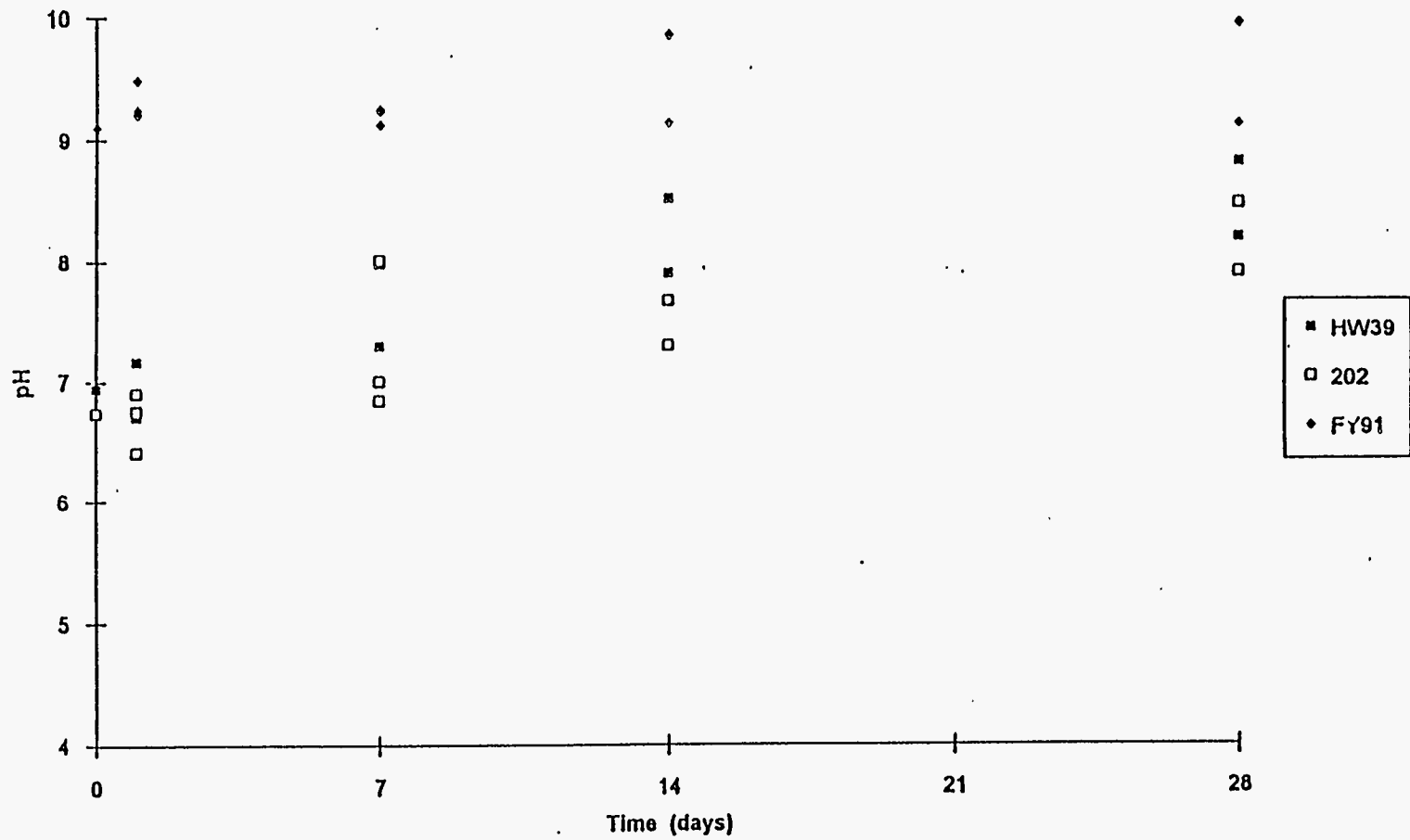
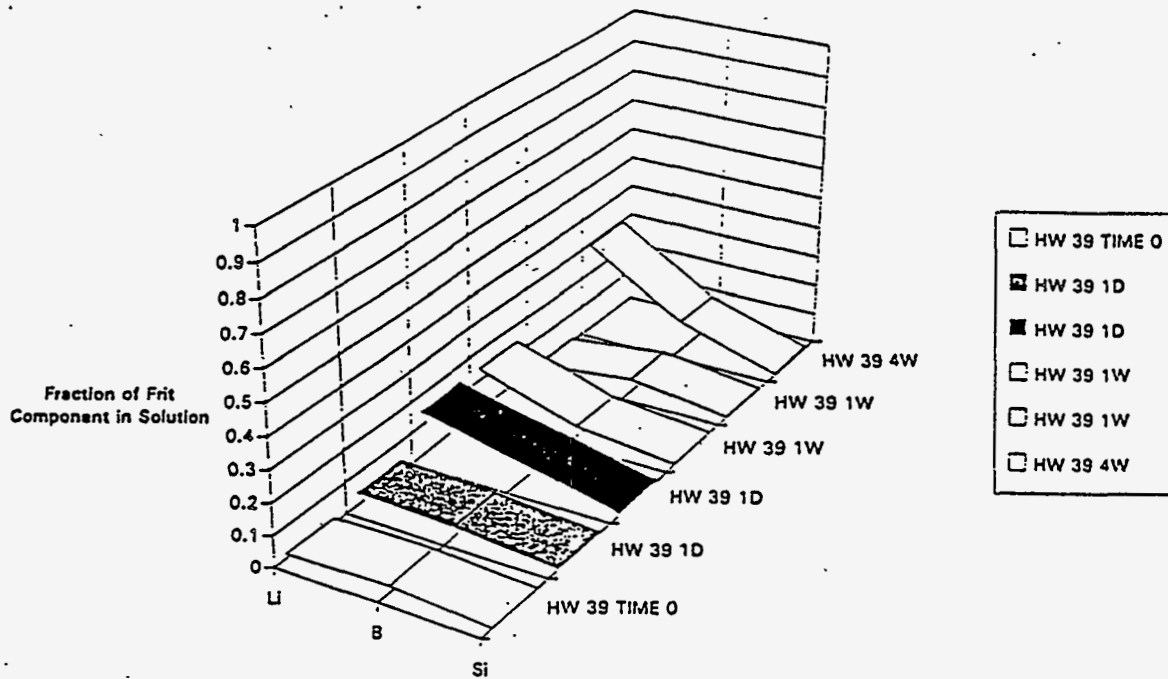**Figure 5.9.** pH Versus Age for the Frit Comparison. These samples were boiled for 2 h.

Figure 5.10c. HW-39 Melter Feed Supernatant Analysis for 2-h Boiling

the yield stress as a function of pH. However, for higher pH values, there is a wider range of yield stress values. This may be cautiously attributed to gel network susceptibility. Specifically, higher pH values indicate increased leaching whose result provides the basis for network formation via a condensation reaction.

To investigate the effect of pH on the rheological properties of the NCAW simulant, the electrokinetic sonic amplitude (refer to section 3.4 for description) was measured as a function of pH (see Figure 5.12).[a]. Simply, a higher mobility should correspond to a more dispersed system, and a lower viscosity and yield stress would be expected provided that the surface chemistry did not change. The pH of the unformated NCAW waste simulant was lowered by the addition of 6 M HNO_3. The magnitude of the ESA did not change appreciably over the measured pH range. These results imply that the waste particles do not disperse differently over the tested pH range. Therefore, changes in melter feed rheology are likely dependent on the response of the frit, provided that all other conditions are maintained.

(a)   The phase angle for this measurement was maintained between 0° and 15° over the entire pH range.

5.14

Figure 5.11. Yield Stress of HWVP NCAW Melter Feed Simulants Versus pH
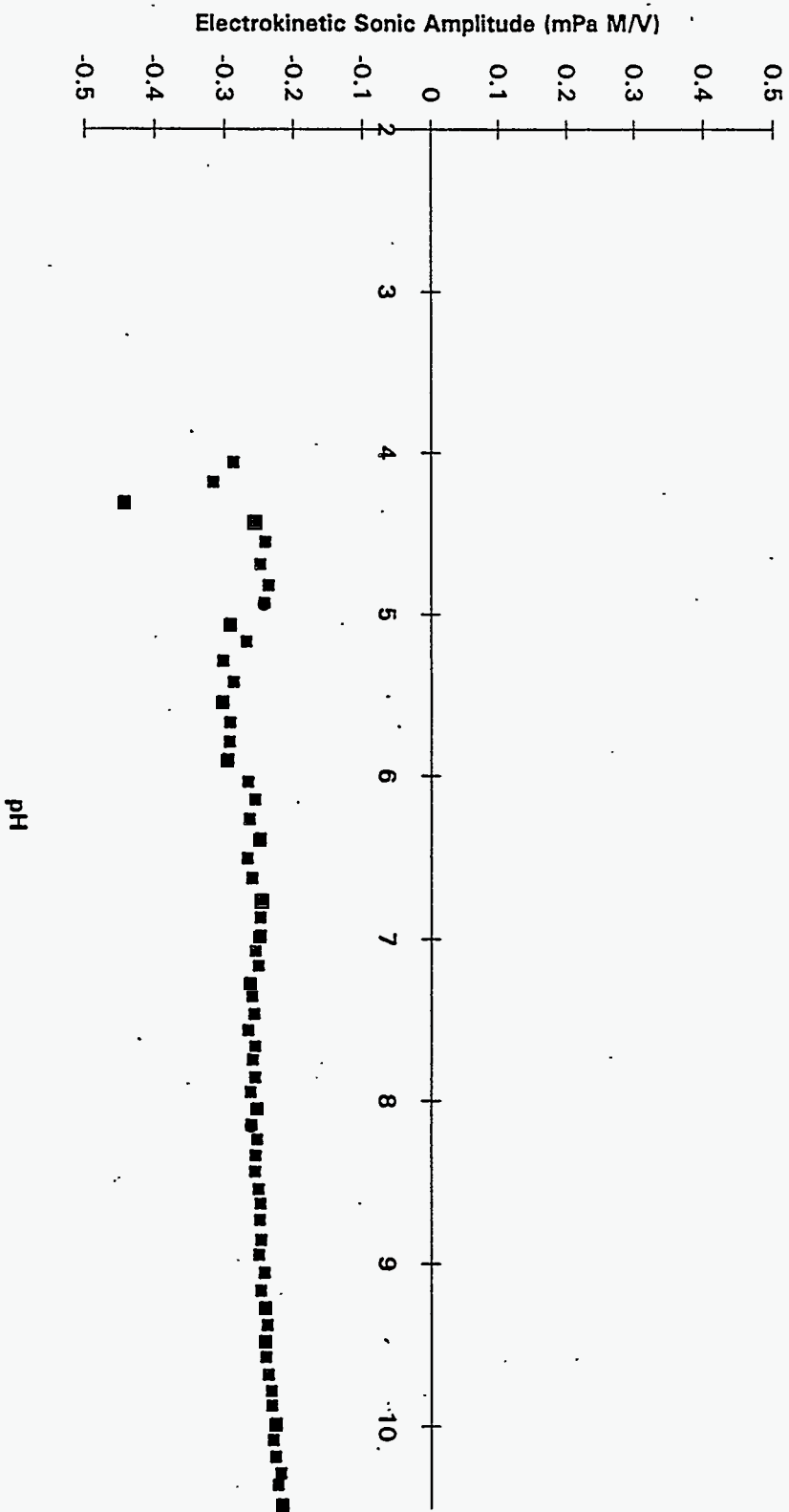
Figure 5.12. Electrokinetic Sonic Amplitude Versus pH of an Unformated HWVP NCAW Simulant Tritrated with HNO_3

5.4 Rheology of 202 and FY 91 Melter Feeds: pH < 5

The pH of the 202 and FY 91 melter feeds was maintained below 5 during a 4-week aging period. The pH of the FY 91 melter feed was approximately 9 after a 2-h boil. The pH of the 202 melter feed was approximately 7.5. The suspensions were immediately titrated with 6 M HNO_3 to lower the pH to below 5. The resulting titration curves and pH data are shown in Figure 5.13. These tests were performed for three reasons. First, HNO_3 was added to the melter feed in the KfK tests (see Section 6.2) for rheological mitigation. Second, Si is less soluble at lower pH. Third, Si is less soluble in HNO_3 (Elmer and Nordberg 1958). Note that the acid titration diluted the FY 91 melter feed solids, as clearly depicted in Figure 5.14.

Viscosity as a function of aging is shown in Figure 5.15. The viscosities of the compared melter feeds were similar over the 28-day period. For the 1- and 28-day samples, the FY 91 melter feed had a higher viscosity. The yield stresses for the two melter feeds are shown in Figure 5.16. The yield stress for the FY 91 melter feed generally rose over the aging period. The yield stress is consistently between 0.5 and 3 Pa for the 202 melter feed, excepting the 1-day sample. Generally, the yield stresses were slightly lower for the pH < 5 melter feed samples compared to the melter feeds in the pH 8-10 range. This reduction in yield stress may not warrant acidifying melter feed. These rheology data (Figures 5.15, 5.16) must be cautiously compared because of solids loading differences, which result from the acid titrations.

The pH versus time description (Figure 5.13) showed that the FY 91 melter feed required significantly more HNO_3 compared to the 202 melter feed. This can largely be attributed to the prevalent leaching that occurs in the FY 91 melter feed. Figure 5.17 shows that the Li was readily released in the FY 91 melter feed. The amount of Li leached for the FY 91 melter feed pH < 5 sample was comparable to the FY 91 melter feed without pH control (see Figure 5.10). The Li leaching for the 202 melter feed pH < 5 sample was smaller compared to the 202 melter feed that was permitted to rise in pH (see Figure 5.10). In addition, Figure 5.17 shows that Si was not detected for either pH-controlled melter feed sample. The FY 91 and 202 melter feed B release was similar for the samples shown in Figures 5.10 and 5.17, which implies that the solubility of B did not change as a function of melter feed pH.

5.5 FY 91 and 202 Melter Feeds at 600 g TO/L

Figure 5.18 shows the viscosity data for the 202 and FY 91 melter feeds at waste loadings of 500 and 600 g TO/L. The 202 and FY 91 melter feeds at 500 g TO/L were discussed previously. For the 600 g TO/L samples, the viscosity of the FY 91 melter feed was consistently higher than the 202 melter feed throughout the aging period. Additionally, the viscosities of the 600 g TO/L samples generally decreased over the aging period. Examination of the weight percent solids data (see Figure 5.19) showed that the measured percent solids decreased during the aging period. The decreased viscosity is likely linked to the measured percent solids decrease.

Chart1
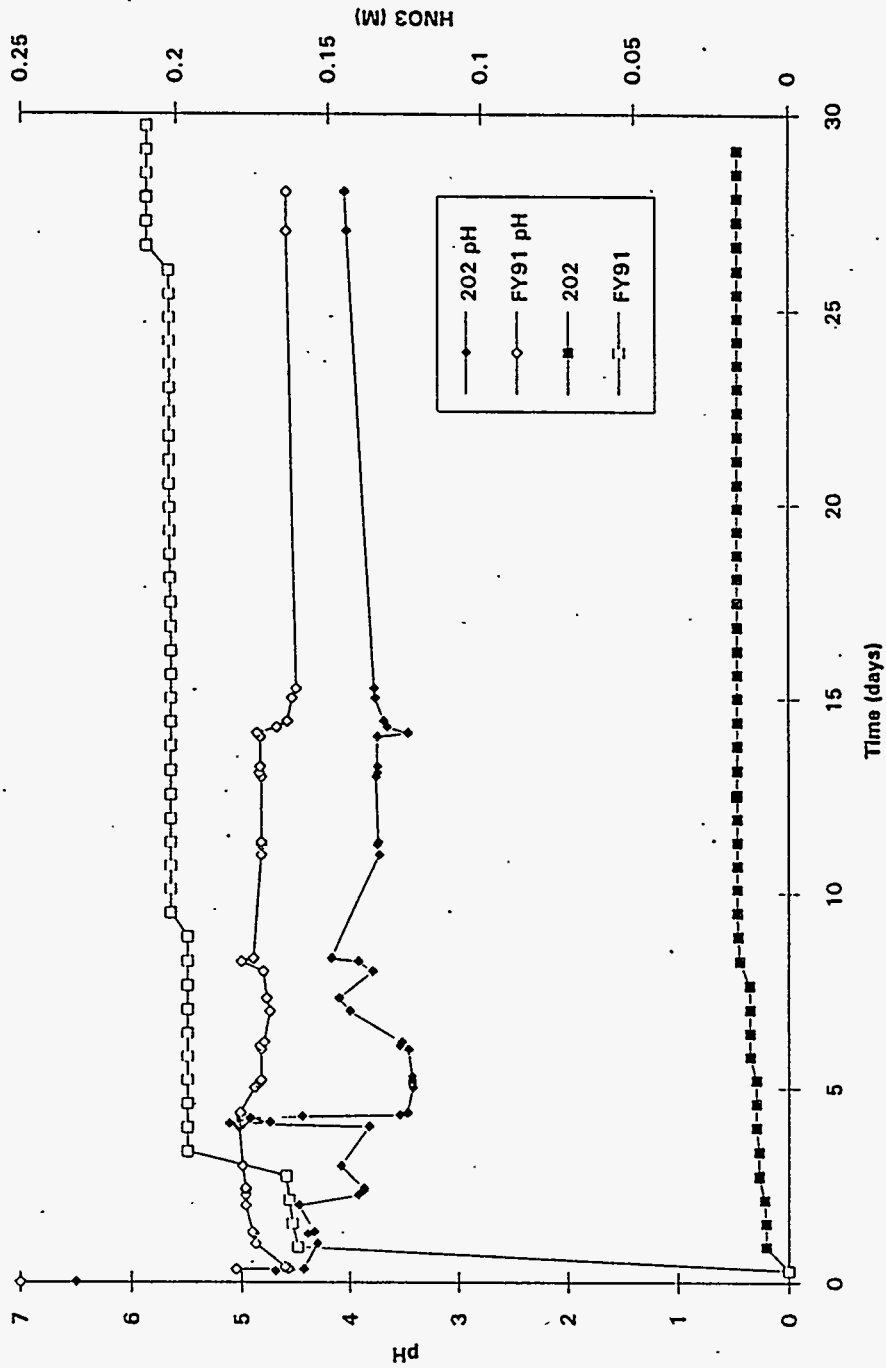
Figure 5.13. pH, Dose of HNO_3 Versus Time for the pH <5 Melter Feeds

5.18
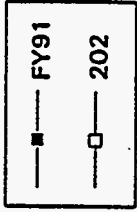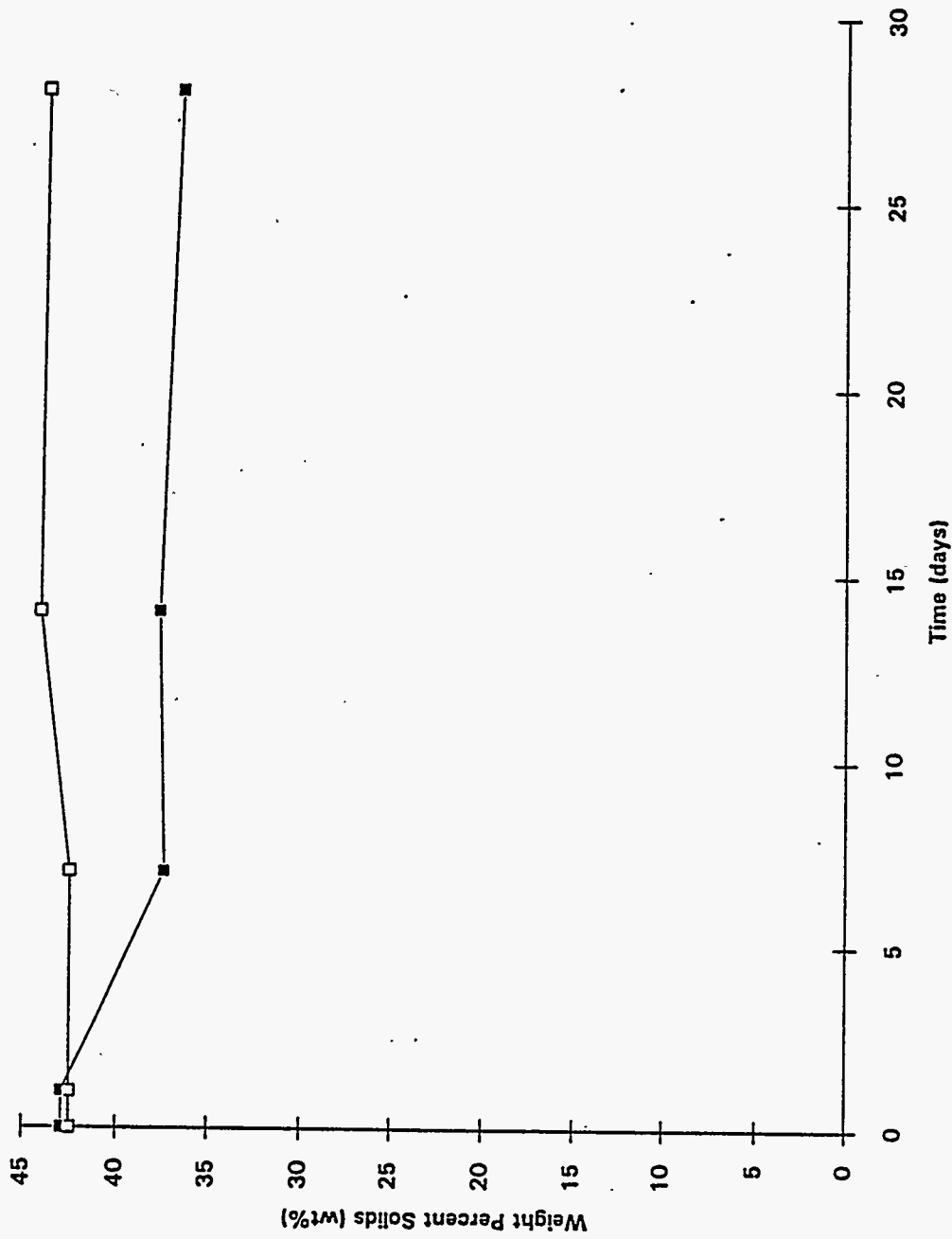
Figure 5.14. Weight Percent Solids Versus Time for the pH-Controlled Melter Feeds

5.19
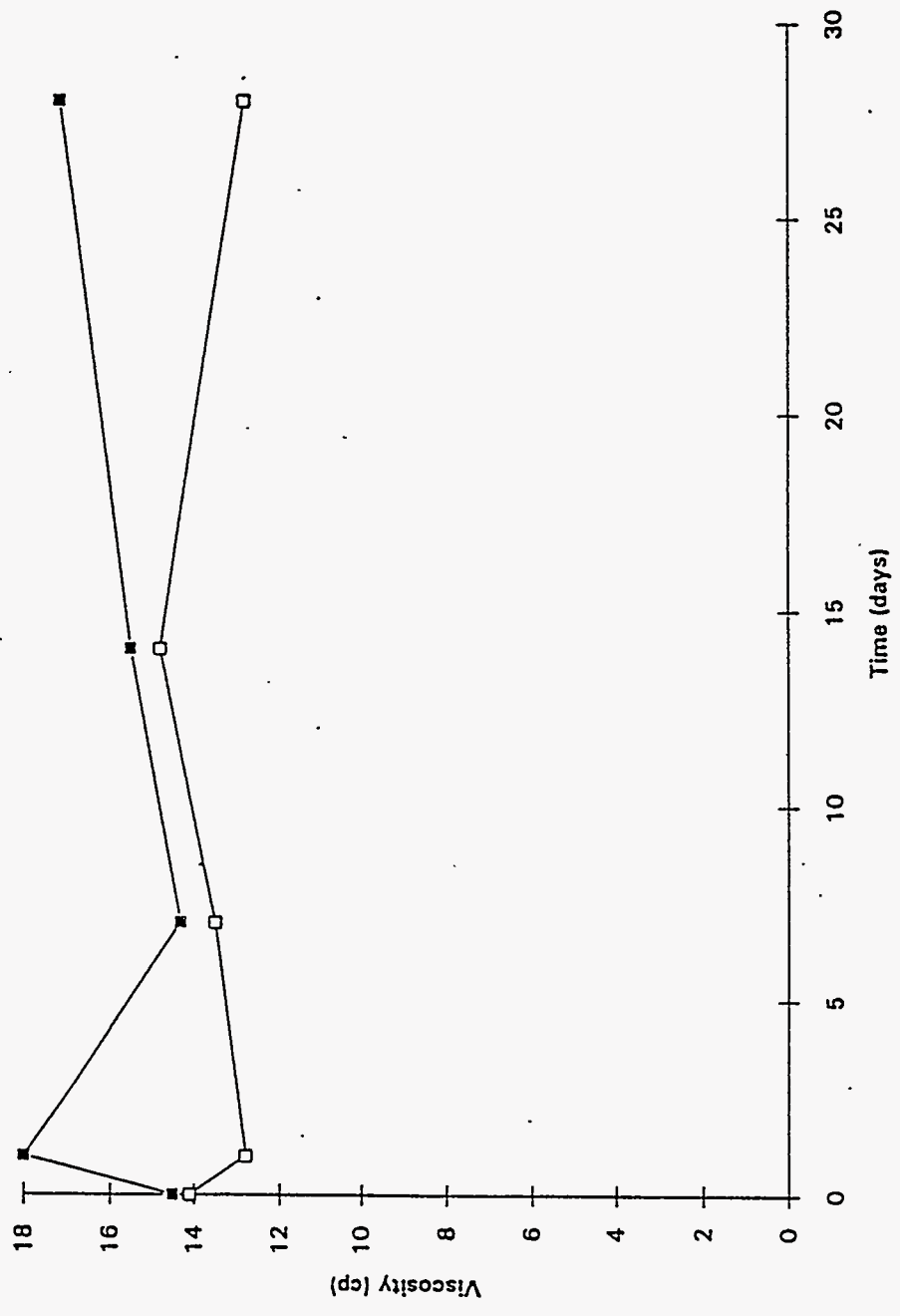
Figure 5.15. Viscosity Versus Time for the pH-Controlled Melter Feeds

5.20
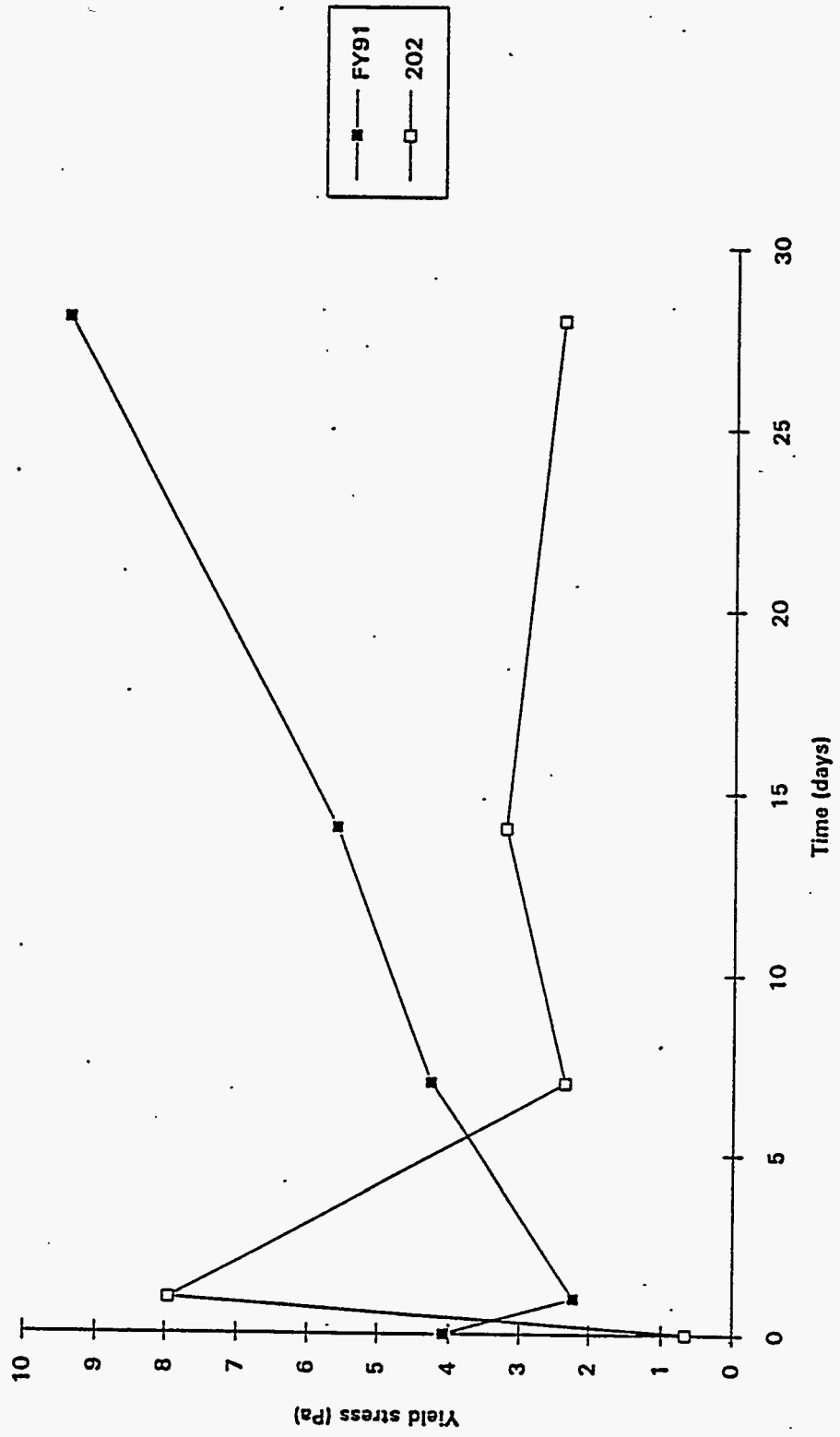
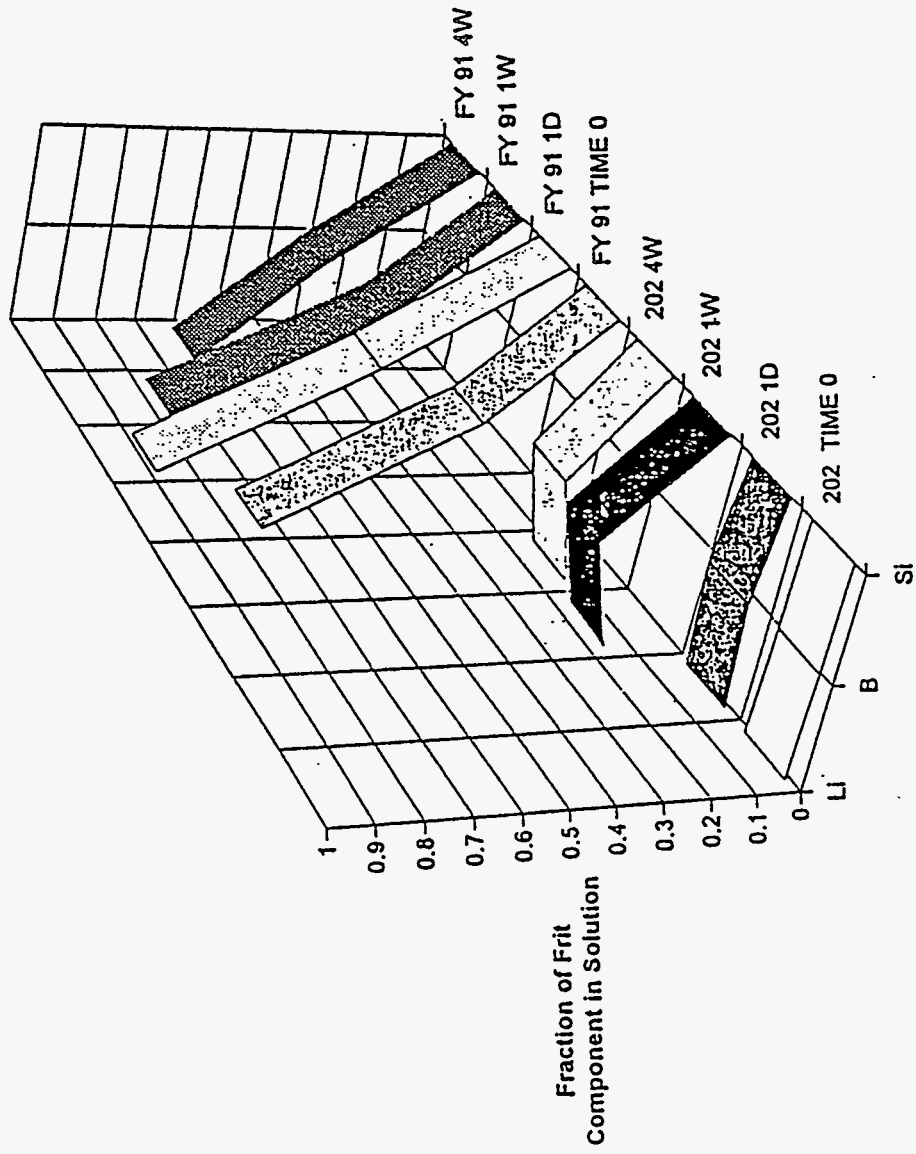**Figure 5.16.** Yield Stress Versus Time for Samples pH < 5

5.21

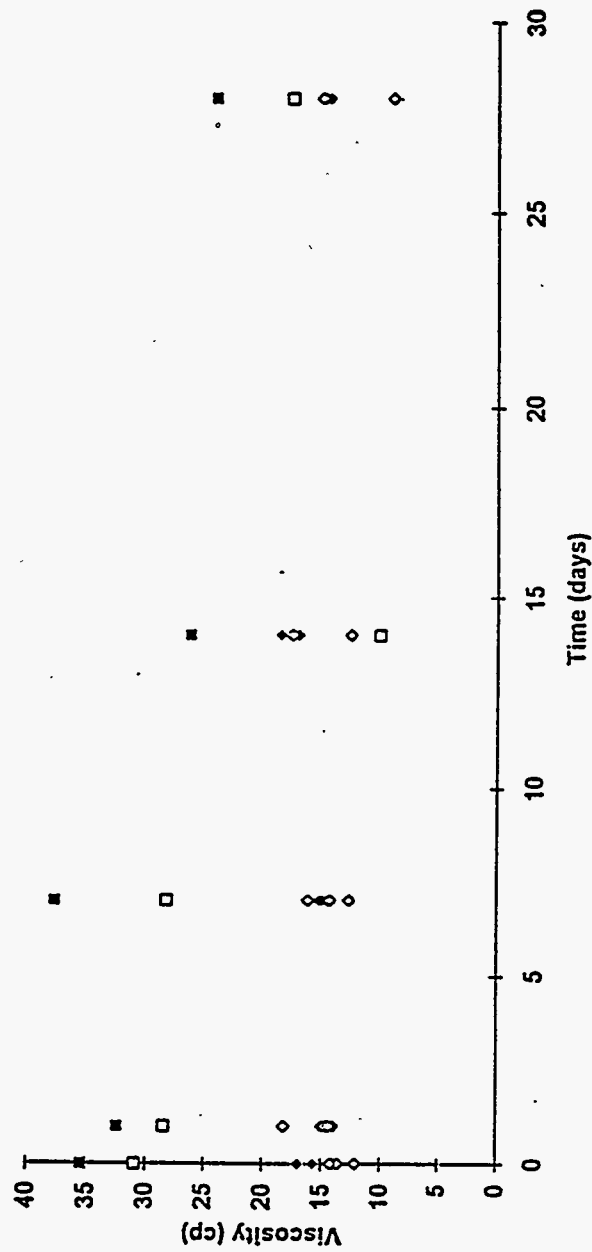**Figure 5.17.** Supernatant Analysis for the Melter Feeds Maintained at pH < 5

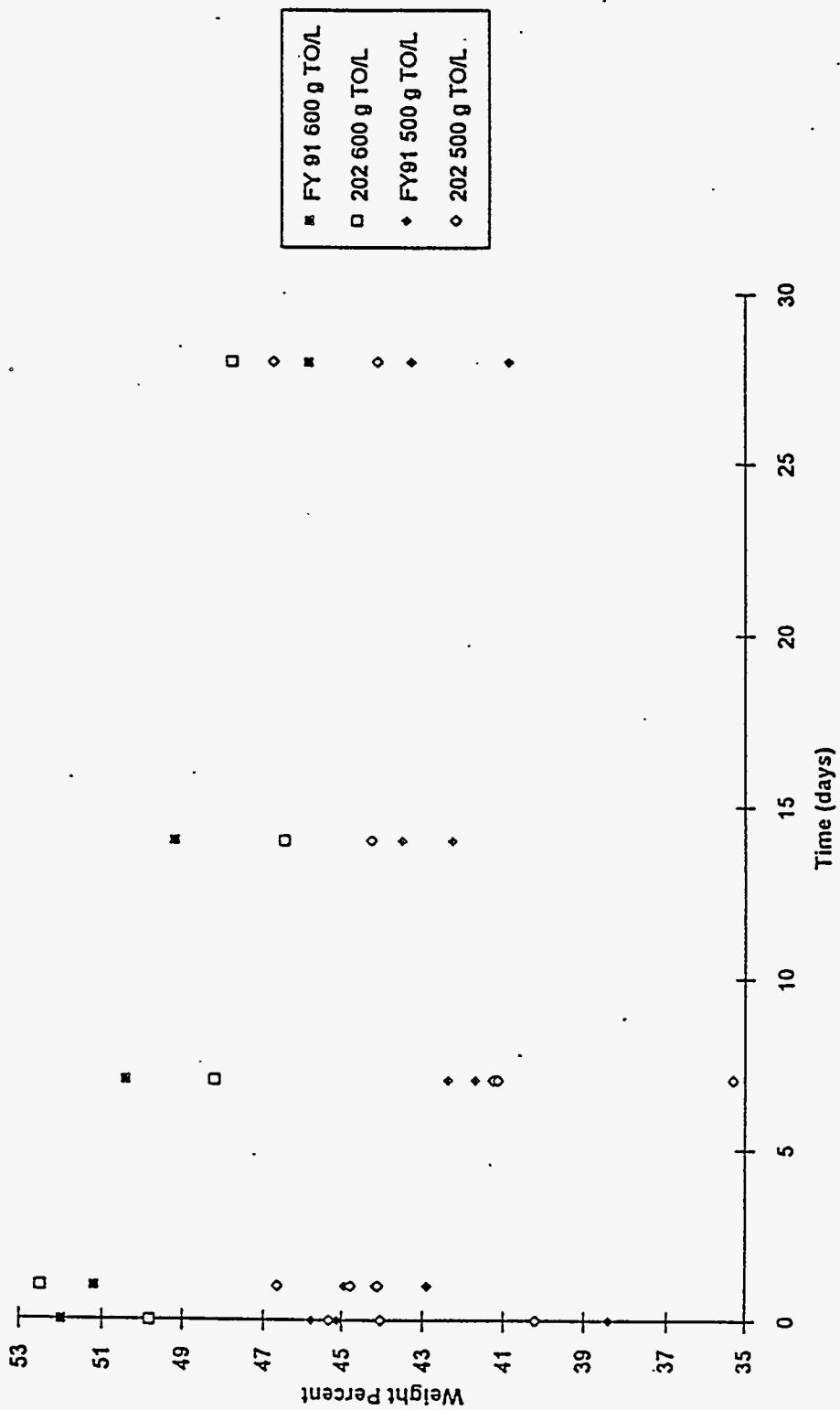**Figure 5.18.** Viscosity Versus Time for 500 and 600 g TO/L

5.23

Figure 5.19. Weight Percent Solids Versus Time for 500 and 600 g TO/L

5.24

Figure 5.20 shows the yield stress versus time for the 600 g TO/L FY 91 and 202 melter feeds. As expected, the 600 g TO/L showed higher yield stresses compared to the 500 g TO/L melter feeds. No other trends could be extracted from this data. Note that the FY 91 600 g TO/L sample for 4 weeks of aging showed the lowest yield stress for the 600 g TO/L samples. However, the FY 91 600 g TO/L suspension also showed the lowest weight percent solids of the 600 g TO/L. Lastly, the pH (Figure 5.21) and the chemical analysis (Figure 5.22) of the 600 g TO/L samples did not differ significantly from the 500 g TO/L counterparts, though pH showed a modest increase with aging time.

5.5.1 Concentration Cycling of the FY 91, 202, and HW-39-4 Melter Feeds

The degree of leaching depends on frit composition. Increasing the melter feed concentration by evaporation may cause the leached frit particles or other solids to bond to one another and/or entrap water. This experiment was designed to test the effect of concentration cycling on the development of bonds. Samples of the FY 91, 202, and HW-39 melter feeds were prepared at 500 g TO/L and initially aged for 10 days. After 10 days, the solids loading was increased to 600 g TO/L by evaporating water from the mixing vessel. The samples were aged at 600 g TO/L for 10 days and then returned to 500 g TO/L for 15 days.

Figure 5.23 shows the results of the concentration cycling on the melter feed solids loading. The viscosities of the three melter feeds are shown in Figure 5.24. The HW-39 viscosity showed a significant increase after the initial concentration to 600 g TO/L. However, the viscosity measurement at 14 days was similar to the FY 91 melter feed viscosity. The yield stress versus time for the concentration cycled samples is shown in Figure 5.25. The 202 melter feed yield stress showed a significant increase in yield stress for the 10-day sample (initial concentration). However, the 202 melter feed yield stress was similar to the FY 91 and HW-39 melter feeds at 14 days of aging. Furthermore, no significant hysteresis was observed for the rheological properties of the compared melter feeds. This data suggests that the evaporation of the water required to reach 600 g TO/L in an aged melter feed (analogous to leached frit) did not cause condensation reactions, and consequently, the expected yield stress increased. Therefore, irreversible bonds were not formed between frit particles in the laboratory. Furthermore, water was not entrapped during the concentration cycling, which would have resulted in a viscosity versus time hysteresis.

5.6 Noble Metal Effects on Melter Feed Rheology

Noble metal effects were investigated for influence on 202 and FY 91 melter feed rheology. In general, the presence of noble metal results in a higher pH before frit addition for the formated NCAW simulant.[a] The influence of the noble metal in a formated NCAW simulant was shown in the melter

---

(a) Smith, H. D., K. D. Wiemers, M. H. Langowski, M. R. Powell, and D. E. Larson. 1993. Evaluation of HWVP Feed Preparation Chemistry for an NCAW Simulant - Fiscal Year 1993: Evaluation of Offgas Generation and Ammonia Formation.
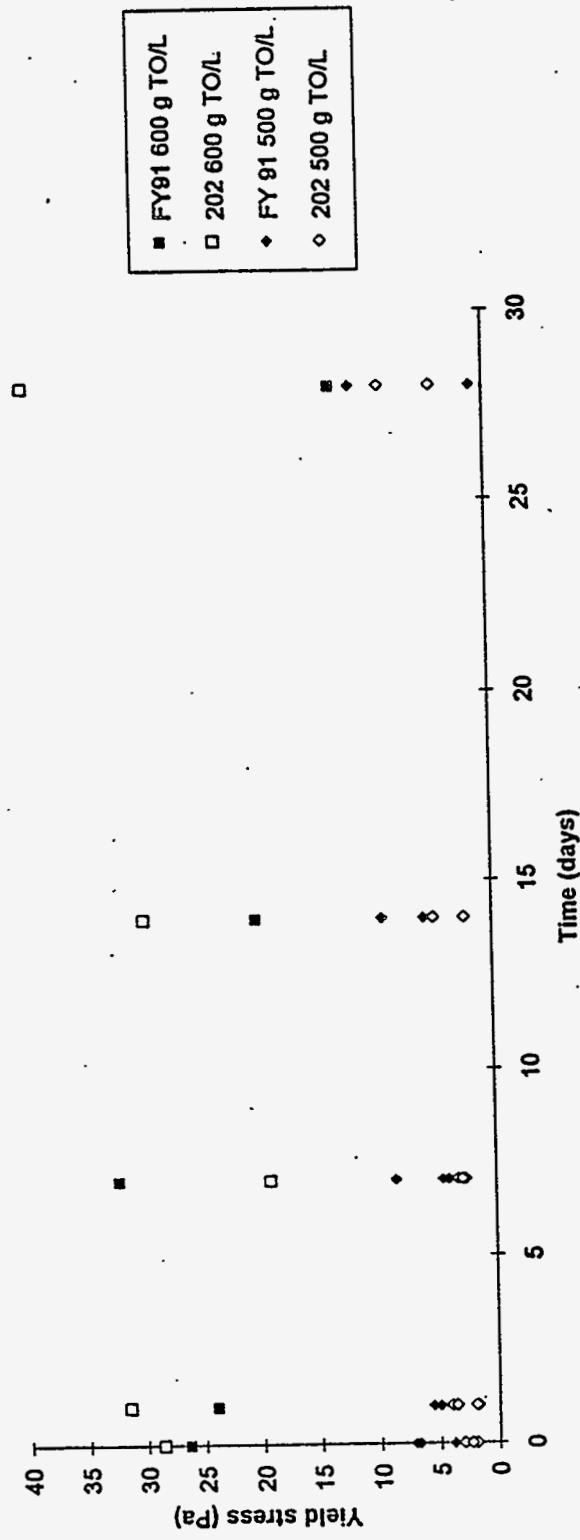
Figure 5.20. Yield Stress Versus Time for the 500 and 600 g TO/L

Legend:
- ■ FY91 600 g TO/L
- □ 202 600 g TO/L
- ◆ FY 91 500 g TO/L.
- ◇ 202 500 g TO/L

X-axis: Time (days)
Y-axis: Yield stress (Pa)
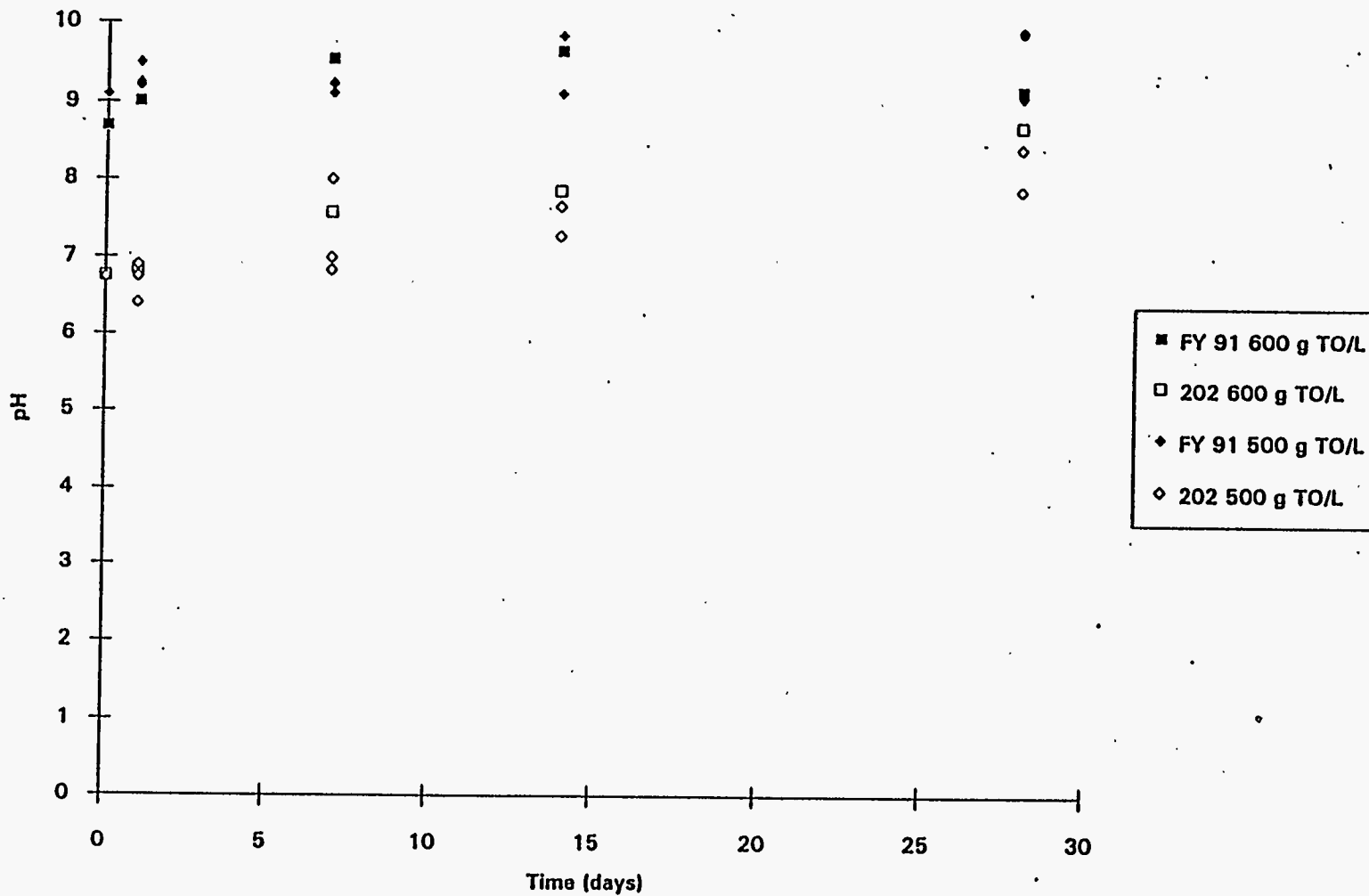
Figure 5.21. pH Versus Age for 500 g TO/L and 600 g TO/L Melter Feeds

5.27
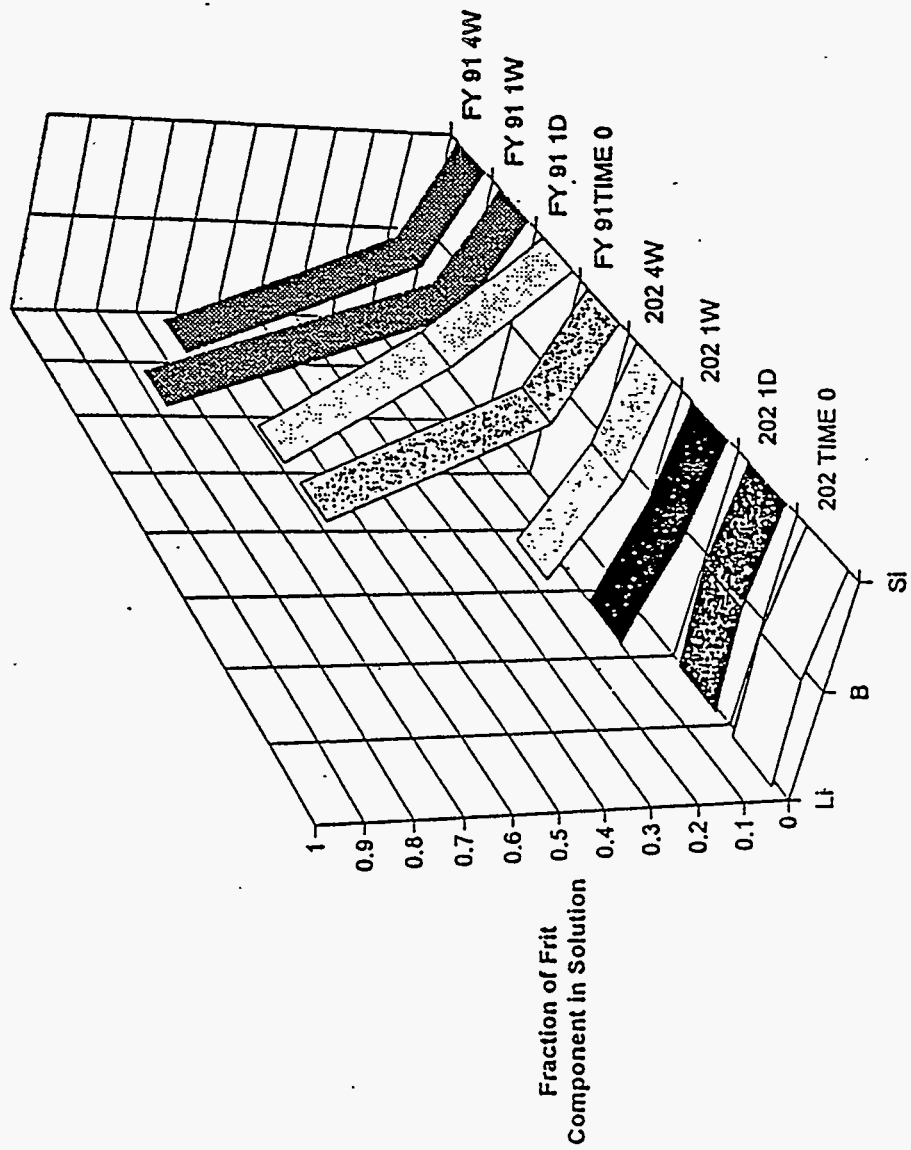
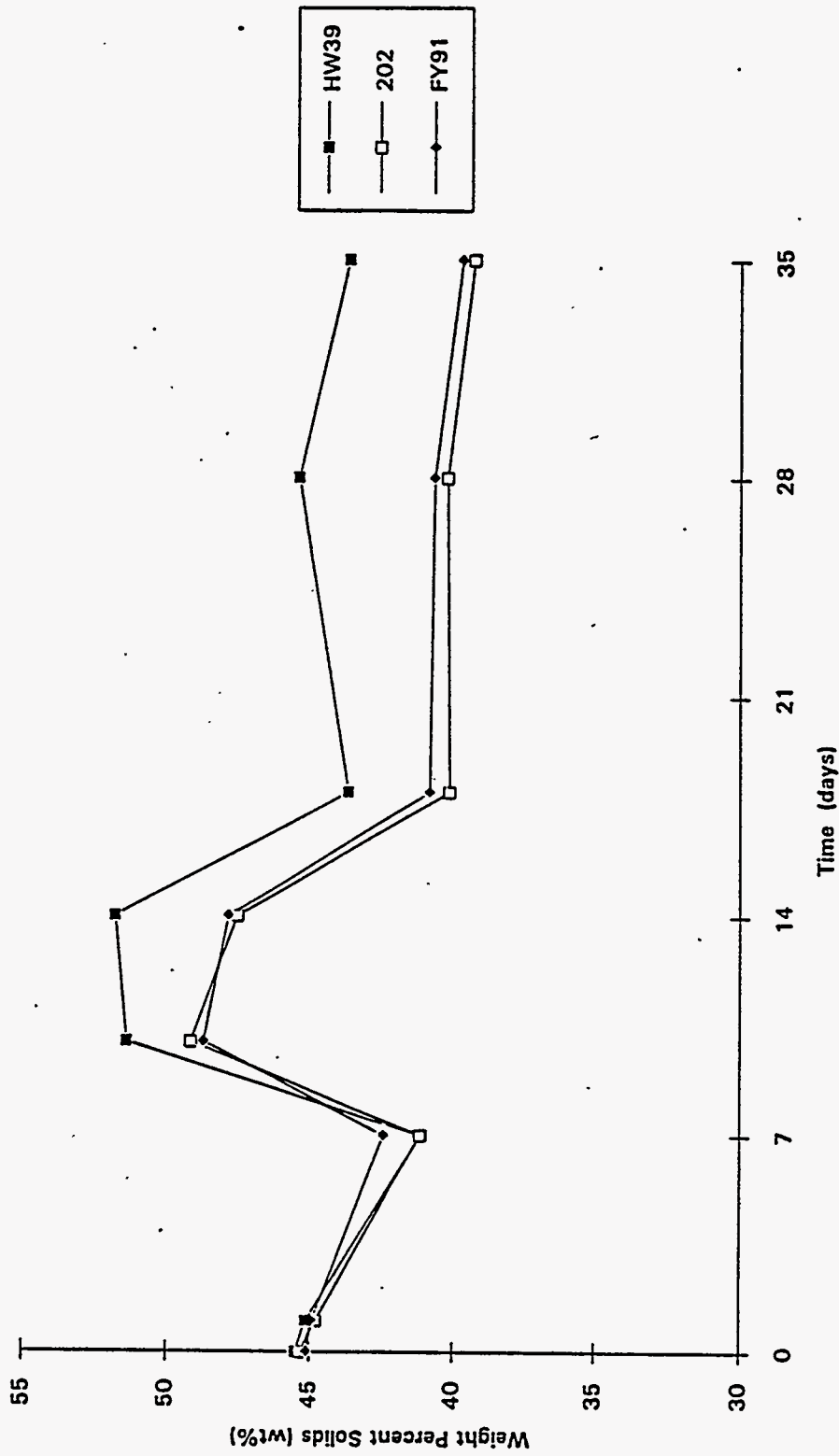**Figure 5.22.** Supernatant Analysis for the 600 g TO/L Melter Feeds

5.28

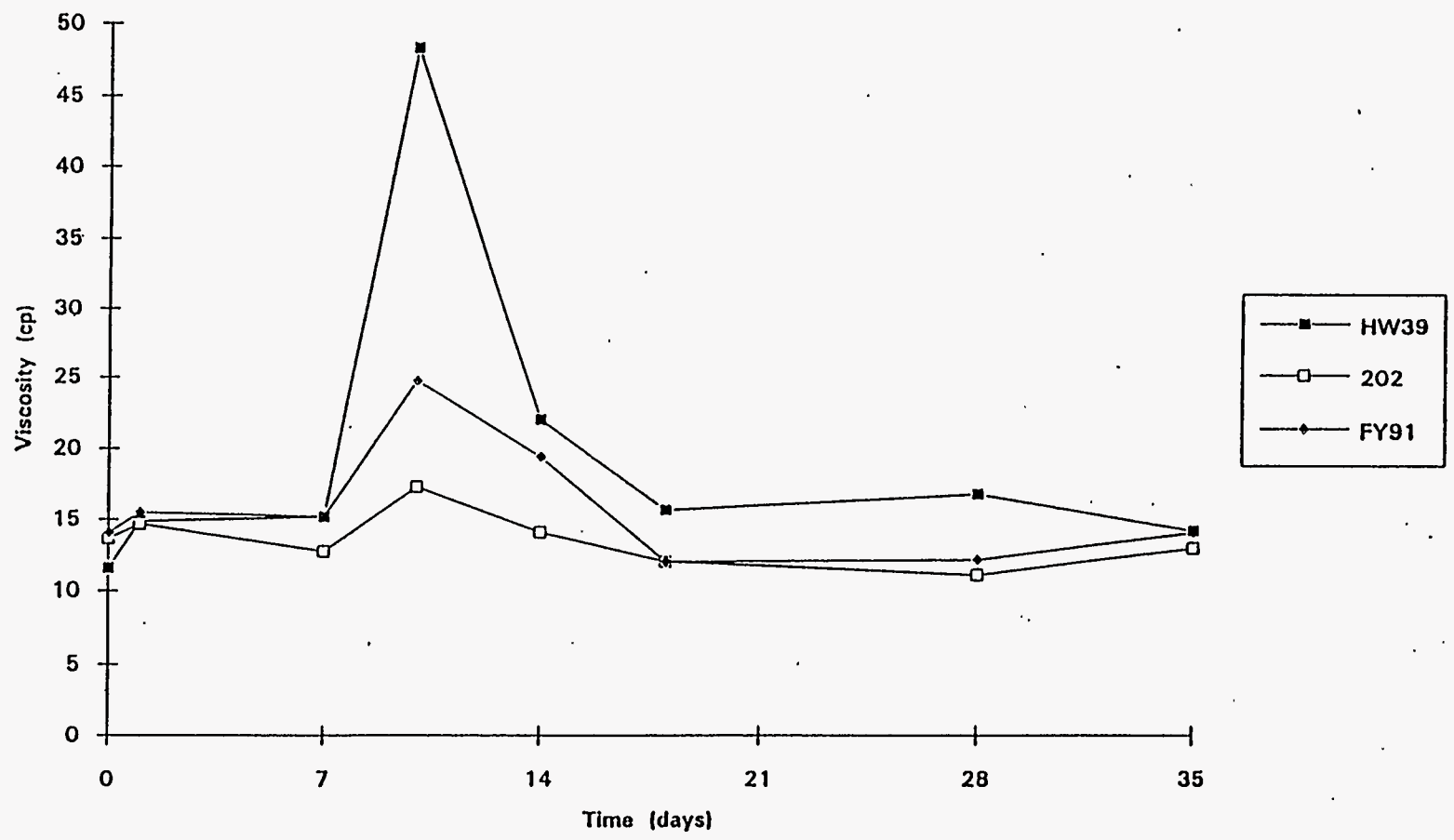Figure 5.23. Concentrated Samples: Weight Percent Solids Versus Time
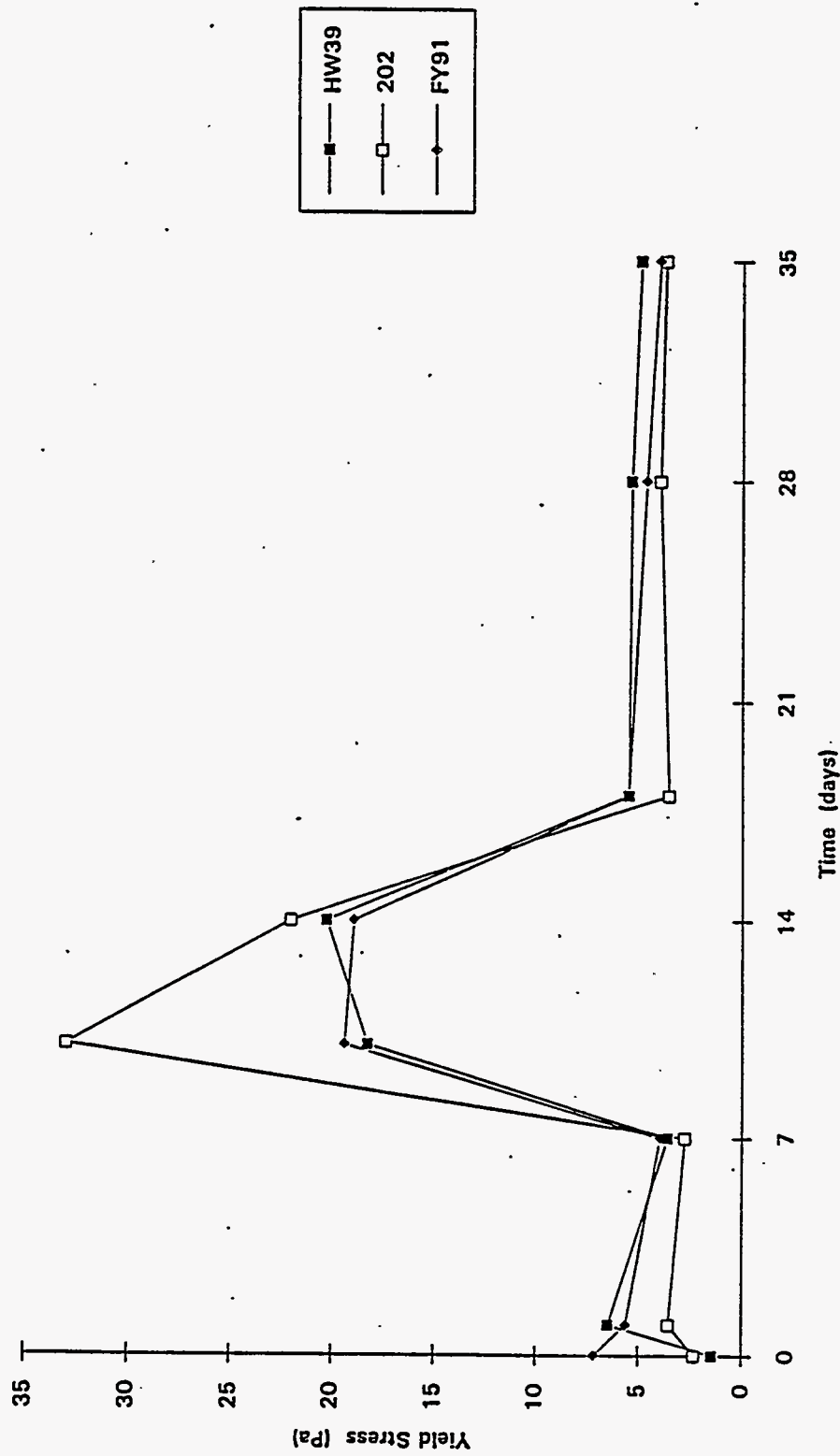
Figure 5.24. Concentrated Samples: Viscosity Versus Time

Figure 5.25. Concentrated Samples: Yield Stress Versus Time

5.31

feed pH over the 4-week aging period. The 202 noble metal-containing melter feed showed higher pH values than the 202 melter feed composition minus noble metal (see Figure 5.26). The pH values of the noble metal-containing FY 91 melter feed were generally higher for the first 7 days of aging; this difference decreases with time. In addition, the chemical analysis of the melter feed supernatant liquid did not show leaching behavior different than the nonnoble metal feeds of corresponding composition (Figure 5.27).

With the exception of the 1-day noble metal FY 91 melter feed, the viscosity of the compared melter feeds show no difference based on noble metal presence (see Figure 5.28), but the yield stress of the noble metal-containing 202 melter feed was higher (see Figure 5.29). Based on the weight percent solids data (Figure 5.30) noble metal 202 melter feed had higher solids loading, which may have resulted in the measured increase for the yield stresses. Based on these results, noble metals did not appear to significantly influence the NCAW melter feed rheology.

5.7 FY 1992 Experimental Data

During FY 1992, scoping tests were performed that focused on frit composition, noble metals, and aging. These tests were performed in vessels that permitted evaporation and did not afford close temperature control. The examined melter feeds were FY 91 with and without noble metals, HW-39 without noble metals, and 202 with noble metals. These melter feeds were formulated at 500 g TO/L. Rheology data were available after 4 weeks of aging; pH data were available over the same domain with two additional measurements taken at 6 weeks of aging. The results are shown in Figures 5.31 to 5.33.

The FY 1992 viscosity data were typical of the results obtained in FY 1993 (refer to Figure 5.6). However, the yield stress data showed a value of 28 Pa for the FY 91 melter feed without noble metals, which was higher than the values typically measured for the FY 91 melter feed. Further, the value recorded for the FY 91 melter feed with noble metals was typical. Also, the HW-39 rheology results appeared to be somewhat higher than the FY 1993 results (see Section 5.2). These increases in yield stress may have resulted from evaporation. Additionally, the weight percent solids was not measured for any of these samples. While the weight percent solids data are not entirely reliable (see Section 5.9), it could have provided relevant information. Lastly, the pH data corresponded to the data obtained in FY 1993.

5.8 X-Ray Analysis of Melter Feed

X-ray diffraction was performed on several samples from the boiling time comparison test. The analysis was performed in an effort to detect the formation of any deleterious phases that may have resulted due to frit leaching and/or aging. The XRD results are shown in Appendix B [new frit (NF)
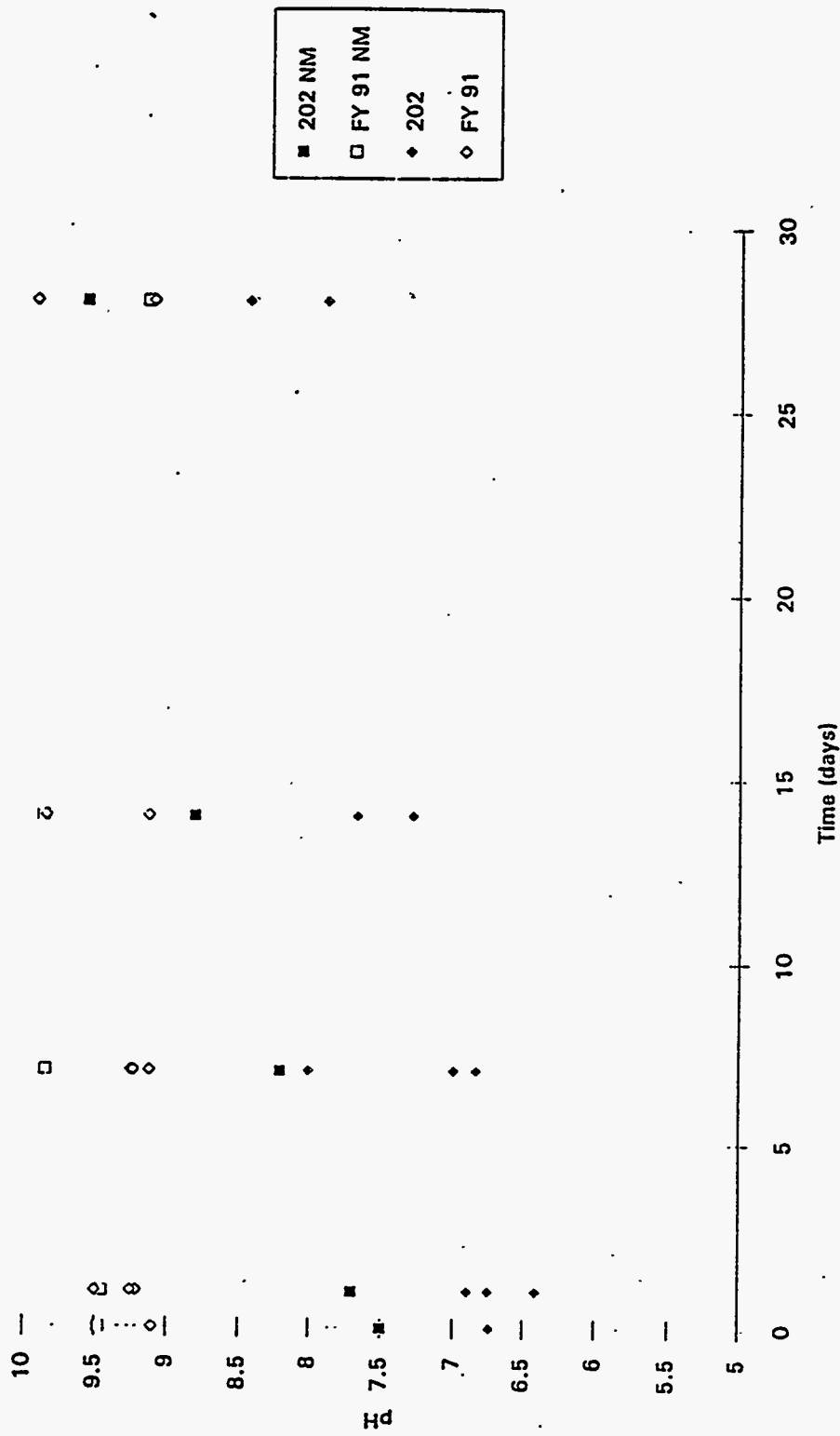
Figure 5.26. Noble Metal Influence on an HWVP NCAW Melter Feed Simulant, pH Versus Time

5.33
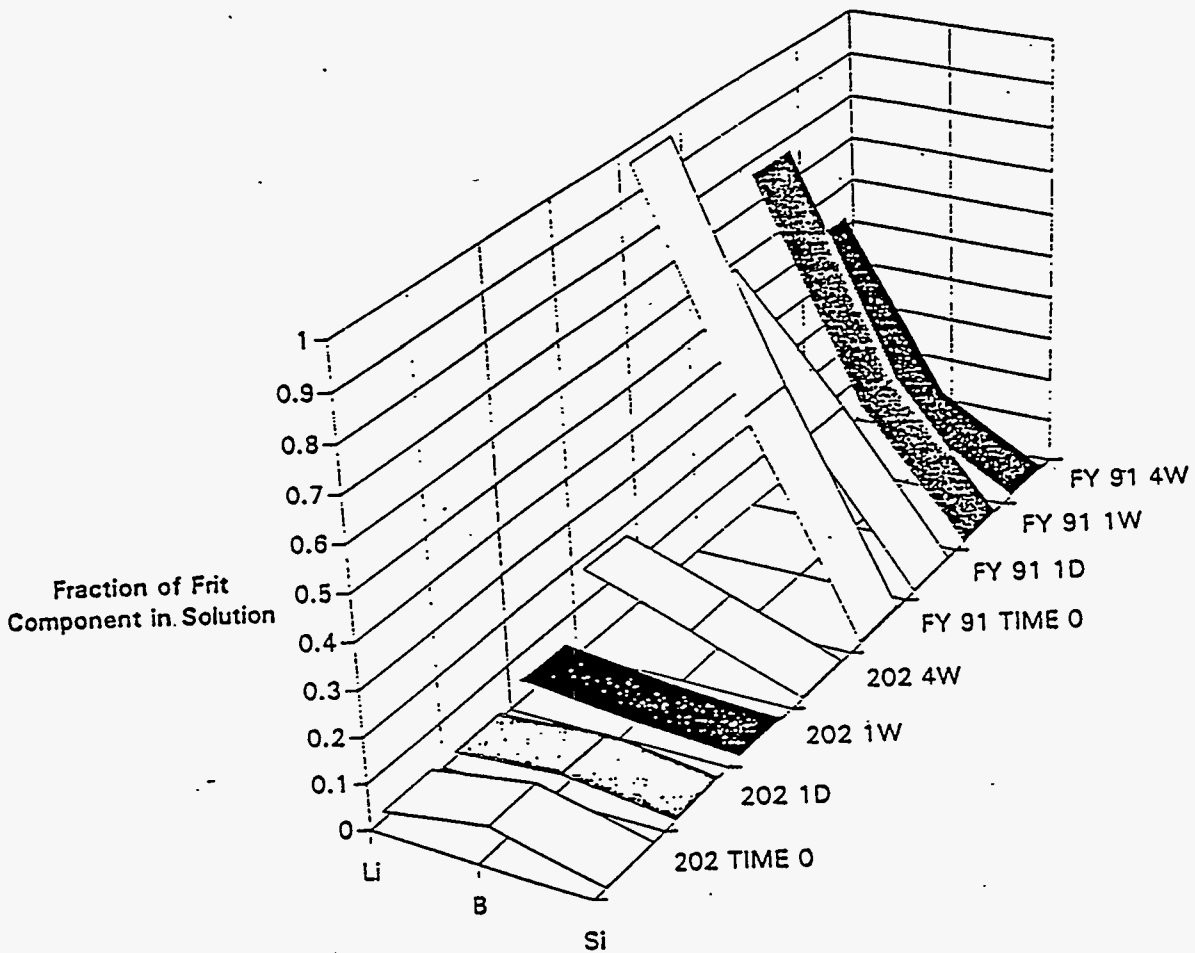
Figure 5.27. Supernatant Analysis of Noble Metal Melter Feeds

corresponds to FY 91]. These results are from the FY 91 and 202 melter feeds; they were boiled for 0, 2, 8, and 24 h and were aged for 0, 1, and 7 days. The results show the significant presence of the following expected phases:

- oxide hydroxide, goethite, FeOOH, ICDD# 29-713

- silicon dioxide, quartz, SiO_2, ICDD# 33-1161

- sodium nitrate, nitratine, $NaNO_3$, NCDD# 7-271.

Because of the complex and varied feed chemistry, other phases were not detected, and the analysis was not further pursued.

5.34
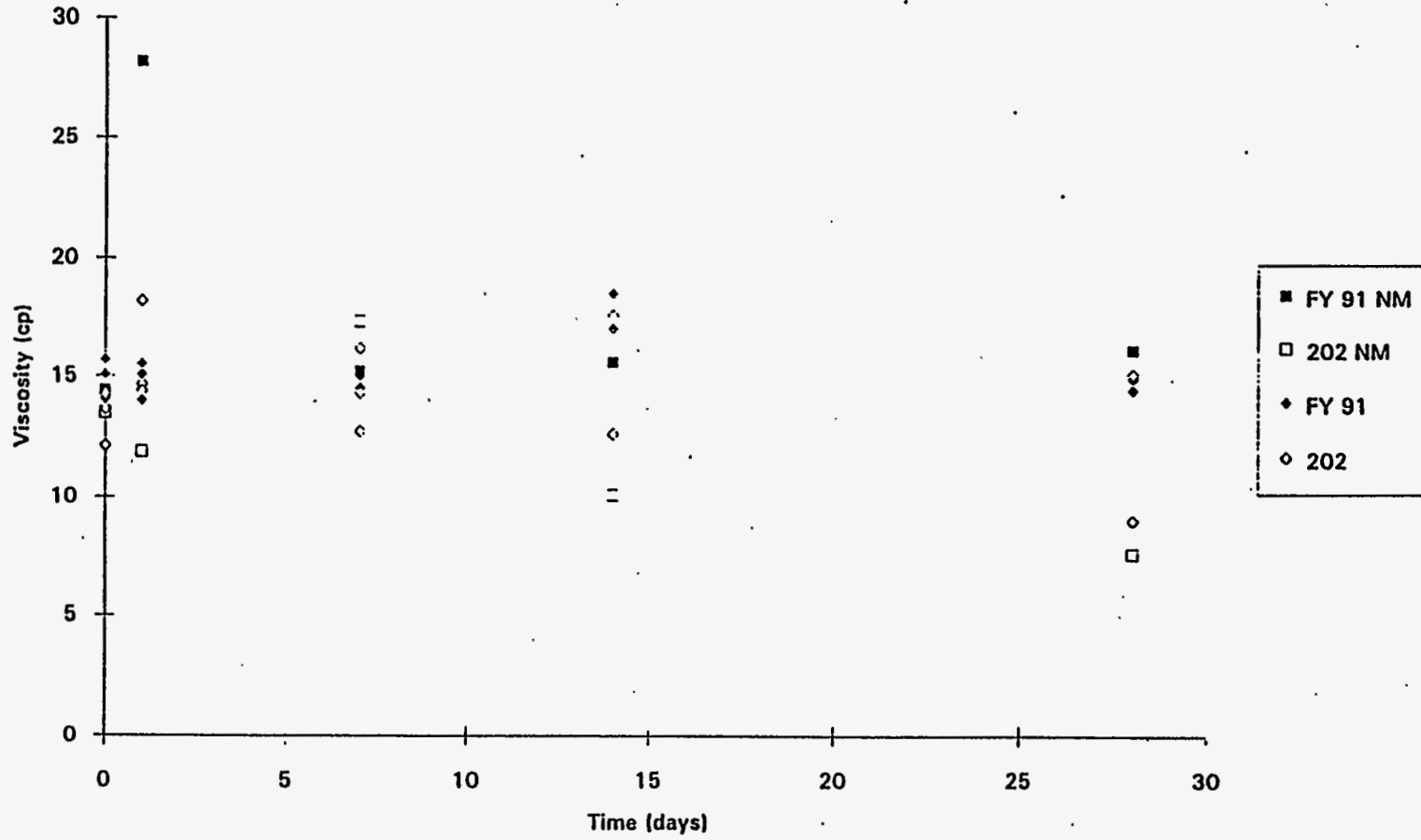
Figure 5.28. Noble Metal Influence on an HWVP NCAW Melter Feed Viscosity
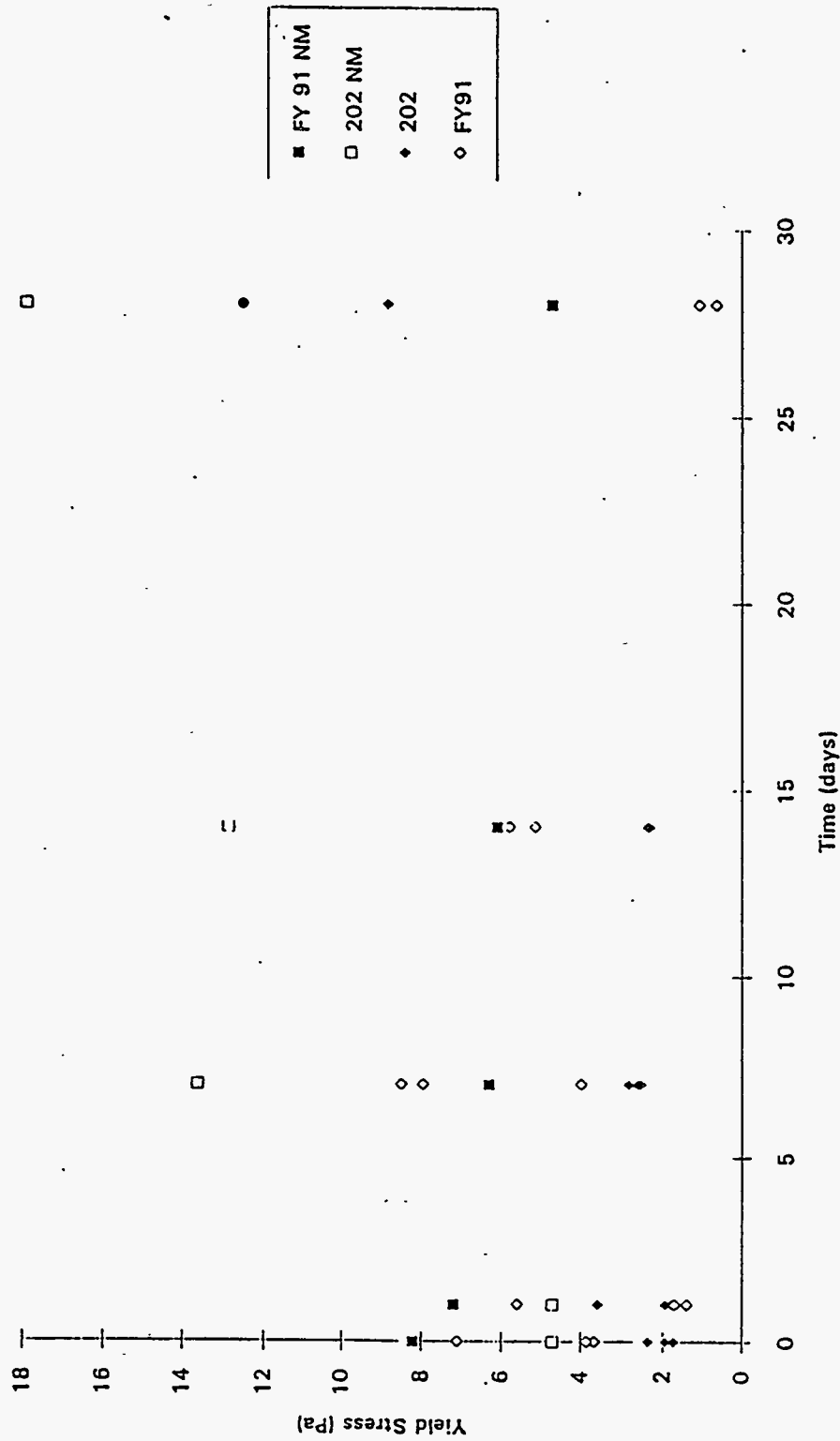
Figure 5.29. Noble Metal Influence on an NCAW HWVP on Yield Stress
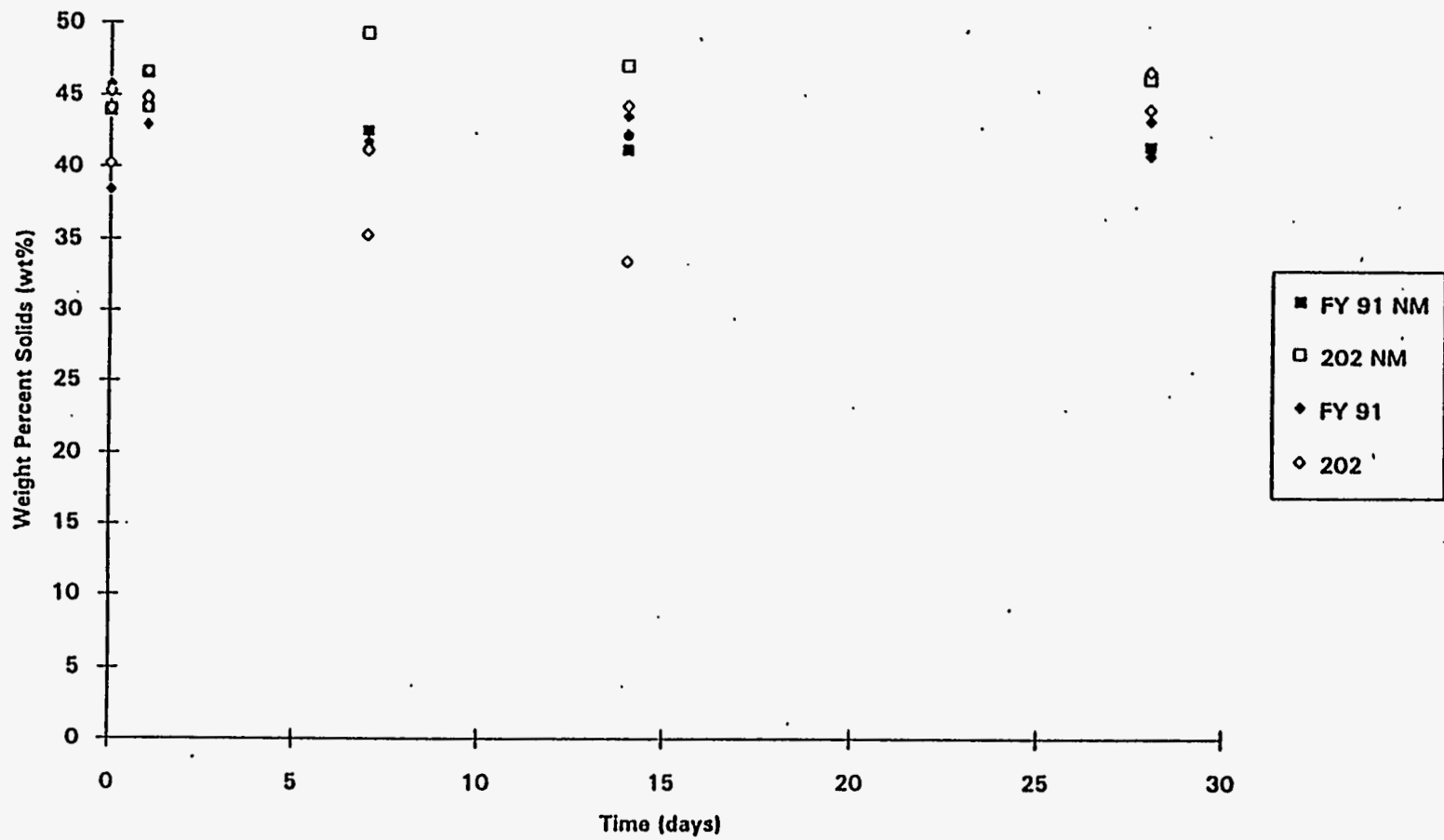
Figure 5.30. Weight Percent Solids for the Noble Metal-Containing Melter Feed
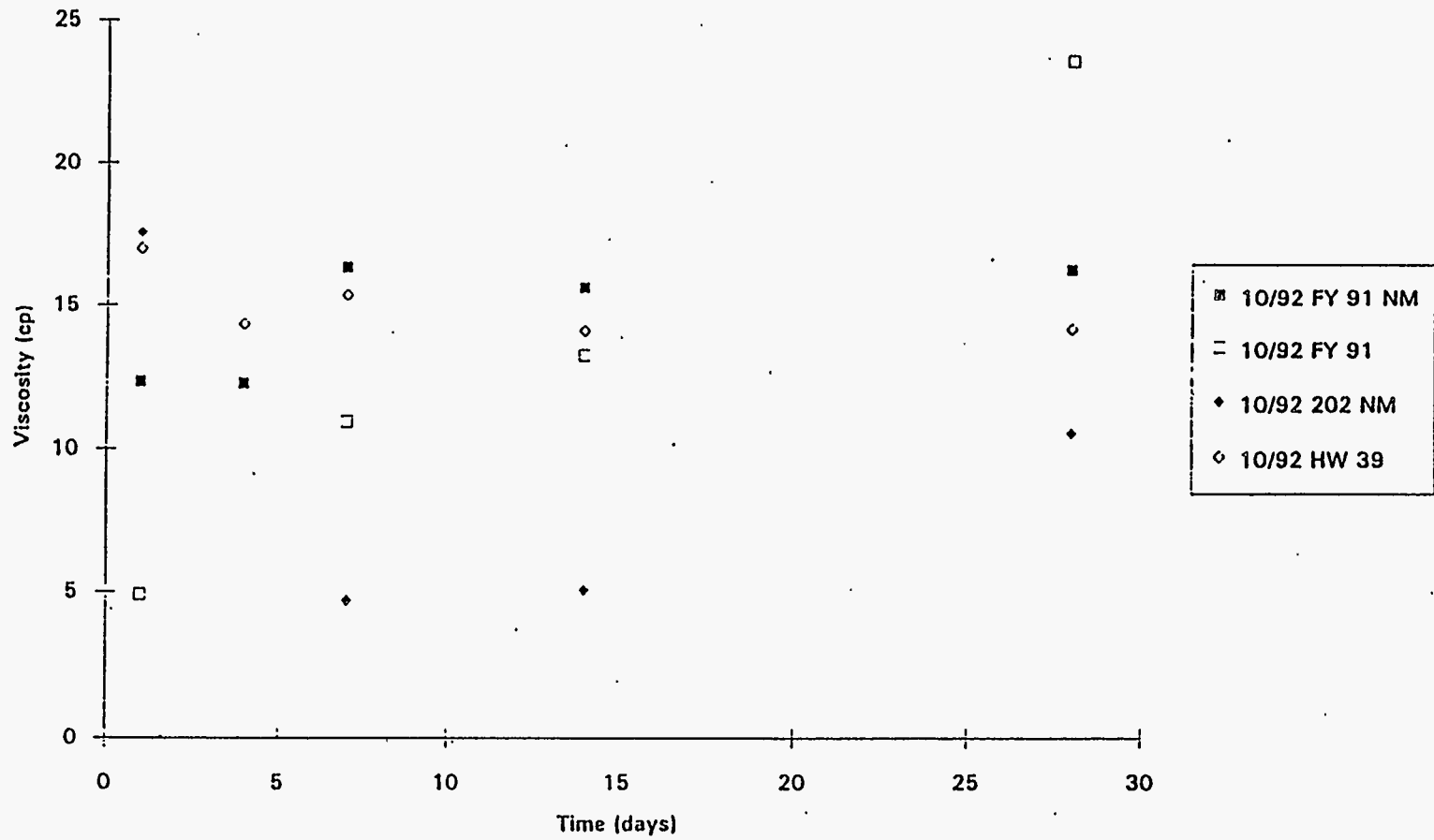
Figure 5.31. Viscosity Data from the FY 1992 Experiment
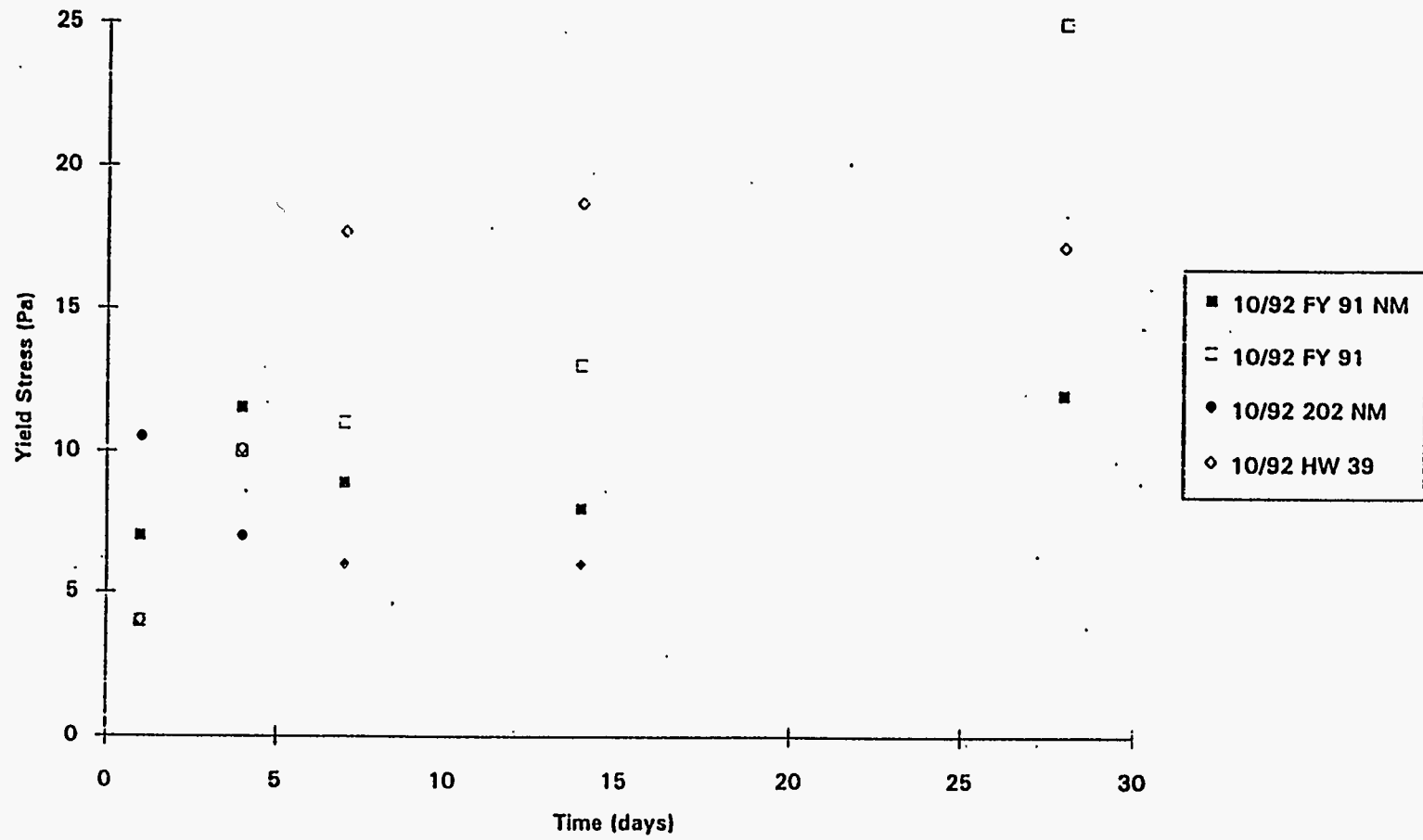
Figure 5.32. Yield Stress Data from the FY 1992 Experiment
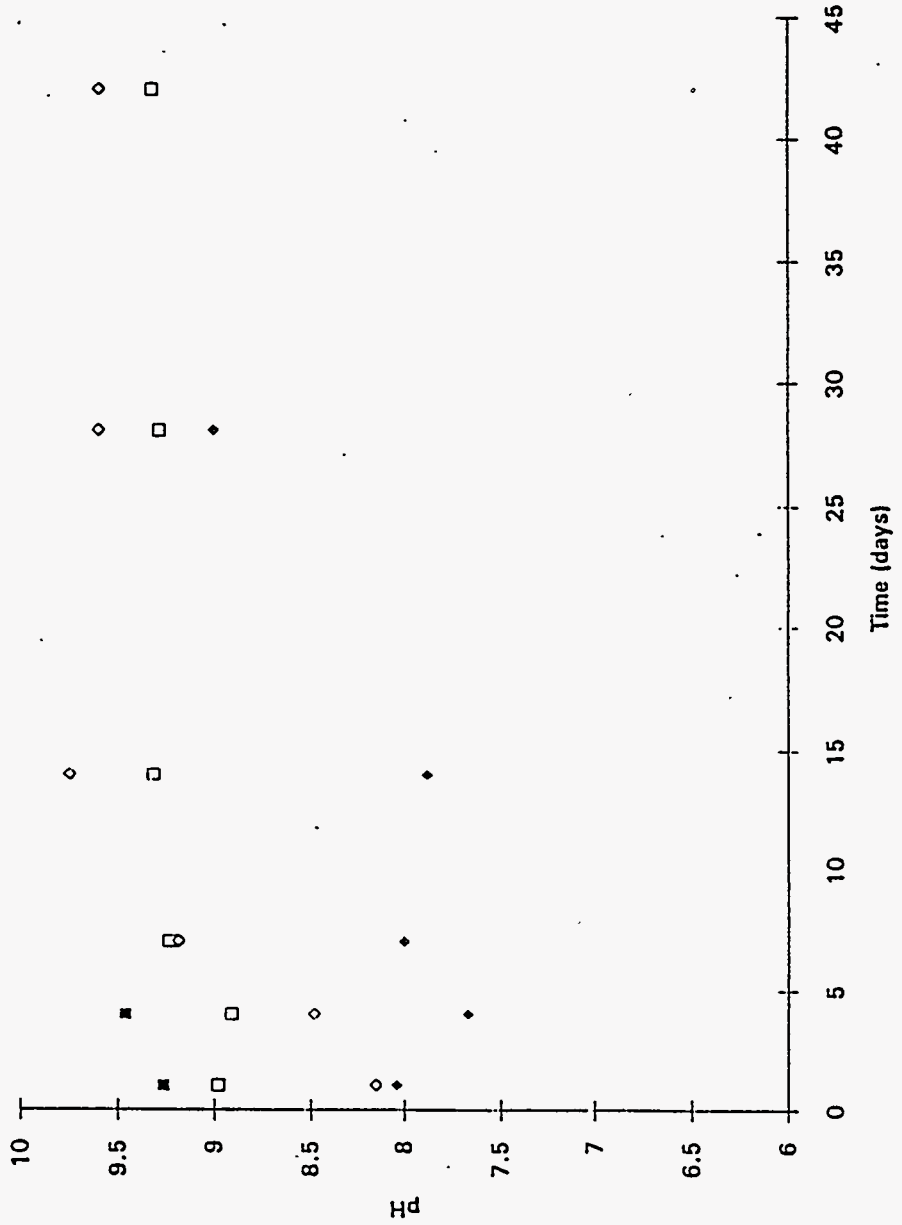
Figure 5.33. pH Data from the FY 1992 Experiment

Legend:
- ■ 10/92 FY 91 NM
- □ 10/92 FY 91
- ◆ 10/92 202 NM
- ◇ 10/92 HW 39

5.40

5.9 Weight Percent Solids Data

The weight percent solids of melter feed presented in this report were obtained by evaporating the water at 105°C for 24 h in a crucible. The drying oven was exposed to atmosphere. The starting sample weight was typically 10 g. The measurement does not provide the true solids content since chemically and physically adsorbed water was not removed. Therefore, the weight percent solids measurements have been reported for relative though useful purposes.

5.10 Average Particle Size of the 202 and FY 91 Melter Feed Used in the Boiling Time Comparison

The particle size was measured to determine whether the frit type, boiling time, or aging changed the average size. Change in average size would be the result if a ripening mechanism were prevalent. Figure 5.34 shows the average particle size as a function of time. Note that this analysis is based on a number weighted distribution. Therefore, smaller particles have the greater influence in a distribution of sizes. For the melter feeds, the measured particle size was largely sensitive to the waste's particle size. The analytical results showed an average size ranging from 0.75 to 1.15 μm.

There are no clear trends for particle size changes based on frit type or boiling time. There was a broader distribution of average sizes for melter feeds aged 28 days. Based on these particles size measurements, there was no evidence of any specific phenomenon that would influence rheology.
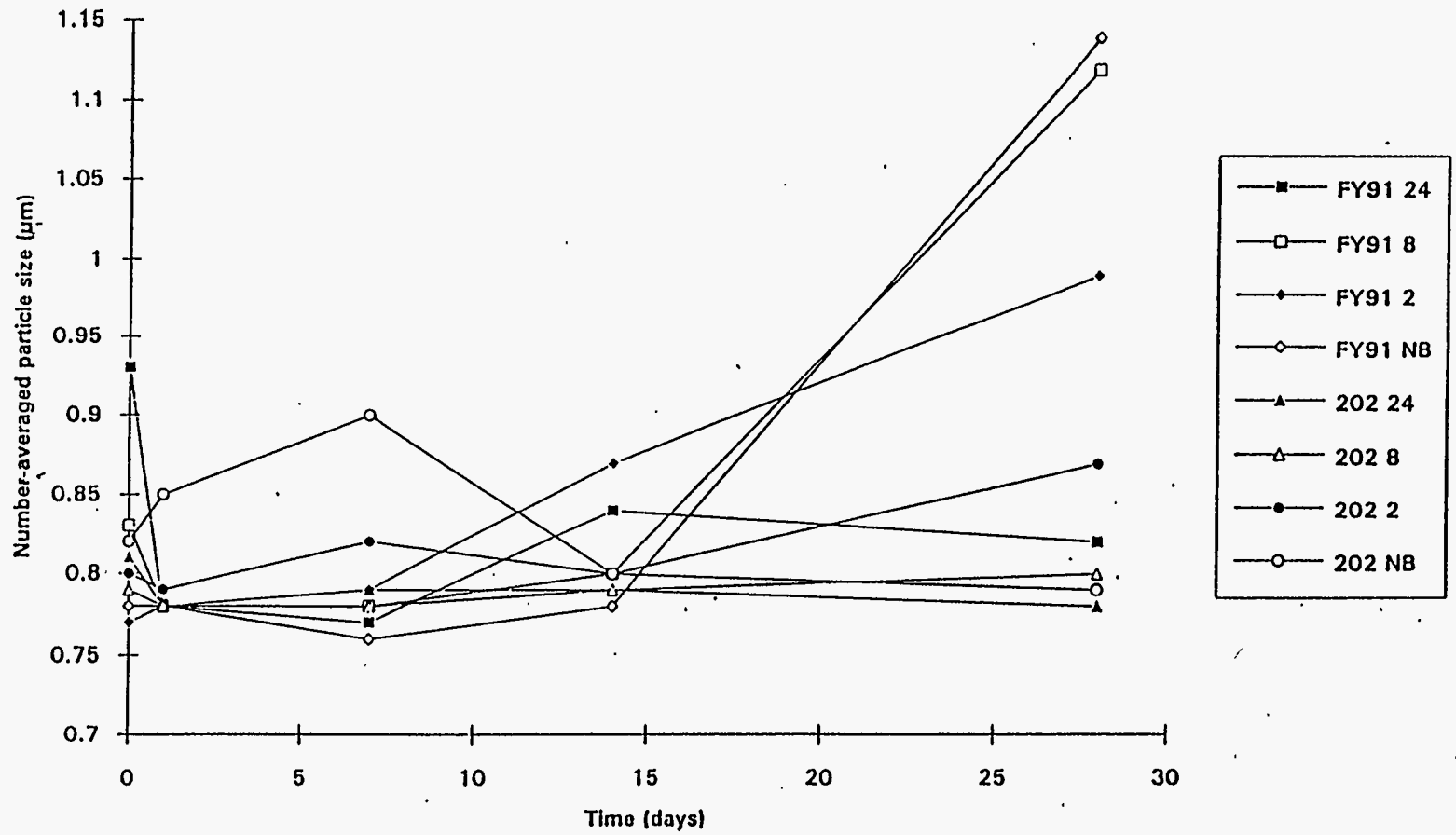
Figure 5.34. Average Particle Size of the NCAW Melter Feed Simulant from the Boiling Time Comparison

6.0 Review of Related Rheology Data: Large-Scale Testing

Three large-scale tests, the Integrated DWPF Melter System (IDMS), Kenaforschungzentrum Karlsruhe (KfK), and the Research-Scale Melter (RSM) tests, were performed using FY 91 frit and the NCAW simulant. Although these tests did not specifically focus on rheology, the test data are reviewed here to gain understanding of large-scale rheology. In this section, the tests are discussed individually; the following topics will be covered: rheology, pH before frit addition, attempts to mitigate cold cap behavior, the presence of a heel, and frit preparation. The basic aspects of feed preparation are described in section 6.1. There were differences in the feed preparation for the three tests, but this description is germane to all three tests.

6.1 Integrated DWPF Melter System

Two tests of the HWVP NCAW melter feed were performed at Savannah River Technology Center (SRTC). The focus of these tests was to determine material balances, to characterize the evolution of off-gas products, to determine the effects of noble metals, and to obtain general HWVP design data (Hutson 1992). A review of the rheological information obtained from the work of Hutson is presented here. The same information was recently reviewed by Seymour (1993).[a]

The melter feed consisted of 28 wt% waste oxides, 3 wt% recycle waste stream (RWS), and 69 wt% frit oxides. The mixed hydroxide slurry representing the waste oxides was prepared by Optimum Chemicals, Inc. Hutson summarized the procedure:

1. The hydroxides of Fe, Zr, Ni, and the dioxide form of Mn are precipitated from nitrate feedstocks.

2. The solution is washed to remove excess nitrate and Na.

3. Separately, the hydroxide of Al is precipitated from a nitrate feedstock.

4. The Al solution is washed to remove excess nitrate and Na.

5. The Al solution is blended with the solution resulting from step 2.

The primary chemicals (see Table 6.1.) were then added, followed by the secondary chemicals, the noble metals, and cadmium compounds (see Table 6.2 .)

(a) DSI from R. G. Seymour to D. E. Larson, April 2, 1993, *IDMS Feed Preparation History*.

Table 6.1. Primary Chemicals (Hutson 1992)

Chemical Name	Formula
Nitrates/Nitrites	
Chromium nitrate	$Cr(NO_3)_3 \cdot 9H_2O$
Cesium nitrate	$CsNO_3$
Potassium nitrate	KNO_3
Sodium nitrite	$NaNO_2$
Sodium nitrate	$NaNO_3$
Lead nitrate	$Pb(NO_3)_2$
Rubidium nitrate	$RbNO_3$
Samarium nitrate	$Sm(NO_3)_3 \cdot 6H_2O$
Praseodymium nitrate	$Pr(NO_3)_3 \cdot 6H_2O$
Zinc nitrate	$Zn(NO_3)_2 \cdot 6H_2O$
Yttrium nitrate	$Y(NO_3)_3 \cdot 4H_2O$
Oxides/Hydroxides	
Barium hydroxide	$Ba(OH)_2 \cdot 8H_2O$
Selenium dioxide	SeO_2
Calcium hydroxide	$Ca(OH)_2$
Cerium hydroxide	$Ce(OH)_4$
Germanium oxide	GeO_2
Lanthanum oxide	La_2O_3
Magnesium hydroxide	$Mg(OH)_2$
Niobium oxide	Nb_2O_5
Neodymium oxide	Nd_2O_3
Silicon dioxide	SiO_2
Tin oxide	SnO
Strontium carbonate	$SrCO_3$
Tantalum oxide	Ta_2O_5
Tellurium oxide	TeO_2
Titanium oxide	TiO_2
Molybdenum oxide	MoO_3
Salts/Others	
Boric acid	H_2BO_3
Lithium chloride	$LiCl$
Sodium chloride	$NaCl$
Sodium carbonate	Na_2CO_3

Table 6.1. (contd)

Chemical Name	Formula
Sodium oxalate	$Na_2C_2O_4$
Sodium fluoride	NaF
Sodium iodide	NaI
Sodium phosphate	Na_3PO_4
Sodium sulfate	Na_2SO_4
Copper sulfate	$CuSO_4 \cdot 5H_2O$

Table 6.2. Secondary Trim Chemicals (Hutson 1992)

Chemical Name	Formula
Silver nitrate	$AgNO_3$
Rhodium nitrate solution	$Rh(NO_3)_3$ [a]
Palladium nitrate solution	$Pd(NO_3)_2$ [b]
Cadmium hydroxide	$Cd(OH)_2$
Ruthenium chloride	$RuCl_3$ [c]

(a) Solution is 4.933 wt% Rh.

(b) Solution is 8.769 wt% Pd.

(c) Salt is 42 wt% Rh; $RuCl_3$ is converted to a nitrosyl ruthenium form prior to addition to the Slurry Receipt and Adjustment Tank (SRAT).

Formic acid molarity was 22.64 for test 1 and 22.45 for test 2. The RWS was composed of trim chemicals, zeolite, and diatomaceous earth components. The composition is listed in Table 6.3. The frit composition was measured and compared to the specification. The results are provided in Table 6.4.

Hutson (1992) critiqued the batch history of the two tests and listed several observations; the observation of residual frit was rheologically significant. For the first test, analyses showed higher than expected SiO_2 concentrations that were attributed to the presence of residual DWPF frit (that was left in the tank). (The DWPF frit composition was assumed to be (in wt%): 77% Si_2, 8% B_2O_3, 7% Li_2O, 6% Na_2O, and 2% MgO.) The second test analysis showed considerably higher concentrations of Si, B, and Li, which were attributed to the presence of residual FY 91 frit. Since frit affects rheology, the presence of residual frit must also affect rheology. However, the rheological impact of residual frit has not been established. Alternatively, the residual frit presence implies either inadequate mixing or sedimentation of the frit particles.

6.3

Table 6.3. Trim Chemicals Used to Compose the RWS (Hutson 1992)

Chemical Name	Formula
Sodium nitrate	$NaNO_3$
Manganese dioxide	MnO_2
Sodium chloride	$NaCl$
Sodium phosphate	Na_3PO_4
Sodium oxalate	Na_2C2O_4
Cadmium hydroxide	$Cd(OH)_2$
Diatomateous earth	[a]
Zeolite	[b]

(a) Manville Standard Super-Cel™.
(b) Union Carbide Ionsieve IE-96 (-125 mesh).

Table 6.4. IDMS/HWVP Frit Composition (Hutson 1992)

Major Oxides	Composition (wt%)	Specification (wt%)
SiO_2	73.135	72.260
B_2O_3	18.902	20.450
Li_2O	6.972	7.290
Minor Oxides		
Na_2O	0.302	
CaO	0.088	
Fe_2O_3	0.039	
TiO_2	0.103	
ZrO_2	0.039	
Al_2O_3	0.189	
BaO	0.016	
K_2O	0.031	
ZnO	0.078	
Total Oxides	99.894%	

Formic acid addition must be considered in terms of the IDMS rheological behavior. From a plot of pH versus time into formic cycle, the pH of the waste stream was approximately 8 after the digestion period. The pH value resulting from the formating process is usually between 6.5 and 7.0. This difference was not called out specifically. Seymour (1993) plotted pH, g TO/L, and temperature versus time and event (see Figure 6.1), which showed that waste pH was 8.77 with added recycle. This pH value was higher than prototypical laboratory experience. In addition, the waste loading was lower than the nominal conditions of 500 g TO/L. The lower waste loading typically results in lower yield stresses and different pH.

For the second HWVP test, Hutson (1992) found that an insufficient quantity of formic acid was added to the HWVP waste sludge simulant. Seymour (1993) showed that the pH was 9.53 before frit addition to the waste with recycle. This pH value was higher than prototypical experience. Based on the understanding detailed in Section 3.2, this pH could significantly affect the leaching of the SiO_2.

Formic acid addition requirements for DWPF operation included compensation for acid consumption based on the reactions:

$$2HCOOH + 3NO_2^- \rightarrow NO_3^- + 2NO + 2HCOO^- + H_2O \tag{6.1}$$

and

$$3HCOOH + 2NaNO_2 \rightarrow 2NO + CO_2 + 2H_2O + 2NaCOOH \tag{6.2}$$
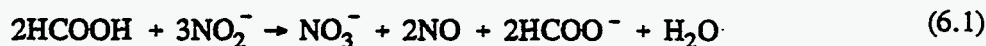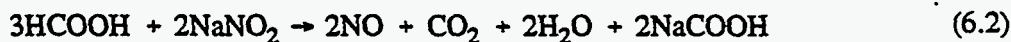
Hsu (1990)[a] assumed the first reaction was the predominant of the two and recommended 0.75 moles of formic acid per mole of nitrite. Hutson (1992) concluded that the assumption does not apply to HWVP NCAW wastes. Hsu did not account for $NO_2 \rightarrow N_2O$ which has been observed in processing the NCAW simulant. This reaction consumes acid in quantities greater than the DWPF relevant 0.75 moles $HCOOH/NO_2^-$ ratio. In addition, the presence of frit in the heel may have contributed to acid consumption. Insufficient formic acid was added for both tests performed at IDMS.

Hutson (1992) presented rheological data for the two tests. The tests included sampling during formic acid addition, during recycle addition, and after frit addition as a function of aging and dilution. In the quality assurance analysis, the Haake RV3 viscometer used to take the measurements was termed "quite old and unreliable." The rheology data "seems to be biased high." Further, the data were

---

(a)   Memo from C. W. Hsu to J. R. Knight, July 5, 1990. *Formic Acid Requirement in The DWPF Chemical Processing Cell, WSRC-RP-90-0554.*

6.5

Feed Preparation History For HWVP IDMS Run #1

6.6

Start
HCOOH Addition Start
HCOOH Addition End
Digest Start
Digest End
Dead Time Start
Dead Time End
Addition Concentration Start
Addition Concentration End
RWS Addition Start
RWS Additional End
RWS Concentration Start
RWS Concentration End
1st Frit Addition Start
1st Frit Addition End
1st Frit Concentration Start
1st Frit Concentration End
2nd Frit Additional Start
2nd Frit Addition End
2nd Frit Concentration Start
2nd Frit Concentration End
3rd Frit Addition Start
3rd Frit Addition End
3rd Frit Concentration Start
3rd Frit Concentration End
Melter Feed Reaches 30 °C
Addition Of NaNO3
MFT Transfer #1
MFT Transfer #2
Last Canister Poured For Run 1

g TO/L
600.0
500.0
400.0
300.0
200.0
100.0
0.0

pH
10.0
9.0
8.0
7.0
6.0
5.0

Temperature
120
100
80
60
40
20

Time (Hrs)
0.0   25.0   50.0   75.0   100.0   125.0   200.0   400.0   600.0   800.0   1000.0
11/12/91   12/15/91

Figure 6.1A. Solids Loading, pH and Temperature Data from the HWVP IDMS Test Run #1

Figure 6.1B. Solids Loading, pH and Temperature Data from the HWVP IDMS Test Run #2

described as having been obtained correctly, but "should be used with caution." The data are actually counter intuitive. For example, a rise in yield stress and consistency was measured after a dilution in the second test. The rheology data should be ignored.

For the first test, the analyzed sample was close to the target composition and was assumed to be processable. For the second test, dilution of the melter feed was required. In terms of yield stress and viscosity, this feed rheology was worse than any of the previously processed slurries at IDMS. The obvious difference between the two HWVP tests and previous IDMS tests was the frit composition. Hutson stated that the FY 91 frit would cause gelling and that an alternative acid should be considered. While the statements may be correct, the supporting evidence is lacking. Further, some differences in the testing (i.e. presence of residual frit, less than prototypic formic acid addition) may have contributed to the stated rheological differences.

6.2 KfK

Based on the IDMS experience, Elliott performed preliminary rheological tests for the KfK tests. Elliot's tests were done to elucidate the best remedy for anticipated rheological problems at KfK. The KfK testing primarily focused on noble metal effects on the vitrification of the NCAW simulant (Grunewald et al. 1993). In this section, the experiments performed at PNL will be described and then, the observations made at KfK will be reviewed.

A description of the PNL tests for the KfK testing follows. The waste simulant was formated at 125 g WO/L; recycle was added as a slurry. The formate to nitrate molar ratio was 3:1. Formic acid was added at a rate of 0.46 mL/min. The temperature during formating was 96°C. Dow Corning 544 antifoam was added at a concentration of 100 ppm. FY 91 frit was added dry at $T = 80$°C. The slurry was concentrated to 493 g TO/L at $T = 96$°C.

The melter feed suspension was agitated for 5 days at 50°C. During that period, pH remained constant at 9.2. The yield stress and consistency factor were measured over the 5-day period. The data (see Figure 6.2) showed increases in yield stress and consistency as time elapsed.

Mitigation options were explored as a result of the yield stress and consistency increases. The effects of formic acid (22.5 M), HNO_3 (8 M), and water on yield stress were tested. The HNO_3 concentration in the melter feed was 0.19 M, the resulting pH was 8.6. The HNO_3 concentration was increased to 0.41 M, which resulted in pH 6.2.

The formate concentration in the melter feed was 0.38 M, and the resulting pH was 7.3. In a subsequent sample, the formic acid concentration was increased and the pH was 6.3. Dilution with water brought the loading to 400 g TO/L, pH rose to 9.4. Suspensions were aged at 50°C. Rheograms of these samples were obtained for times of 24, 120, and 182 h at $T = 25$°C.
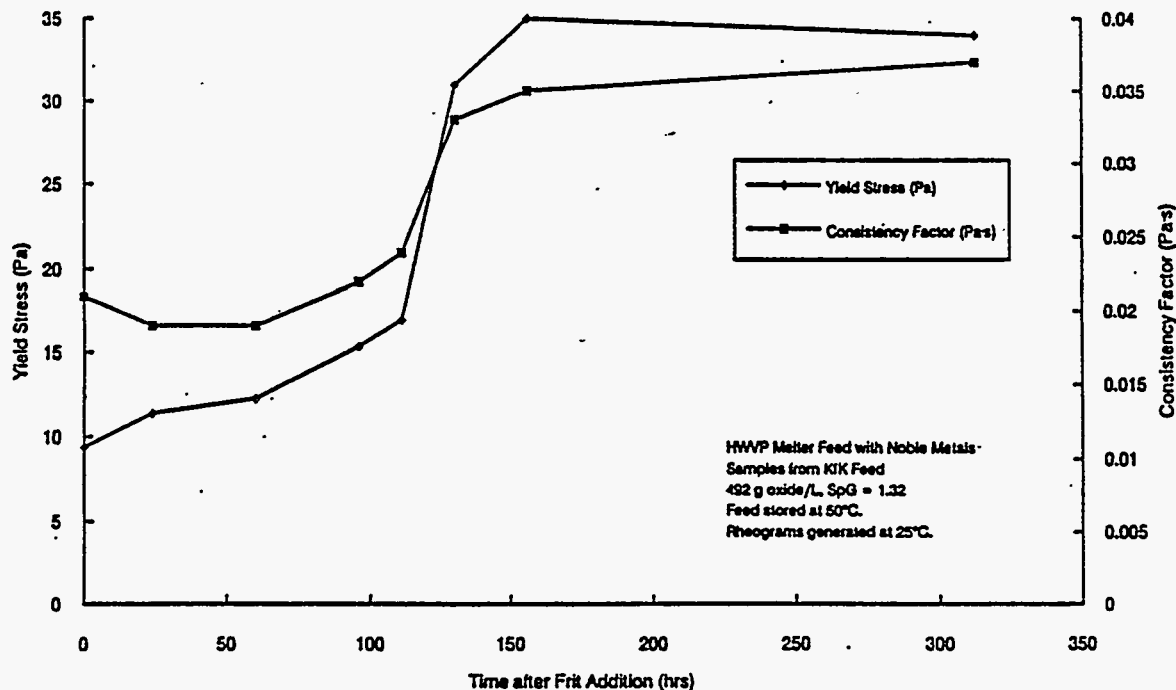
Figure 6.2. Rheological Properties for Reference Sample

The formic acid rheograms are shown in Figure 6.3. The second formic acid addition reduced the solids loading by 2 weight percent. As time progressed, the yield stress and consistency increased. The pH increased from 6.3 to 7.8.

The HNO_3 rheograms are shown in Figure 6.4. The second HNO_3 addition reduced the solids loading by 5 weight percent. As time progressed, yield stress and consistency increased. These increases were less than the changes observed in the samples with formic acid. The pH increased from 6.2 to 7.7. After 12 h, the yield stress was 19 Pa, and the consistency was 20 cp. Based on these measurements, HNO_3 can be considered a short term remedy for thickened feed; however, its effectiveness is lost after 5 days.

During the KfK test, the feed was continuously stirred in the melter feed tank (MFT). The temperature of the feed reached 40° to 50°C, and the feed was slowly concentrated by evaporation. Observation showed that rheology was a function of time. Although not specifically stated, the rheological problems may have stemmed from the concentration.

The problems at KfK were feed nozzle and feed line plugging and poor cold cap spreading. The feed in the MFT became more viscous with time (in terms of days) after the frit was added to the formic acid waste. This increased the pluggage risk between the MFT and engineering-scale melter (ESM); when plugging occurred, it was attributed to "irregular shaped nondissolved feed material." Poor cold cap spreading was attributed to increased feed viscosity. The increased viscosity led to poor

6.9
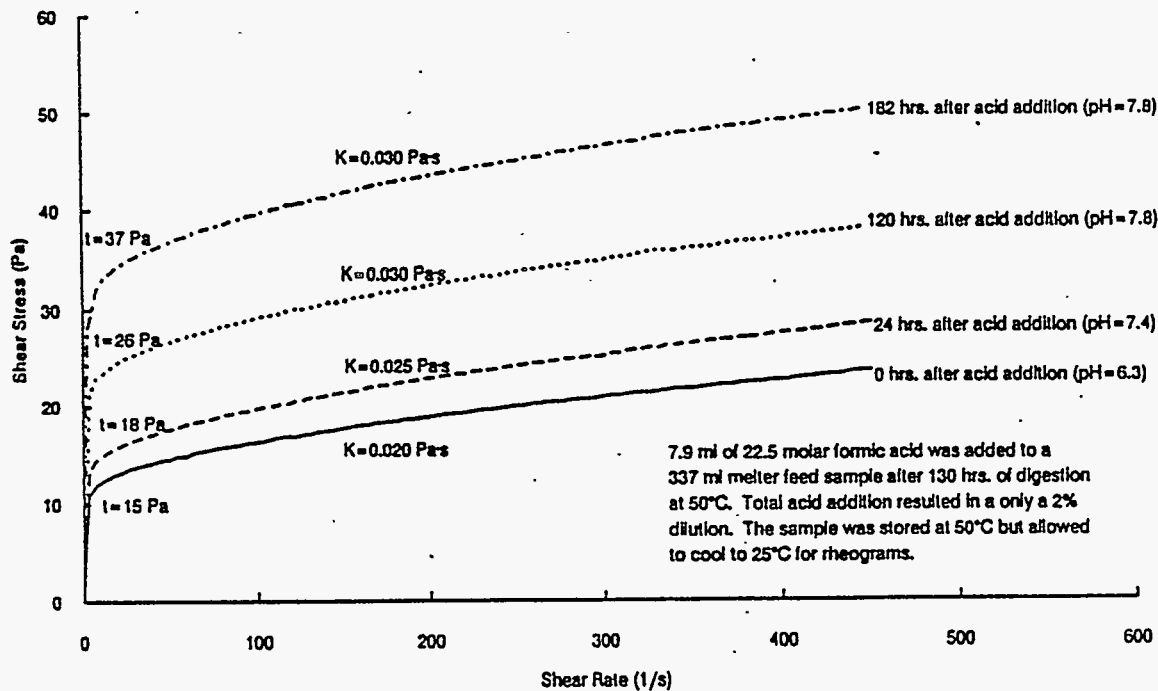
Figure 6.3. Yield Stress Reduction Experiments--Formic Acid
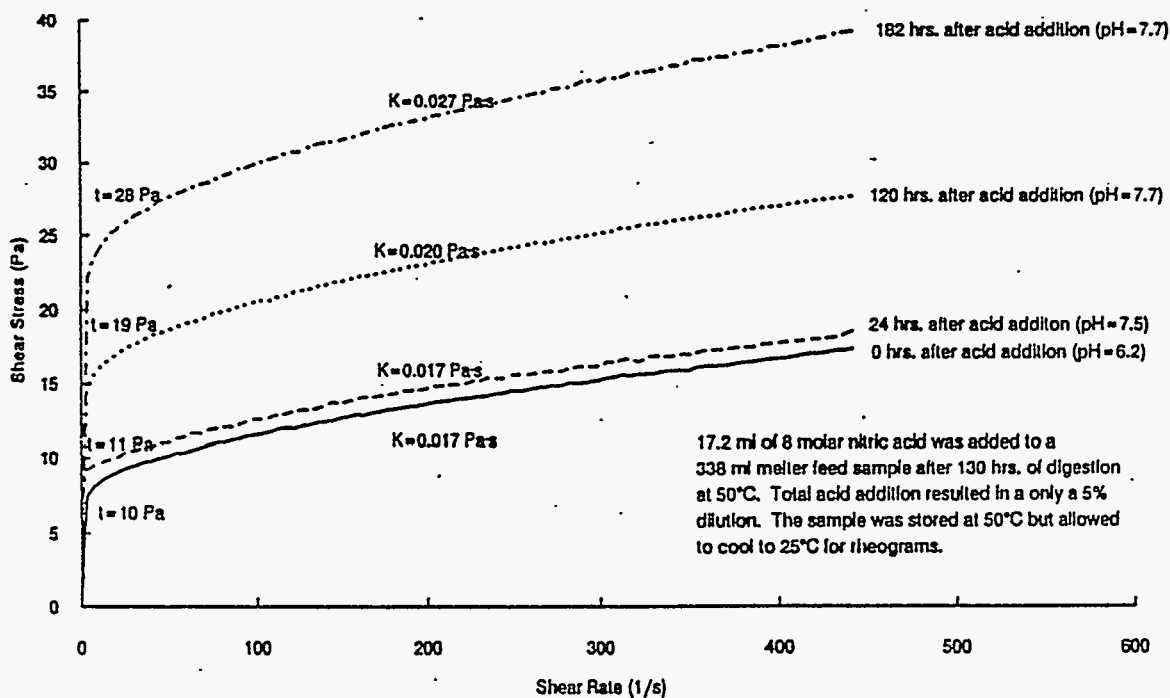
Figure 6.4. Yield Stress Reduction Experiments--HNO₃

6.10

slurry spreading; therefore, dry feed formed stalagmites on the cold cap surface. Specifically, the feed formed piles 5 to 10 cm in diameter and up to 30 cm high until the feed income channel of the feed tube was blocked by the top of the pile. To facilitate the melting process, the feed must remain liquid and spread across the cold cap surface. To avoid these conditions, the feed was diluted in the MFT by adding water ($< 5\%$) or nitric acid.

The KfK investigators made two statements that gave credence to the rheology-concentration relationship. First, only a few percent water was required to be added when the concentration effect was too high (Grunewald et al. 1993). Restating, small dilutions improved flow. Second, small grains in the suspension apparently have the same composition ranges as larger grains in the agglomerates, indicating a somewhat different thermal history (INE 1992). These dilutions by water addition facilitated cold cap spreading and avoided plugging. Essentially, this water replenished the water lost during evaporation.

An inspection of the feed suspension particle assemblages indicated a difference in thermal history of the melter feed. Grains of different size were analyzed for composition; compositions were similar regardless of grain size. So, what does grain size mean? Grain size is often defined as the dimensions of a single crystal or as the ultimate crystal size and is commonly determined by XRD. Several grains can compose a particle. However, grain size is often misstated as particle size. Since, an XRD analysis of crystal size was not included in the report, the data will be considered as particle assemblage information.

Grunewald et al. (1993) stated the difference in feed particle assemblage size was attributed to thermal history difference. It can be reasoned that particles receiving elevated temperature or time became fused or coagulated. Since water additions mitigated the rheological problems, it is likely that the particles were flocced rather than fused.

The KfK rheology results must be viewed retrospectively. The test focused on noble metal behavior during the vitrification of the NCAW simulant. However, the rheology information is substantial. During testing, cold cap spreading was problematic, and plugging occurred in the feed pipes. These problems were overcome by dilution. The use of HNO_3 reduced feed pluggages and facilitated slurry spreading on the cold cap (Grunewald et al. 1993). Ultimately, the rheology was sufficient to feed the melter. Evaporation was named as a specific influence on rheology. Further, the nature of the particle assemblages may also be inferred. For these reasons alone, the KfK testing has contributed to the rheological understanding of the melter feed.

6.3 RSM

The RSM test focus was melter behavior, not rheology. Since the thrust of the test was melt related, the rheology problems were overcome by avoiding time effects. Melter feed was constituted on a daily basis. A heel was present throughout slurry make up; heel effects have not been investigated in any study.

The RSM melter feed was formulated at concentrations of 500 g TO/L and 400 g TO/L. The pH before frit addition was approximately 9. The pH of all melter feeds ranged from 10.0 to 10.3. Pumping problems were observed for melter feed transport. A lack of melter feed spreading on the cold cap was encountered. The slurry on the cold cap was characterized as thick and rigid. Stalagmites were present on the cold cap. These data and observations provide the basis for investigating the rheology aspects of the RSM tests. (Cooper et al. 1993).

Suspension history was believed to have a significant rheological influence. Aging was believed to be the cause of the lack of spreading on the cold cap. In response, the melter feed was constituted every 12 h with the goal to avoid aging effects. To examine aging effects, a sample of melter feed was aged in the laboratory.

Rheograms were obtained for three test scenarios. The first set of rheograms measured the effect of TO loading (400 g TO/L and 500 g TO/L). These samples were agitated in the melter tank. The second set of rheograms compared fresh feed and feed aged for 14 h. These samples were agitated in the melter feed tank and contained two times the nominal concentration of noble metals. The third set of rheograms showed melter feed that was made in the melter feed tank but aged in the laboratory for 12 days. These samples contained two times the noble metal concentration. All rheograms were taken at 25°C.

Figure 6.5 shows the effect of TO loading on the RSM melter feed. The 400 g TO/L samples had a significantly lower yield stress compared to the 500 g TO/L samples, as expected. The influence of aging is unclear based on these rheograms. For the 400 g TO/L test, samples aged for 8.0 h and 4 days[a] were measured. As seen in Figure 6.6, the yield stress was reduced during aging. However, since the feed tank was not observed during the time period, sedimentation may have occurred. Sedimentation would lessen the solids in the suspension sample and could account for the lower yield stress. This information was not obtained during the experimentation. It is difficult to make any conclusions based on the 400 g TO/L feed.

The 500 g TO/L data (see Figure 6.7) compared a newly prepared sample and a sample aged for 10 h. The yield stress increased during the elapsed time. The conclusion is that aging of melter feed with concentration of 500 g TO/L affected the yield stress.

Figure 6.8 compares melter feed at 400 g TO/L with twice nominal noble metal concentration. Melter feed tank samples were measured at time 0 and 14 h. The yield stress increased 3-fold during the elapsed time. Speculatively, this dramatic change in yield stress may be linked to the increased presence of noble metals. However, substantial cause-effect reasoning based on noble metal rheological influence does not exist for aqueous melter feed. Thus, yield stress increase is attributed to aging but the influence of noble metals remains unresolved for this experimentation.

(a) The samples aged for 4 days because of an incident unrelated to HWVP that required building evacuation.

6.12
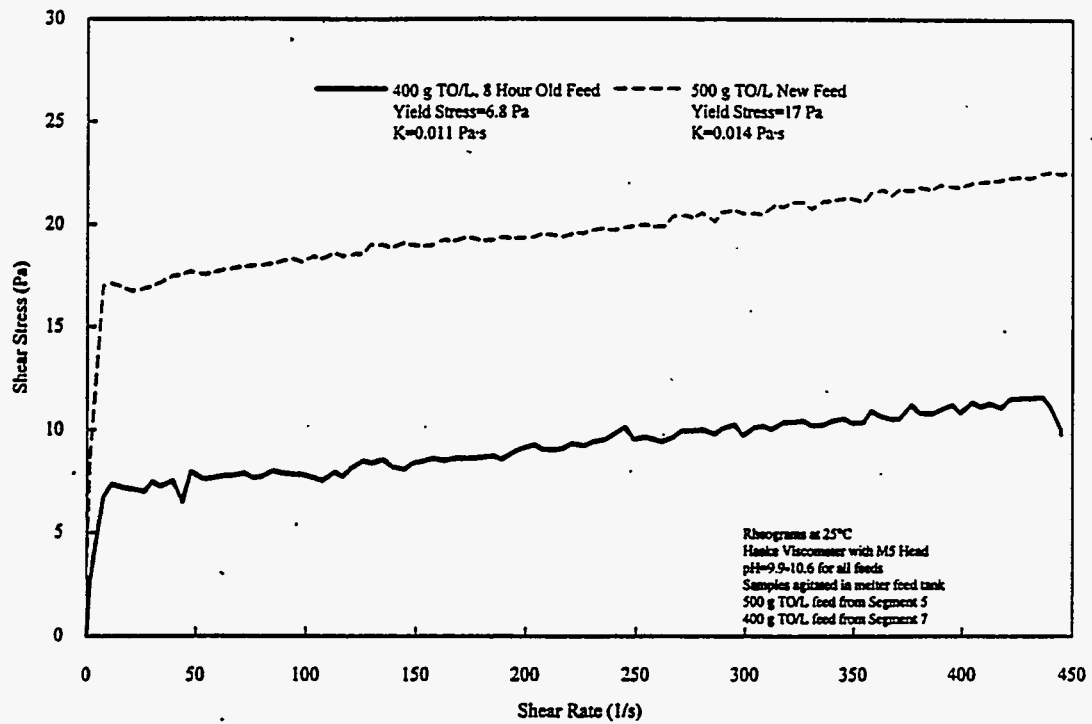
Figure 6.5. RSM Rheograms of 400 g TO/L for 8 Hours of Aging and 500 g TO/L of New Melter Feed
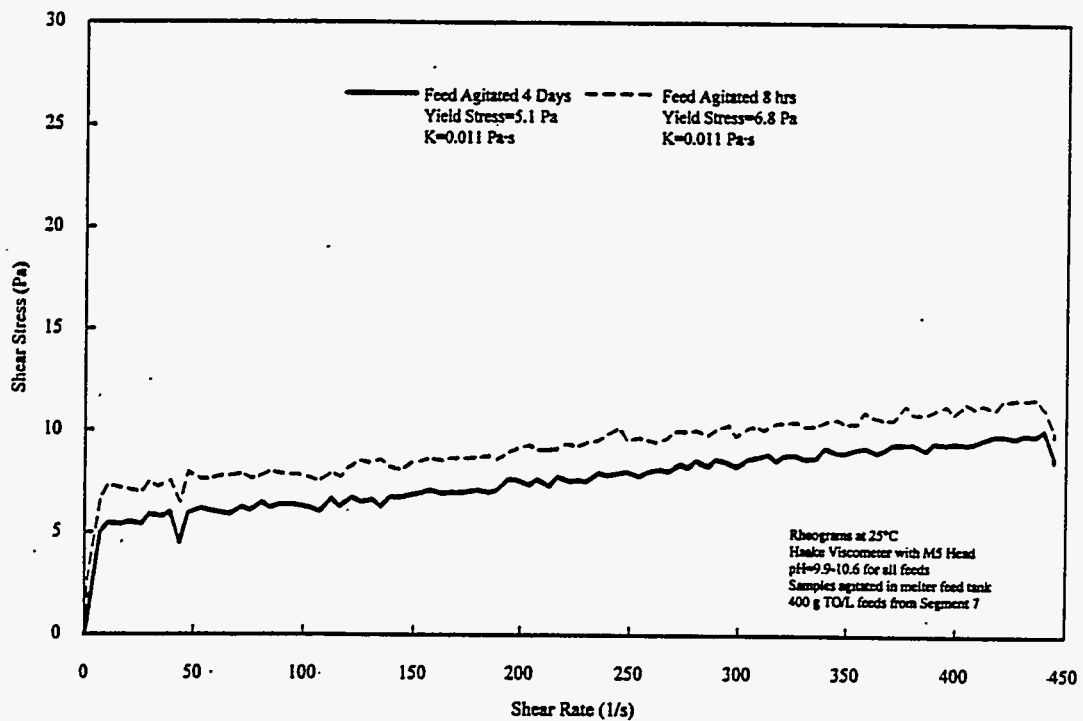
Figure 6.6. RSM Rheograms of 400 g TO/L Melter Feed

6.13
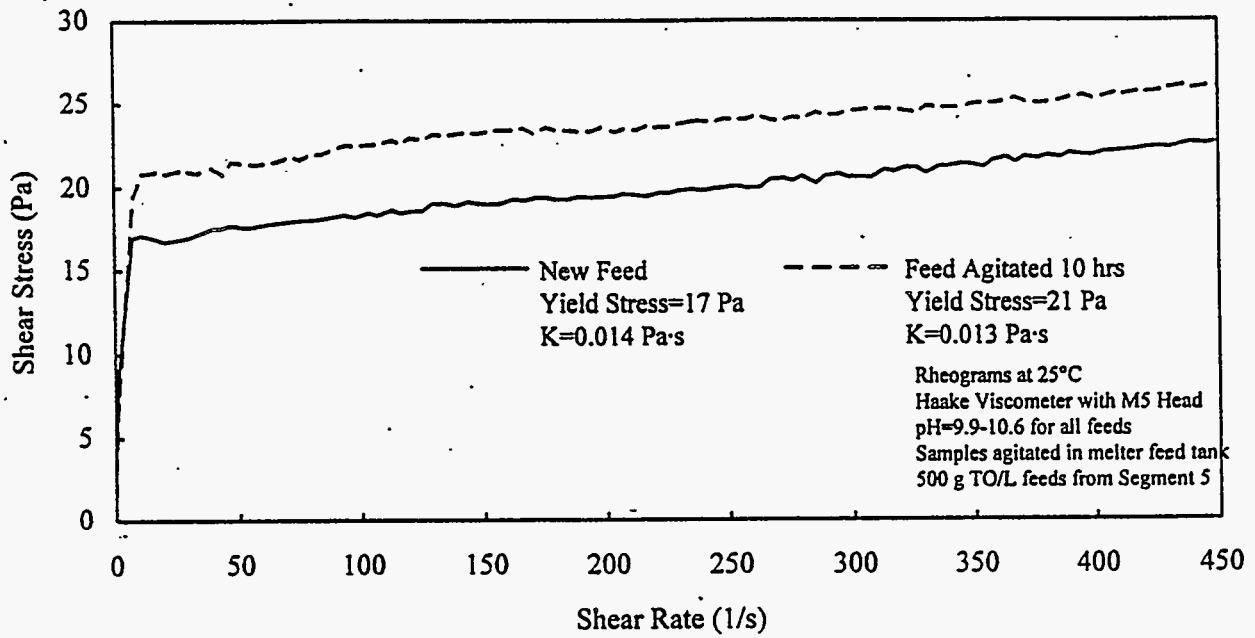
Figure 6.7. RSM Rheograms of 500 g TO/L Melter Feed
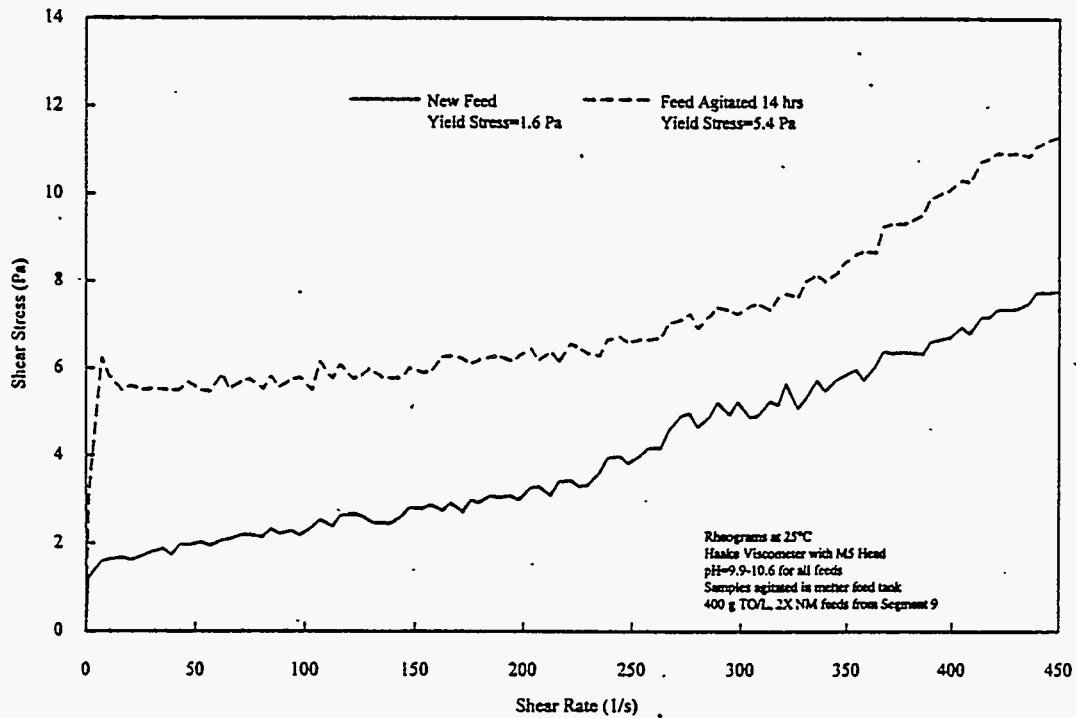
Figure 6.8. RSM Rheograms of Melter Feed Containing 2 Times Nominal Noble Metal Concentration

Chemical analysis of the supernatant liquid was performed on the RSM samples with nominal and 2 times the noble metal concentration. This test was performed to detect the presence of any Si that may have resulted in a gel network. The chemical analysis results are typical of the FY 93 laboratory results for the FY 91 melter feed (see Figure 6.9). The TO loading was unavailable for the samples, and therefore, the data could not be put in terms of the fraction of frit component in solution.

The rheology was termed "problematic" due to cold cap spreading difficulties. The relationship between cold cap spreading and rheology has been investigated on a limited basis, and the variables of importance have not been identified (Yasuda and Hrma 1991). The frit composition was never considered, though it may exert a significant influence on spreading. Based on the large-scale testing results, frit composition influences cold cap spreading. However, the functionality of this influence has not been determined.
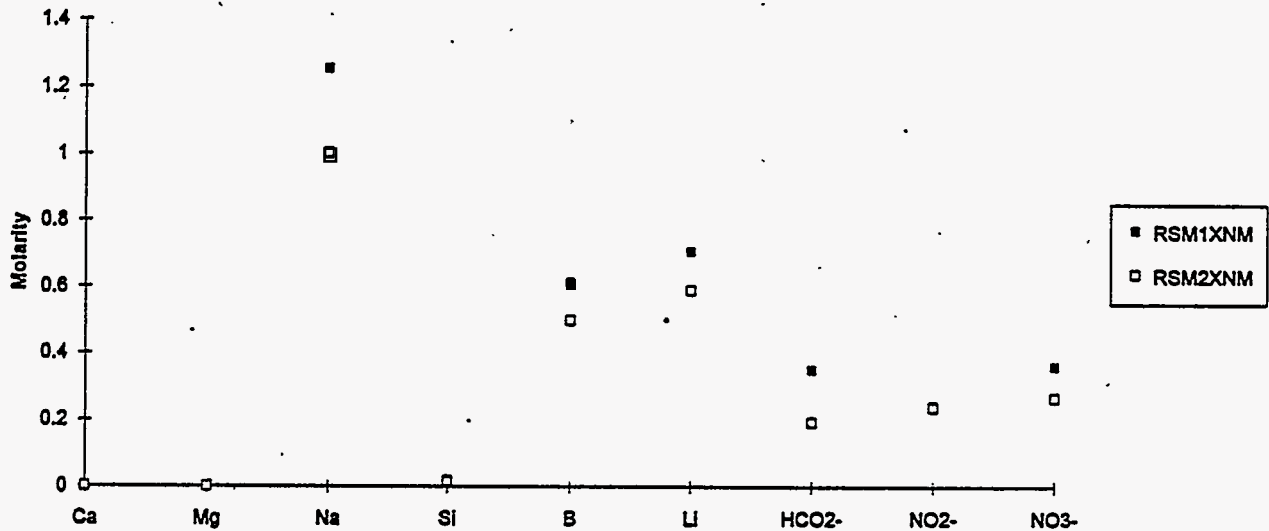
Figure 6.9. Chemical Analysis Data for Simulated Waste Slurry
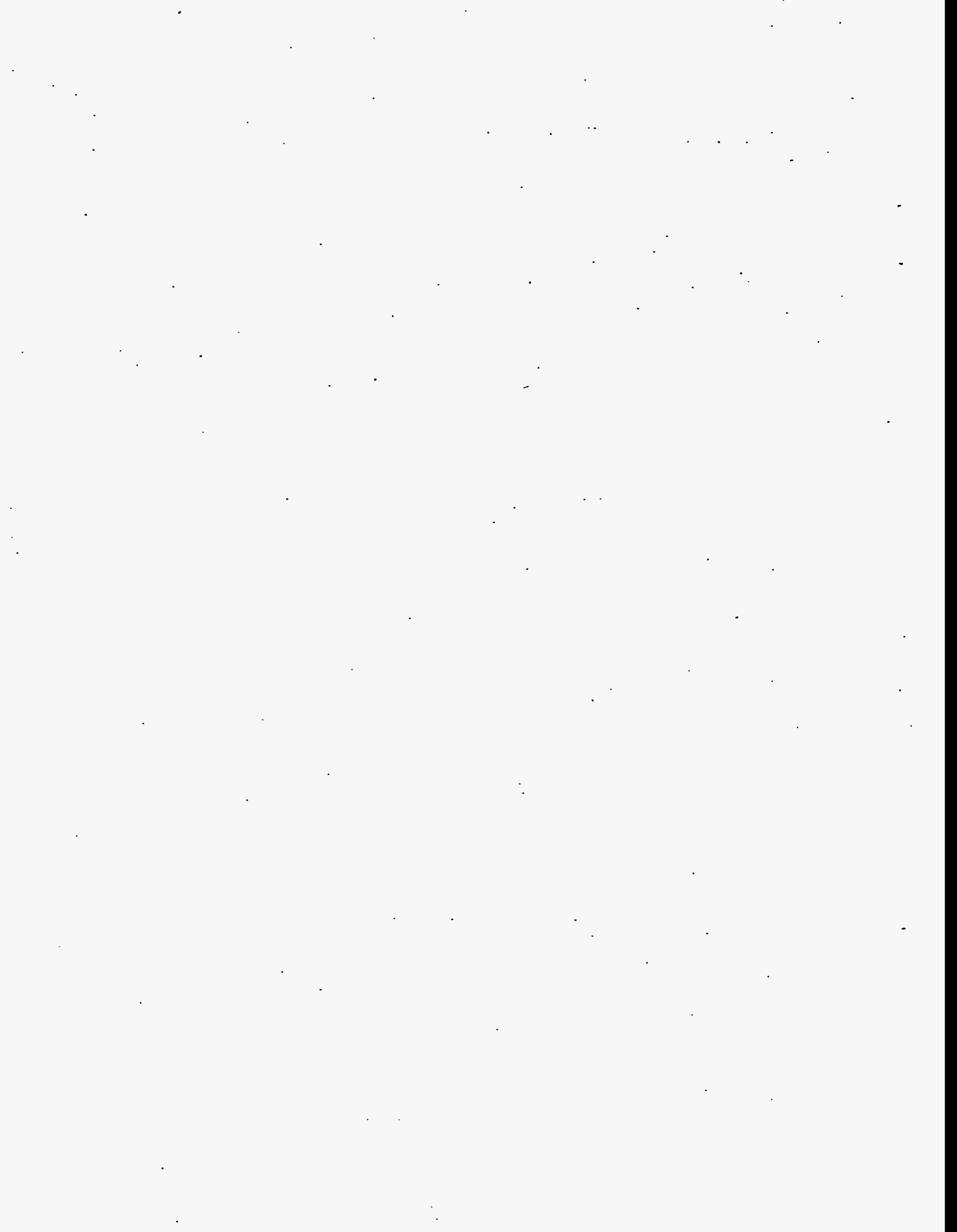
7.0 Analysis of NCAW Melter Feed Rheology Data

A variety of melter feed rheology data have been presented in this report. These FY 1992 data (Subsection 5.7) and FY 1993 data (Subsections 5.1 to 5.6) were obtained under a wide range of conditions. The conditions for the FY 1993 rheology testing were controlled and well described. The FY 1992 testing was not controlled as well considering the apparatus' shortcoming and the lack of solids content data. The large-scale testing conditions (described in Section 6) were not well described, which was a result of foci other than rheology. Despite the variability in test conditions, several relevant observations can be made:

- Two global measurements relate to the melter feed rheology: rheogram and pH. From the rheogram, the Bingham model is usually used to obtain viscosity and yield stress. The most recent HWVP specifications (see Table 7.1) describe the melter feed in terms that are not clearly related to transport. Therefore, satisfying the HWVP specification does not ensure melter feed will be pumpable in the plant.

- Several facts are apparent from Sections 5 and 6. The yield stresses of the samples tested at 500 g TO/L were within the design range. A limiting pH of 8 would preclude the FY 91 frit and for aging times greater than 2 weeks, 202 and HW-39 would not be within the HWVP specification. However, meeting pH specifications will not ensure transport.

- The real concern is that pumping problems were encountered in RSM and KfK testing. The apparatus used in the laboratory tests performed in FY 1992 and 1993 was quite different than large-scale equipment. Also, there was increased variability in the conditions the melter feed was subjected to in large-scale testing. RSM and KfK tests with FY 91 melter feed resulted in slurry transport difficulties. The FY 1993 laboratory testing did not provide results which would have predicted this behavior.

Table 7.1. HWVP Melter Feed Properties[a] Taken from the HWVP Technical Data Package

	Nominal	Design Range
Apparent viscosity (cp at 25° C)		
at 10 s^{-1}	700	80 to 3000
at 25 s^{-1}	300	30 to 1200
at 183 s^{-1}	70	5 to 170
Yield stress (dyne/cm^2)	100	5 to 260
pH	6	3.5 to 8

(a) Based on synthetic NCAW feeds without transuranic recycle.

- The FY 91 frit composition has allegedly been responsible for the large-scale rheological testing problems. From the FY 1993 testing, it is obvious that this frit is not durable. This lack of durability did not result in an increase in yield stress or viscosity over the time period examined in the FY 1993 testing. It could be postulated that this lack of durability may provide the basis for the FY 91 melter feed to gel under certain conditions. These conditions may be present in the large-scale testing. In addition, frits with higher durability may be less likely to gel and thus, pumping problems may be avoided in large-scale testing. However, this hypothesis has not been validated, and the rheology experiments performed thus far have not been aimed at gathering this information. The current HWVP rheology melter feed test consists of a strain rate sweep from 0 to 451 s^{-1} in 2 min. The structure is broken down in the first second of the measurement. To characterize gelling in this manner is erroneous. If this gelation requires an investigation, critical strain or stress relaxation experiments will be needed.

- Large-scale process flowsheets require that the frit be added to the waste as an aqueous slurry. In an aqueous environment, the FY 91 frit releases Si. However, in the melter feed, the Si is not detected because it precipitates as it is released. In large-scale testing, it is likely that Si in the aqueous frit slurry could cause gelling. So, the current process flowsheet enhances the opportunity for gel formation and thus, yield stress increases.

7.1 Comment on FY 1993 Data

The quality of the data from the FY 1993 testing requires discussion. The rheology information gathered in the FY 1993 testing shows significant scatter. The chemical analysis data must be termed reasonably consistent considering the complexity of melter feed chemistry. Also, the pH data were reproducible. The chemical analysis and pH correspond with large-scale and FY 1992 experiments. Unfortunately, the rheology results do not correspond to the large-scale testing and do not provide a self-consistent description of melter feed behavior.

The scatter in the FY 1993 rheology results may have originated from a variety of sources. It is difficult to identify these sources since the experimentation was focused on testing several effects. In addition, aging was an effect that was tested throughout the experiment. Only a limited number of samples were duplicated because of the time spent examining the effect of aging. The FY 1993 testing was not designed to look at reproducibility.

So, why are the data scattered? There are the inherent difficulties of experimentation that always lead to error. However, this scatter goes beyond the typical experimental error. Some error was attributed to dilution, which was shown in the weight percent solids samples.

Examine the complex nature of the melter feed. It has a variety of soluble and insoluble waste components and frit particles. The waste components contribute ions to the solution and the average size of the waste particles is 1 mm. The frit contributes dissolution products, > 75-mm particles and possibly a gel layer. Each of these properties influences the melter feed rheology through colloidal and hydrodynamic interactions.

It is difficult to describe which property controls the melter feed rheology; however, the frit particles are clearly subject to sedimentation based on particle size. This could be a source of error throughout any experimentation (Sections 5 and 6). Sedimentation effects are present in sampling and rheology testing.

It has been postulated that gellation may be the result of pumping difficulties encountered in large-scale testing with FY 91 melter feed. Again, the chemical analysis data from FY 1993 testing certainly support this possibility; unfortunately, the rheology testing did not. In the FY 1993 testing, the time between sampling and measuring was minimized. Correspondingly, the FY 1993 testing samples were consistently agitated. This agitation may have precluded gel formation and led to the differences in FY 1993 testing and large-scale experience.

Further speculation would not clarify the information. From the FY 1993 testing, the influence of aging has been shown clearly in the pH data. Future testing can be better focused by removing the aging tests. A method for rheological characterization can be developed that yields reproducible results.
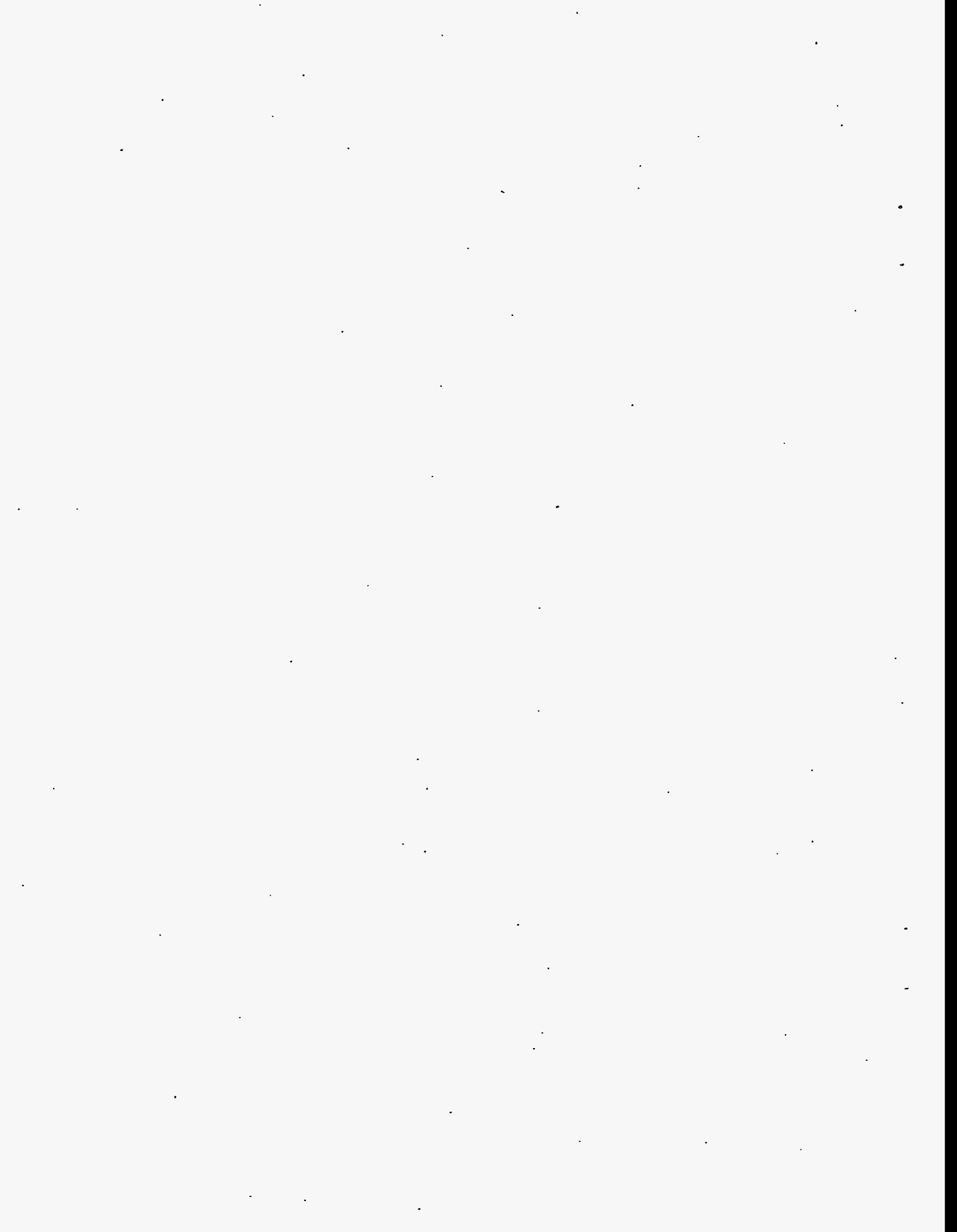
8.0 References

Allen, L. H., and E. Matijevic. 1969. "Stability of Colloidal Silica In Effect of Simple Electrolyes." *J. of Coll. Int. Sci.*, 31 (3):287-296.

Andrade, E., and J. Fox. 1949. "Mechanism of Dilatancy." *Proc. Roy. Soc.* London 62:843.

Baumann, H. 1955. *J. Beitr. Silikose-Forsch.* 37:47.

Brinker, C. J., and G. W. Scherer. 1990. "The Physics and Chemistry of Sol-Gel Processing." *Sol-Gel Science*, Academic Press, Inc., New York.

Bunker, B. C., F. J. Hendley, and S. C. Douglas. 1984. "Gel Structures in Leached Alkali Silicate Glass." *Mat. Res. Soc. Symp. Proc.* 32.

Chaffey, C. E., and I. Wagstaff. 1977. "Shear Thinning and Thickening Rheology II. Volume Fraction and Size of Dispersed Particles." *J. Coll. Int. Sci.* 59:1:63-75.

Chang, J. C., B. V. Velamakinni, F. F. Lange, and D. S. Pearson. 1991. "Centrifugal Consolidation of A1203 and A1203/Zr02 Composition Slurries vs Interparticle Potentials: Particle Packing and Mass Segregation." *J. Am. Ceram. Soc.* 74:9:2201-2204.

Chou, C. C., and M. Senna. 1987. "Correlation Between Rheology Behavior of Aqueous Suspensions of Alumina and Properties of Cast Bodies: Effects of Dispersant and Ultrafine Powders." *Am. Cer. Soc. Bull.* 66:7:1129-1133.

Collins, E. A., D. J. Hoffman, and P. L. Soni. 1979. "Rheology of PVC Dispersions I. Effect of Particle Size and PSD." *J. Coll. Int. Sci.* 71 (1):21-29.

Einstein, A. 1909. "A New Determination of Molecule Dimension." *Ann. Physik* 19:289.

Elmer, T. H., and M. E. Nordberg. 1958. "Solubility of Silica in Nitric Acid Solutions." *J. Am. Ceram. Soc.* 41:517.

Green, H. 1949. "Industrial Rheology and Rheological Structures." John Wiley and Sons, New York.

Grunewald, W., G. Roth, W. Tobie, S. Weisenburger, and K. Weiss. 1992. "Investigation of Bubble Rich Glass Product Taken from the Outer Melt Surface of the ESM Melter During Long-Term Operation." Institut für Nukleare Entsorgungstechnik, Germany.

Grunewald, W., G. Roth, W. Tobie, S. Weisenburger, and K. Weiss. 1993. "Vitrification of Noble Metals Containing NCAW Simulant with an Engineering Scale Melter (ESM)." Campaign Report.

Hamaker, H. C. 1937. "London-Vander Waals at Fractions Between Spherical Particles." *Physica* 4:1058-1072.

Hogg, R., T. W. Healy, and D. W. Fuerstenau. 1956. "Mutual Coagulation of Colloidal Dispersions." *Trans. Faraday Soc.* 62:1638-1651.

Horn, R. G. 1990. "Surface Forces and Their Action in Ceramic Materials." *J. Am. Ceram. Soc.* 73 (5):1117-1135.

Hunter, R. J. 1981. Zeta Potential in Colloid Science. Academic Press, New York.

Hutson, N. D. 1992. (IDMS) Integrated DWPF Melter System Campaign Report: Hanford Waste Vitrification Plant (HWVP) Process Demonstration. WSRC-TR-92-0403, Westinghouse Savannah River Company, Aiken, South Carolina.

Iler, R. K. 1979. The Chemistry of Silica. John Wiley and Sons, New York.

Israelchvili, J. N., and G. E. Adams. 1978. "Measurement of Forces Between Two Mica Surfaces in Aqueous Electrolyte Solutions in the Range 0-100 nm." *J. Chem. Soc. Faraday Trans.* 74:975-1001..

Knickerbocker, I. O. 1976. "Rheological Properties of Flocculated Clay-Water Systems." Master's Thesis, Alfred University, Alfred, New York.

Michaels, A. 1958. "Rheological Properties of Aqueous Clay Systems." *Ceramic Fabrication Process*. John Wiley and Sons, New York.

Mooney, M. 1951. "The Viscosity of a Concentrated Suspension of Spherical Particles." *J. Coll. Sci.* 6:162.

Phelps, G. W., S. G. Maguire, W. J. Kelly, and R. K. Wood. 1983. *Rheology and Rheometry of Clay-Water Systems*. Cyprus Industrial Minerals, Co., Sandersville, Georgia.

Quemada, D. 1978. "Rheology of Concentrated Disperse Systems II. A Model for Non-Newtonian Shear Viscosity in Steady Flows." *Rheol. Acta* 17:632-642.

O'Brien, R. W. 1988. "Electro-acoustic Effects in a Dilute Suspension of Colloidal Particles." *J. Fluid Mech.* 190:71-86.

Reiner, M. 1960. Lectures on Theoretical Rheology. North Holland, New York.

Russel, W. B. 1987. "Theoretical Approaches to the Rheology of Concentrated Dispersion." *Powder Technology* 51:15-25.

Saunders, F. L. 1961. "Rheological Properties of Monodisperse Latex Systems: I. Concentration Dependence of Relative Viscosity." *J. Coll. Sci.* 16:13-22.

Sebera, D. K. 1964. Electronic Structure and Chemical Bonding. Blaisdell Publishing Co., New York.

Smith, T. L. 1972. "Rheological Properties of Dispersions of Particulate Solids in Liquid Media." *J. Paint Tech.* (44):575:71-79.

Thomas, D. G. 1965. "Transport Characteristics of Suspension: VIII. A Note on the Viscosity of Newtonian Suspensions of Uniform Spherical Particles." *J. Coll. Sci.* 20:267-277.

Van Megan, W., and I. Snook. 1984. "Equilibrium Properties of Suspensions." In: *Advances in Colloid and Interface Science*. Elsevier, New York.

Wagstaff, I., and C. E. Chaffey. 1977. "Shear Thinning and Thickening Rheology I. Concentrated Acrylic Dispersions." *J. Coll. Int. Sci.* 59 (1):53-62.

Yasuda, D. D., and P. Hrma. (1991). "The Effect of Slurry Rheology on Melter Cold Cap Formation." In Ceramic Transactions, Eds. G. G. Wicks, D. F. Bickford, L. R. Bunnell, 23:349-359. The American Ceramic Society, Westerville, Ohio. Nuclear Waste Management IV, pp.349-359.
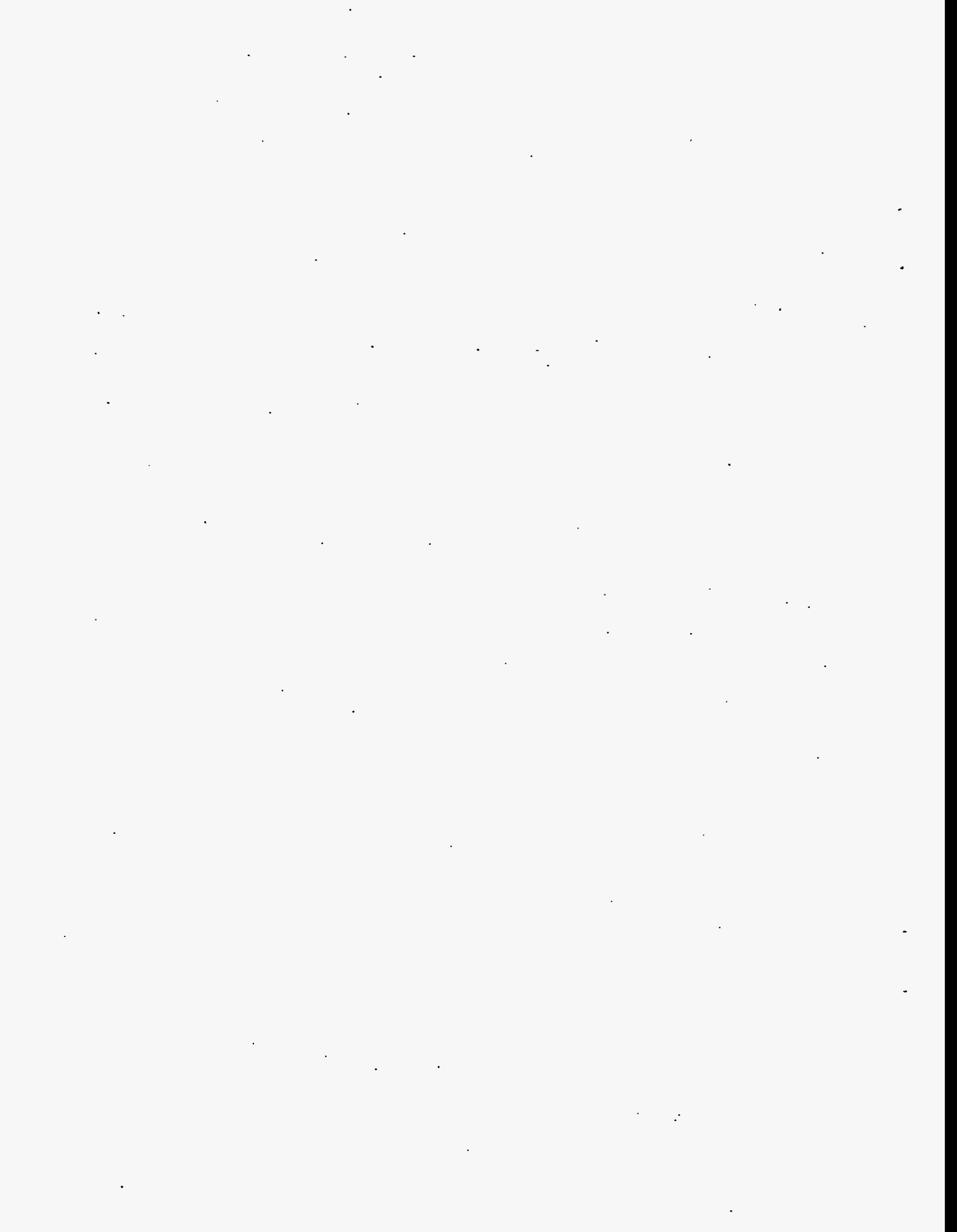
Appendix A

Rheological Data
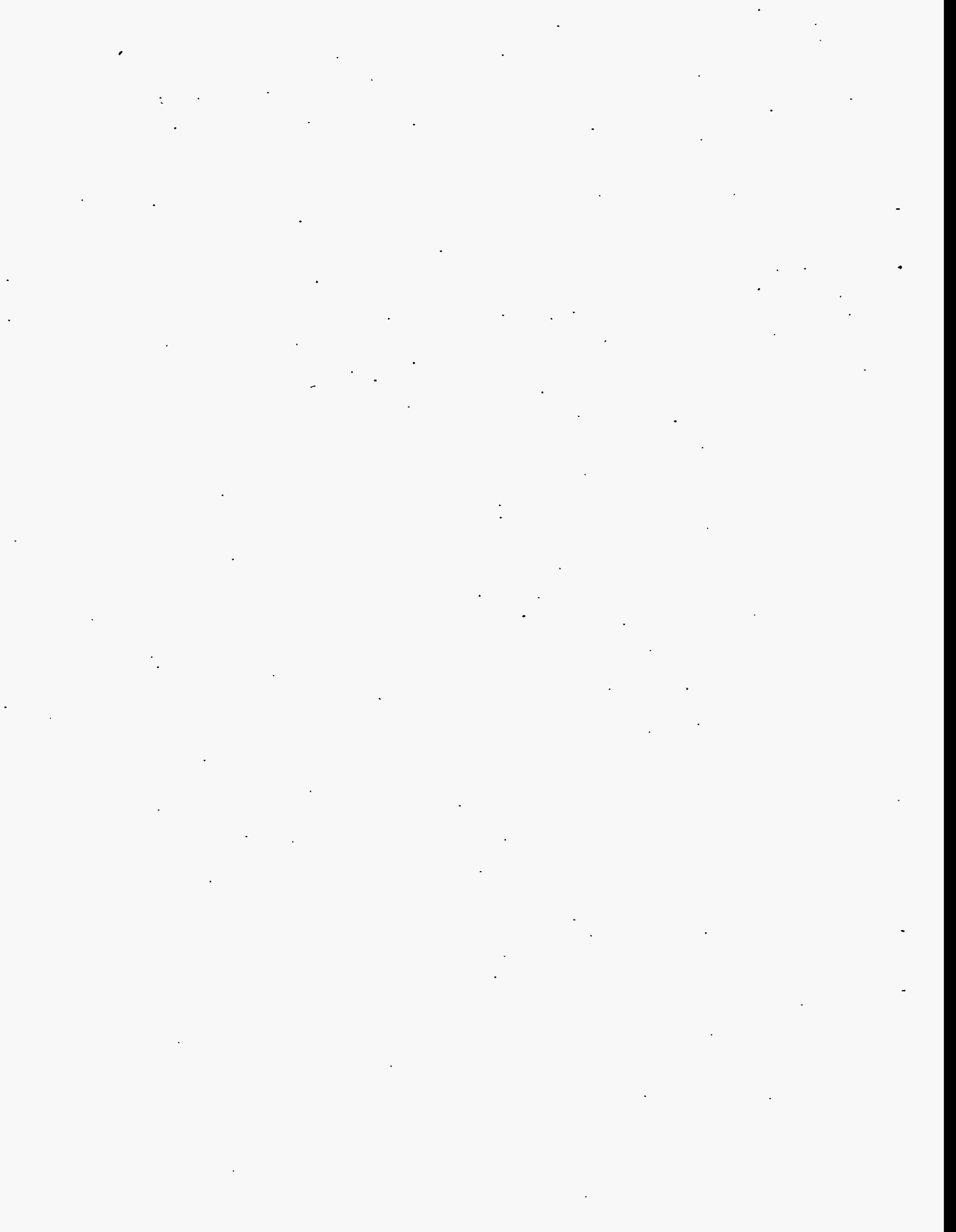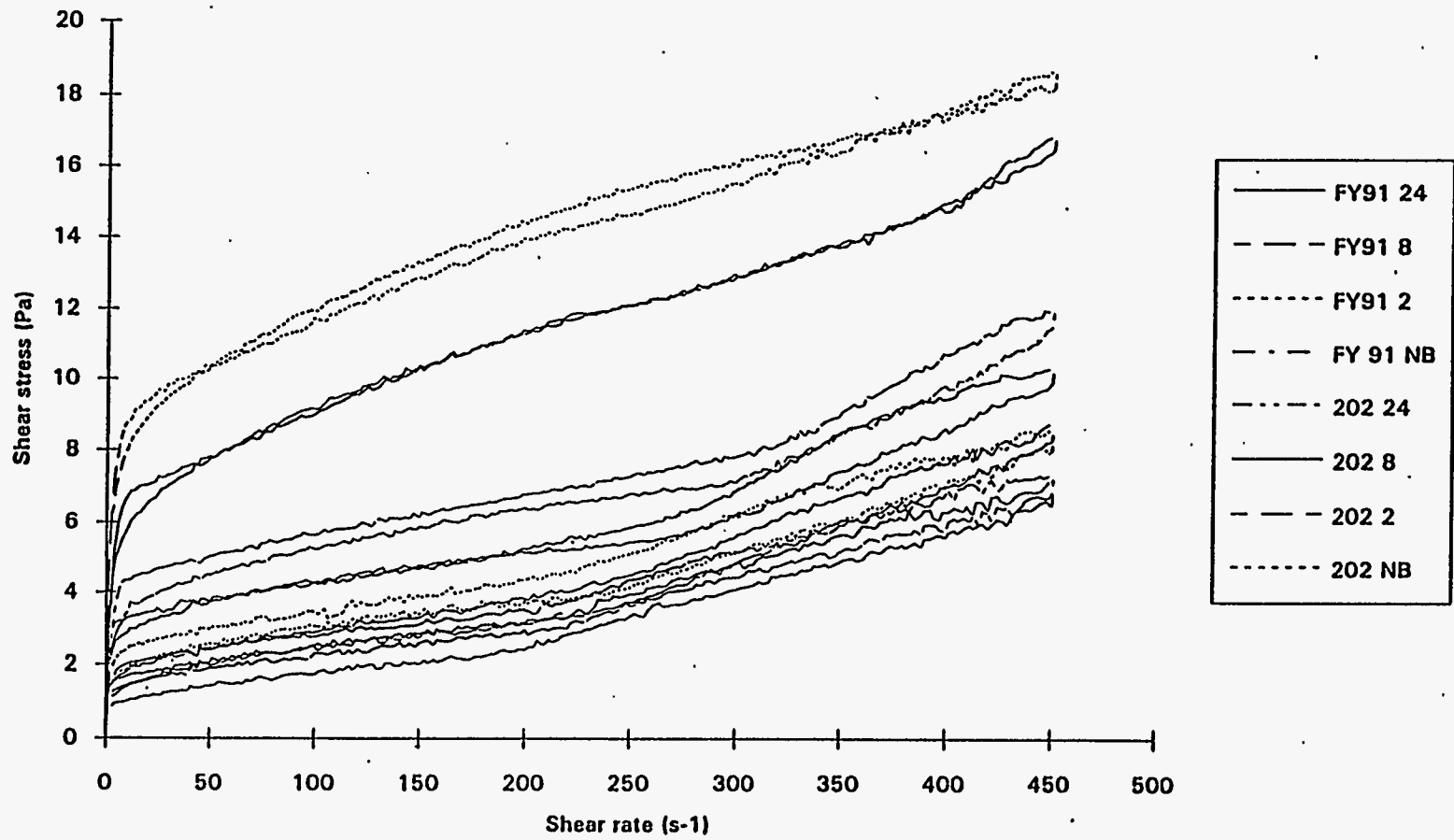
Figure A.1. 202 and FY 91 Rheograms-Boiling Time Comparison, No Aging. 24, 8, and 2 refer to boiling time, NB denotes no boil.
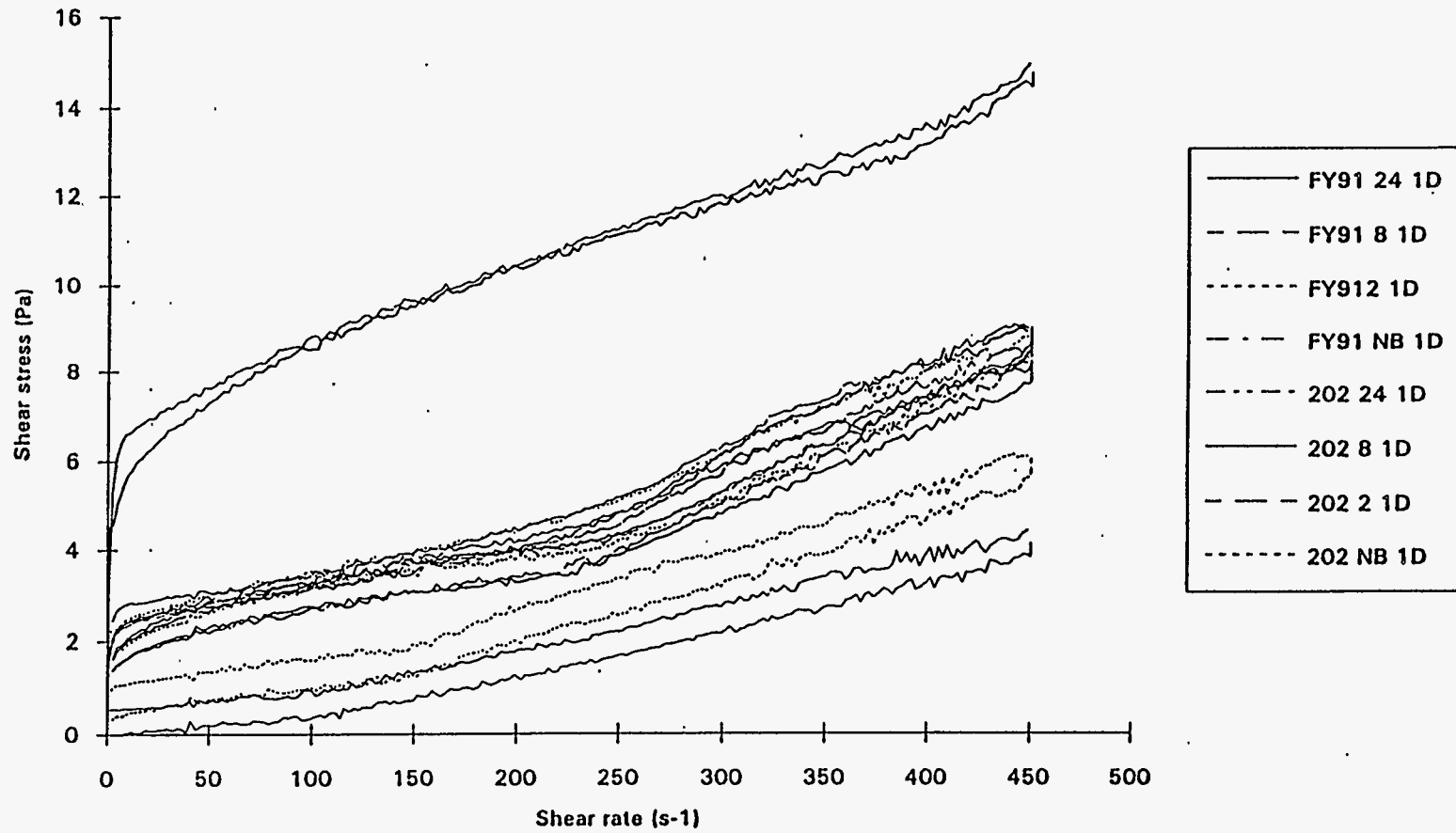
Figure A.2. 202 and FY 91 Rheograms-Boiling Time Comparison, 1 Day of Aging
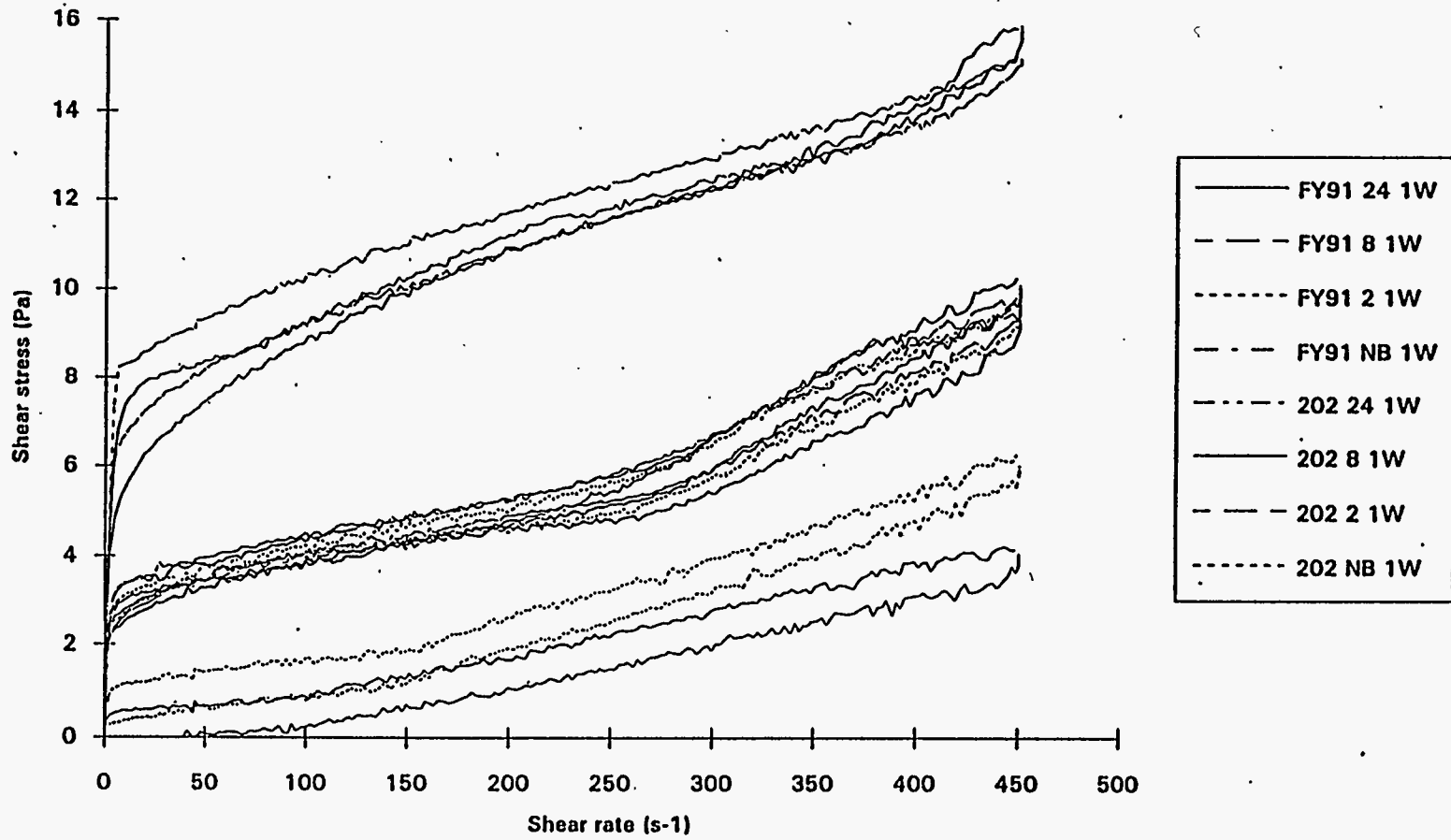
Figure A.3. 202 and FY 91 Rheograms-Boiling Time Comparison, 1 Week of Aging

A.3
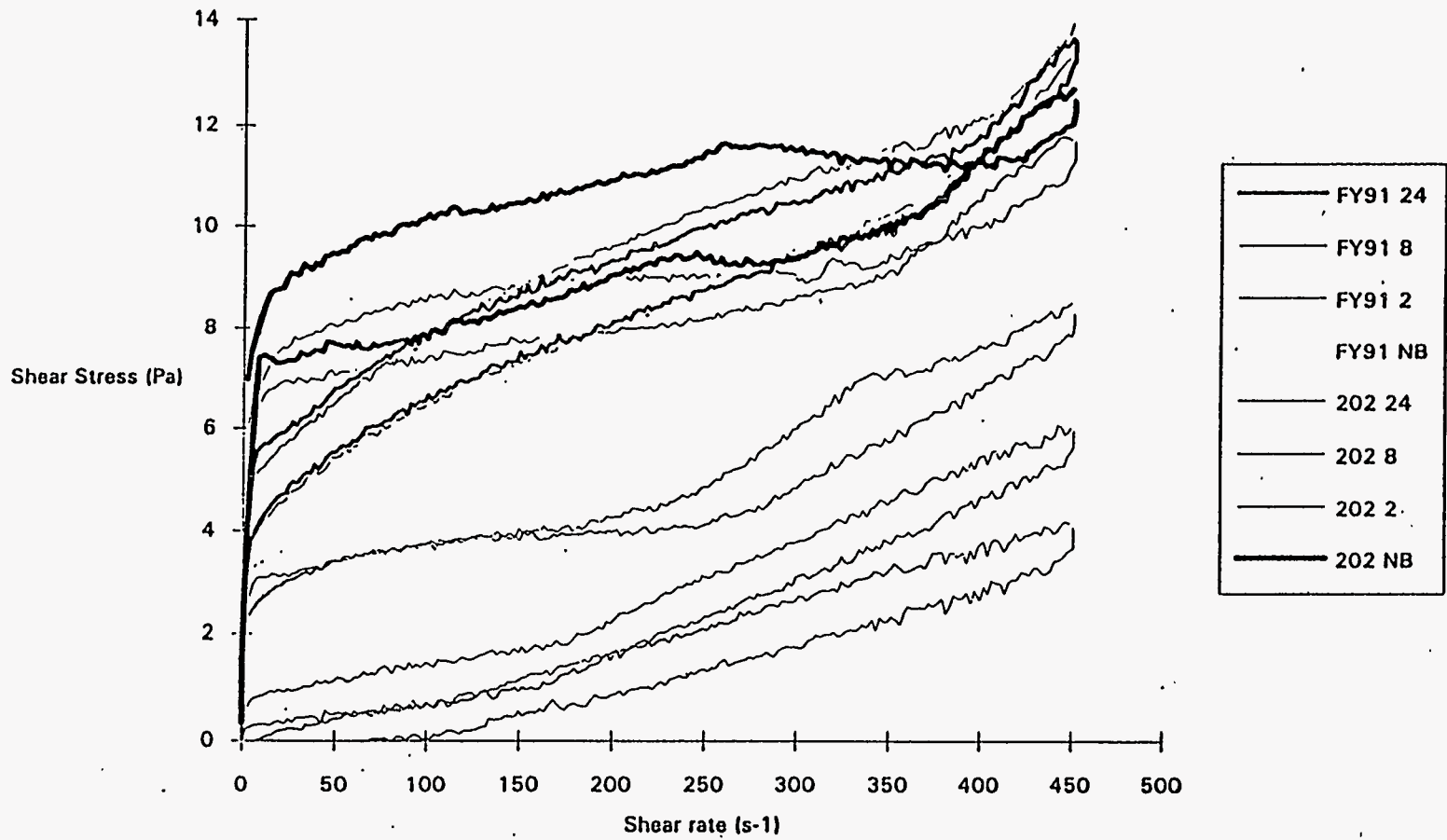
Figure A.4. 202 and FY 91 Rheograms-Boiling Time Comparison, 2 Weeks of Aging
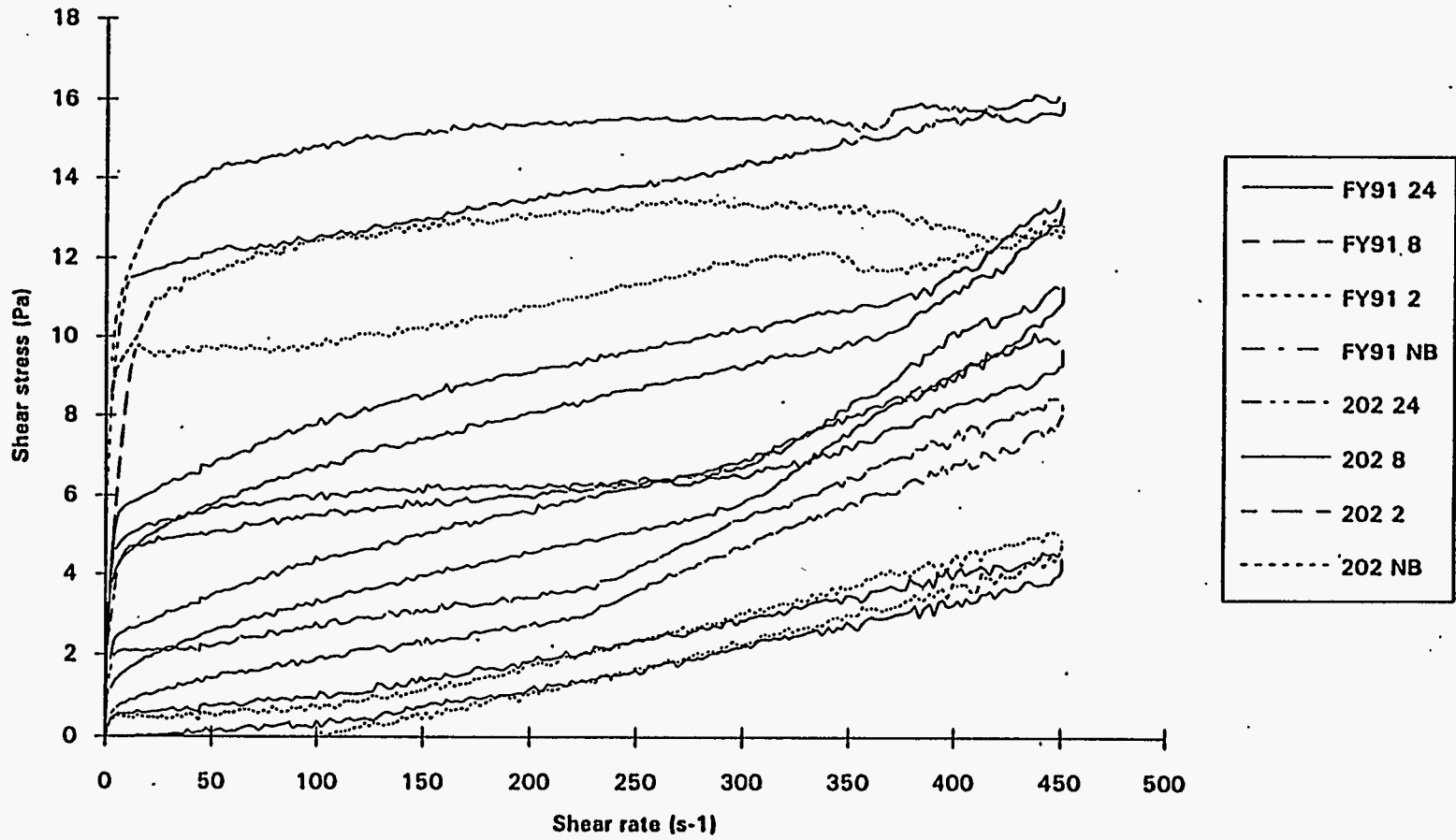
Figure A.5. 202 and FY 91 Rheograms-Boiling Time Comparison, 4 Weeks of Aging
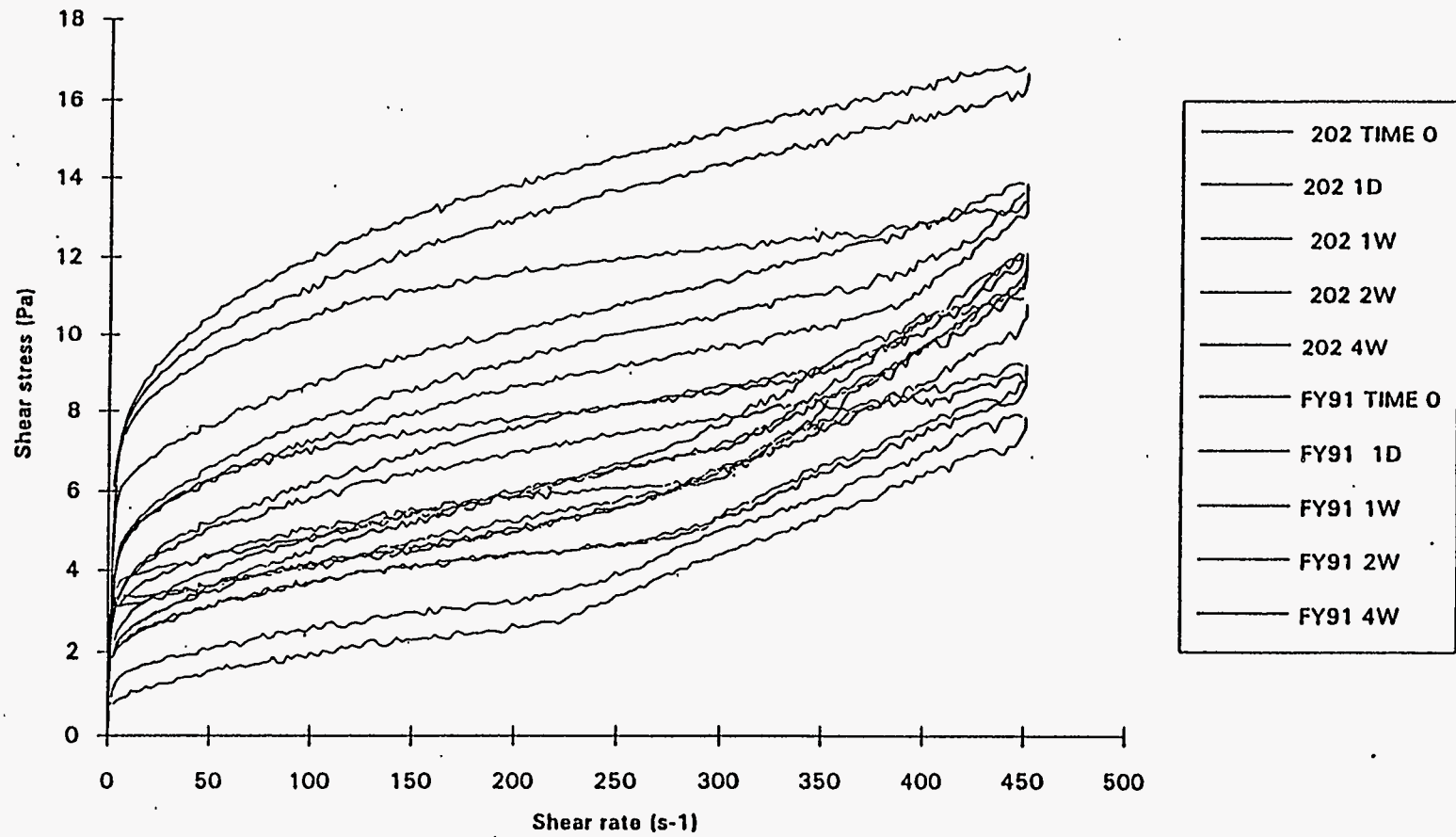
Figure A.6. Rheograms for pH < 5 Samples
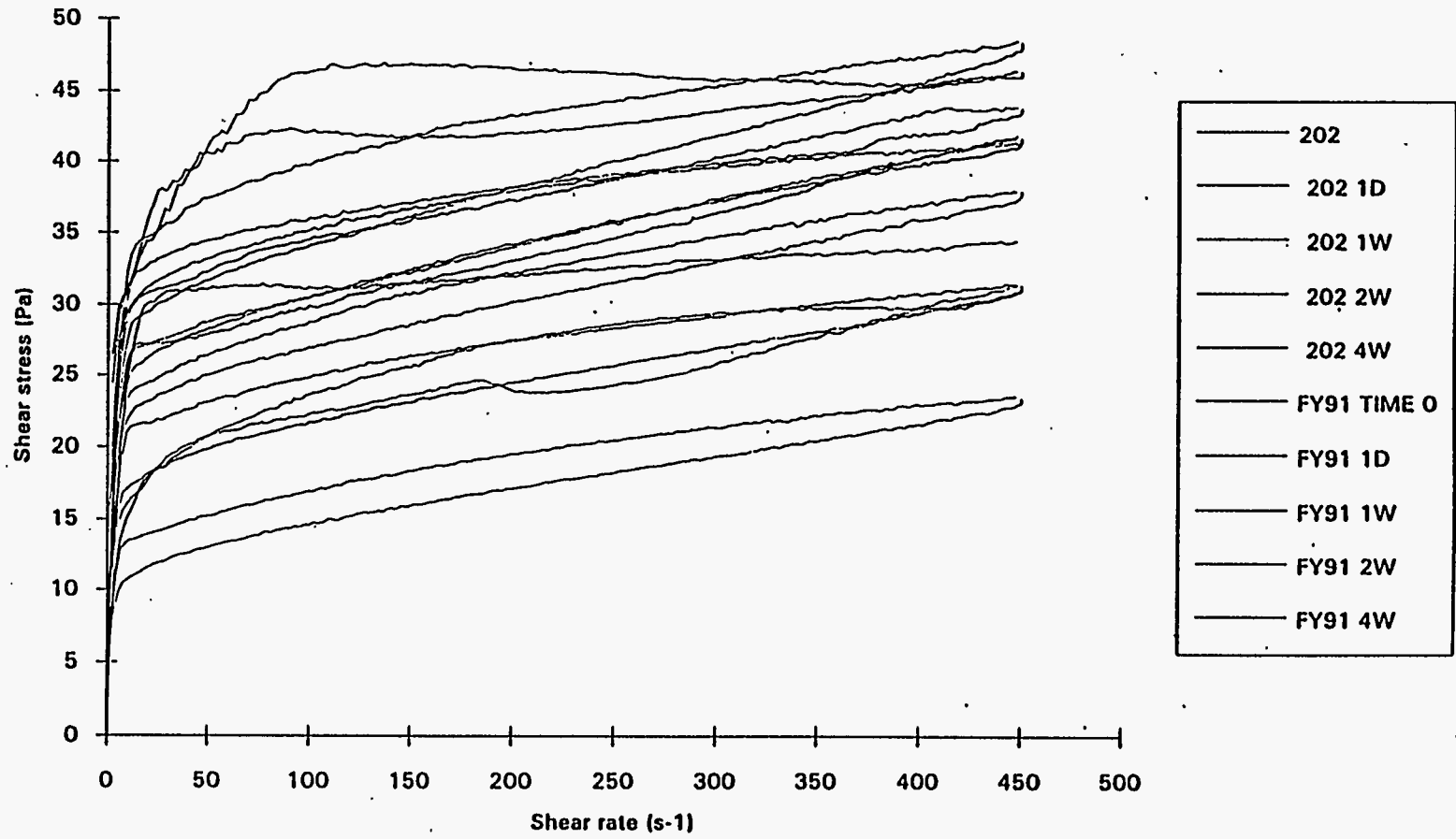
Figure A.7. Rheograms for 600 g TO/L Melter Feed
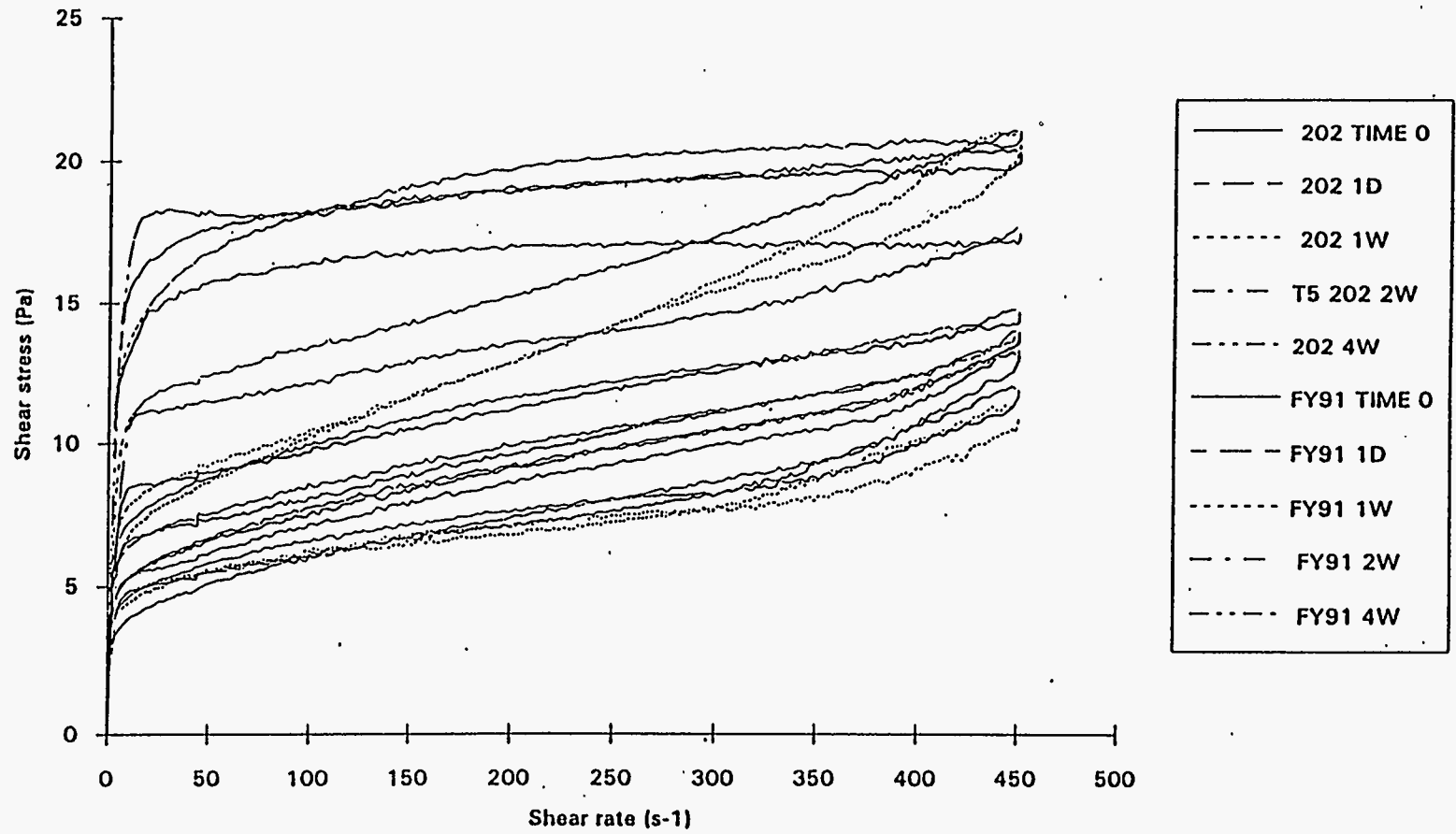
Figure A.8. Rheograms for Noble Metal Slurries

Shear stress (Pa)
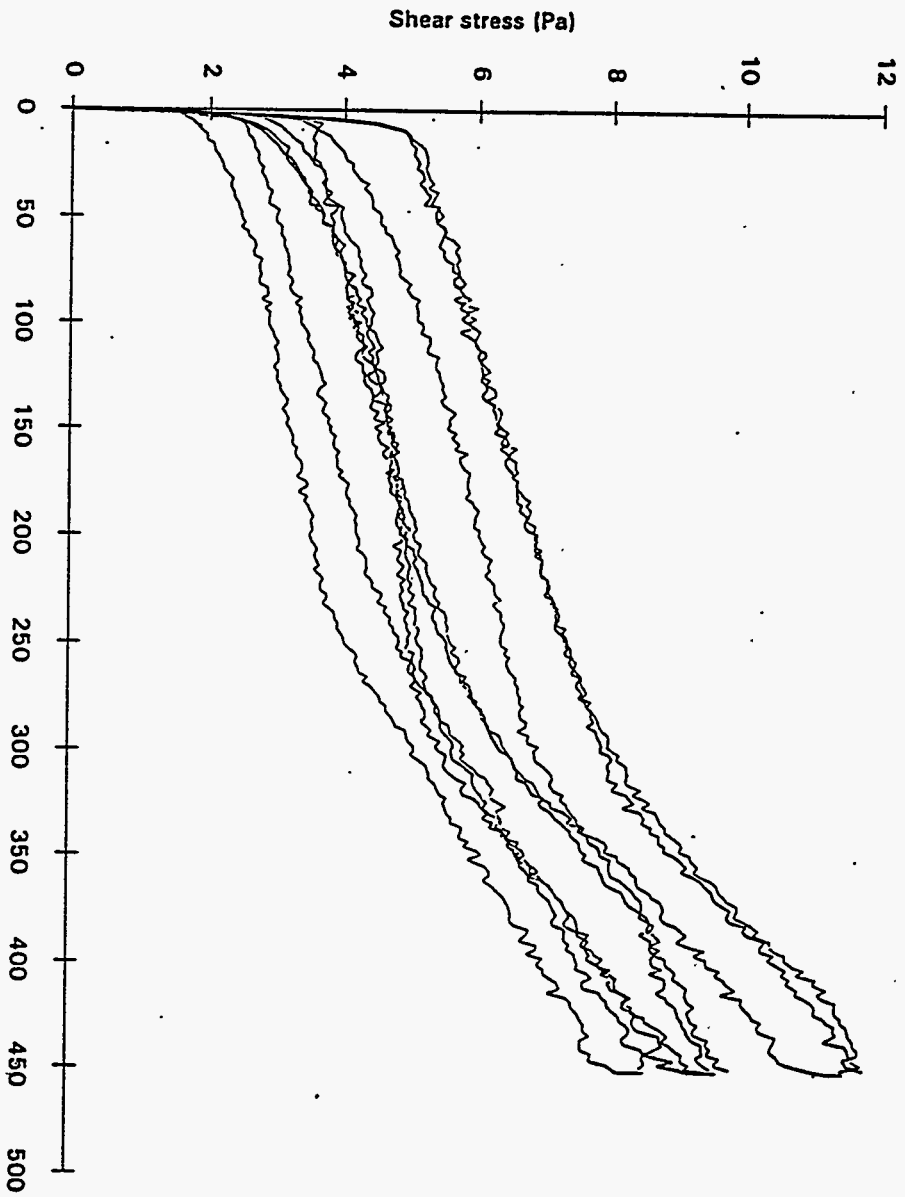
Figure A.9. HW-39-4 Melter Feed Rheograms

HW-39 TIME 0

HW 39 1D

HW 39 1W

HW 39 2W
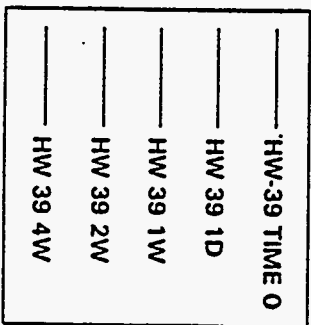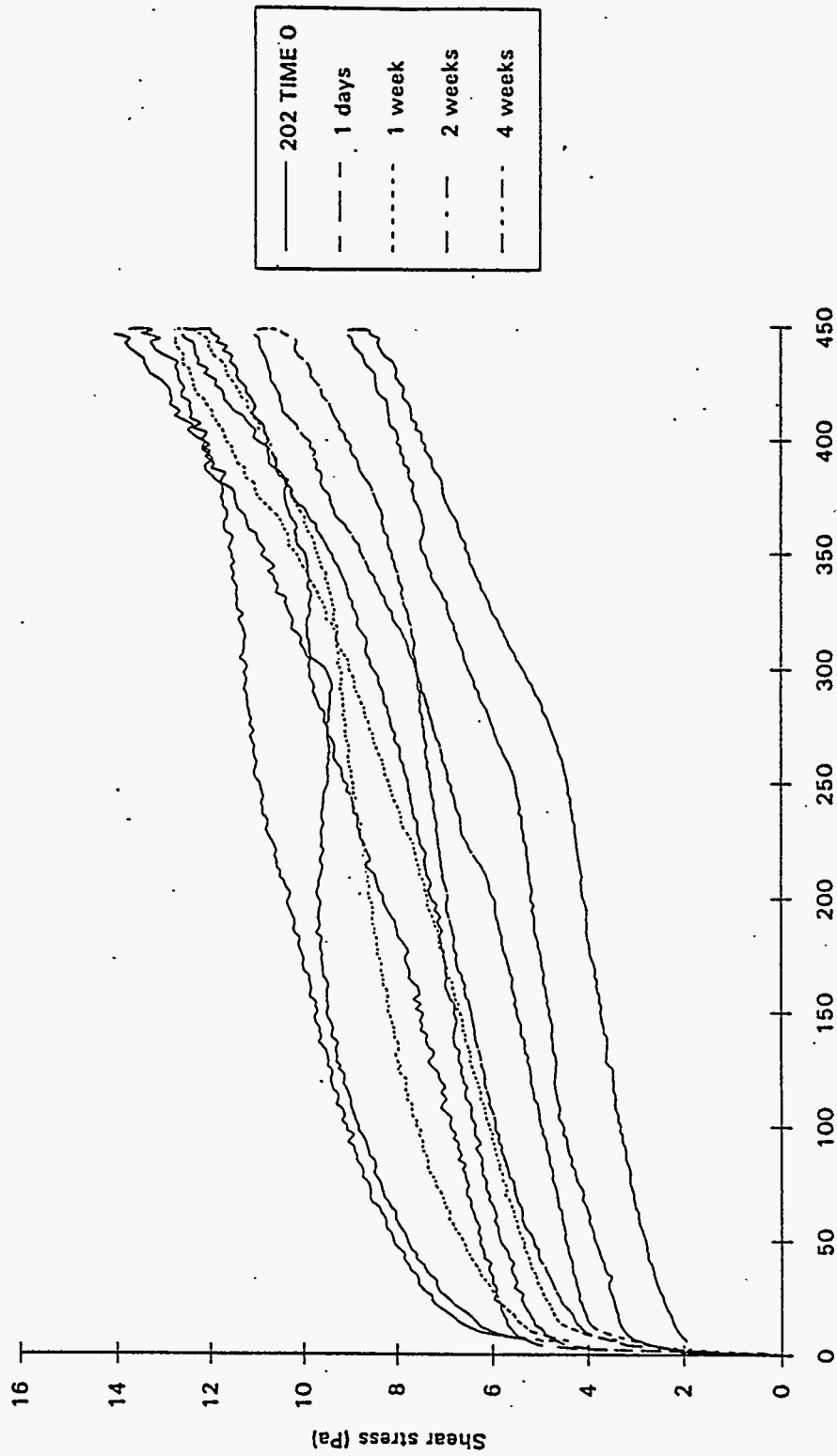
HW 39 4W

Figure A.10. 202 Melter Feed, Boiling Time 2 h, Rheograms from Duplicate Experiments

A.10
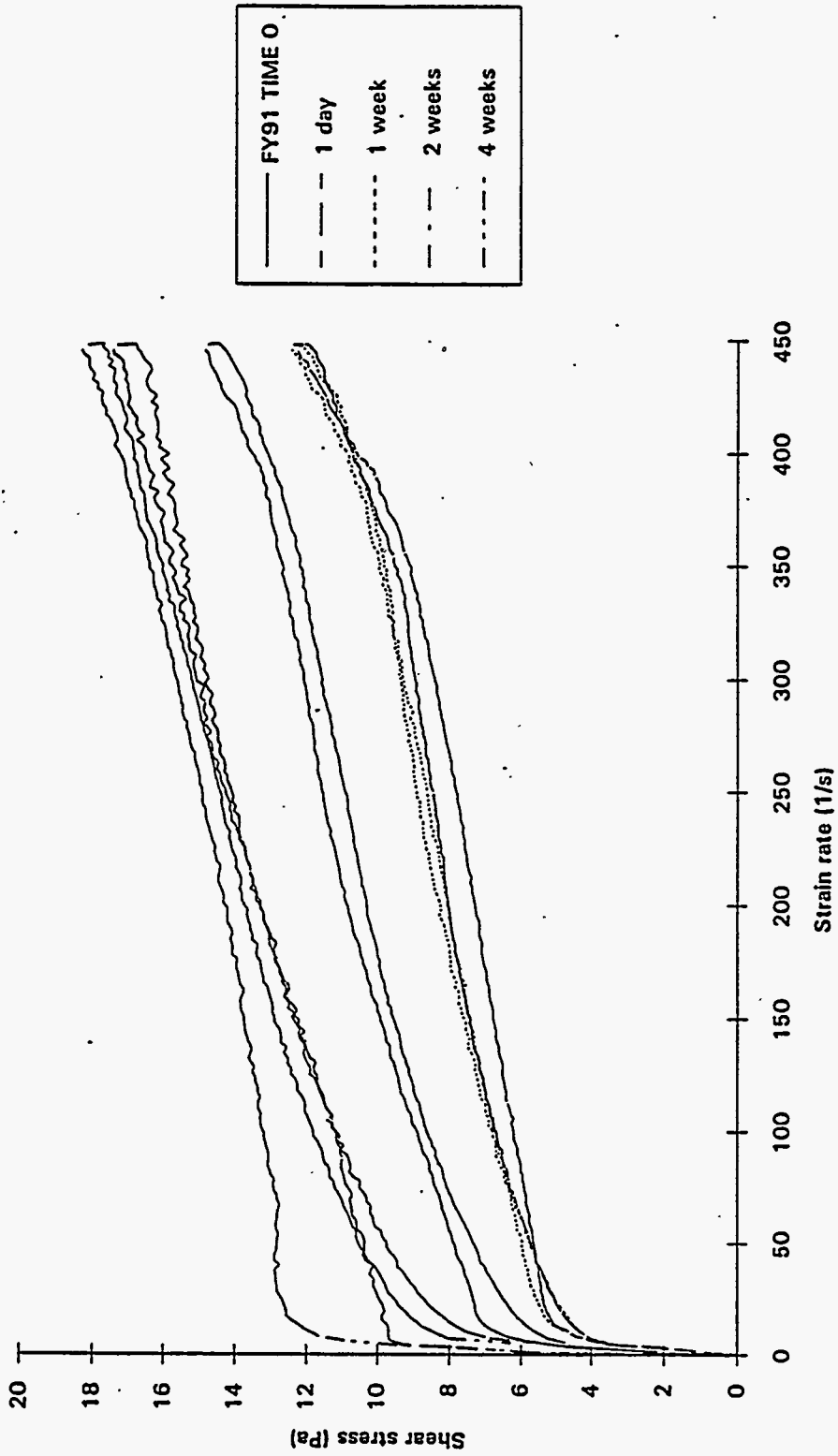
Figure A.11. FY 91 Melter Feed, Boiling Time 2 h, Rheograms from Duplicate Experiments

A.11
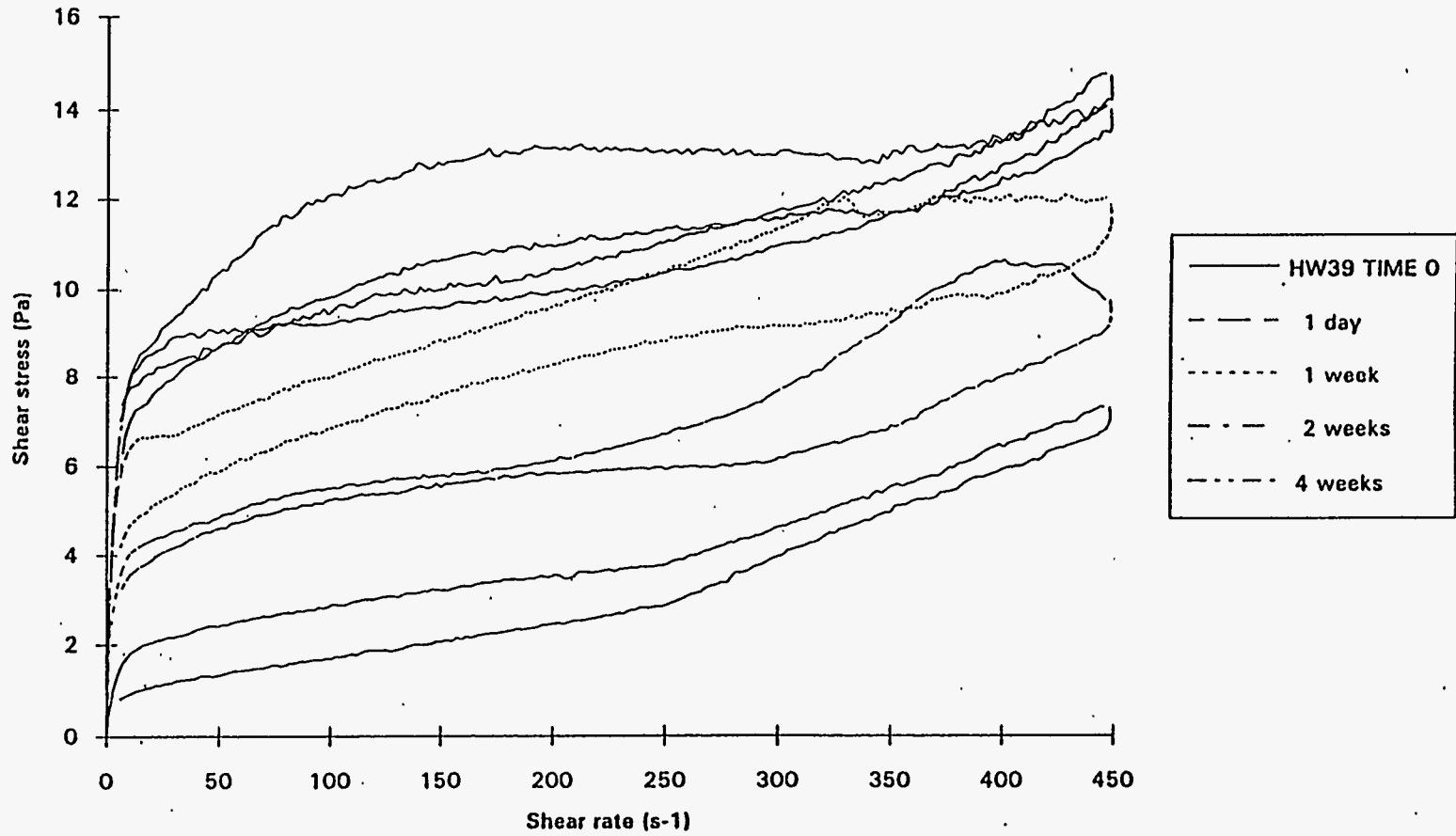
Figure A.12. HW-39-4 Melter Feed, Boiling Time 2 h, Rheograms from Duplicate Experiments
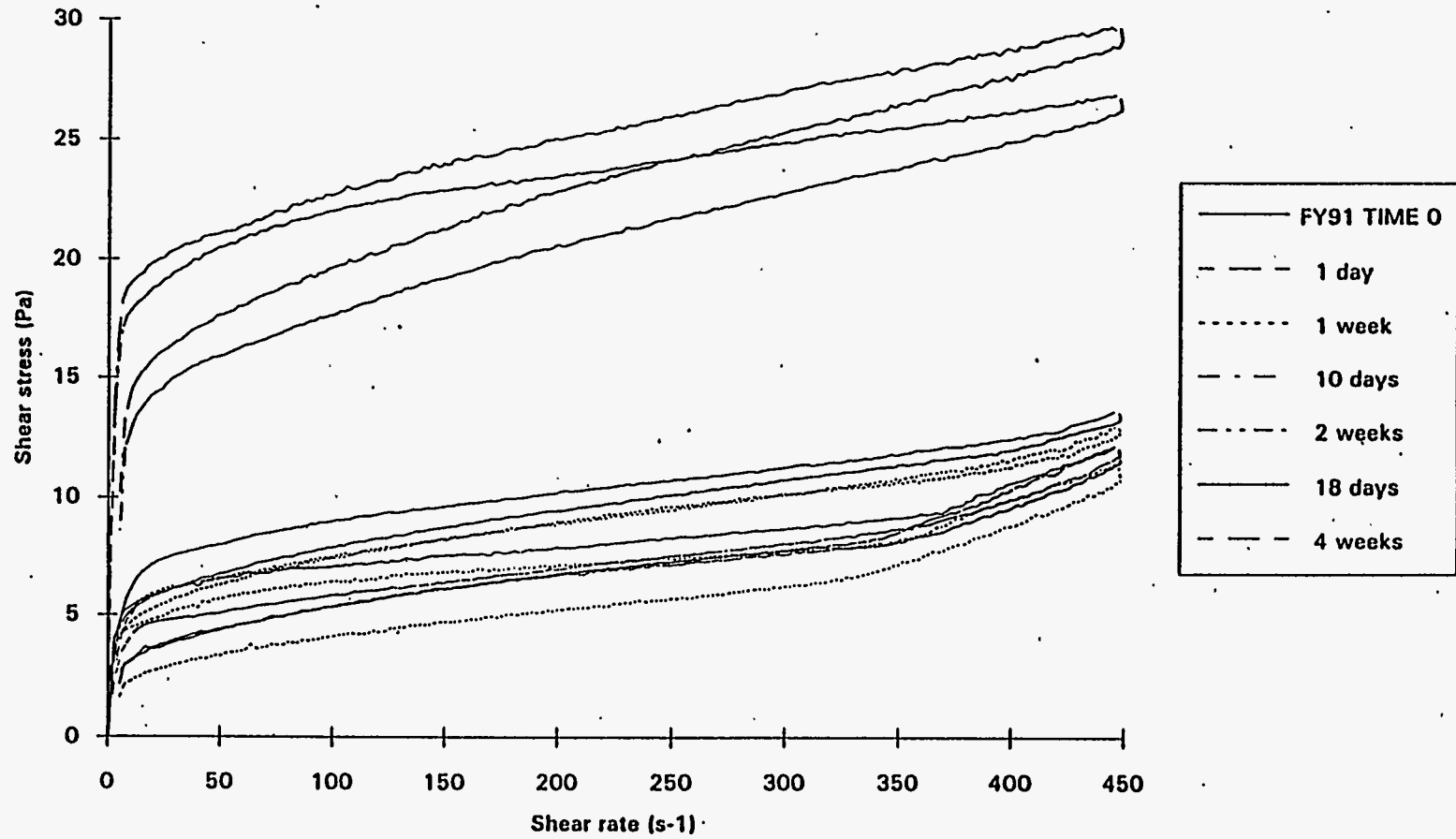
Figure A.13. FY 91 Melter Feed Concentration Cycling Experiment Rheograms
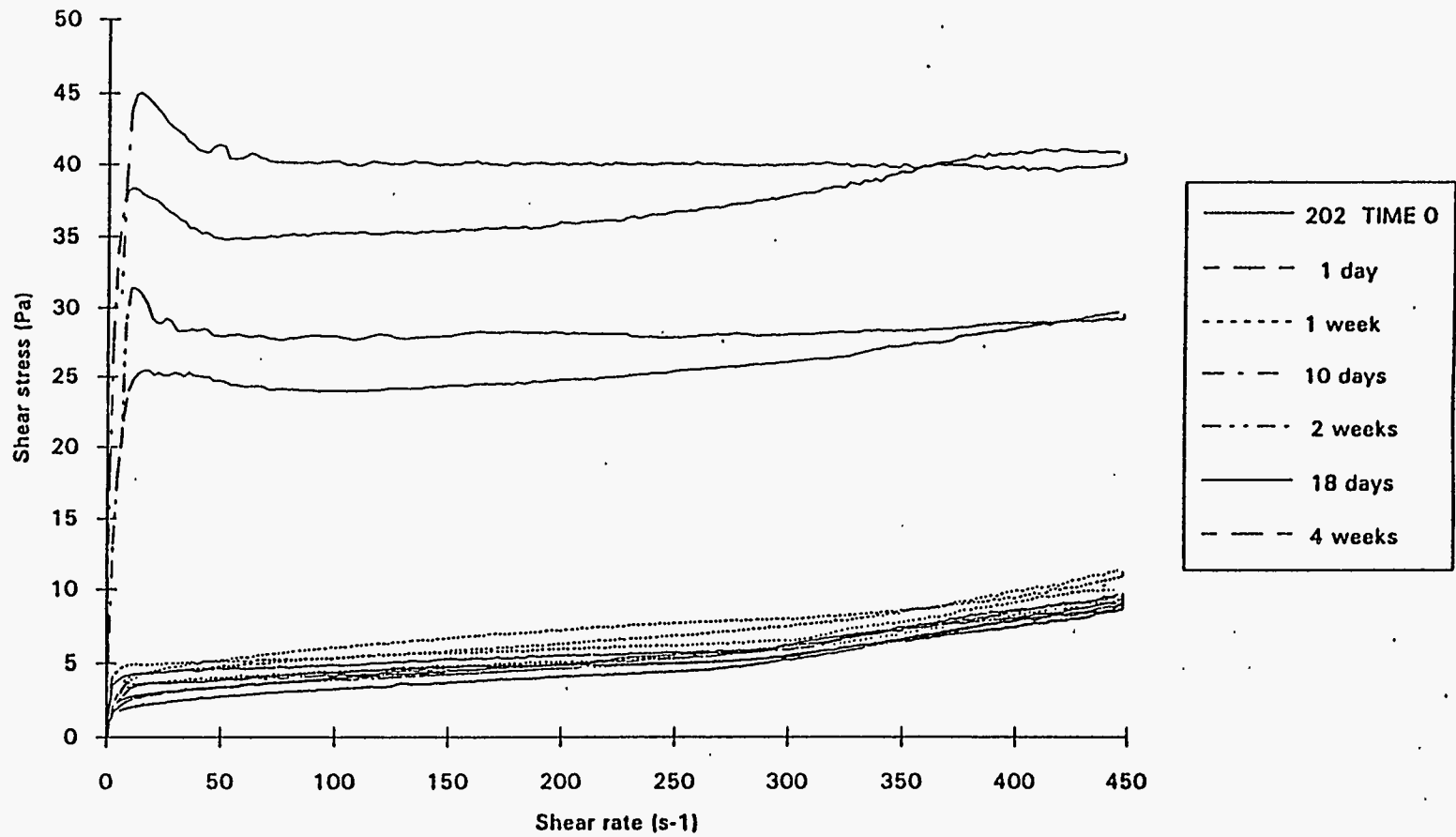
Figure A.14. 202 Melter Feed Concentration Cycling Experiment Rheograms
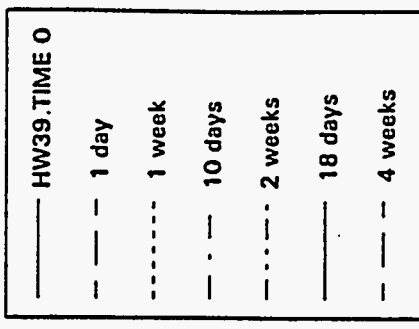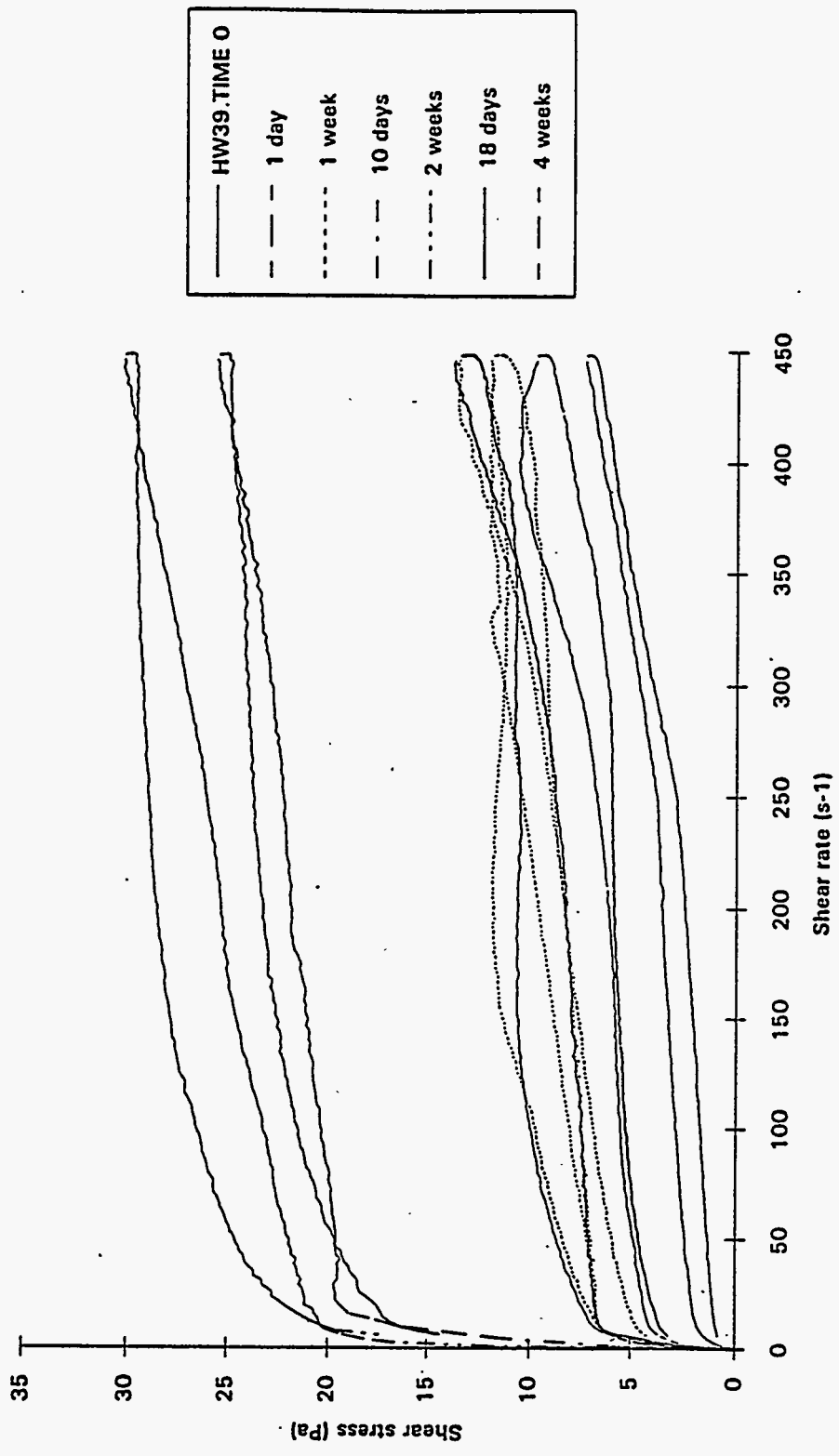
Figure A.15. HW-39-4 Melter Feed Concentration Cycling Experiment Rheograms

Legend:
- HW39.TIME 0
- 1 day
- 1 week
- 10 days
- 2 weeks
- 18 days
- 4 weeks

Shear rate (s-1)

Shear stress (Pa)
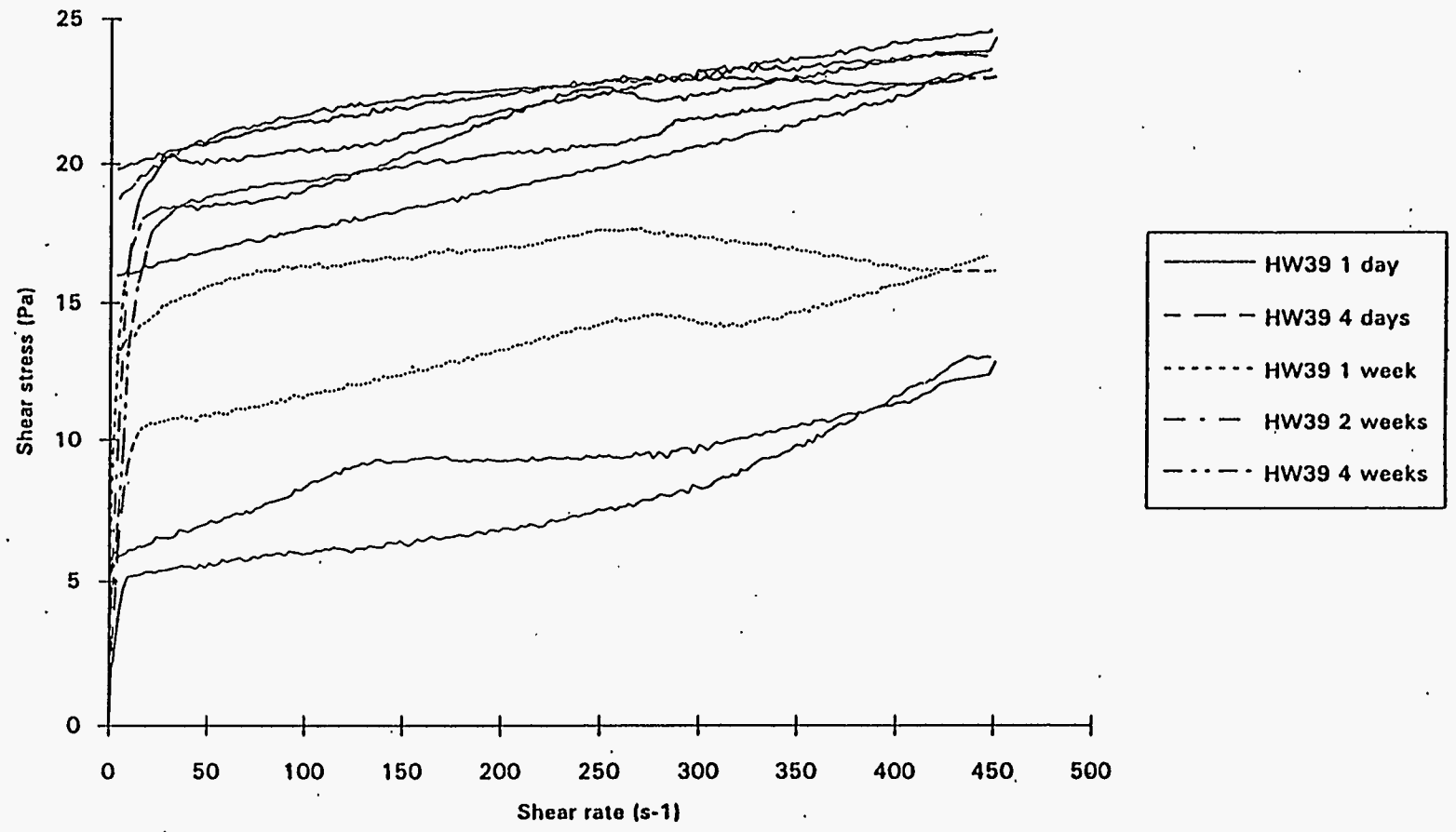
Figure A.16. HW-39-4 Rheograms from FY 1992
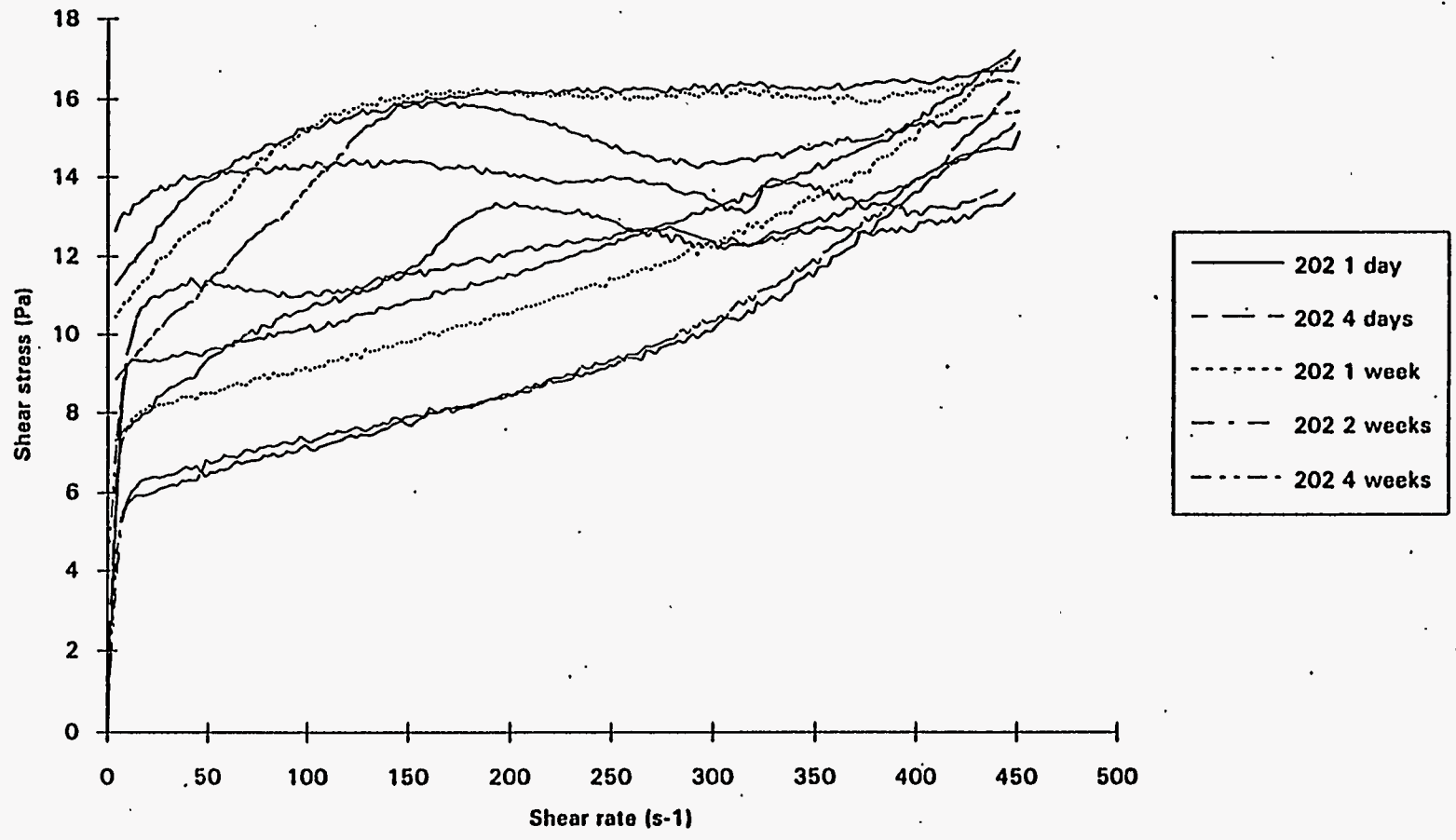
Figure A.17. 202 Melter Feed Rheograms from FY 1992
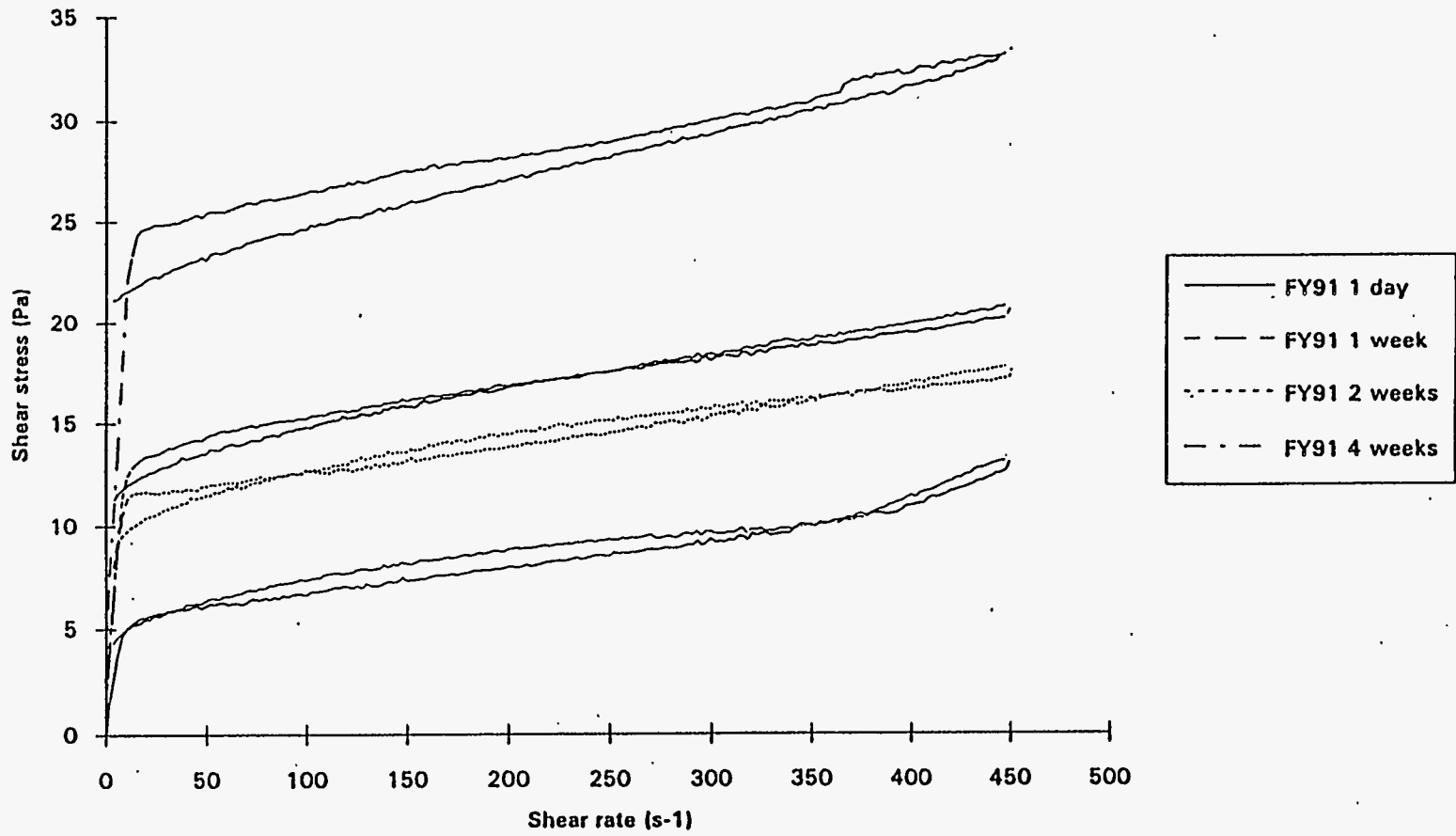
Figure A.18. FY 91 Melter Feed Rheograms from FY 1992
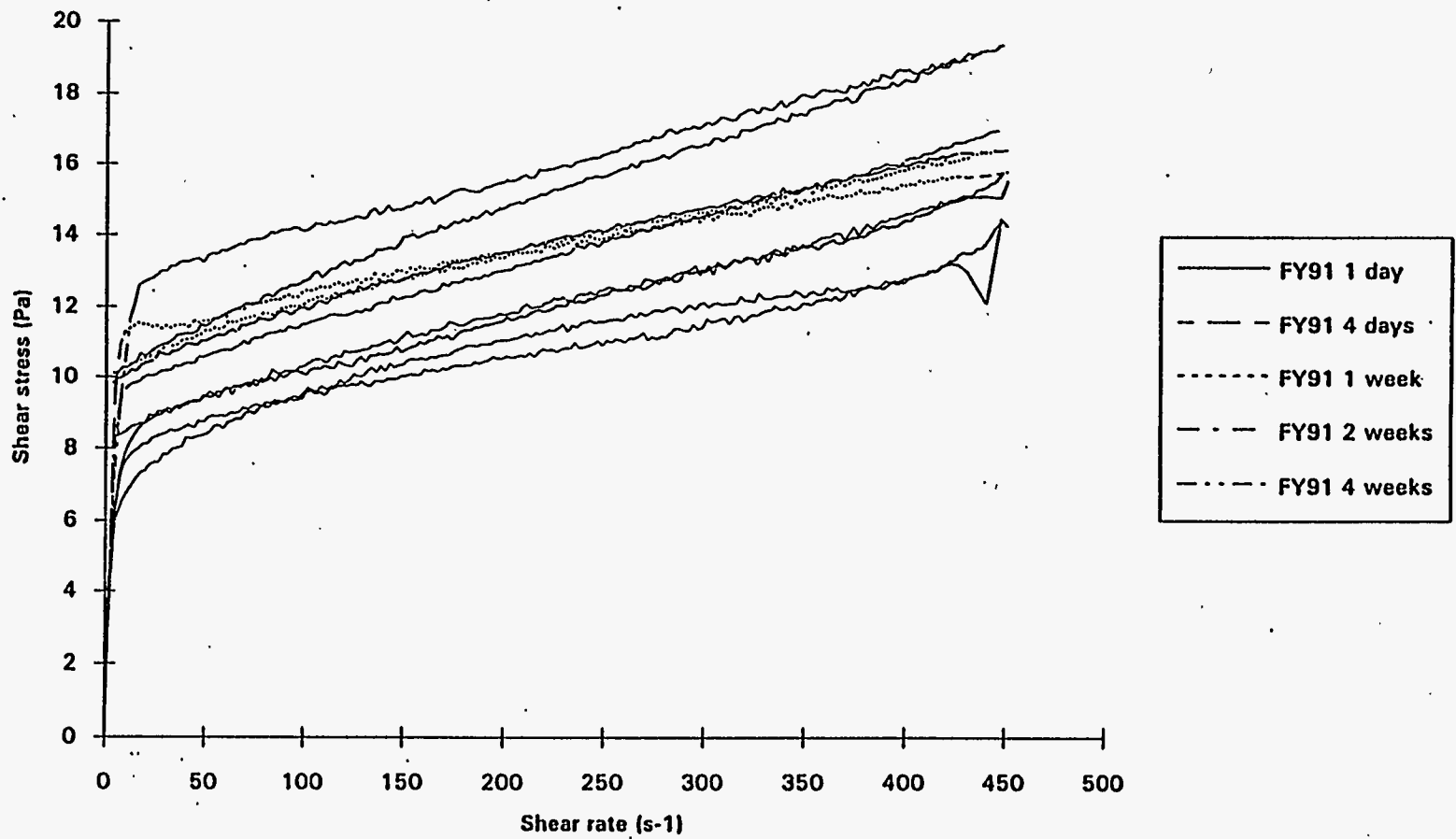
Figure A.19. FY 91 Melter Feed with Noble Metals from FY 1992

Table A.1. Comparison of Rheology Data to Models

Melter Feed	Age	Yield Stress (Pa)	Viscosity (cp)	Fit	Best Alternative Model			
Frit 202	0 days	3	12.15	0.97				
2 hour boil	0 days	1.935	14.25	0.98				
	0 days	2.363	13.64	0.97				
	1 day	3.984	18.18	0.97				
	1 day	1.942	14.38	0.98				
	1 day	3.583	14.66	0.94				
	1 week	2.603	14.31	0.96				
	1 week	2.813	12.74	0.92				
	1 week	3.174	16.17	0.96				
	2 weeks	2.319	12.64	0.94				
	2 weeks	4.915	17.58	0.96				
	4 weeks	4.463	15.13	0.92		a	b	fit
	4 weeks	8.837	9.044	0.72	Logarithmic	4.65	1.221	0.88
FY91	0 days	6.789	16.96	0.93				
2 hour boil	0 days	3.853	15.67	0.94				
	0 days	7.111	14.05	0.88	Logarithmic	1.196	1.779	0.94
	1 day	1.721	14	0.96				
	1 day	4.957	15.05	0.95				
	1 day	5.594	15.05	0.95				
	1 week	3.981	15.21	0.93				
	1 week	4.501	14.5	0.93				
	1 week	8.484	14.99	0.92				
	2 weeks	5.794	17.01	0.94				
	2 weeks	9.284	18.52	0.93				
	4 weeks	1.093	14.93	0.95				
	4 weeks	11.37	14.47	0.8	Logarithmic	5	1.893	0.85
HW39	0 days	1.48	11.55	0.95		a	n	fit
2 hour boil	0 days	1.48	11.55	0.95				
	1 day	3.184	21.54	0.95				
	1 day	3.184	21.54	0.95	Ostwald	3.184	0.2154	0.95
	1 week	3.624	15.19	0.93				
	1 week	3.624	15.19	0.93				
	2 weeks	7.672	14.01	0.92				
	4 weeks	7.638	12.07	0.8	Logarithmic	2.567	1.527	0.8
Concentration Cycling Samples								
202						a	b	fit
	10 days	33	17.34	0.4	Hyperbolic	37.22	-10.01	0.58
	2 weeks	22.04	15.09	0.45	Logarithmic	14.11	2.222	0.63
	18 days	3.573	10.99	0.89				
	4 weeks	3.996	11.12	0.85				
HW39	10 days	17.68	17.84	0.63	Logarithmic	8.364	2.617	0.9
	2 weeks	20.25	22.84	0.78	Logarithmic	9.636	3.089	0.92
	18 days	5.455	15.7	0.87				
	4 weeks	5.341	16.85	0.91				
FY91	10 days	7.961	3.332	0.95				
	2 weeks	18.91	19.46	0.68	Logarithmic	8.533	2.894	0.95
	18 days	5.471	12.04	0.9				

	4 weeks	4.634	12.18	0.8				
Boiling Time Experiments								
Frit 202	0 days	1.493	12.44	0.97				
No Boil	1 day	1.825	15.19	0.98				
	1 week	2.863	13.99	0.96				
	2 weeks	6.632	11.18	0.86				
	4 weeks	7.759	10.95	0.9				
FY91	0 days	2.468	16.34	0.95				
No Boil	1 day	1.864	14.74	0.95				
	1 week	2.645	15.12	0.95				
	2 weeks	2.858	15.74	0.95				
	4 weeks	2.234	17.94	0.96				
Frit 202	0 days	1.162	12.32	0.97				
8 hr boil	1 day	0.1212	8.951	0.98				
	1 week	0.1154	8.902	0.98				
	2 weeks	-0.1159	9.252	0.99				
	4 weeks	0.1233	9.348	0.98				
FY91	0 days	9.755	18.08	0.92				
8 hr boil	1 day	0.5171	11.7	0.98				
	1 week	0.4993	11.8	0.97				
	2 weeks	0.189	12.33	0.97				
	4 weeks	-0.2419	11.85	0.98				
Frit 202	0 days	1.271	15.15	0.97				
24 hr boil	1 day	1.725	13.69	0.97				
	1 week	2.154	15.76	0.95				
	2 weeks	6.024	10.33	0.82				
	4 weeks	4.061	11.39	0.9				
FY91	0 days	4.846	6.795	0.98				
24 hr boil	1 day	6.795	17.3	0.98				
	1 week	6.724	15.29	0.94				
	2 weeks	5.927	15.62	0.94				
	4 weeks	5.97	14.71	0.94				
pH control testing								
Frit 202	0 days	0.964	14.07	0.96				
	1 day	6.799	15.52	0.94				
	1 week	2.58	14.09	0.96				
	2 weeks	3.004	17.04	0.96				
	4 weeks	2.636	13.61	0.96				
FY91	0 days	5.296	12.32	0.88				
	1 day	2.305	18.7	0.96				
	1 week	4.358	14.95	0.95				
	2 weeks	5.748	16.16	0.94				
	4 weeks	9.611	18	0.87	H-Bulkley	2.778	0.268	2.426	0.98
600 g Total Oxide/L								
Frit 202	0 days	25.01	38.52	0.83	Logarithmic	8.83	4.879	0.89	
	1 day	29.88	34.37	0.79	Logarithmic	14.4	4.557	0.93	
	1 week	14.69	16.92	0.83	Logarithmic	7.319	2.195	0.93	
	2 weeks	28.8	14.11	0.39	Logarithmic	19.47	2.455	0.78	

A.21

Table A.1. (Contd)

	4 weeks	37.38	21.11	0.47	Logarithmic	24.26	3.508	0.86	
FY91	0 days	26.13	36.62	0.85	Logarithmic	10.58	4.67	0.92	
	1 day	24.65	32.76	0.83	Logarithmic	10.01	4.322	0.96	
	1 week	34.97	33.83	0.66	Logarithmic	17.26	4.972	0.96	
	2 weeks	21.69	24.43	0.77	Logarithmic	10.22	3.331	0.96	
	4 weeks	14.18	23.2	0.88	H-Bulkley	4.361	0.2374	4.399	0.96
Noble Metal tests									
Frit 202	0 days	4.338	14.82	0.94					
	1 day	4.448	13.14	0.92					
	1 week	10.76	22.44	0.93					
	2 weeks	10.25	15.3	0.84					
	4 weeks	43.93	12.34	0.13	Logarithmic	30.77	3.129	0.54	
T5 FY91	0 days	9.186	14.51	0.91					
	1 day	7.211	29.51	0.98					
	1 week	6.715	14.9	0.93					
	2 weeks	6.416	15.47	0.95					
	4 weeks	5.314	15.82	0.96					
FY92 Testing									
FY91	1 day	4.917	15.73	0.95					
	1 week	10.92	14.74	0.91					
	2 weeks	13.22	17.12	0.89	Herschel-Buckley	4.849	0.1893	0.94	
	4 weeks	23.64	21.95	0.79	Logarithmic	13.64	2.931	0.88	
FY91	1 day	7.976	12.29	0.93					
w/ noble metals	4 days	10.96	12.23	0.89					
	1 week	9.639	16.35	0.95					
	2 weeks	8.39	15.64	0.95					
	4 weeks	12.22	16.38	0.89					
HW39	1 day	4.032	17	0.9					
	4 days	10.08	14.32	0.88	Logarithmic	3.095	1.991	0.91	
	1 week	17.71	15.37	0.85					
	2 weeks	18.7	14.09	0.68	Logarithmic	11.89	2.089	0.89	
	4 weeks	17.25	14.19	0.63	Logarithmic	9.492	2.146	0.82	
Frit 202	1 day	8.253	17.57	0.94					
w/ noble metals	1 week	4.703	21.33	0.94					
	2 weeks	5.069	19.57	0.93					
	4 weeks	10.57	6.19	0.69	Logarithmic	7.528	0.8695	0.85	

A.22

Appendix B

X-Ray Diffraction Data
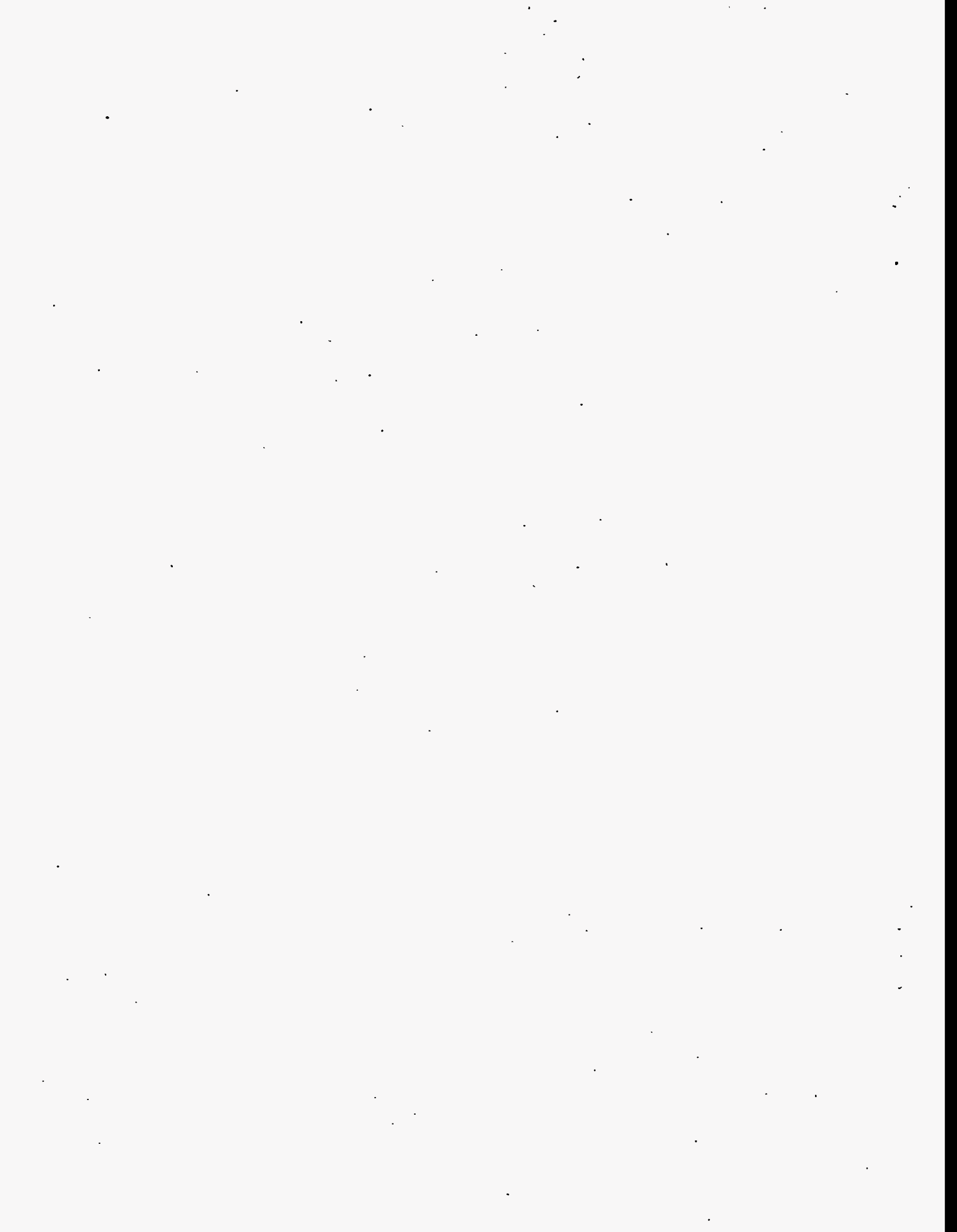
Table B.1. Most Intense Lines of Phases Found During Rheology Test, Baseline Data, NF Samples

Phases Identified	RELATIVE INTENSITY			
ICDD Card Number	NF 24	NF 8	NF 2	NF NB
Na NO3/Nitratine 7-271	1.00	1.00	1.00	1.00
Si O2/Silicon Dioxide 33-1161	0.71	0.54	0.32	0.78
FeO OH/ Goethite 29-713	0.41	0.46	0.42	0.64

Table B.2. Most Intense Lines of Phases Found During Rheology Test, Baseline Data, 202 Samples

Phases Identified	RELATIVE INTENSITY			
ICDD Card Number	202 24	202 8	202 2	202 NB
Na NO3/Nitratine 7-271	1.00	1.00	1.00	1.00
Si O2/Silicon Dioxide 33-1161	0.93	0.70	0.67	0.65
FeO OH/ Goethite 29-713	0.60	0.46	0.46	0.43
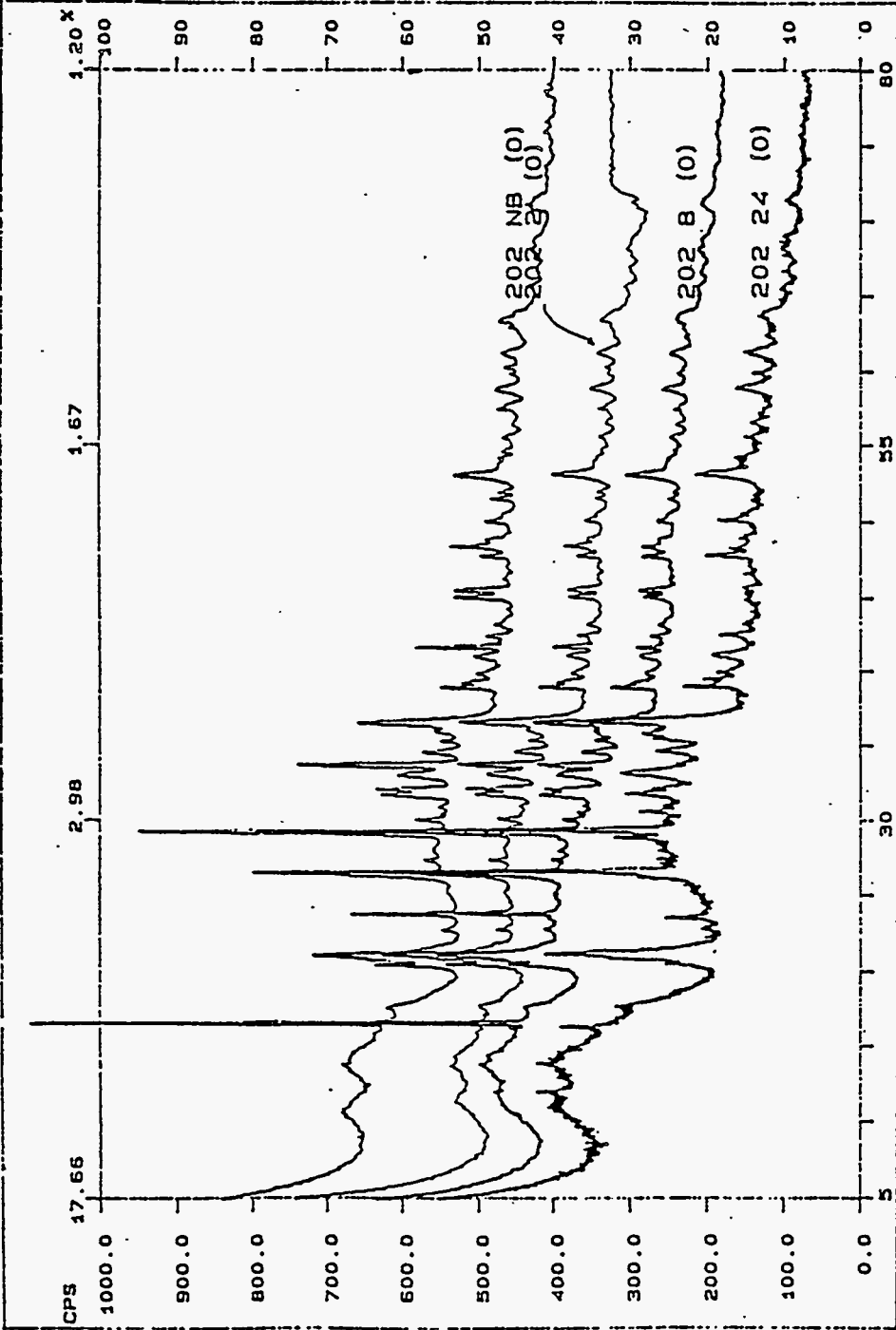
Figure B.1. Composite Plot of Raw Data for Samples 202 24, 202 8, 202 2, and 202 NB Baseline Data

B.2
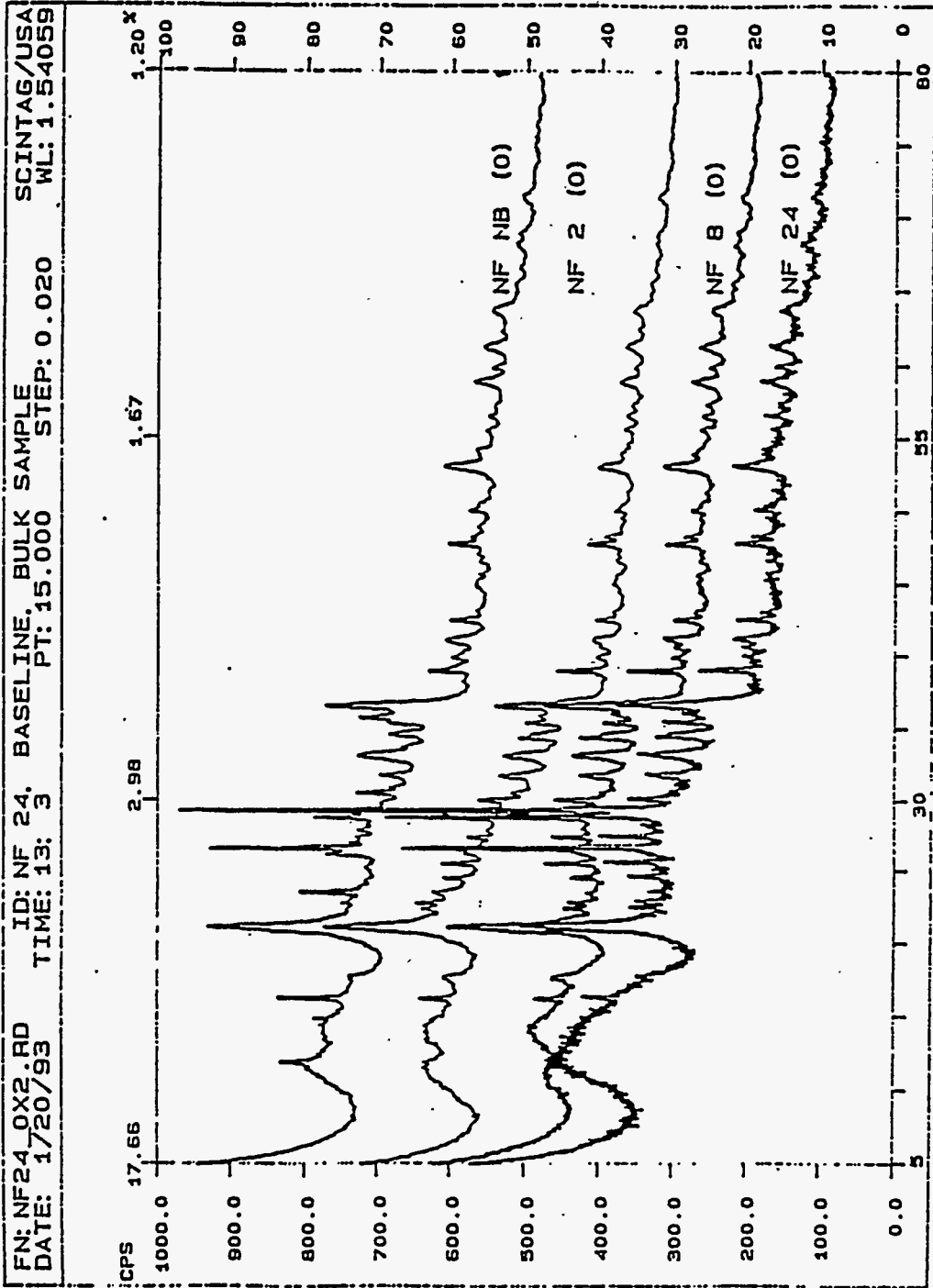
Figure B.2. Composite Plot of Raw Data for Samples NF 24, NF 8, NF 2, and NF NB Baseline Data

B.3
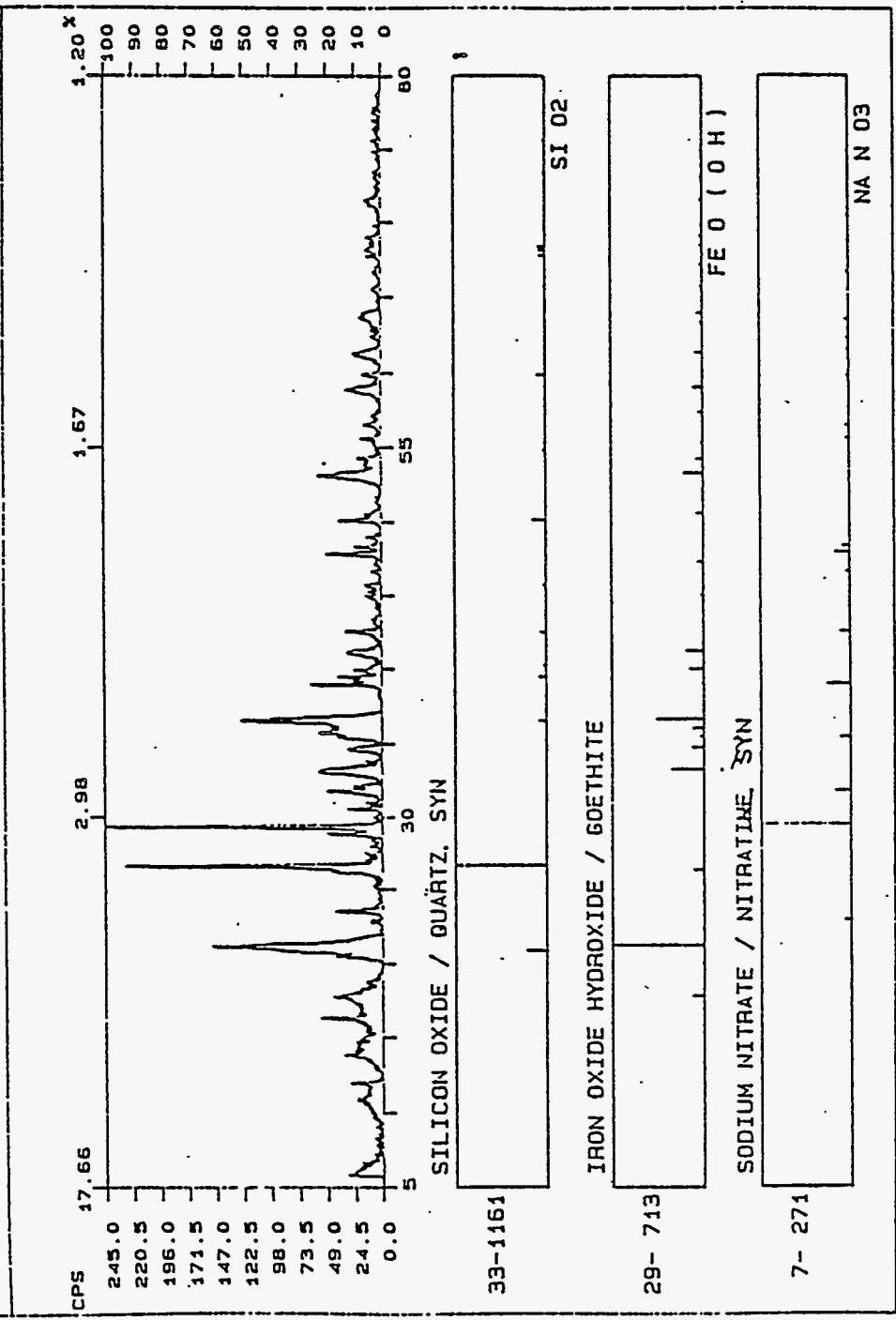
Figure B.3. Net Intensity Plot (background subtracted data) for Sample 202 24, Baseline Data
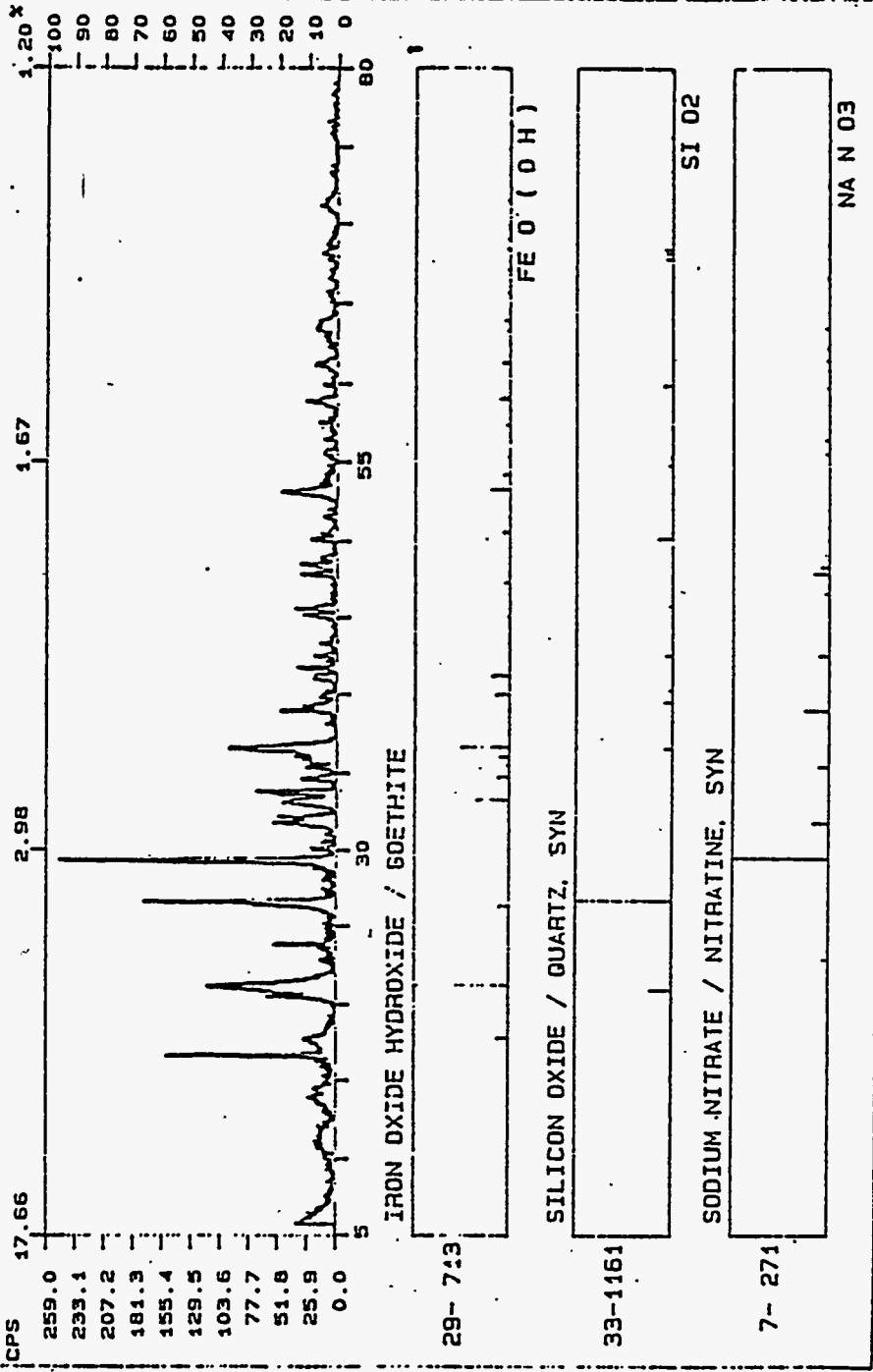
Figure B.4. Net Intensity Plot (background subtracted data) for Sample 202 8, Baseline Data

B.5
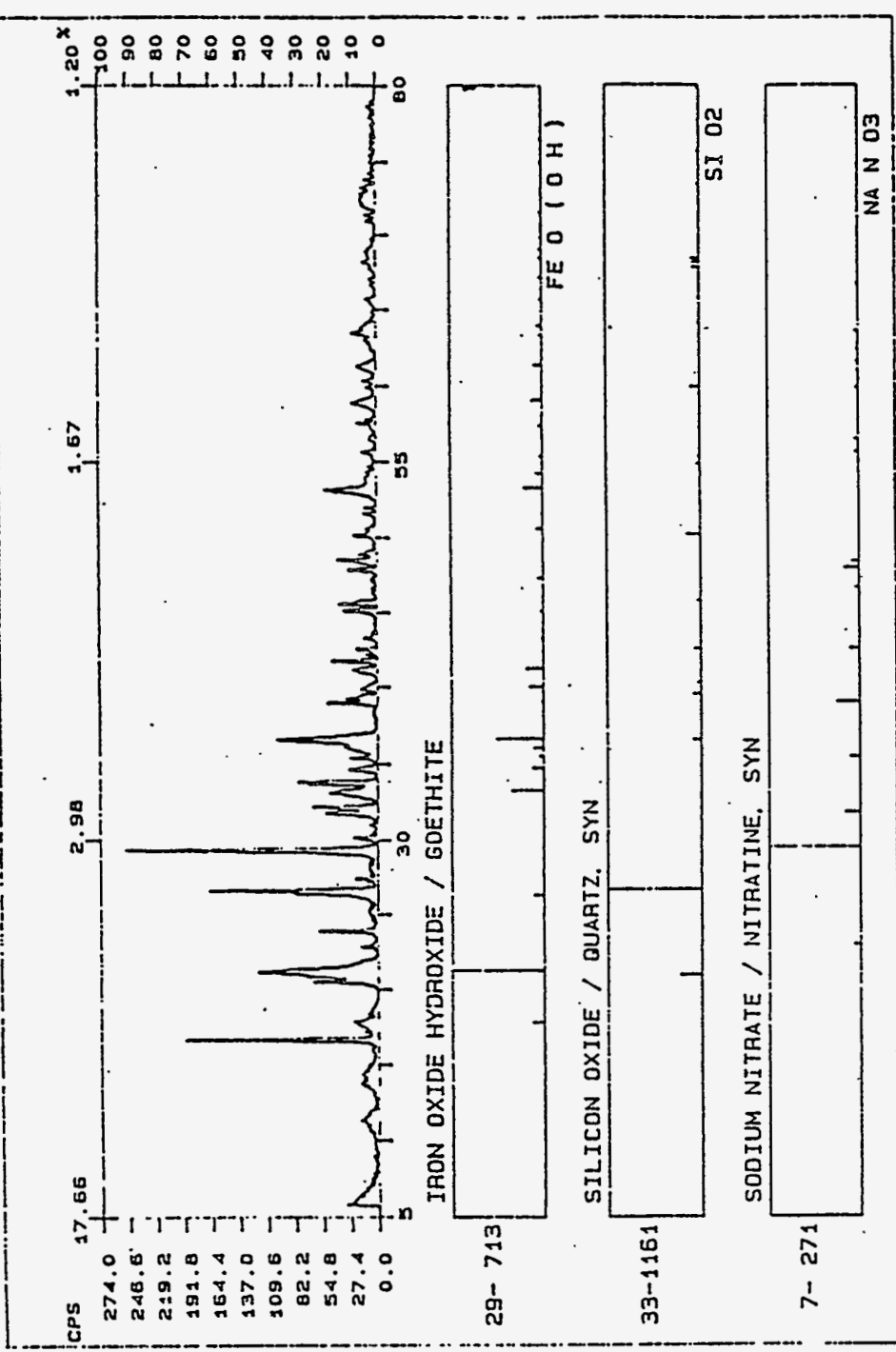
Figure B.5. Net Intensity Plot (background subtracted data) for Sample 202 2, Baseline Data

B.6
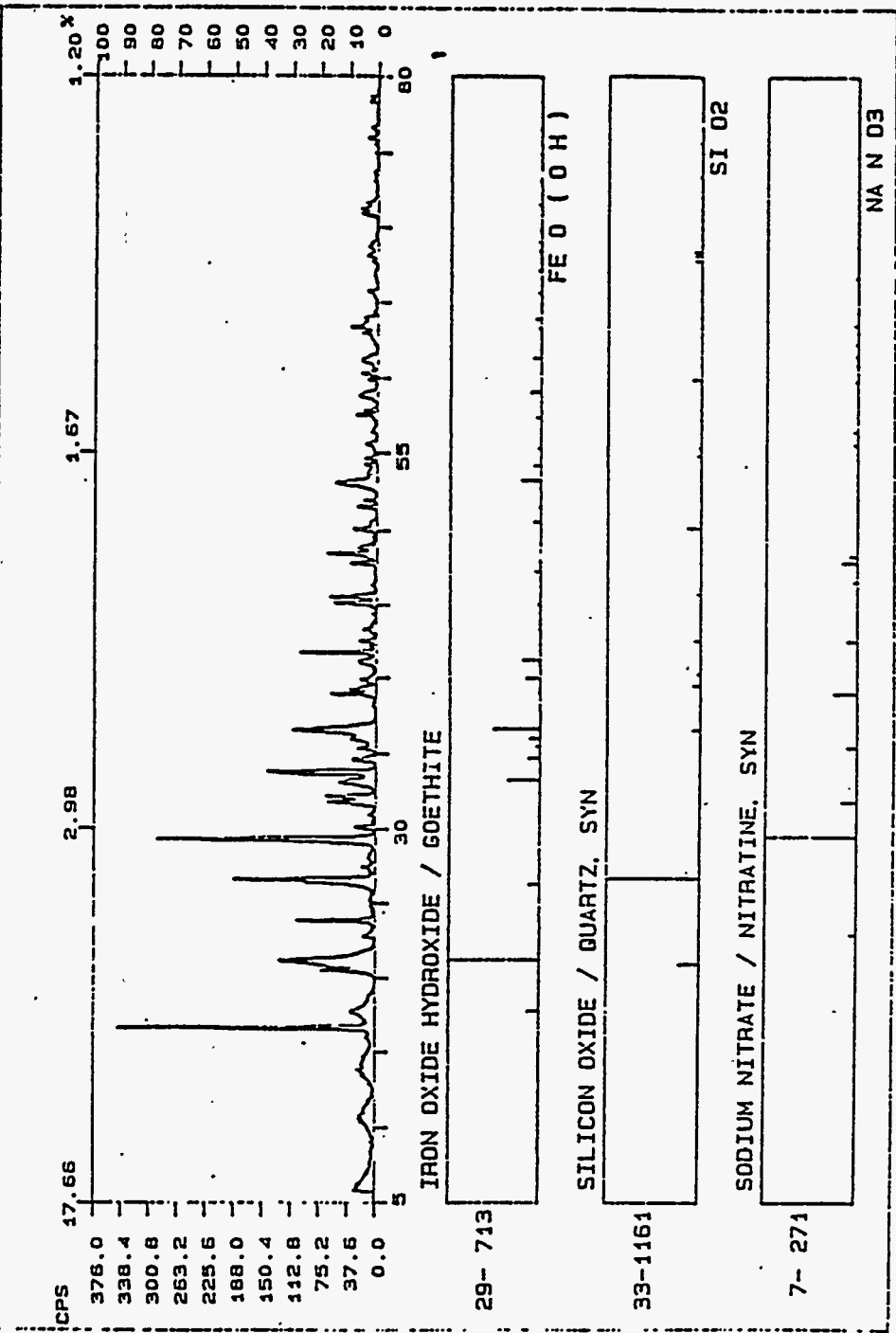
Figure B.6. Net Intensity Plot (background subtracted data) for Sample 202 NB, Baseline Data

B.7
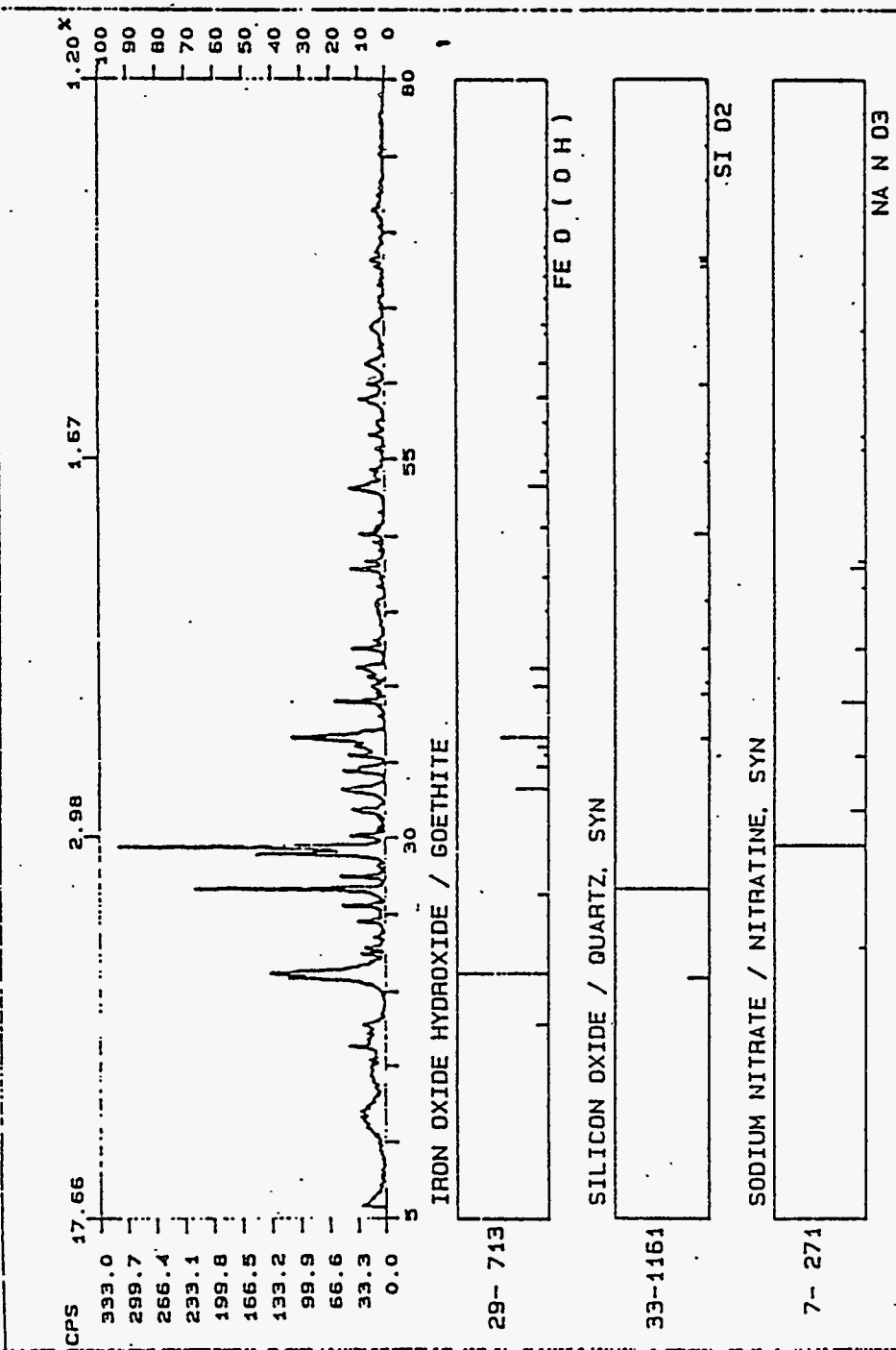
Figure B.7. Net Intensity Plot (background subtracted data) for Sample NF 24, Baseline Data

B.8
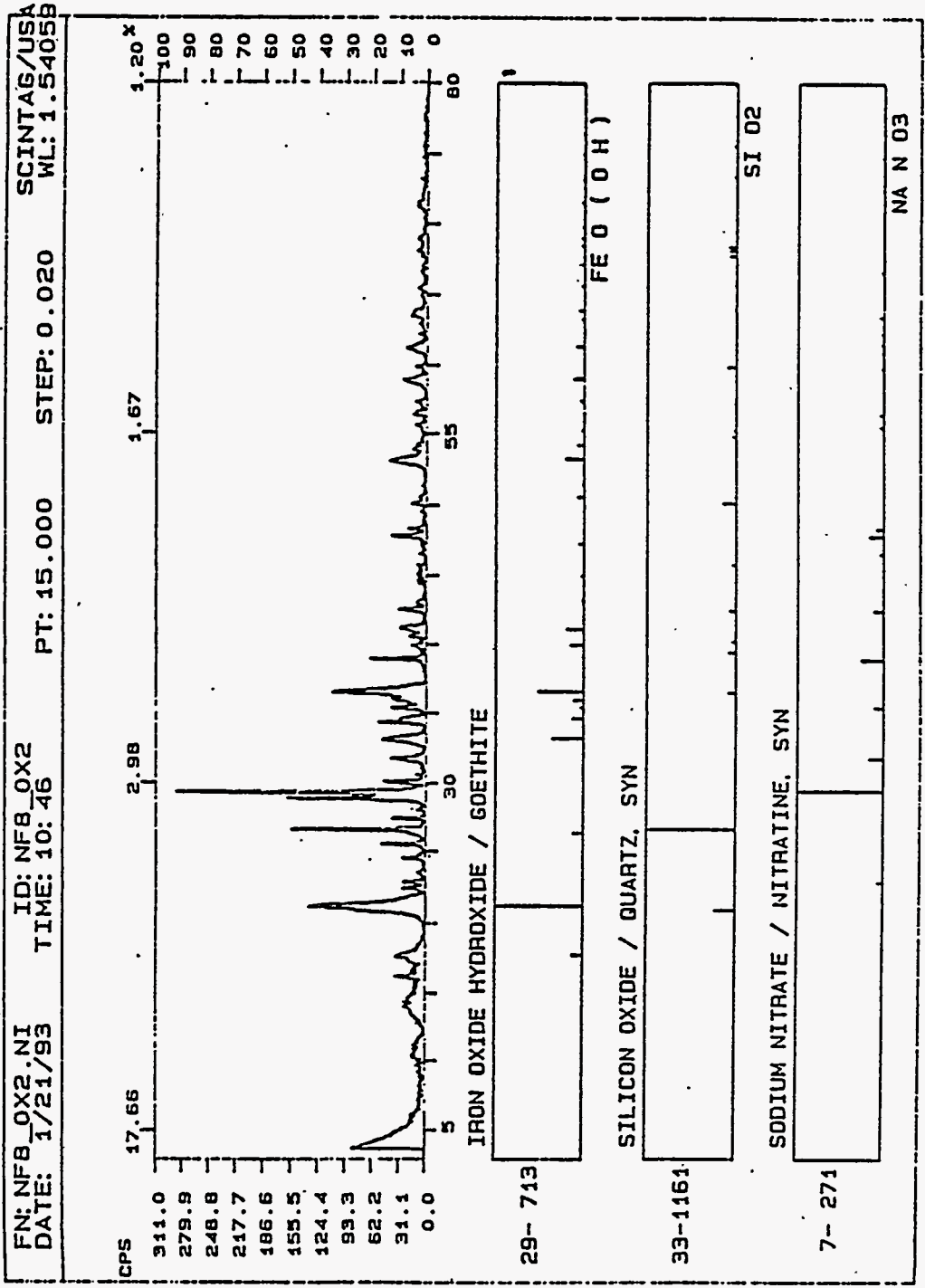
Figure B.8. Net Intensity Plot (background subtracted data) for Sample NF 8, Baseline Data

B.9
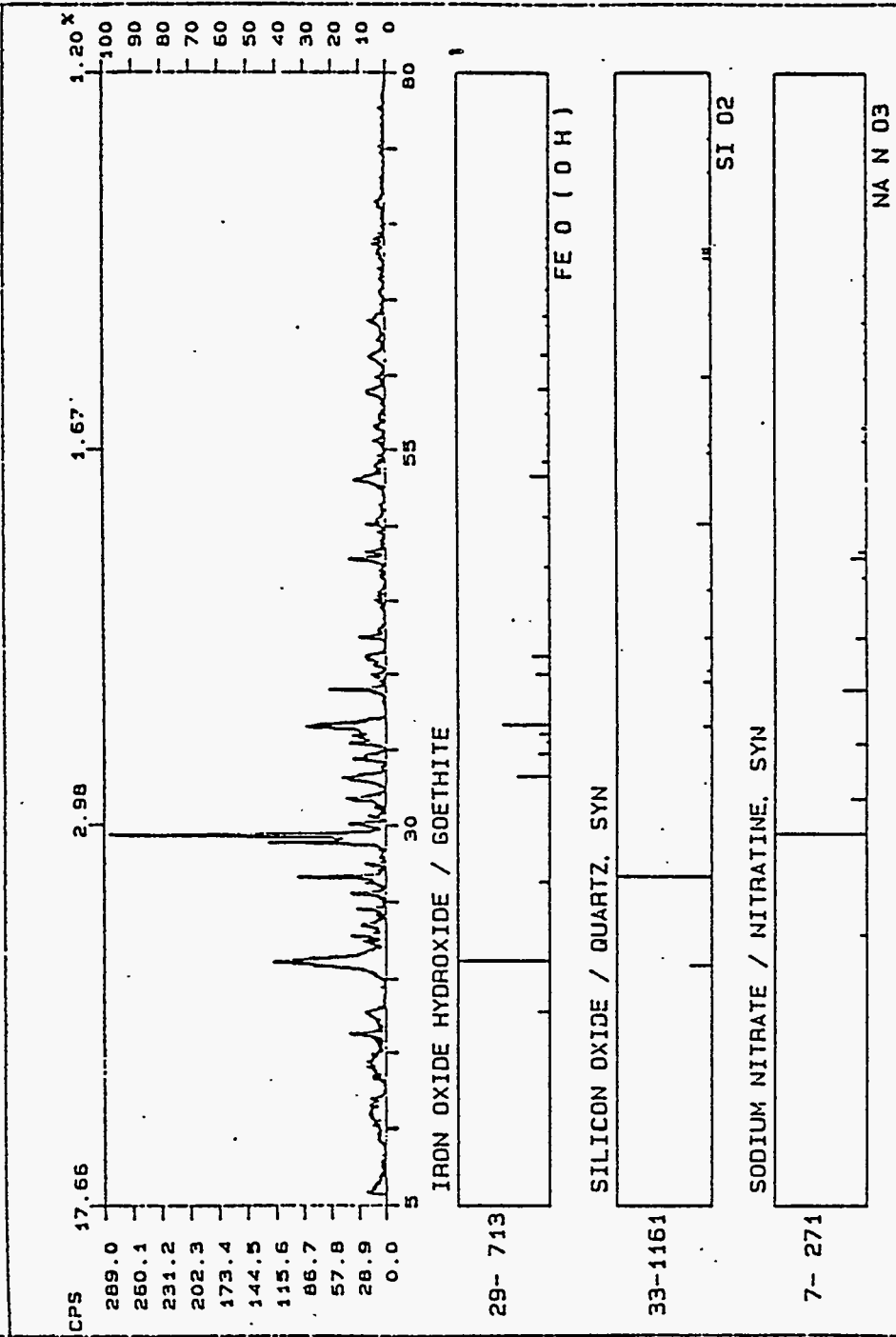
Figure B.9. Net Intensity Plot (background subtracted data) for Sample NF 2, Baseline Data
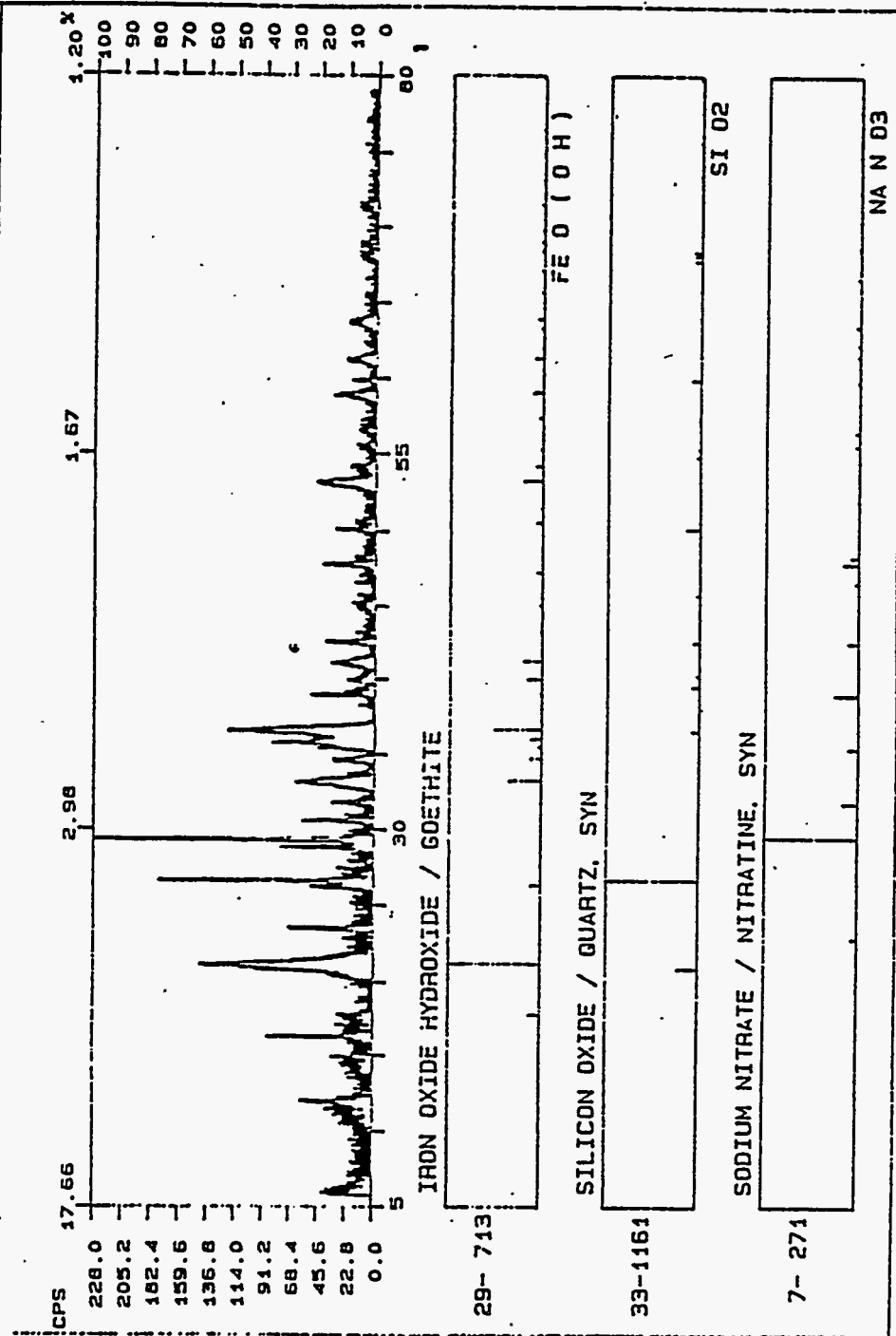
Figure B.10. Net Intensity Plot (background subtracted data) for Sample NF NB, Baseline Data

B.11

Table B.3. Most Intense Lines of Phases Found During Rheology Test, 1-Day Data, NF Samples

Phases Identified	RELATIVE INTENSITY			
ICDD Card Number	NF 24	NF 8	NF 2	NF NB
Na NO3/Nitratine 7-271	1.00	1.00	1.00	1.00
Si O2/Silicon Dioxide 33-1161	0.52	0.42	0.49	0.82
FeO OH/ Goethite 29-713	0.42	0.45	0.51	0.77
Unknown, 16.66 degree 2-theta	0.00	0.00	0.00	0.00

Table B.4. Most Intense Lines of Phases Found During Rheology Test, 1-Day Data, 202 Samples

Phases Identified	RELATIVE INTENSITY			
ICDD Card Number	202 24	202 8	202 2	202 NB
Na NO3/Nitratine 7-271	0.91	1.00	1.00	1.00
Si O2/Silicon Dioxide 33-1161	1.00	0.66	0.69	0.66
FeO OH/ Goethite 29-713	0.69	0.48	0.53	0.50
Unknown peak 16.66 degree 2-theta	0.00	0.40	0.86	1.40*

* Most intense peak considered to be Na NO3 to be consistent with table 1.
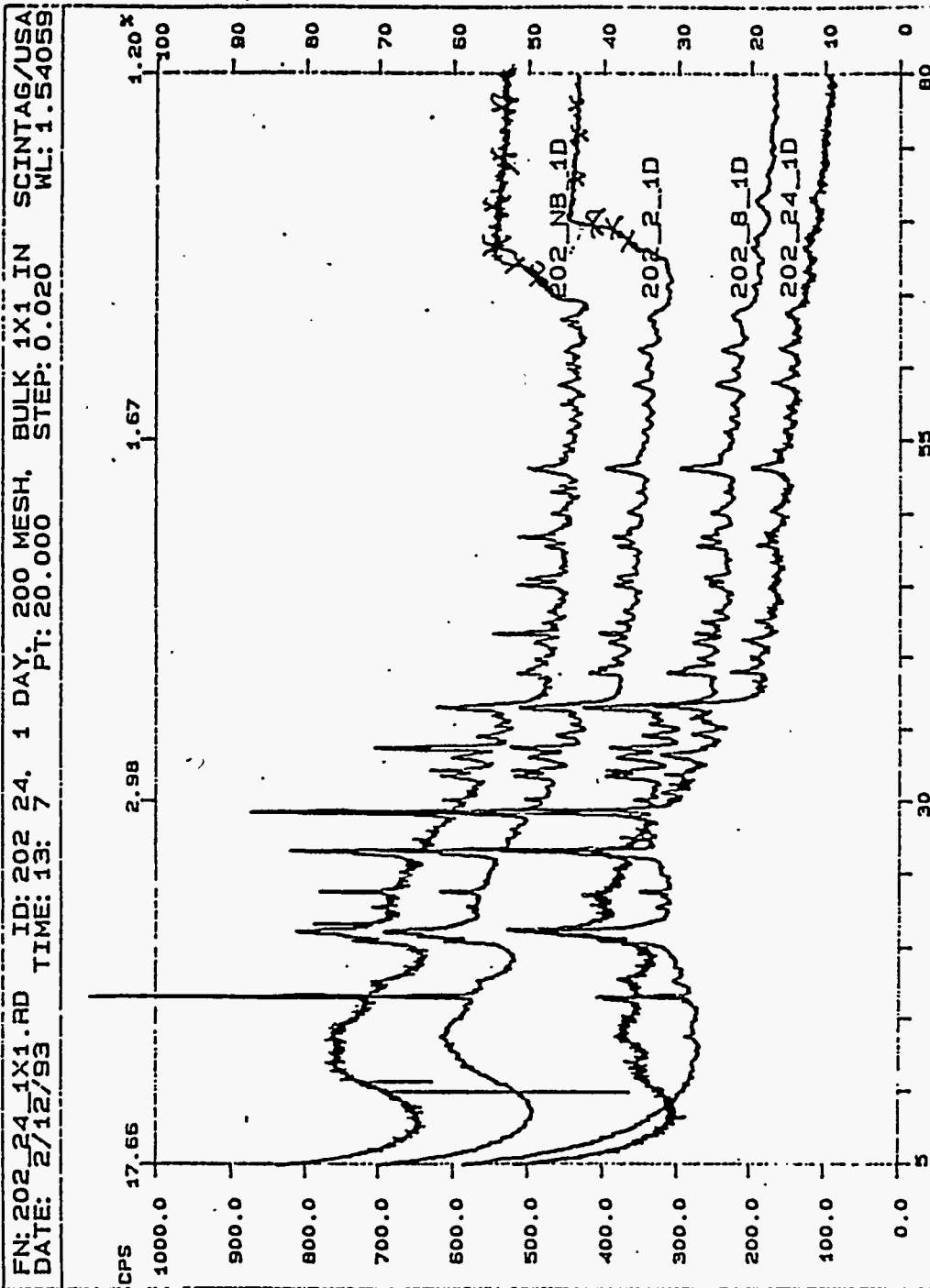
Figure B.11. Composite Plot of Raw Data for Samples 202 24, 202 8, 202 2, and 202 NB, 1-Day Data

B.13
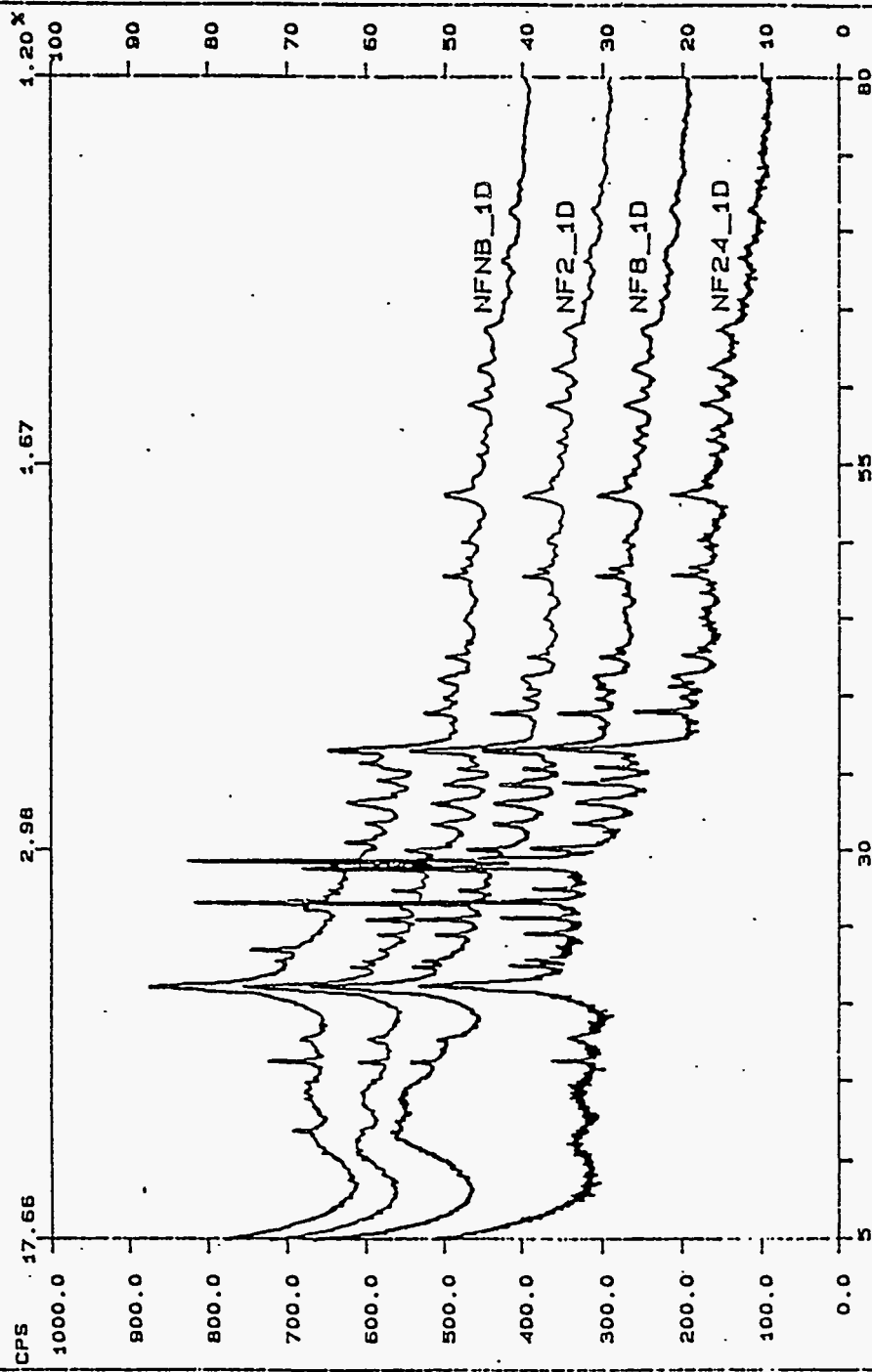
Figure B.12. Composite Plot of Raw Data for Samples NF 24, NF 8, NF 2, and NF NB, 1-Day Data
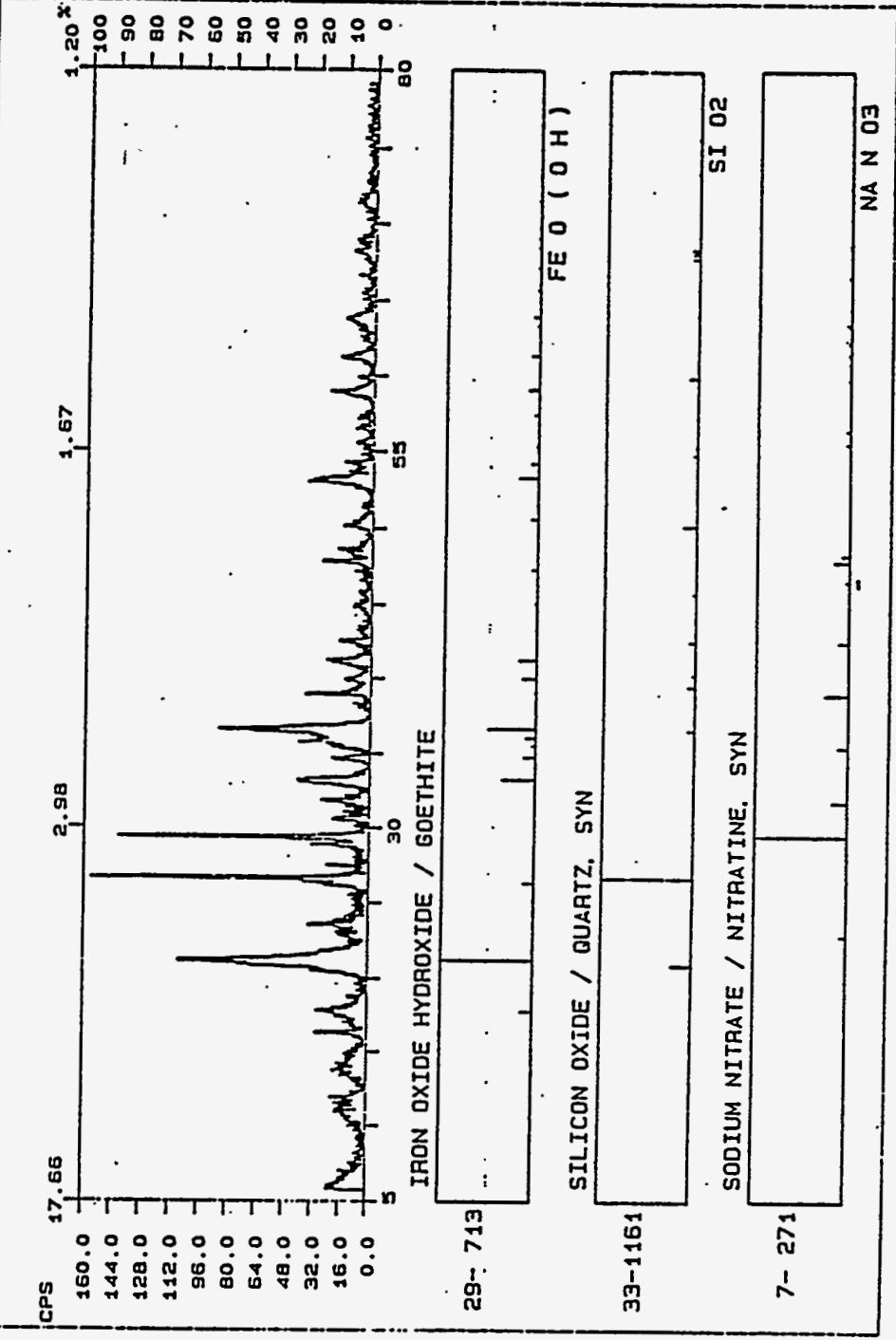
Figure B.13. Net Intensity Plot (background subtracted data) for Sample 202 24, 1-Day Data
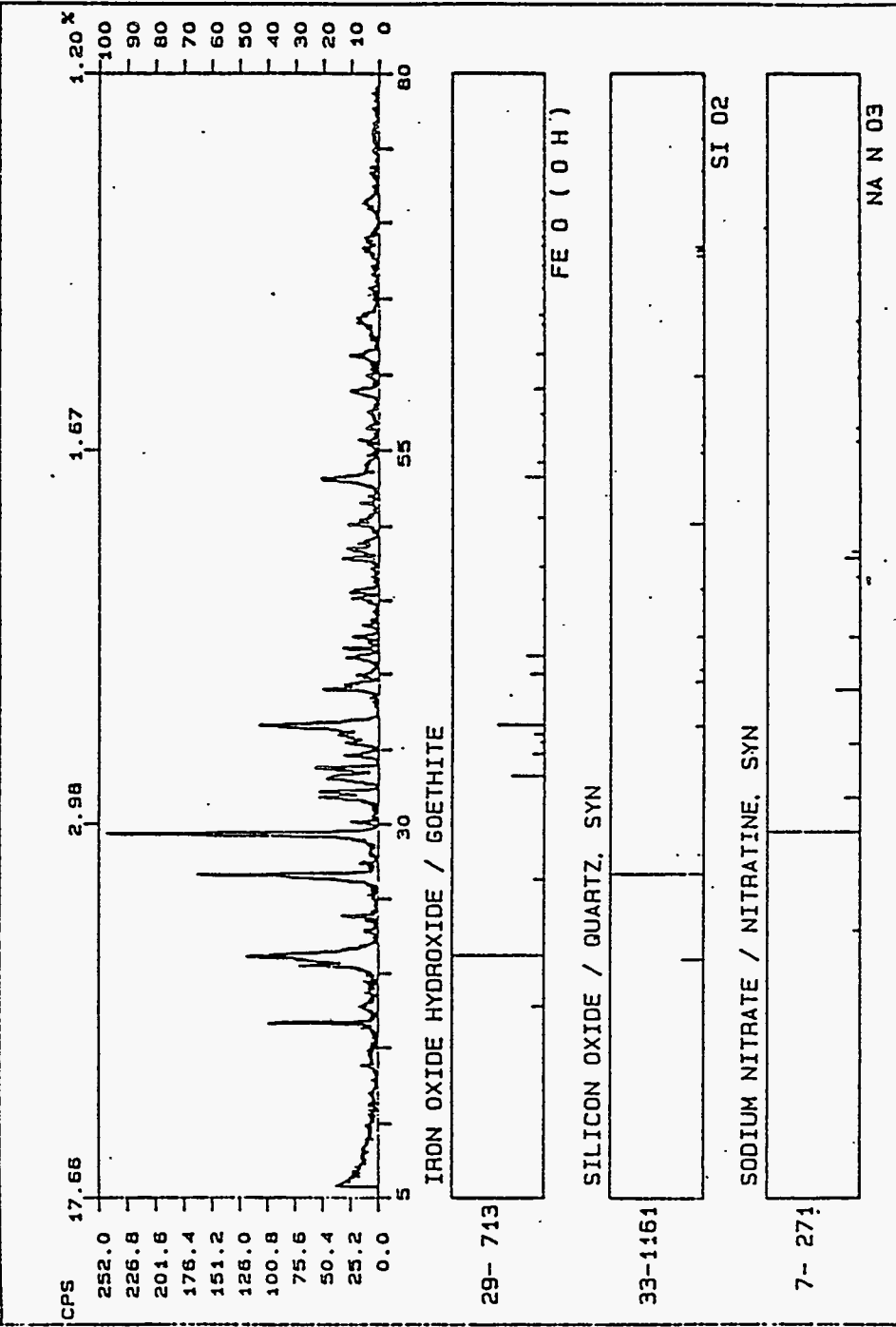
Figure B.14. Net Intensity Plot (background subtracted data) for Sample 202 8, 1-Day Data
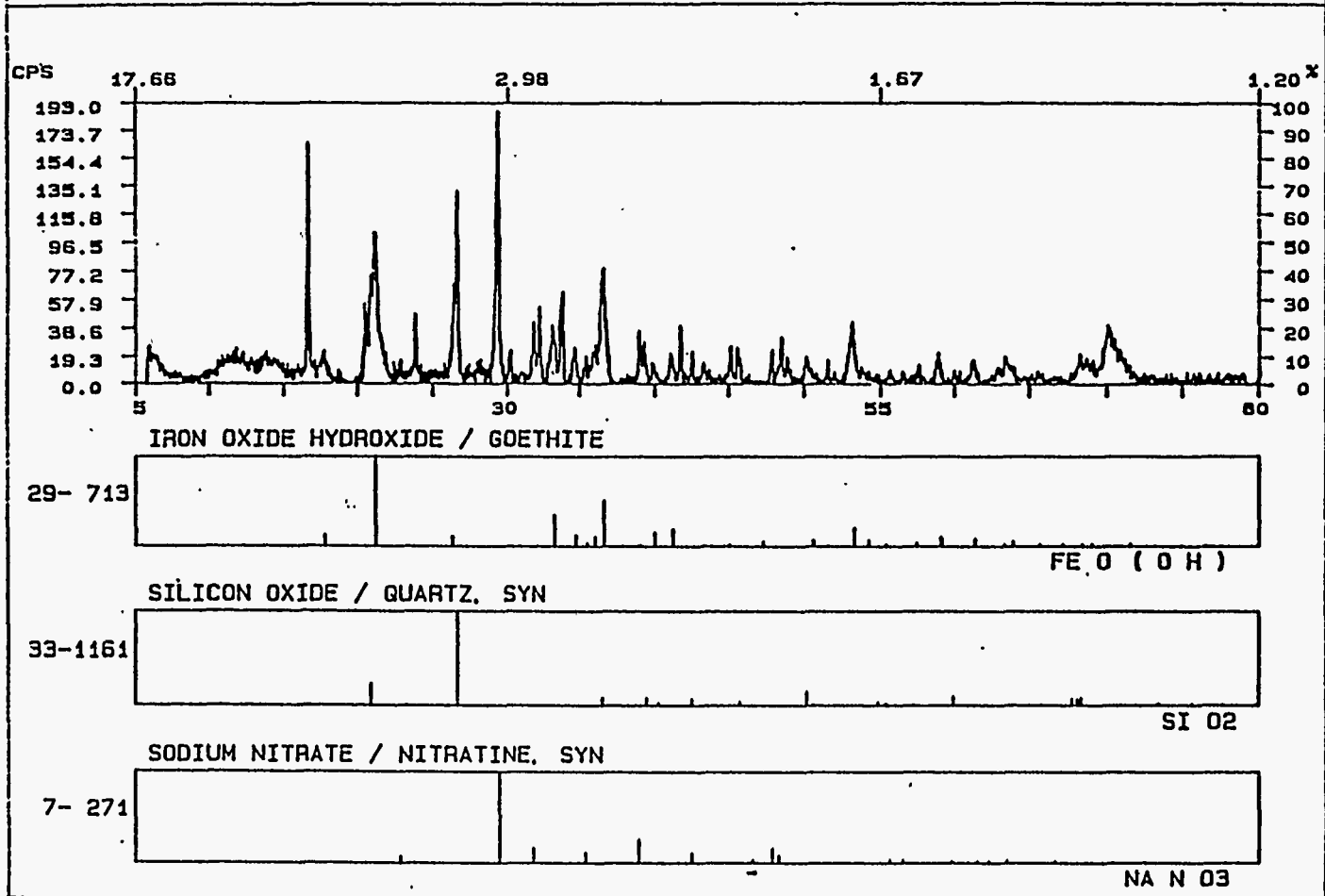
Figure B.15. Net Intensity Plot (background subtracted data) for Sample 202 2, 1-Day Data

FN: 202_NB_1X1.NI   ID: 202_NB.   1 DAY, 200 MESH,   BULK 1X1 IN   SCINTAG/USA
DATE: 2/16/93   TIME: 9: 6   PT: 20.000   STEP: 0.020   WL: 1.54059

CPS

285.0
256.5
228.0
199.5
171.0
142.5
114.0
85.5
57.0
28.5
0.0

17.68   2.98   1.67   1.20 ×

100
90
80
70
60
50
40
30
20
10
0

5   30   55   80

IRON OXIDE HYDROXIDE / GOETHITE

29- 713   FE O (O H)

SILICON OXIDE / QUARTZ, SYN

33-1161   SI O2

SODIUM NITRATE / NITRATINE, SYN

7- 271   NA N O3
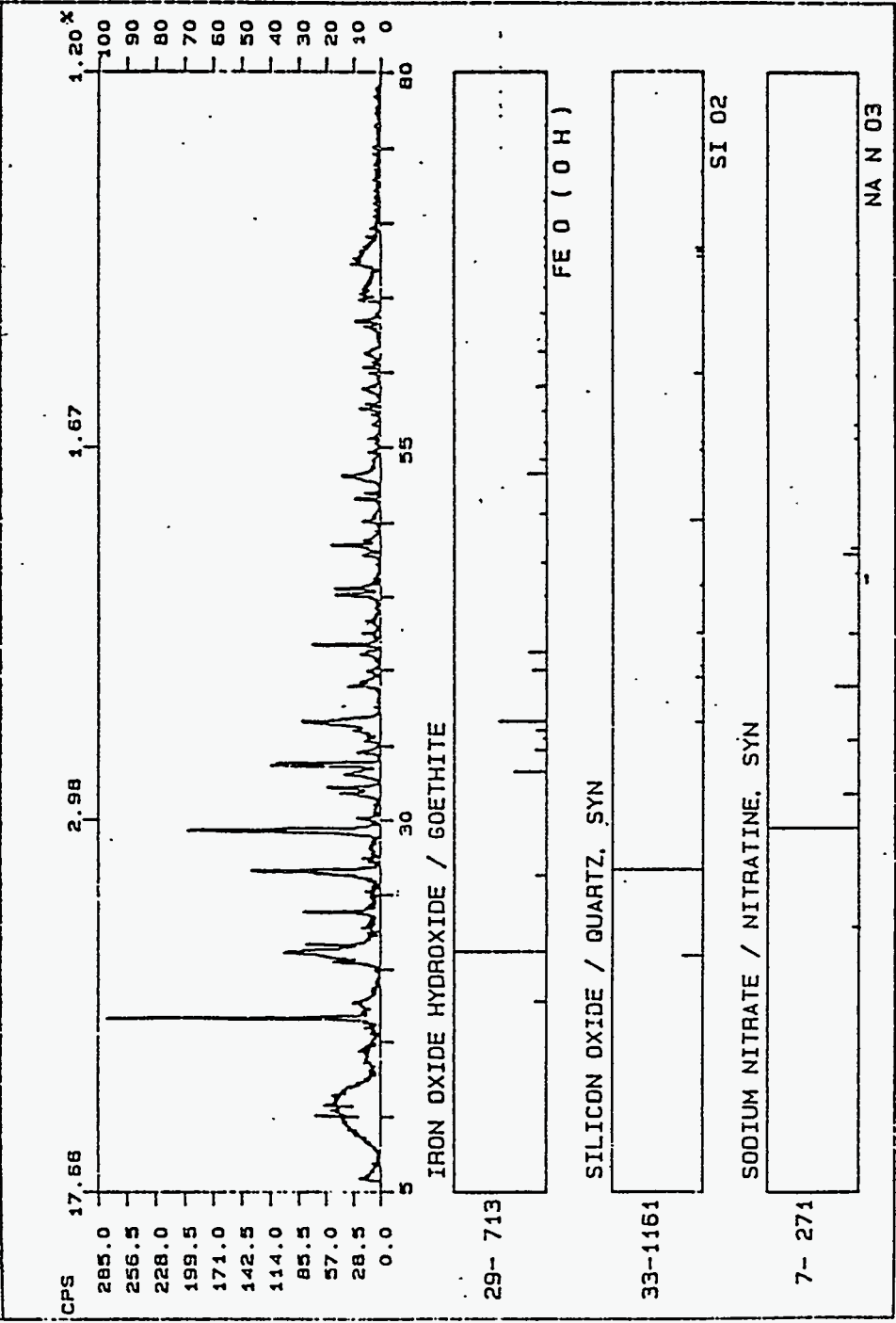
Figure B.16. Net Intensity Plot (background subtracted data) for Sample 202 NB, 1-Day Data

B.18
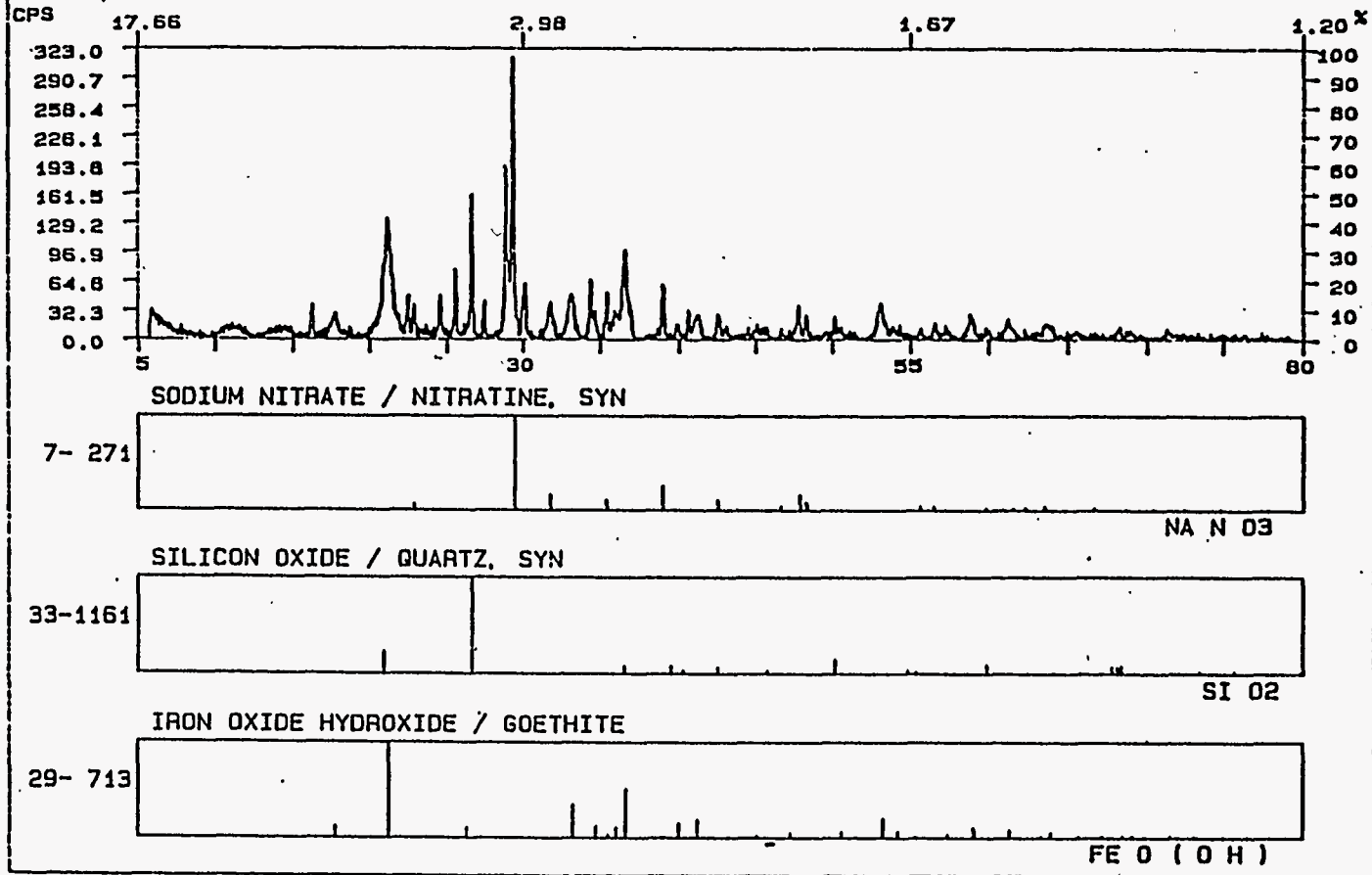
Figure B.17. Net Intensity Plot (background subtracted data) for Sample NF 24, 1-Day Data

FN: NF8_1X1.NI   ID: NF8. 1 DAY, FILTERED PARTICLES, BULK   SCINTAG/USA
DATE: 1/22/93   TIME: 11:45   PT: 20.000   STEP: 0.020   WL: 1.54059
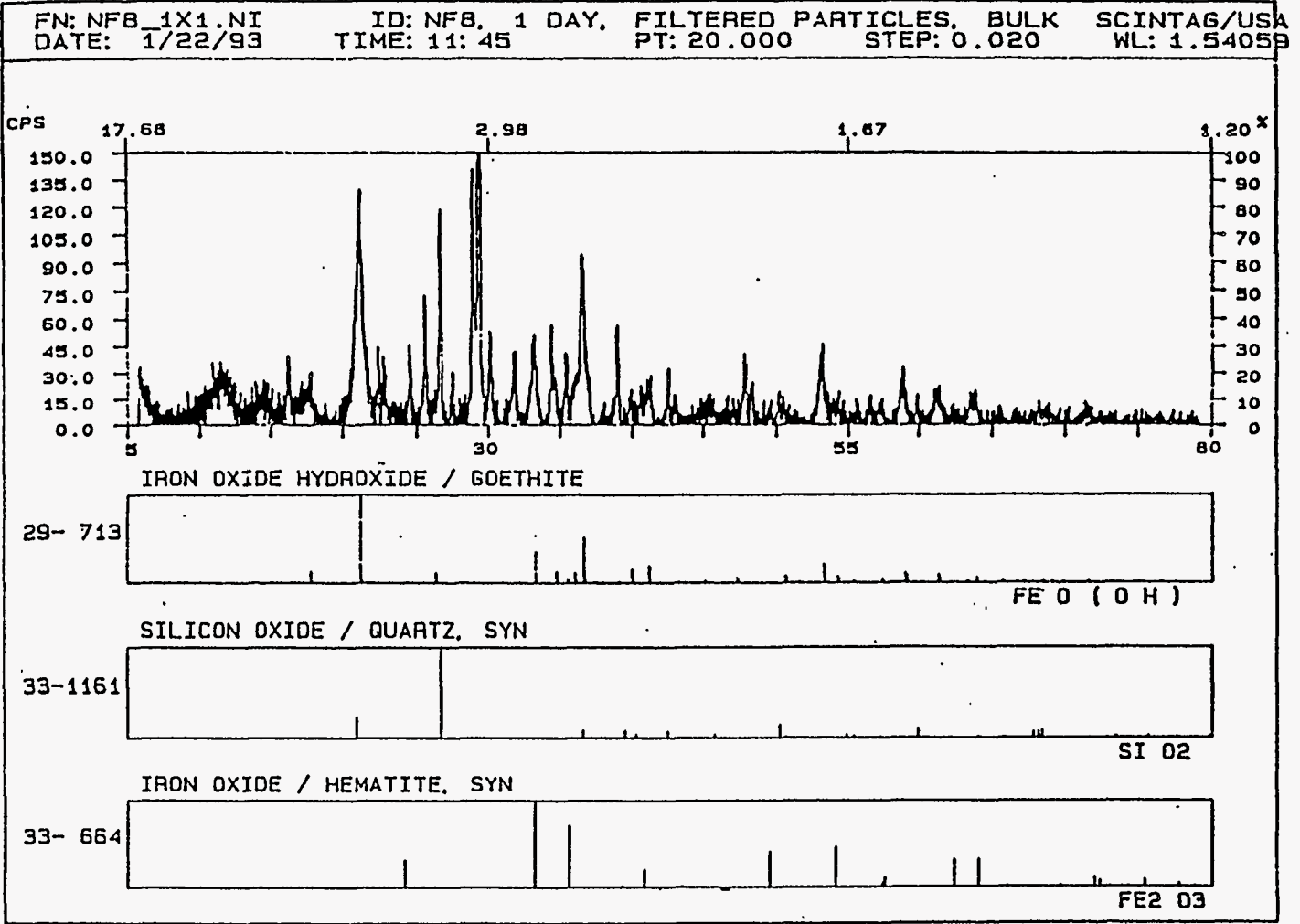
Figure B.18. Net Intensity Plot (background subtracted data) for Sample NF 8, 1-Day Data
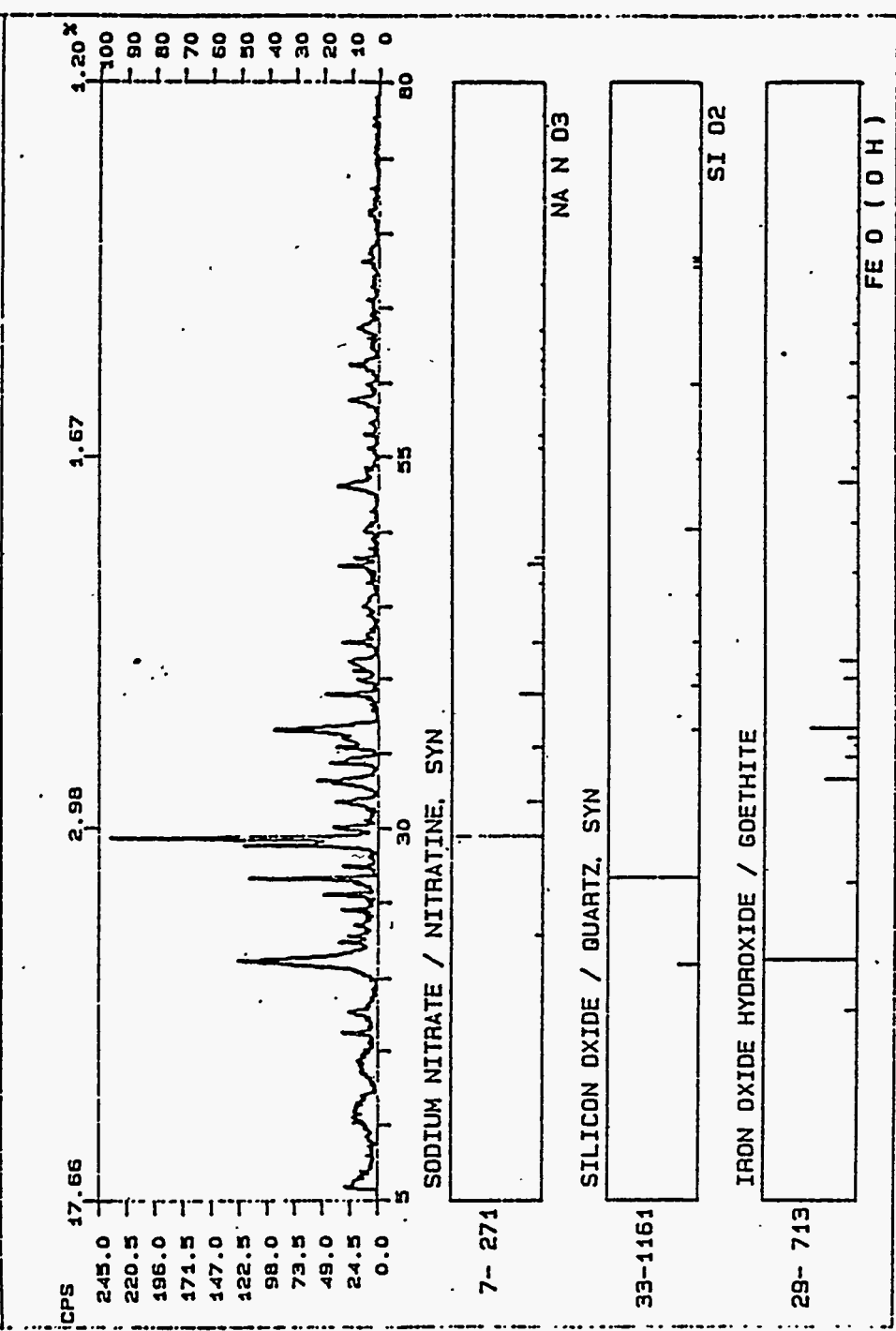
Figure B.19. Net Intensity Plot (background subtracted data) for Sample NF 2, 1-Day Data
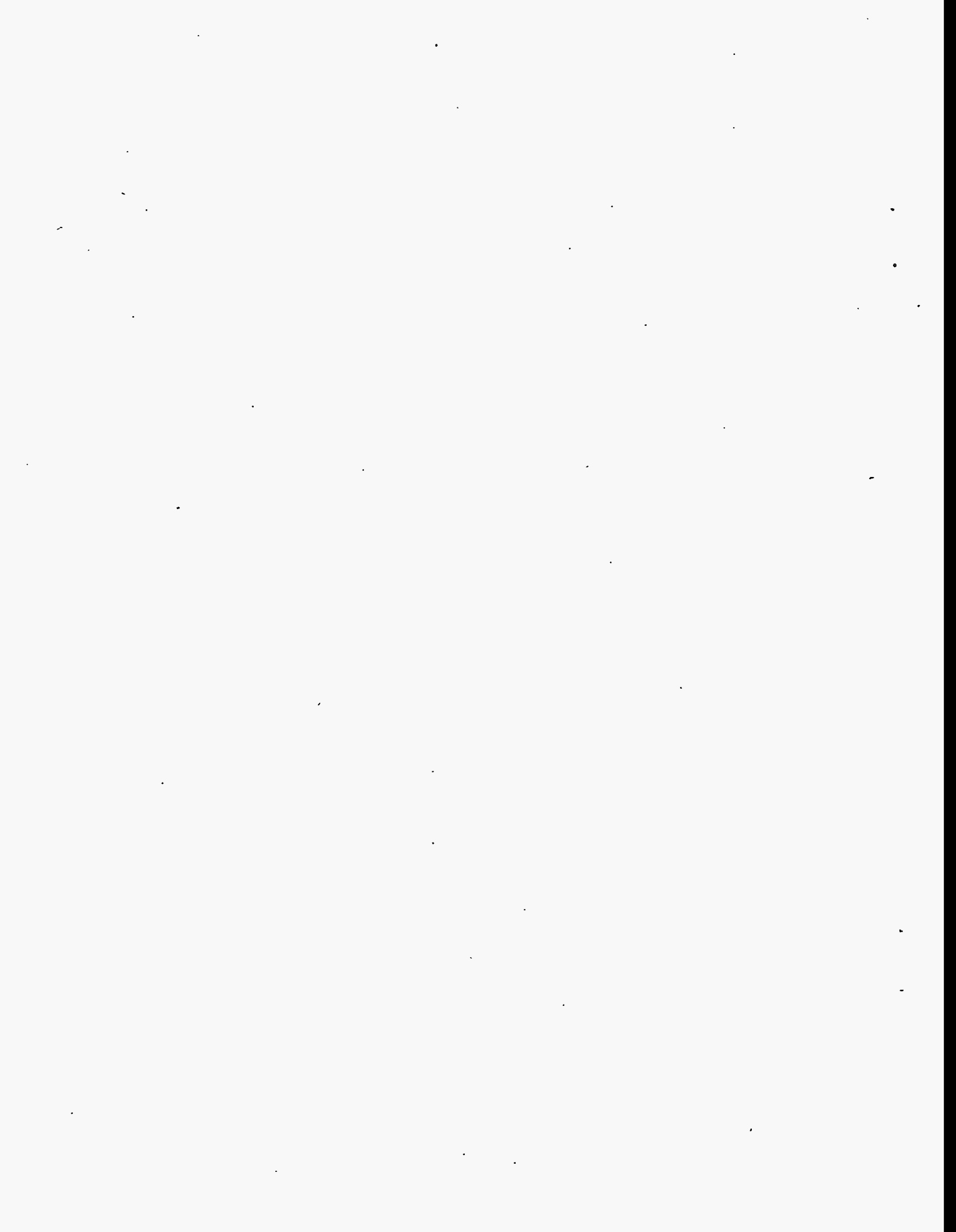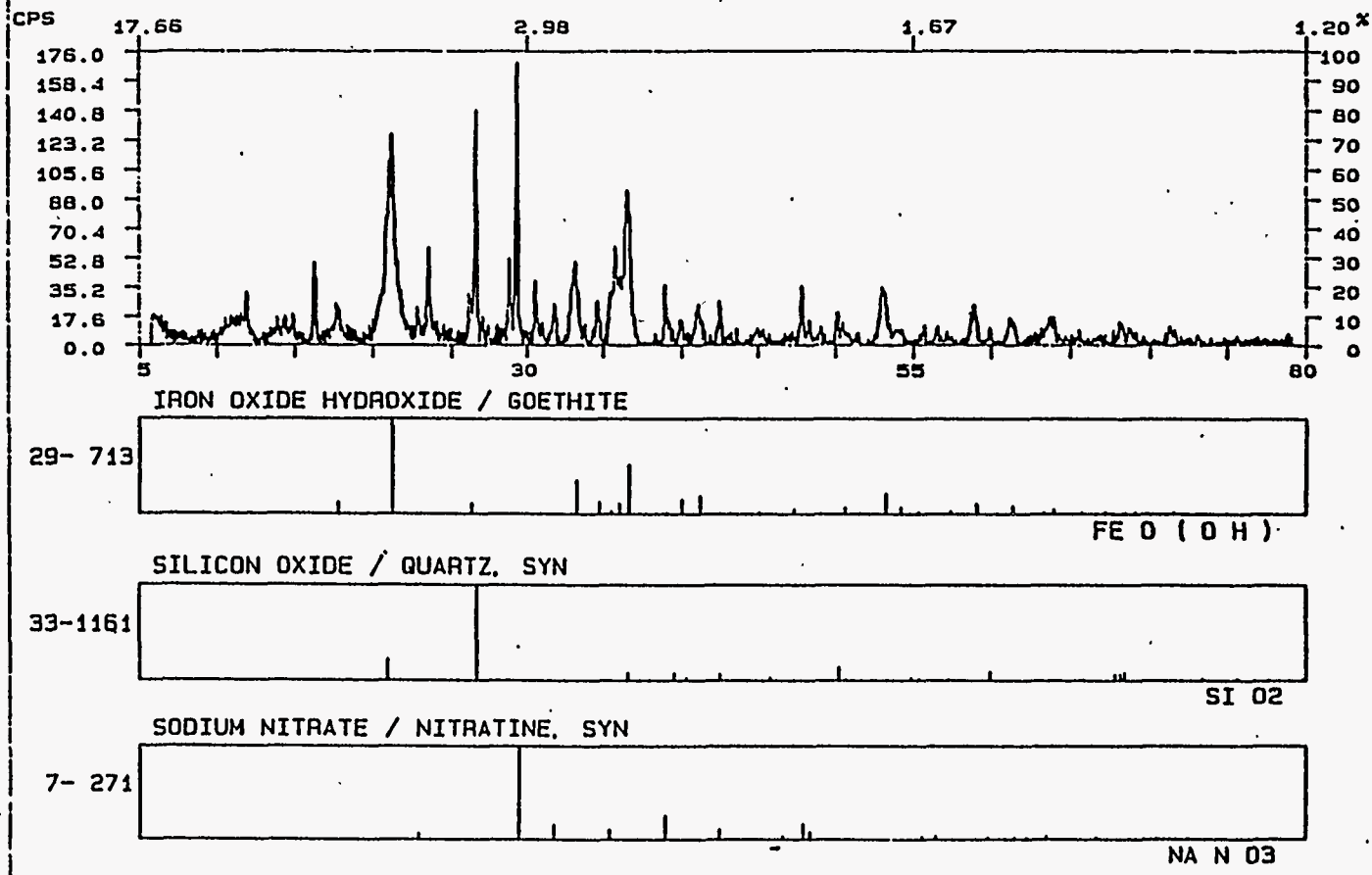
Figure B.20. Net Intensity Plot (background subtracted data) for Sample NF NB, 1-Day Data
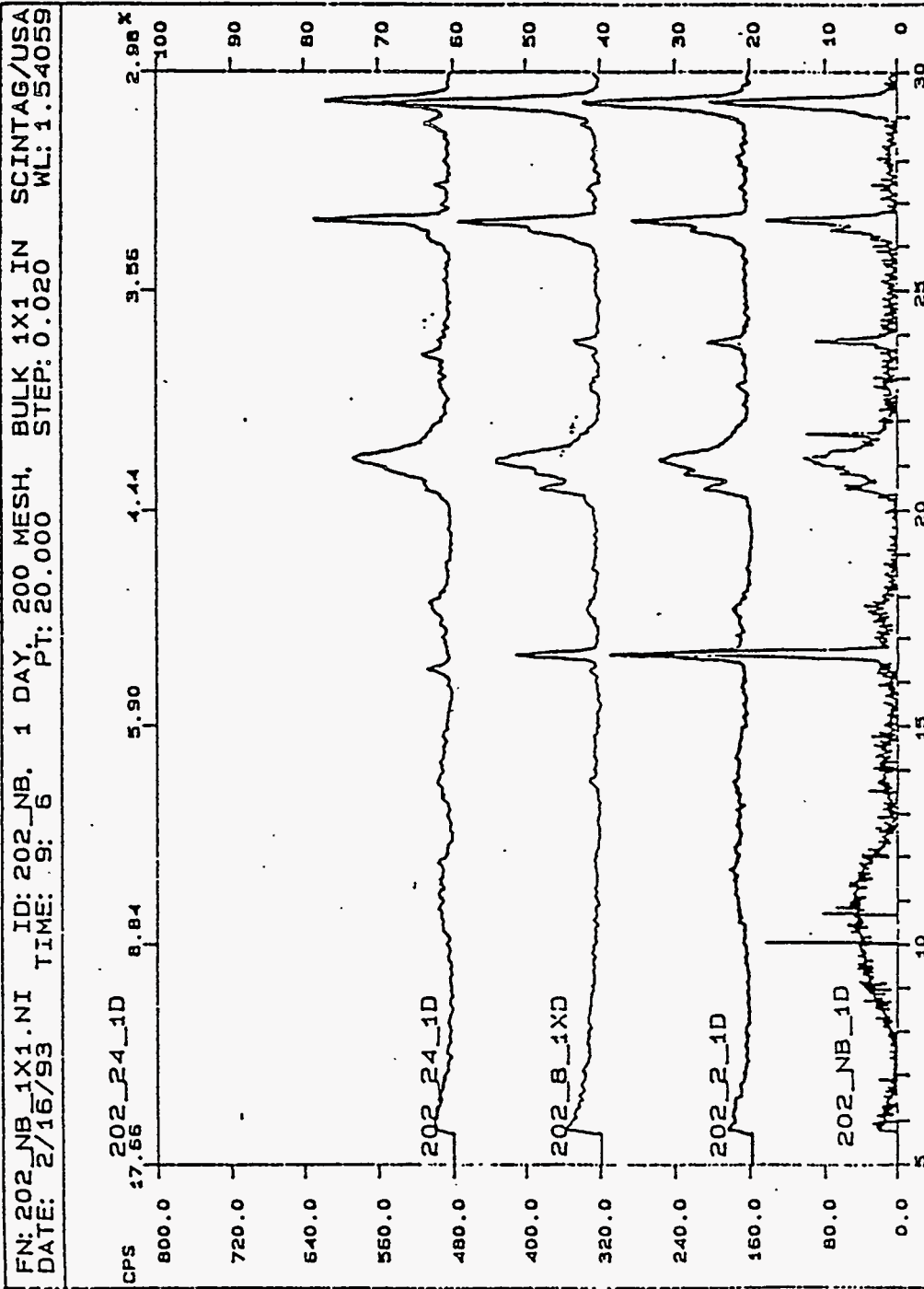
Figure B.21a. Net Intensity Plots (background subtracted data, 1-day data) for Samples 202 NB, 202 2, 202 8, and 202 24. Five to 30 degrees 2-theta, major peaks.
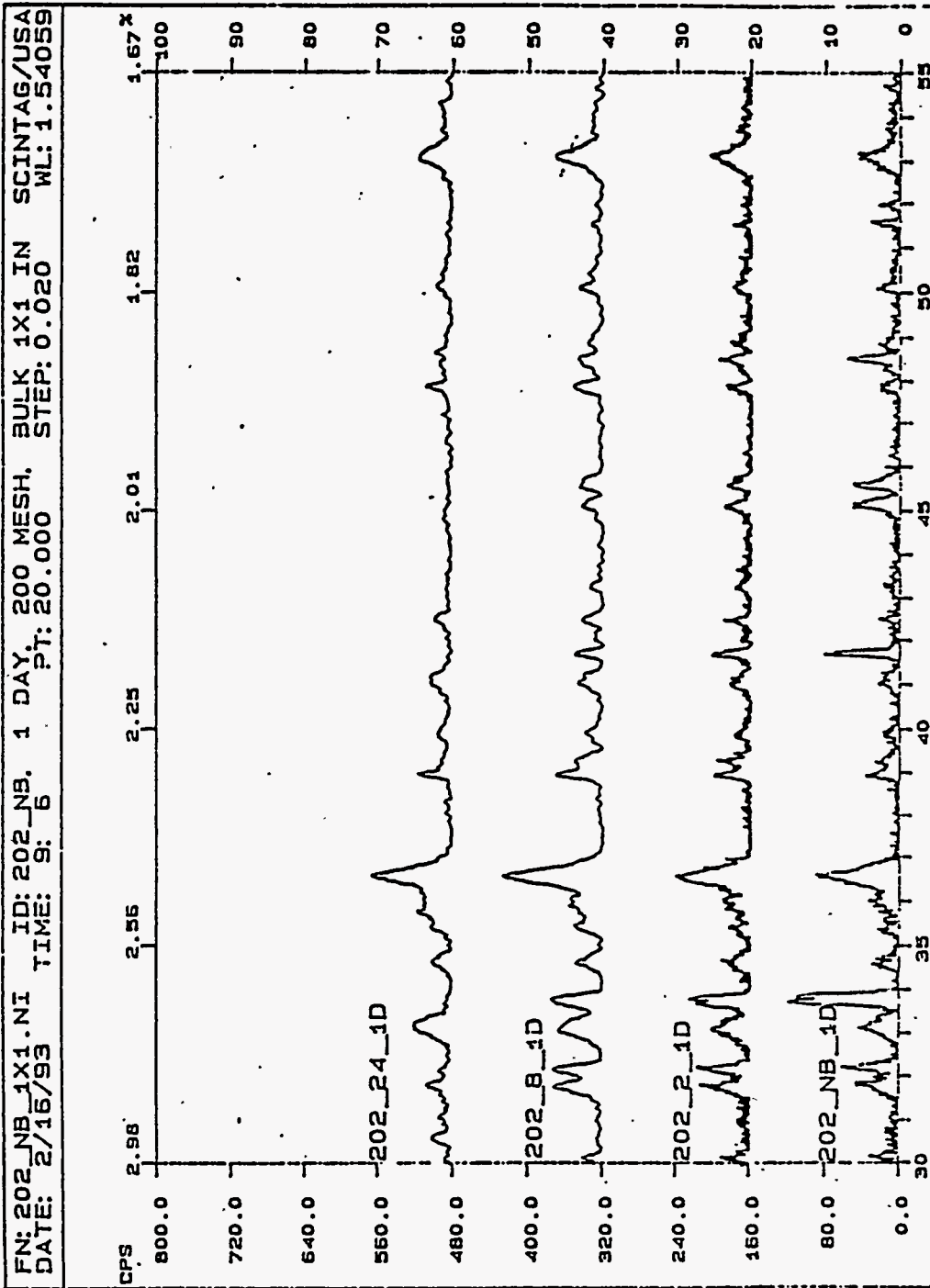
Figure B.21b. Net Intensity Plots (background subtracted data, 1-day data) for Samples 202 NB, 202 2, 202 8, and 202 24. Thirty to 55 degrees 2-theta, major peaks.

B.24

Figure B.21c. Net Intensity Plots (background subtracted data, 1-day data) for Samples 202 NB, 202 2, 202 8, and 202 24. Fifty-five to 80 degrees 2-theta, major peaks.
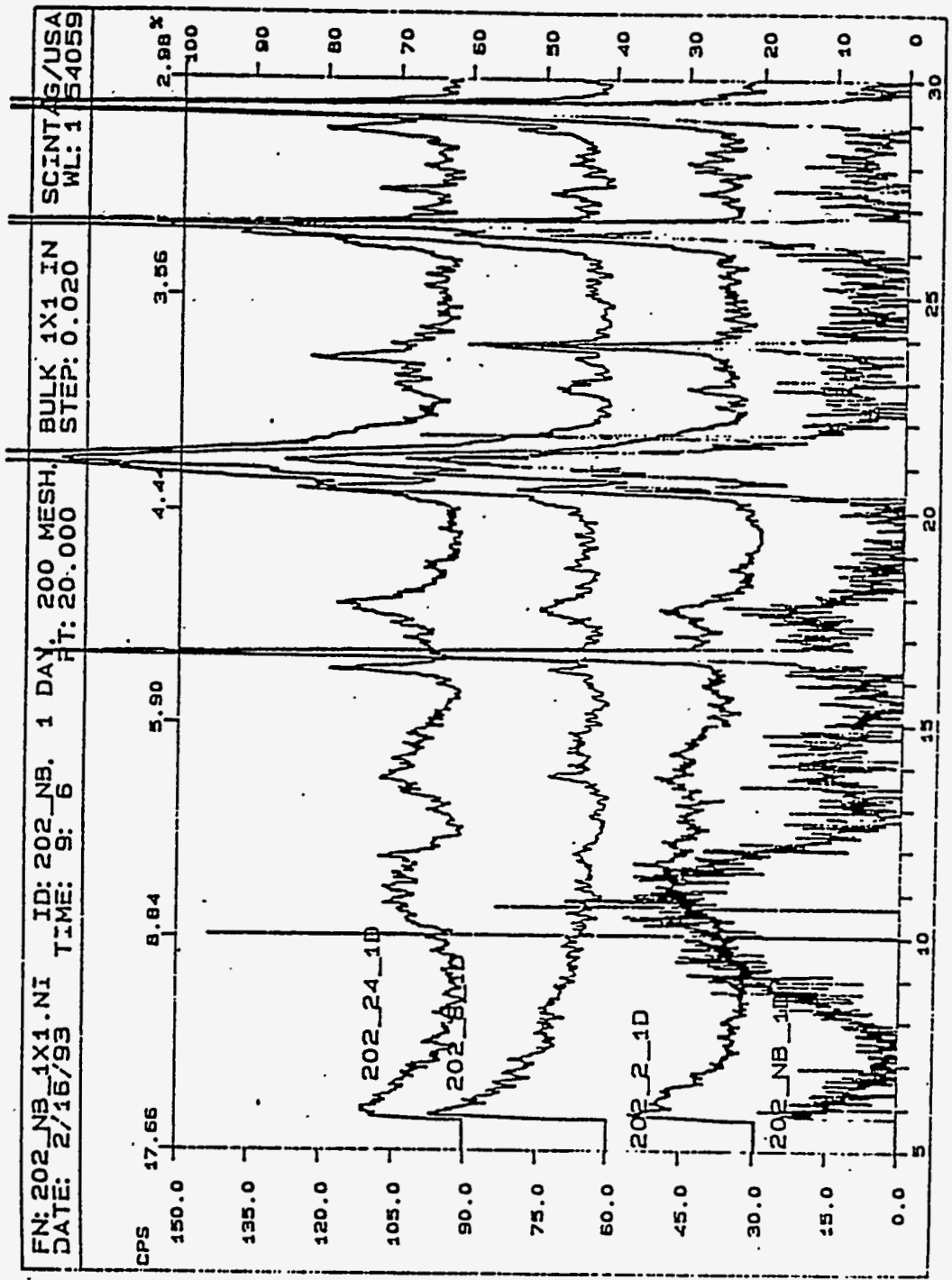
Figure B.22a. Net Intensity Plots (background subtracted data, 1-day data) for Samples 202 NB, 202 2, 202 8, and 202 24. Five to 30 degrees 2-theta, minor peaks.

FN: 202_NB_1X1.NI   ID: 202_NB, 1 DAY, 200 MESH, BULK 1X1 IN   SCINTAG/USA
DATE: 2/16/'93   TIME: 9: 6   PT: 20.000   STEP: 0.020   WL: 1.54059
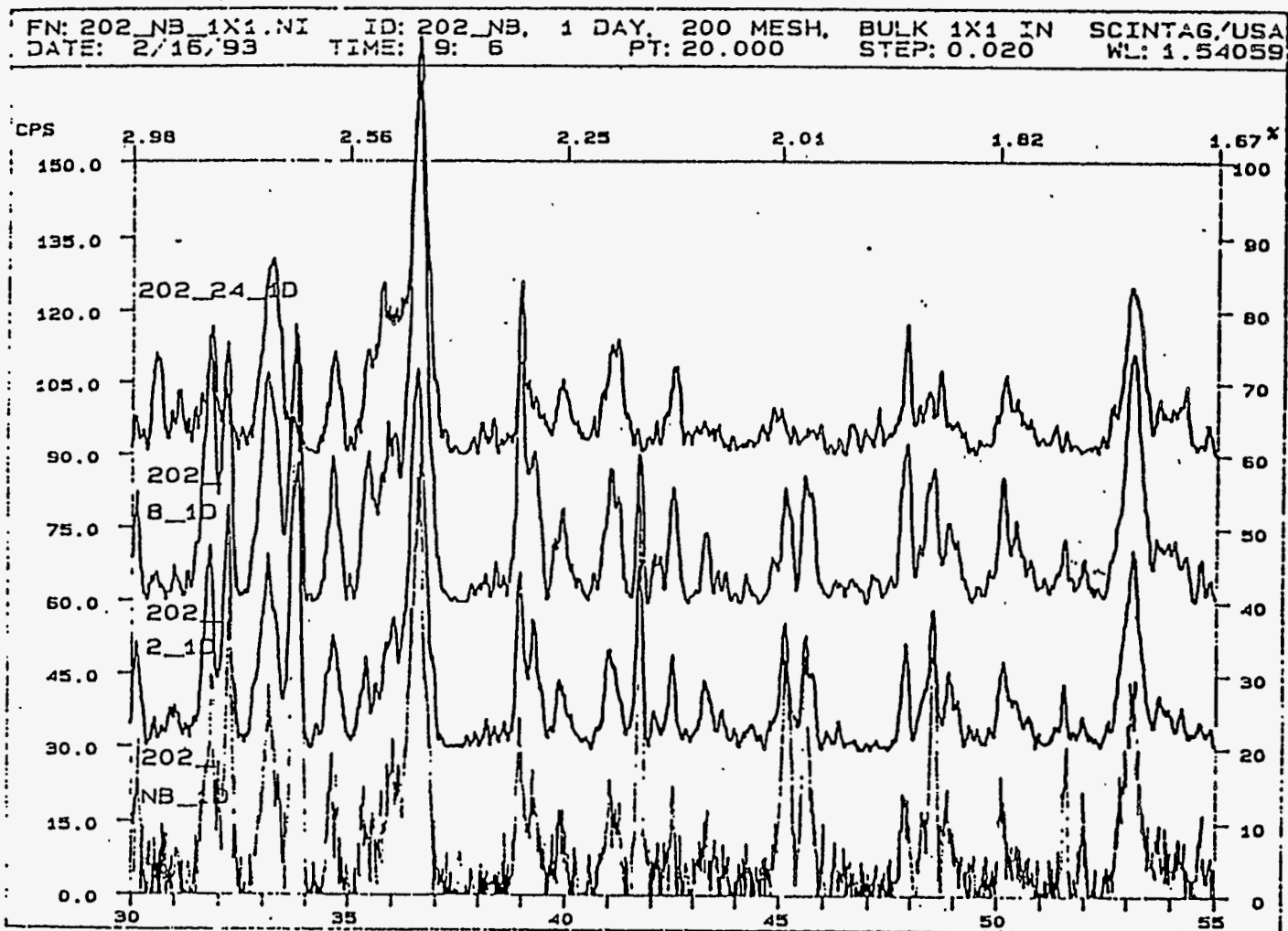
Figure B.22b. Net Intensity Plots (background subtracted data, 1-day data) for Samples 202 NB, 202 2, 202 8, and 202 24. Thirty to 55 degrees 2-theta, minor peaks.
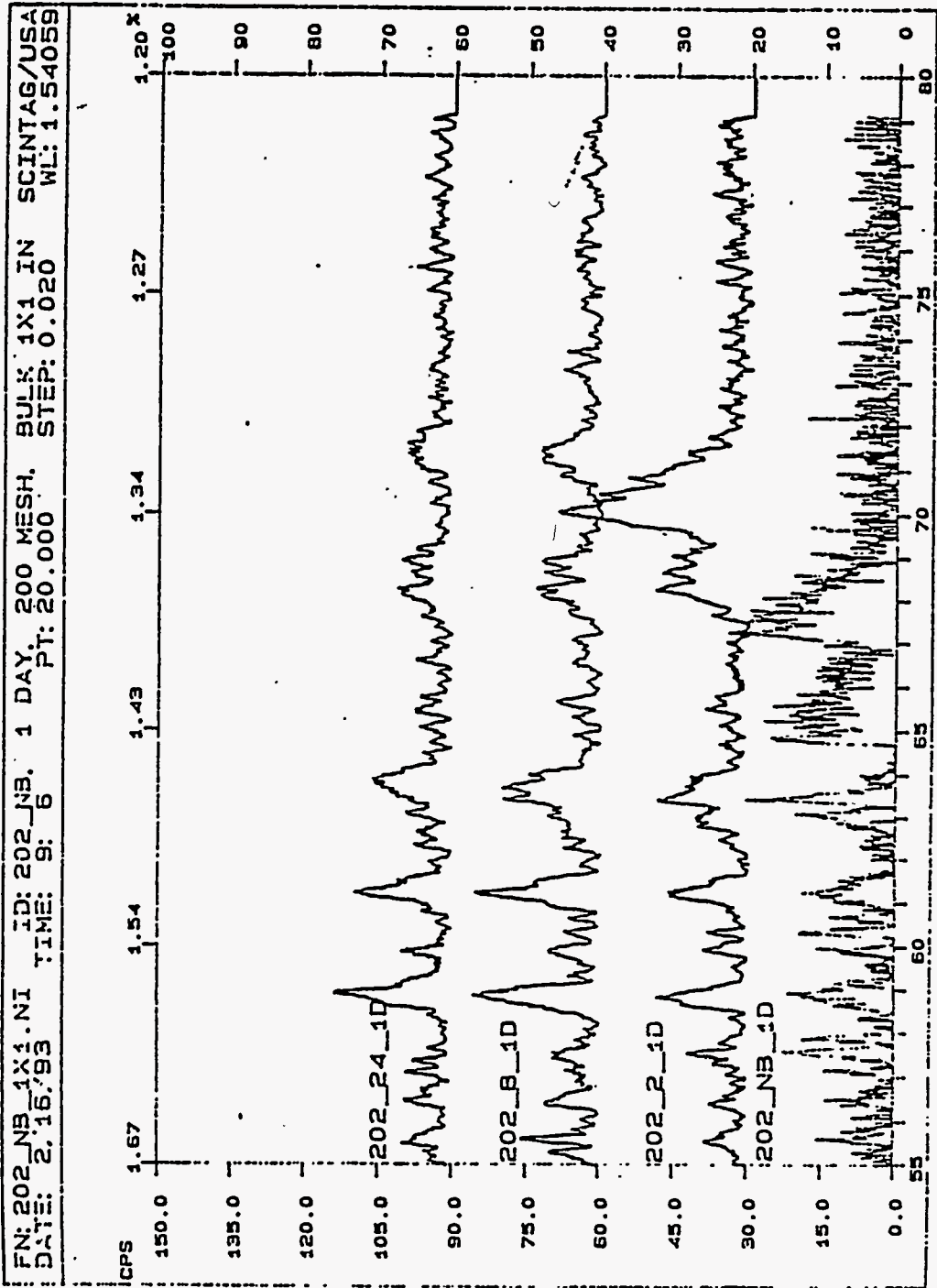
Figure B.22c. Net Intensity Plots (background subtracted data, 1-day data) for Samples 202 NB, 202 2, 202 8, and 202 24. Fifty-five to 80 degrees 2-theta, minor peaks.

B.28
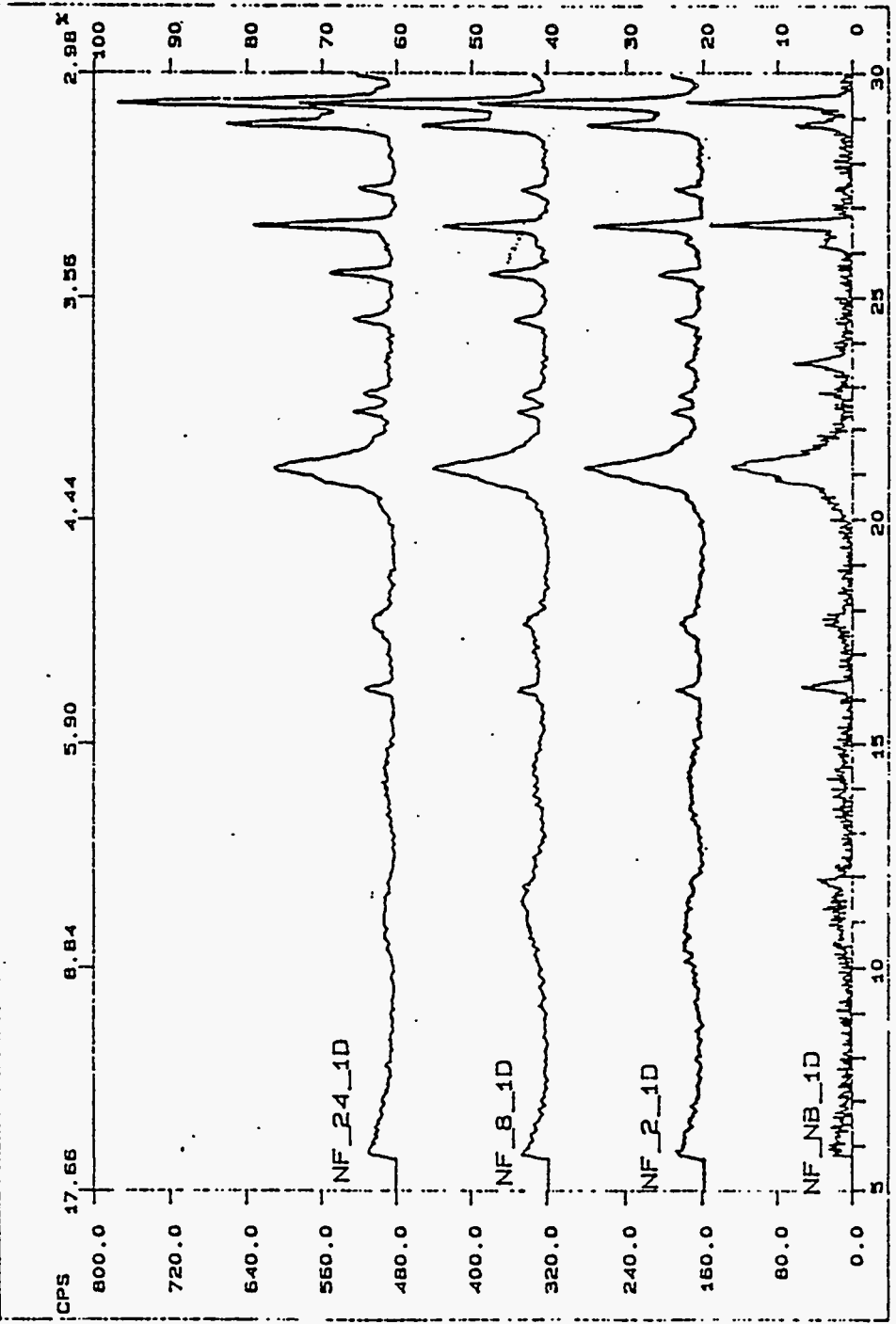
Figure B.23a. Net Intensity Plots (background subtracted data, 1-day data) for Samples NF NB, NF 2, NF 8, and NF 24. Five to 30 degrees 2-theta, major peaks.

B.29
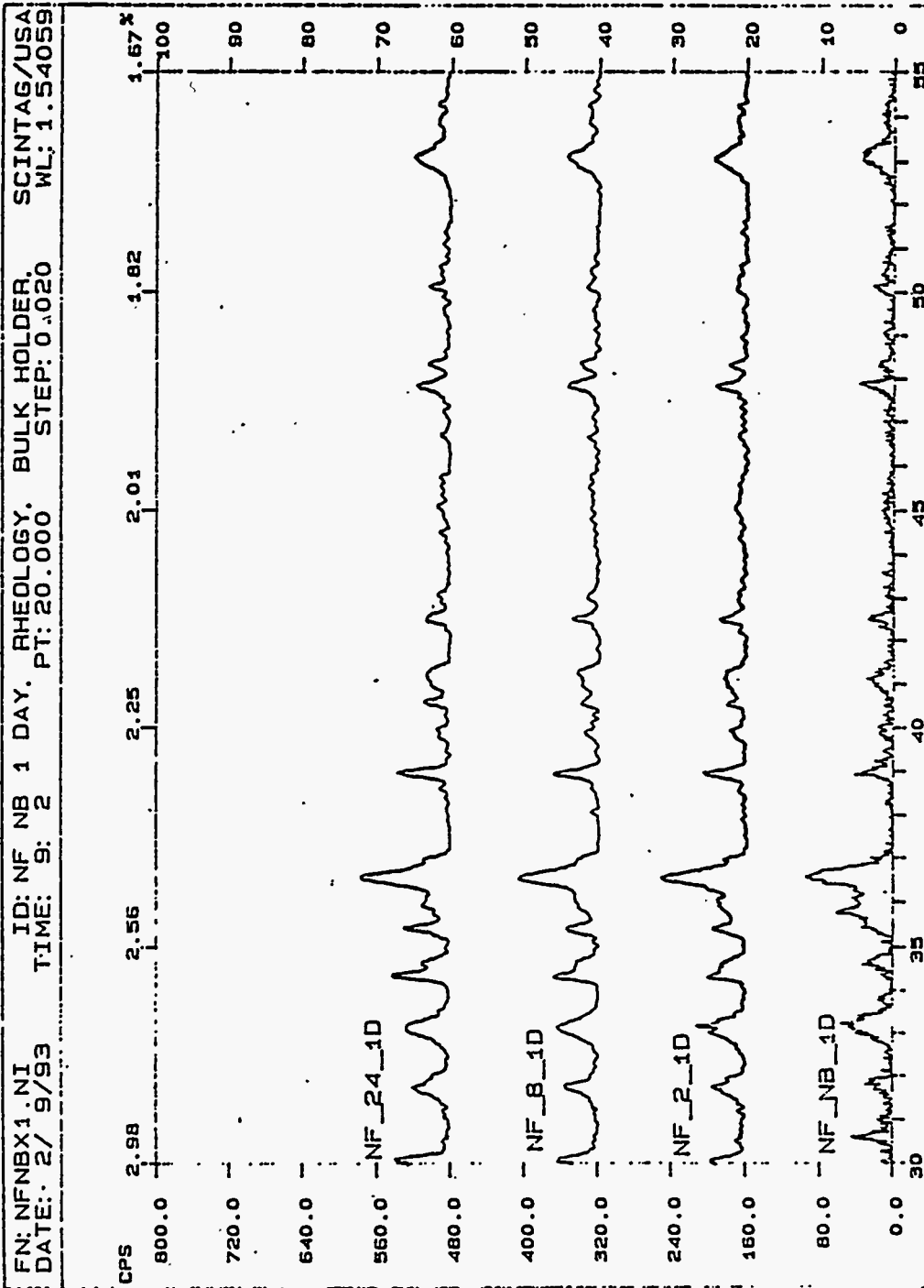
Figure B.23b. Net Intensity Plots (background subtracted data, 1-day data) for Samples NF NB, NF 2, NF 8, and NF 24. Thirty to 55 degrees 2-theta, major peaks.

B.30
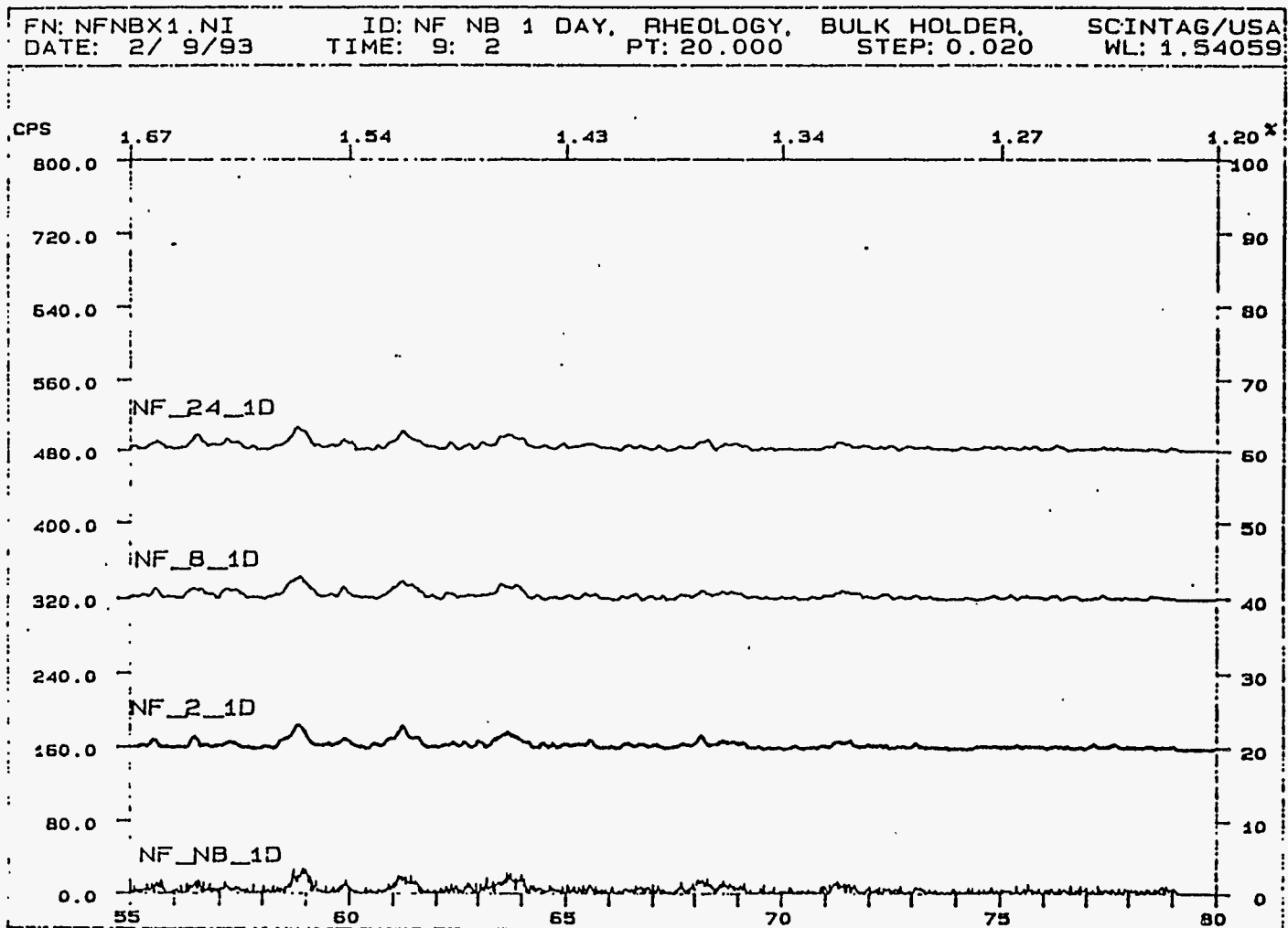
Figure B.23c. Net Intensity Plots (background subtracted data, 1-day data) for Samples NF NB, NF 2, NF 8, and NF 24. Fifty-five to 80 degrees 2-theta, major peaks.
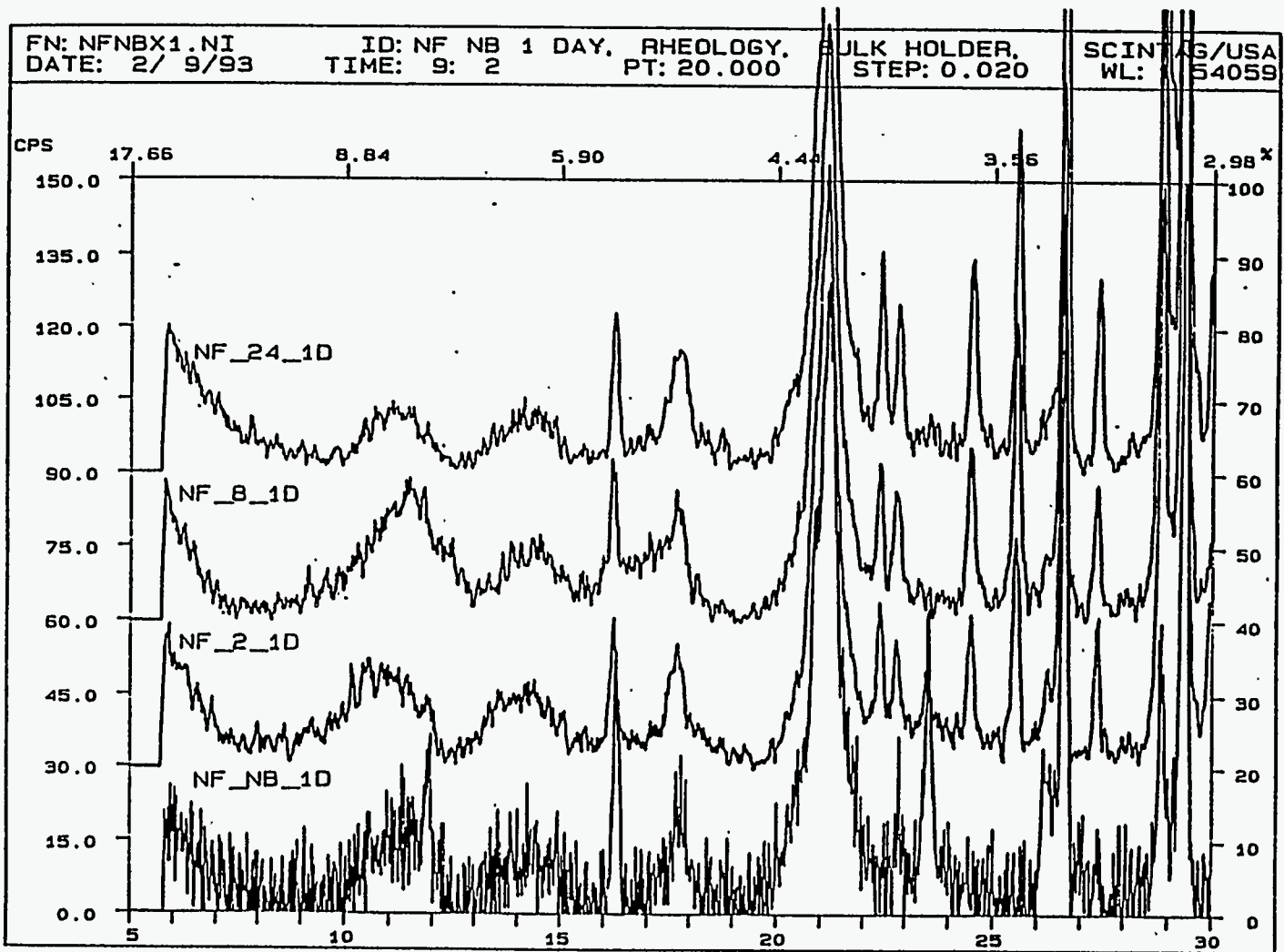
Figure B.24a. Net Intensity Plots (background subtracted data, 1-day data) for Samples NF NB, NF 2, NF 8, and NF 24. Five to 30 degrees 2-theta, minor peaks.
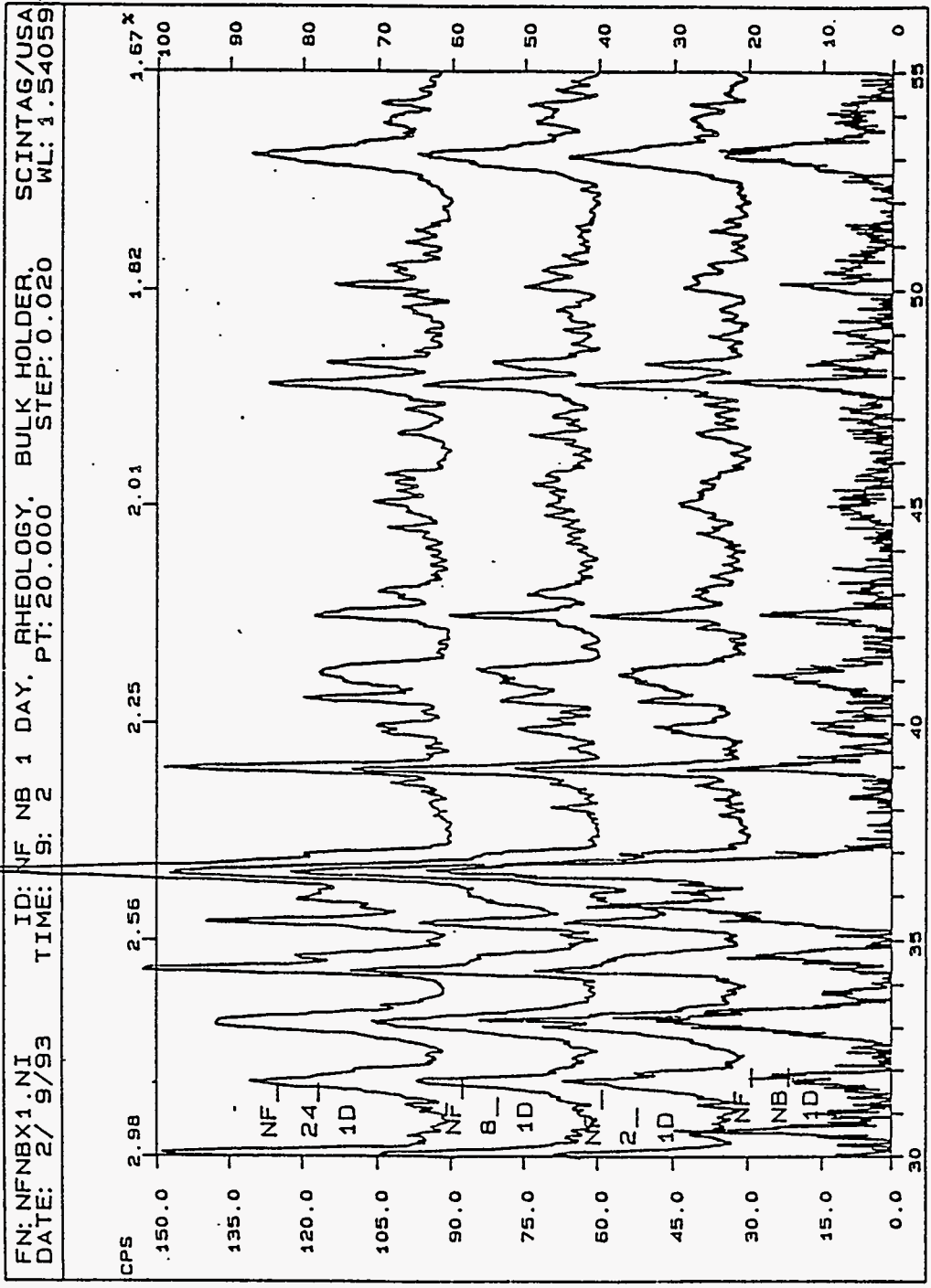
Figure B.24b. Net Intensity Plots (background subtracted data, 1-day data) for Samples NF NB, NF 2, NF 8, and NF 24. Thirty to 55 degrees 2-theta, minor peaks.

B.33
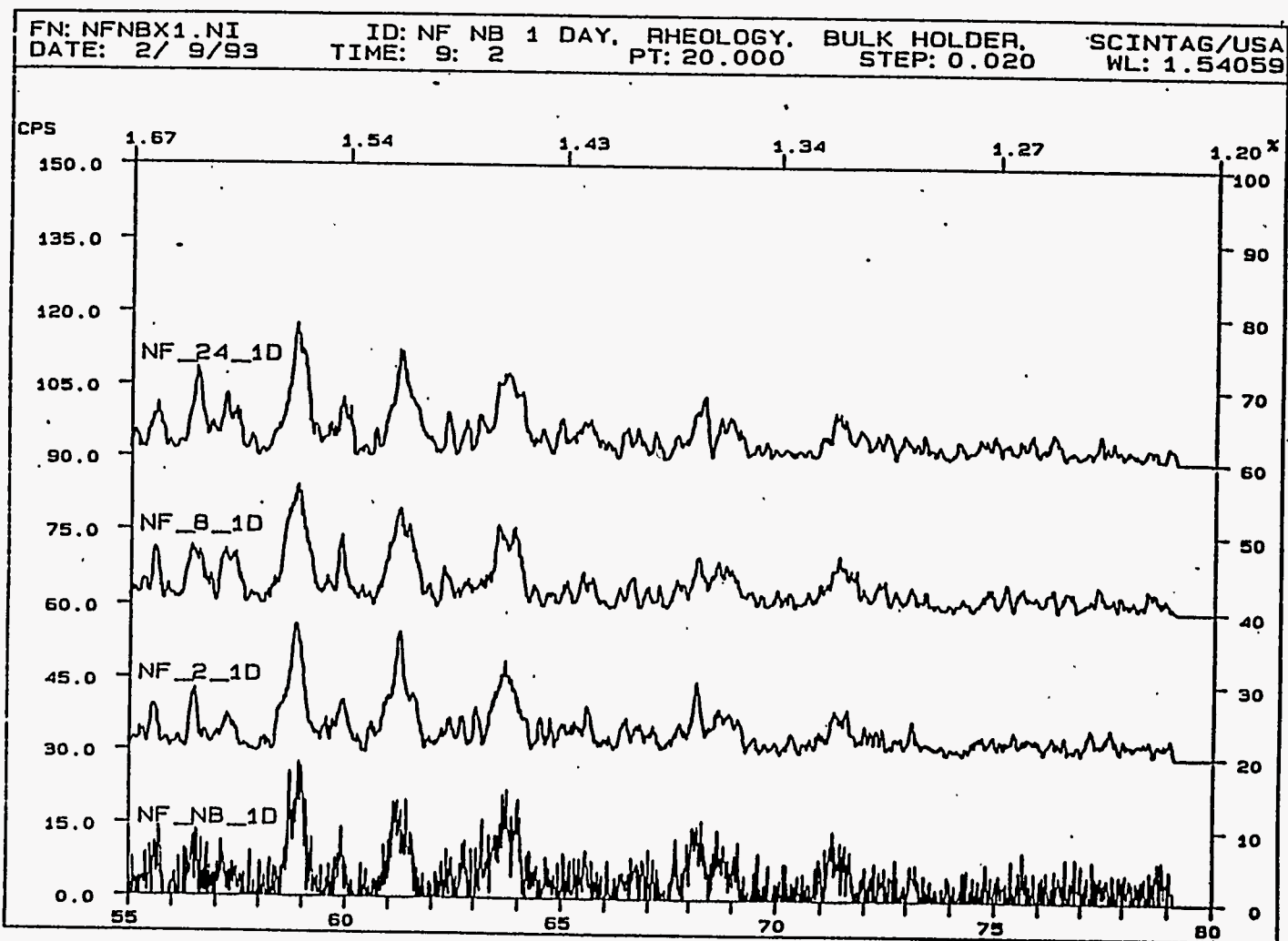
Figure B.24c. Net Intensity Plots (background subtracted data, 1-day data) for Samples NF NB, NF 2, NF 8, and NF 24. Fifty-five to 80 degrees 2-theta, major peaks.

Table B.5. Most Intense Lines of Phases Found During Rheology Test, 1-week Data, 202 Samples

Phases Identified ICDD Card Number	RELATIVE INTENSITY			
	202 24	202 8	202 2	202 NB
Na NO3/Nitratine 7-271	1.00	1.00	1.00	1.00
Si O2/Silicon Dioxide 33-1161	0.44	0.47	0.46	0.75
FeO OH/ Goethite 29-713	0.45	0.44	0.39	0.48
Aluminum borate 29-10	0.00	0.16	0.20	1.23*

* Most intense peak considered to be Na NO3 to be consistent with table 1.

Table B.6. Most Intense Lines of Phases Found During Rheology Test, 4-week Data, NF Samples

Phases Identified ICDD Card Number	RELATIVE INTENSITY			
	NF 24	NF 8	NF 2	NF NB
Na NO3/Nitratine 7-271	1.00	1.00	1.00	1.00
Si O2/Silicon Dioxide 33-1161	0.44	0.47	0.46	0.75
FeO OH/ Goethite 29-713	0.45	0.44	0.39	0.48
Aluminum borate 29-10	0.00	0.00	0.00	0.00

Table B.7. Index to Plots and Location

B.36

Sample	Subject	Figure	
202 24 202 8 202 2 202 NB	Net intensity, 30 - 55 degrees full intensity scale composite plot	12B	23
202 24 202 8 202 2 202 NB	Net intensity, 55 - 80 degrees full intensity scale composite plot	12C	24
202 24 202 8 202 2 202 NB	Net intensity, 5 - 30 degrees enhanced intensity scale composite plot	13A	25
202 24 202 8 202 2 202 NB	Net intensity, 30 - 55 degrees enhanced intensity scale composite plot	13B	26
202 24 202 8 202 2 202 NB	Net intensity, 55 - 80 degrees enhanced intensity scale composite plot	13C	27
NF 24 NF 8 NF 2 NF NB	Net intensity, 5 - 30 degrees full intensity scale composite plot	14A	28
NF 24 NF 8 NF 2 NF NB	Net intensity, 30 - 55 degrees full intensity scale composite plot	14B	29
NF 24 NF 8 NF 2 NF NB	Net intensity, 55 - 80 degrees full intensity scale composite plot	14C	30

Sample	Subject	Figure	
NF 24 NF 8 NF 2 NF NB	Net intensity, 5 - 30 degrees enhanced intensity scale composite plot	15A	31
NF 24 NF 8 NF 2 NF NB	Net intensity, 30 - 55 degrees enhanced intensity scale composite plot	15B	32
NF 24 NF 8 NF 2 NF NB	Net intensity, 55 - 80 degrees enhanced intensity scale composite plot	15C	33

Figure B.25. Samples 202 24, 202 8, 202 2, and 202 NB, 1-week Data. Composite plot of raw data.
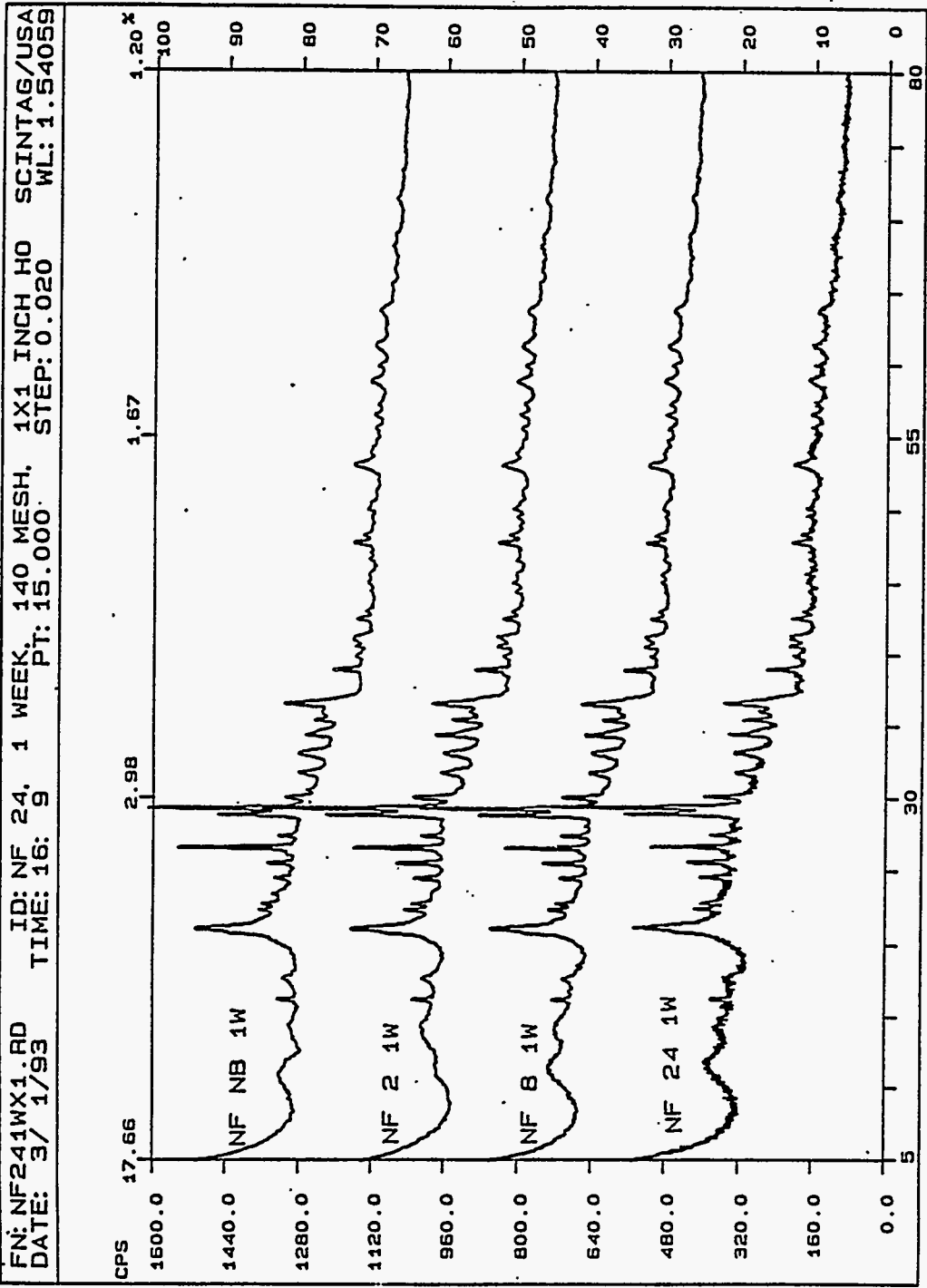
Figure B.26. Samples NF 24, NF 8, NF 2, and NF NB, 1-week Data. Composite plot of raw data.
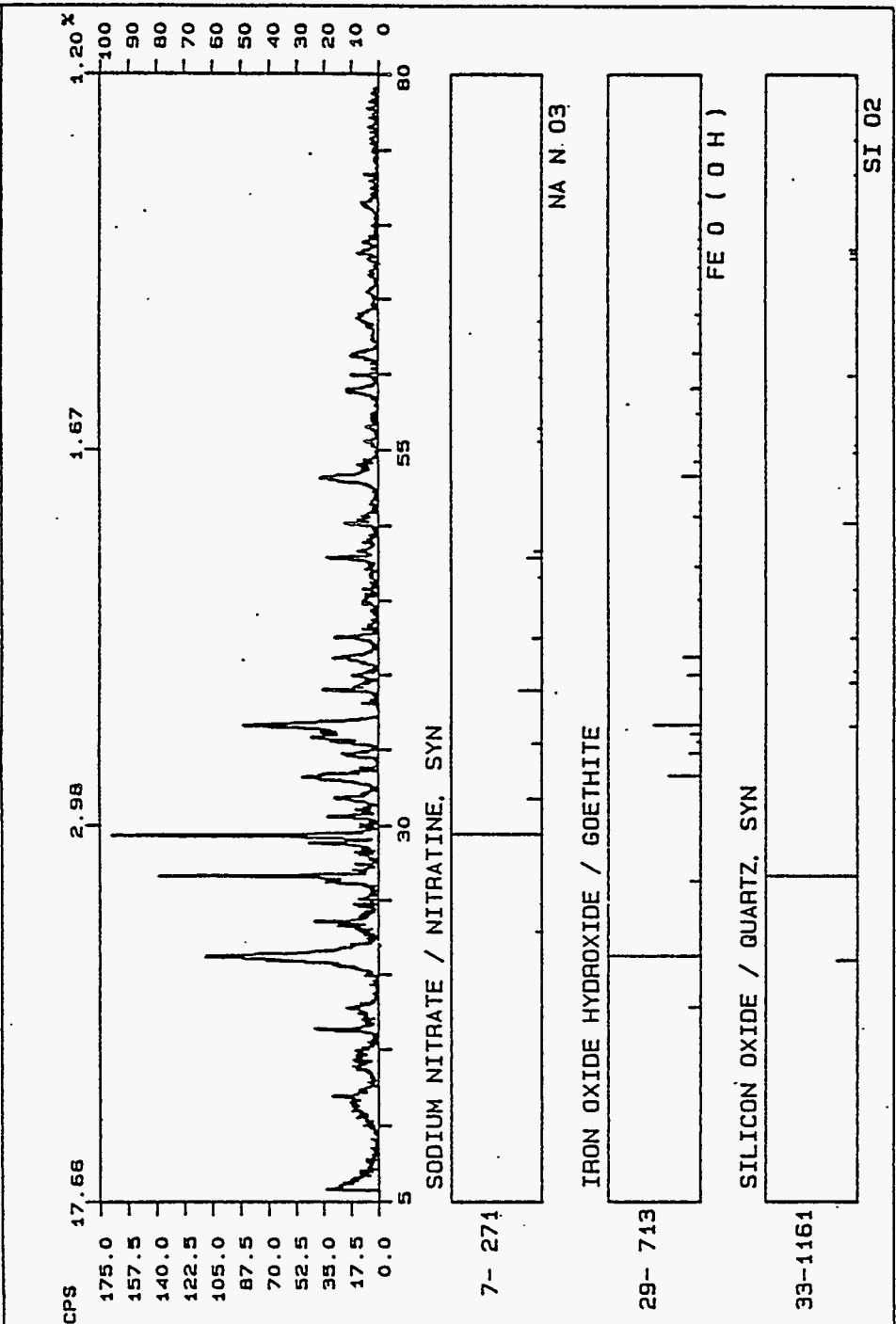
Figure B.27. Sample 202 24, 1-week Data. Net intensity plot with "stick figure" representations of major phases.

B.41
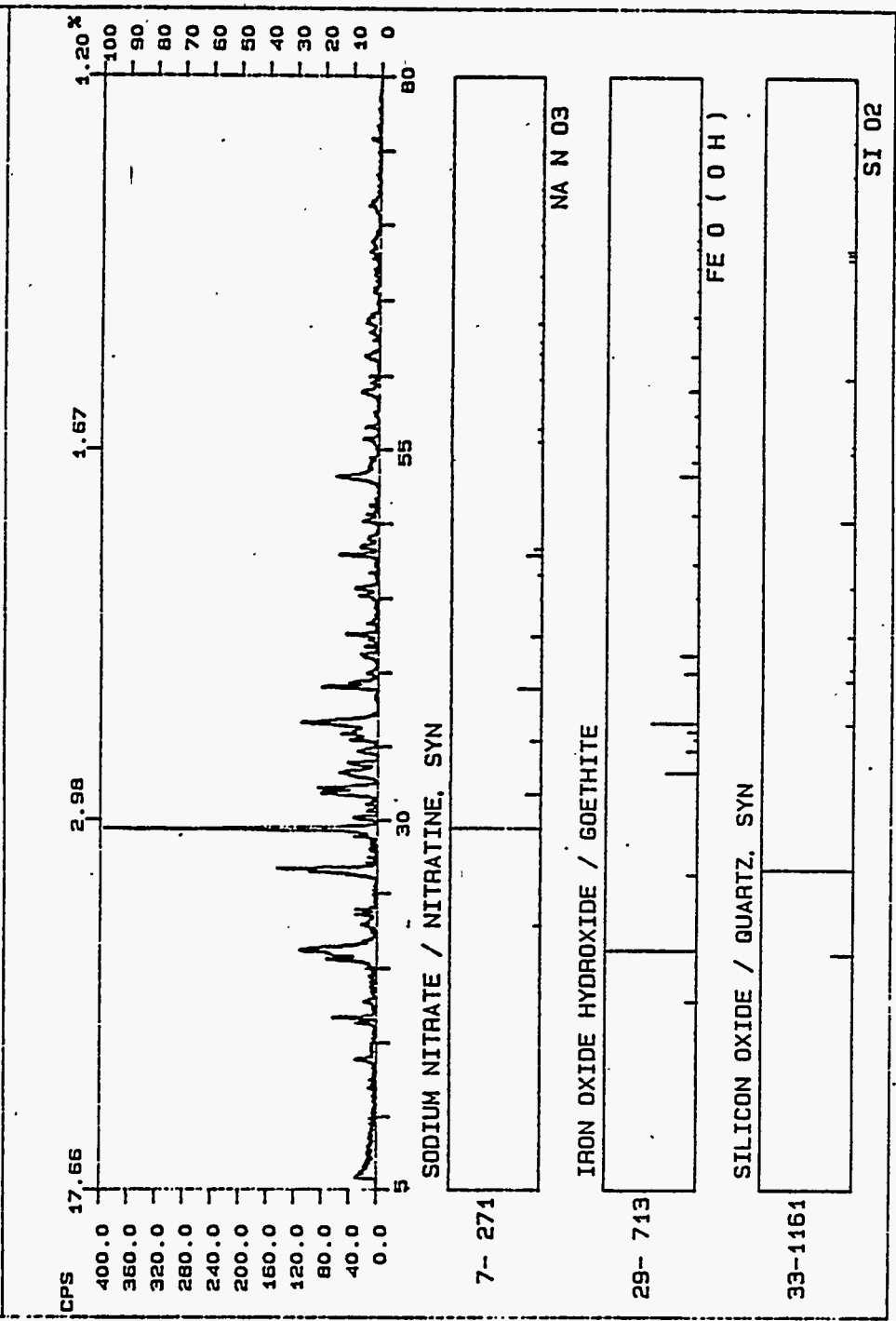
Figure B.28. Sample 202 8, 1-week Data. Net intensity plot with "stick figure" representations of major phases.
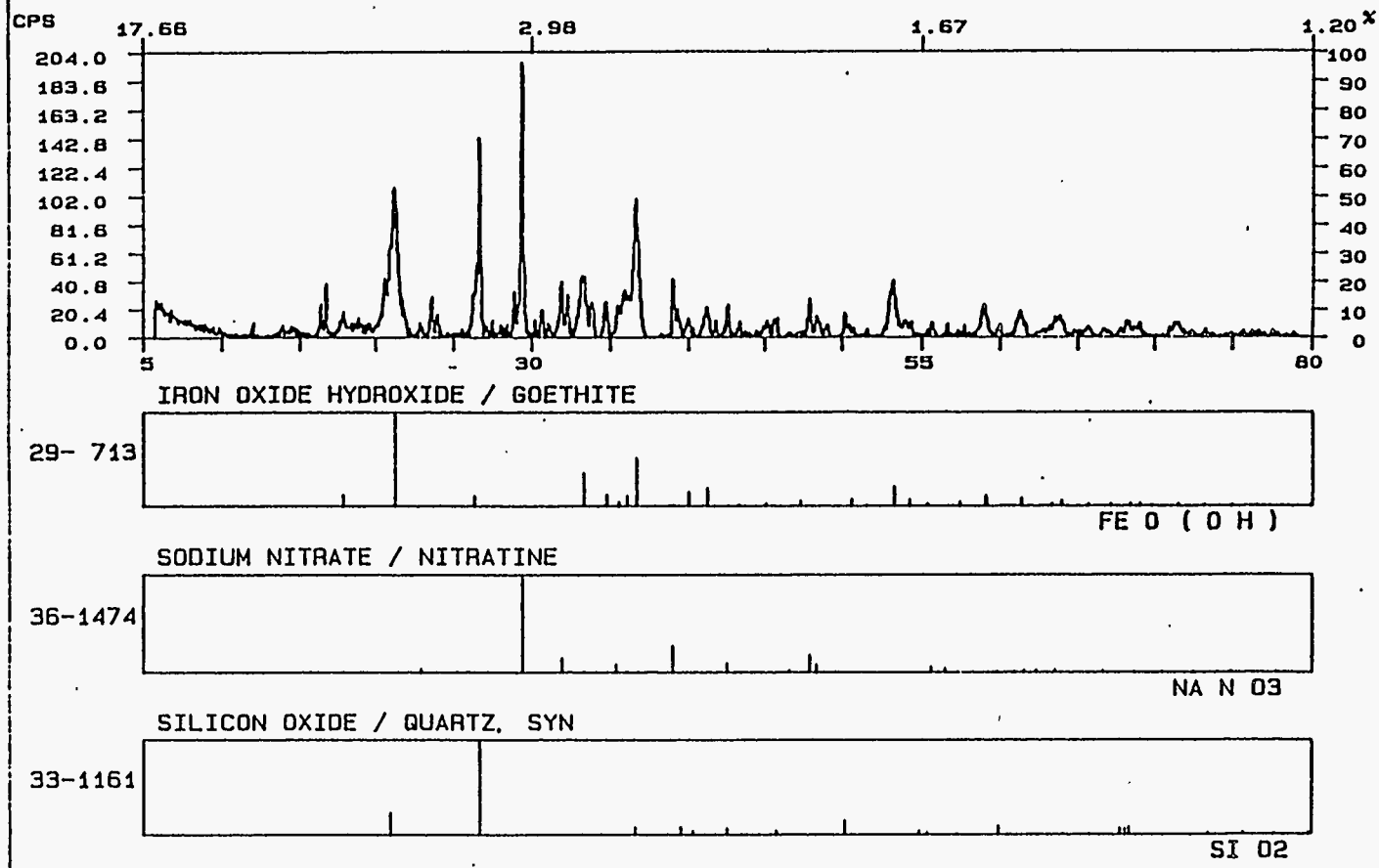
Figure B.29. Sample 202 2, 1-week Data. Net intensity plot with "stick figure" representations of major phases.
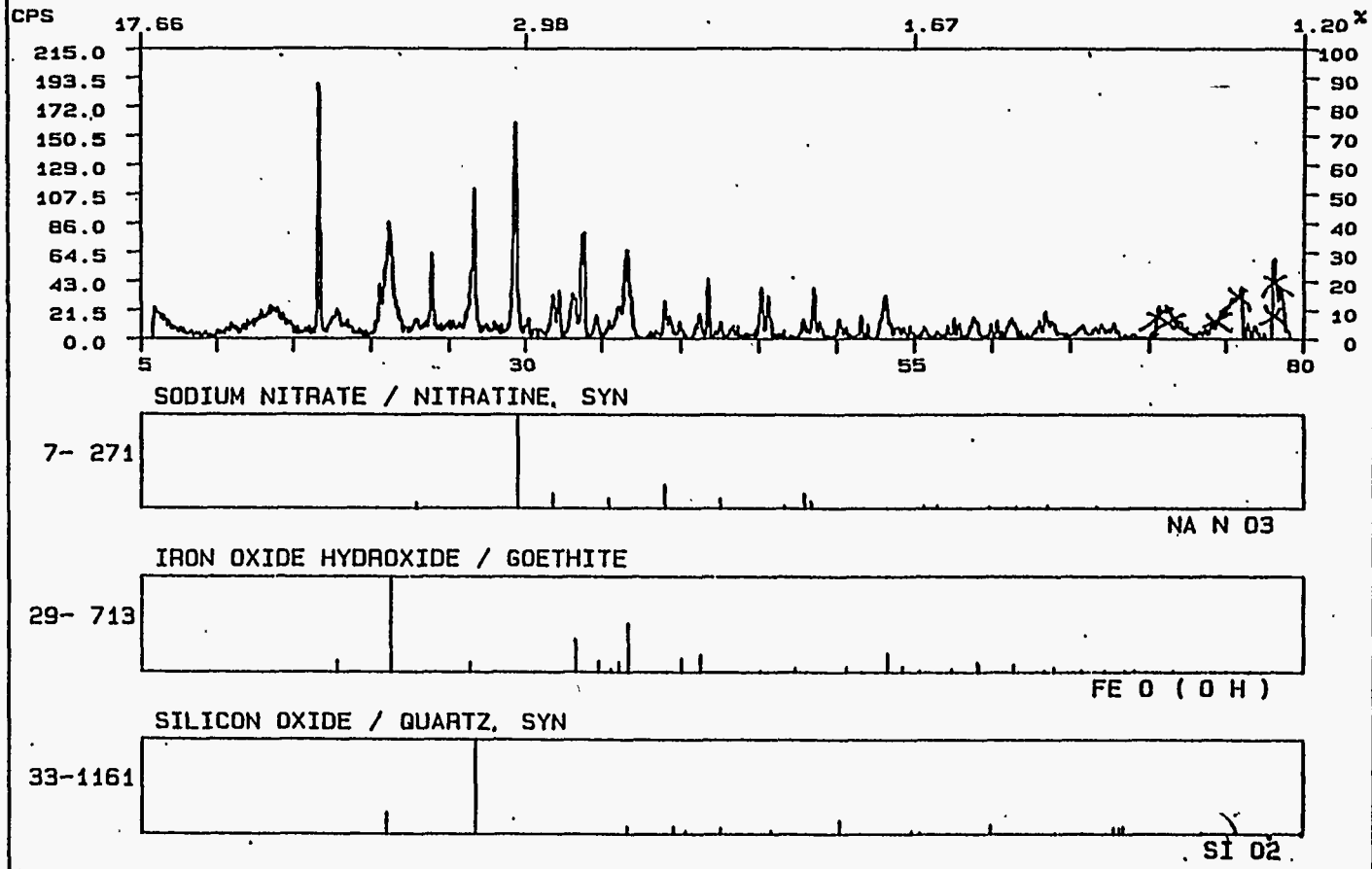
Figure B.30a. Sample 202 NB, 1-week Data. Net intensity plot with "stick figure" representations of major phases.
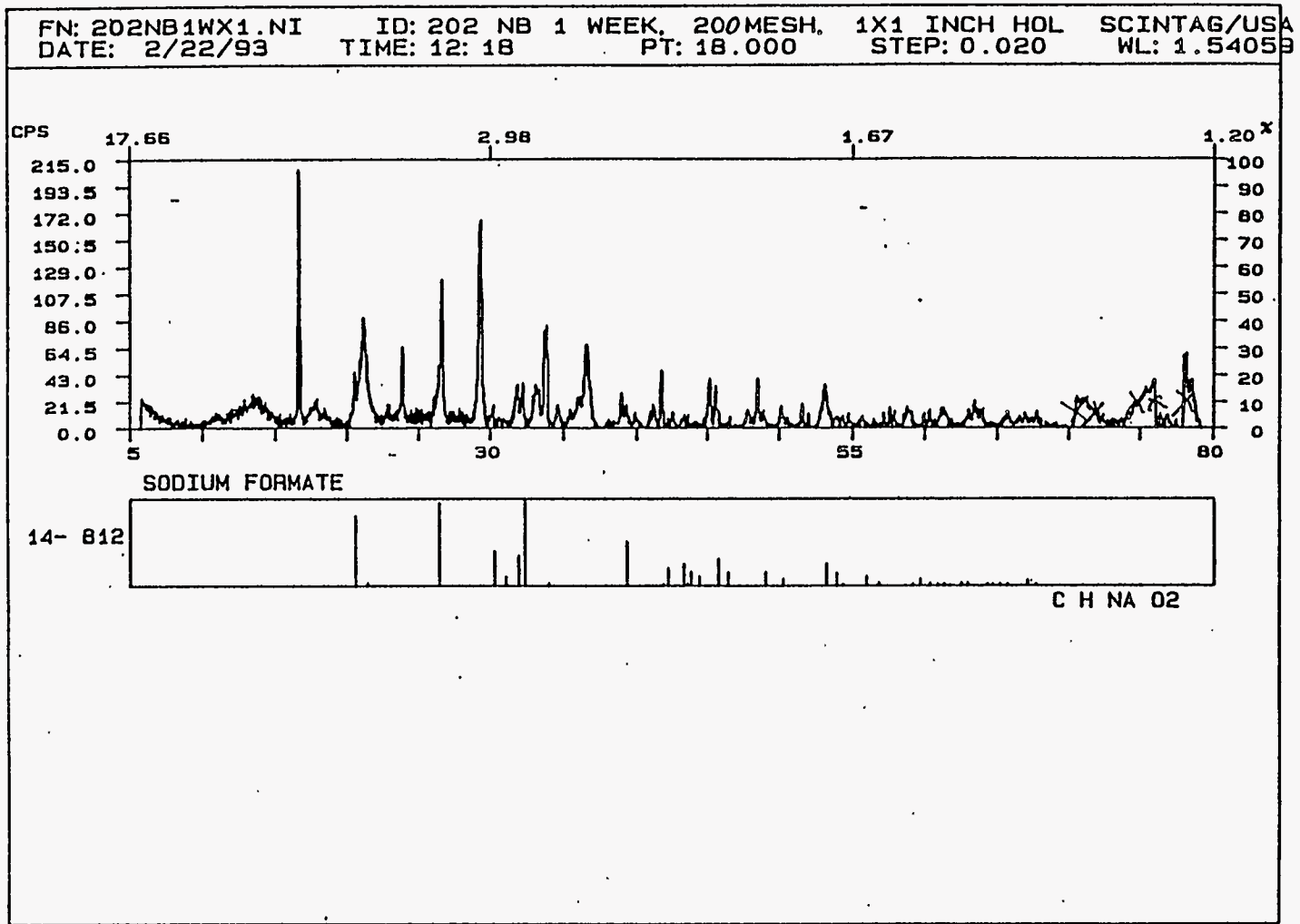
Figure B.30b. Sample 202 NB, 1-week Data. Net intensity plot with "stick figure" representations of sodium formate.
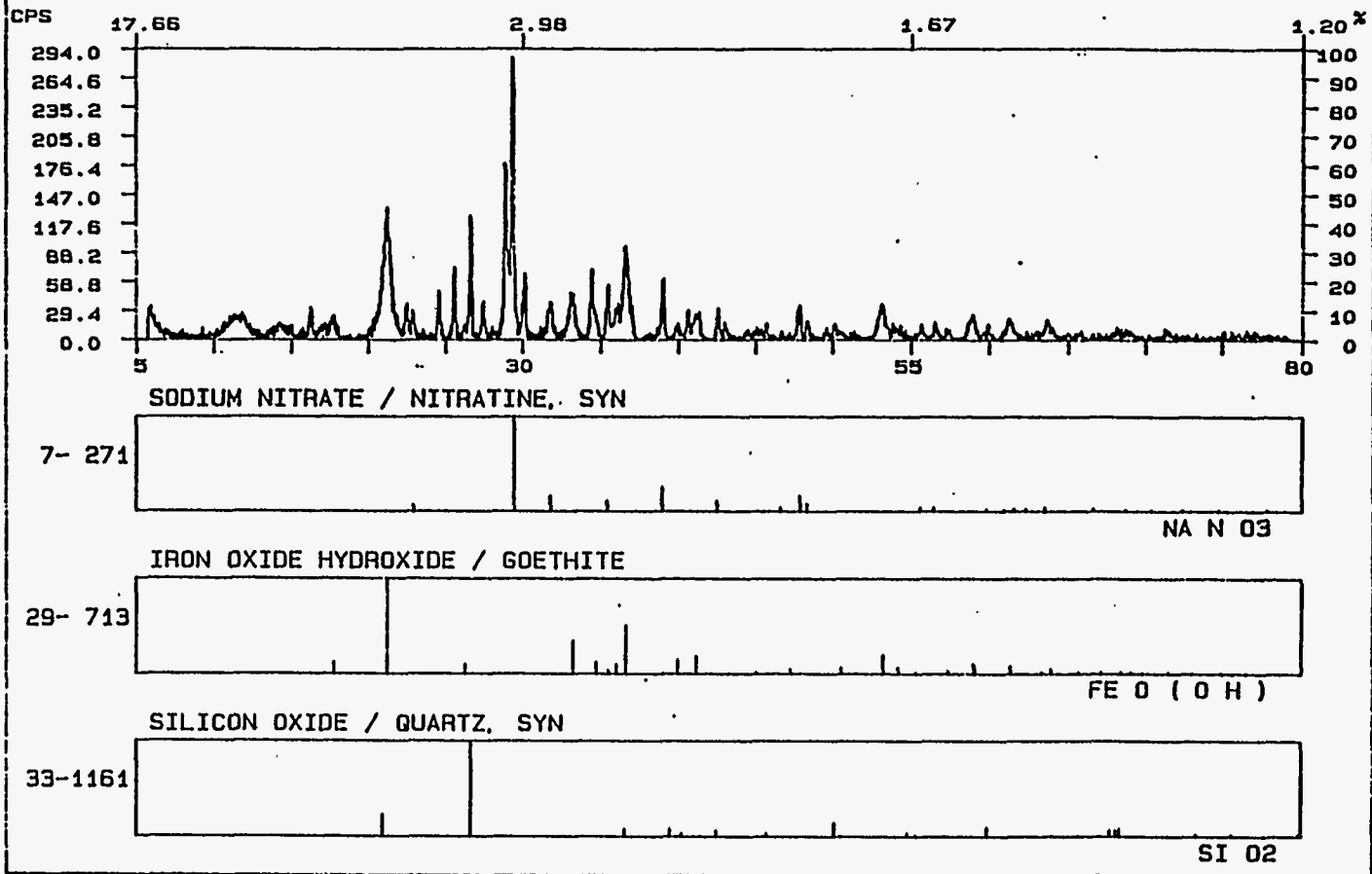
Figure B.31. Sample NF 24, 1-week Data. Net intensity plot with "stick figure" representations of major phases.
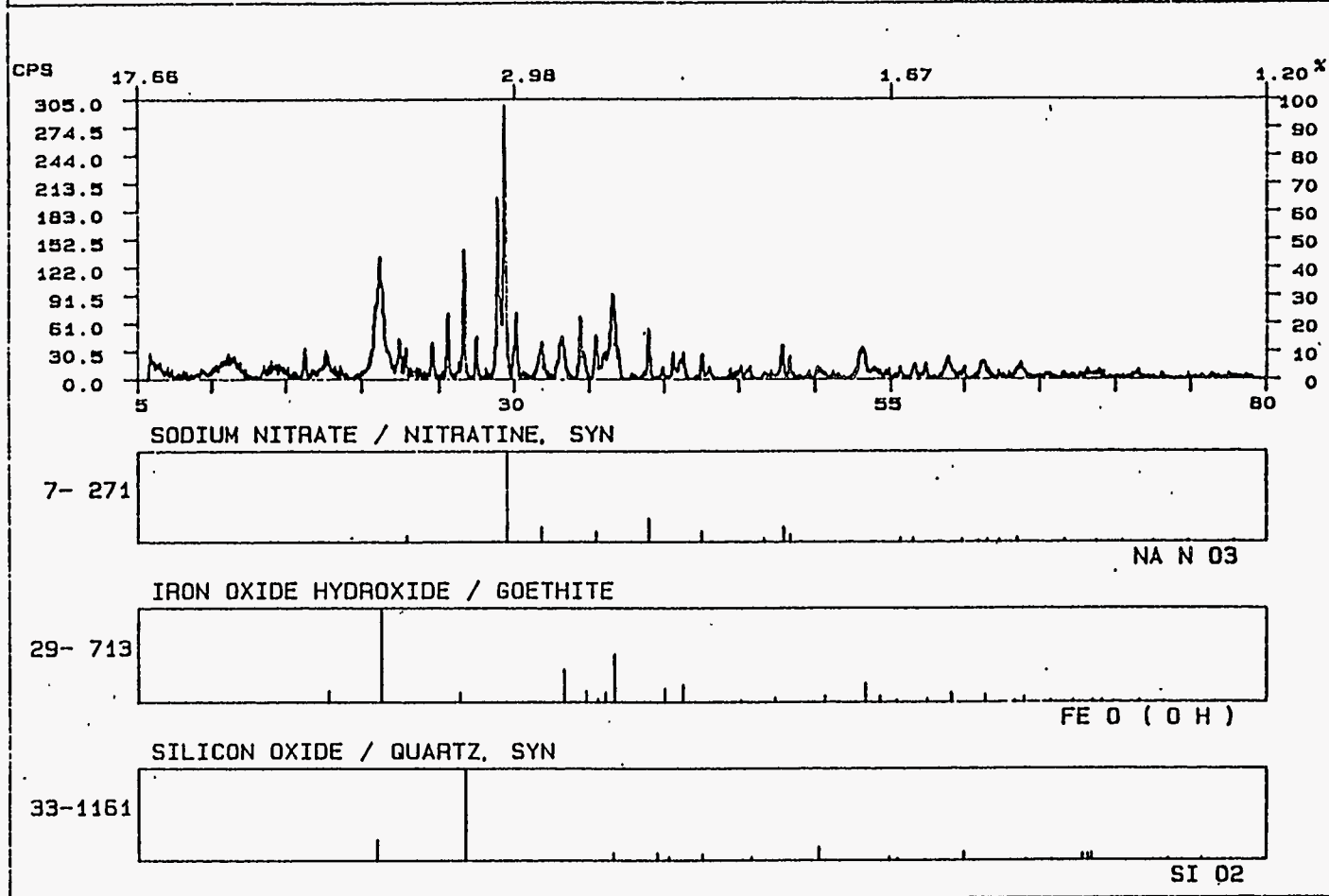
Figure B.32. Sample NF 8, 1-week Data. Net intensity plot with "stick figure" representations of major phases.
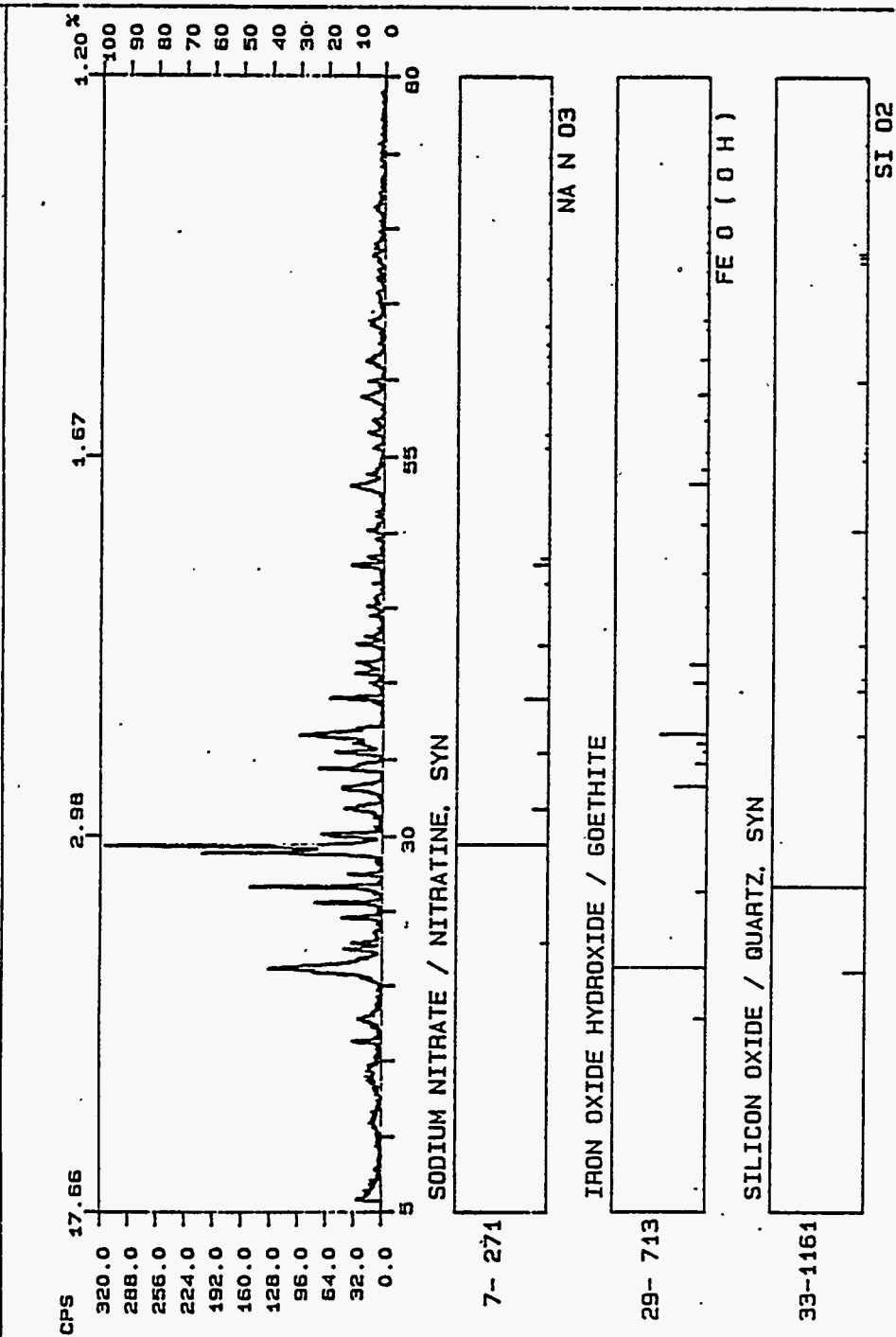
Figure B.33. Sample NF 2, 1-week Data. Net intensity plot with "stick figure" representations of major phases.

B.48
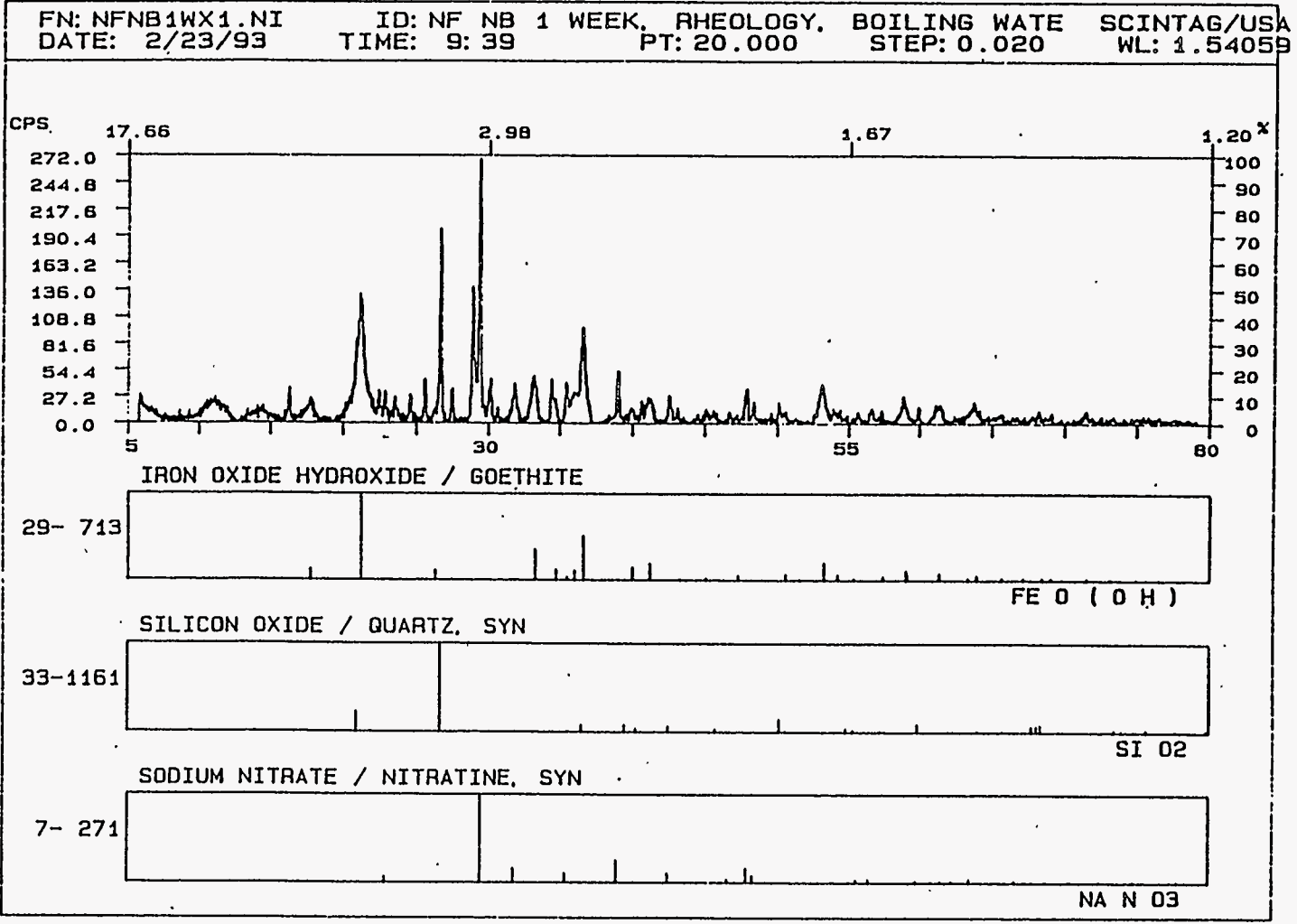
Figure B.34. Sample NF NB, 1-week Data. Net intensity plot with "stick figure" representations of major phases.
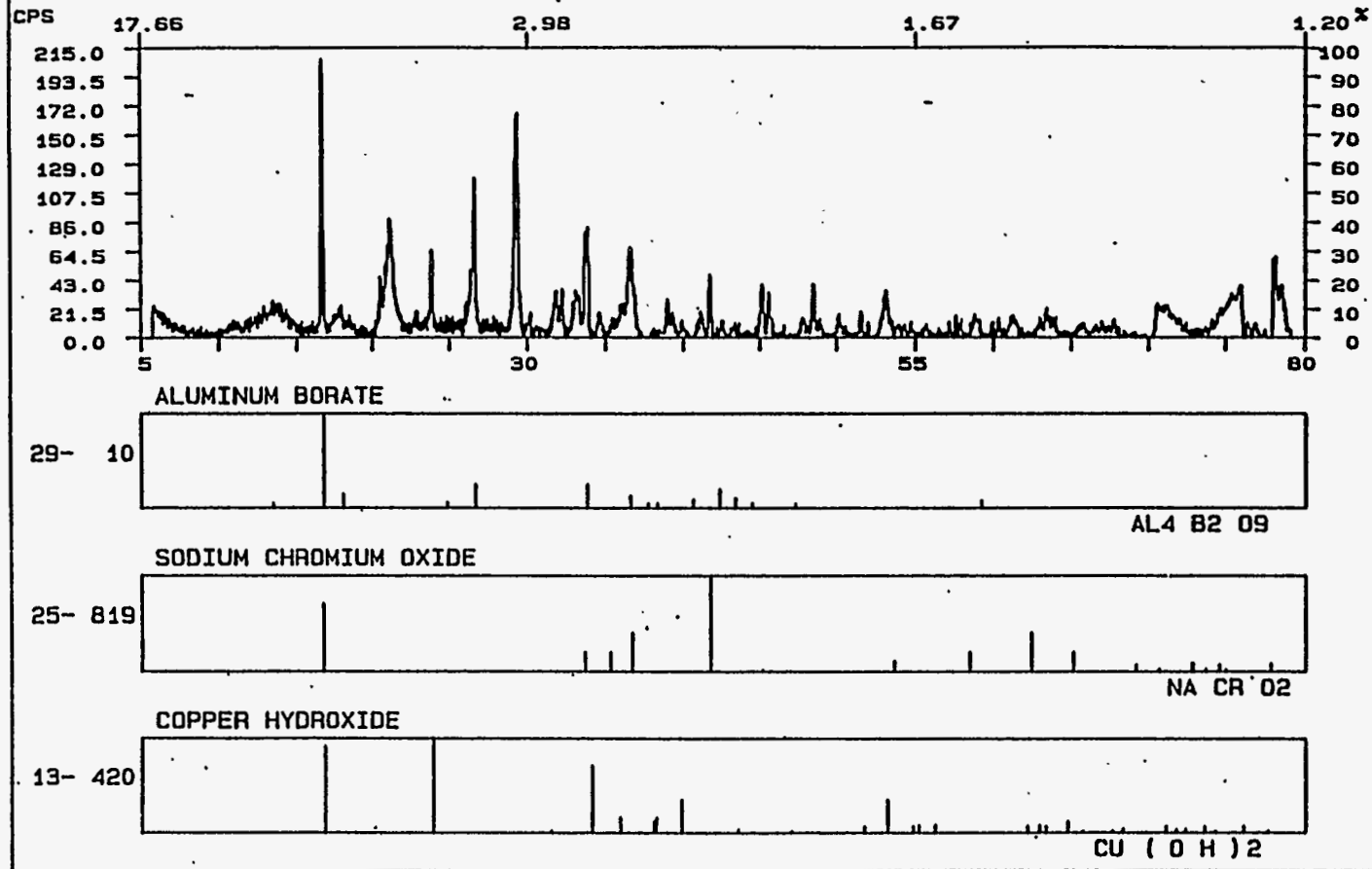
Figure B.35. Sample 202 NB, 1-week Data. Net intensity plot with "stick figure" representations for aluminum borate, sodium chromium oxide, and copper hydroxide.
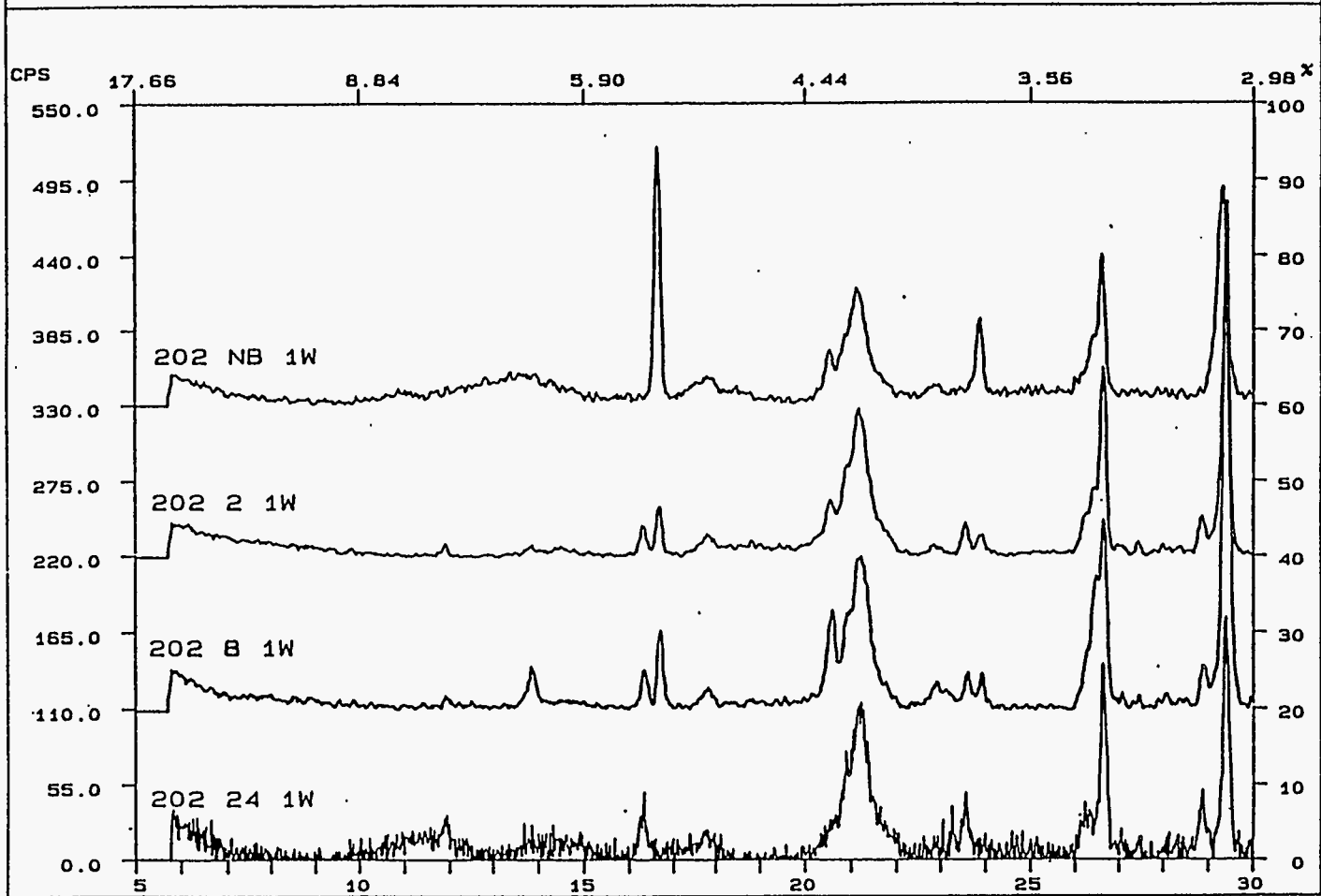
Figure B.36a. Samples 202 24, 202 8, 202 2, and 202 NB, 1-week Data. Expanded 2-theta scale, 5 to 30 degrees. Full intensity scale.
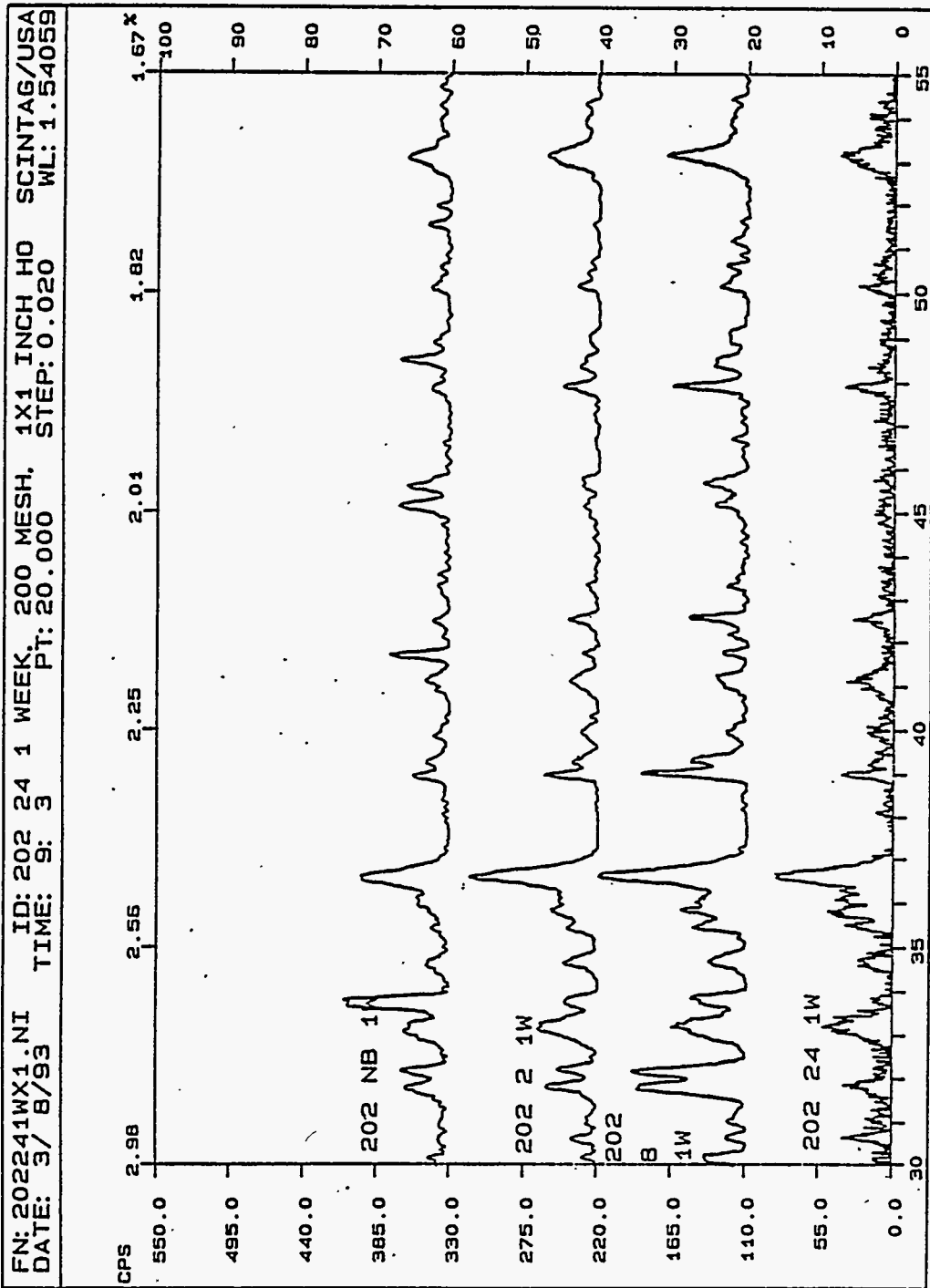
Figure B.36b. Samples 202 24, 202 8, 202 2, and 202 NB, 1-week Data. Expanded 2-theta scale, 30 to 55 degrees. Full intensity scale.
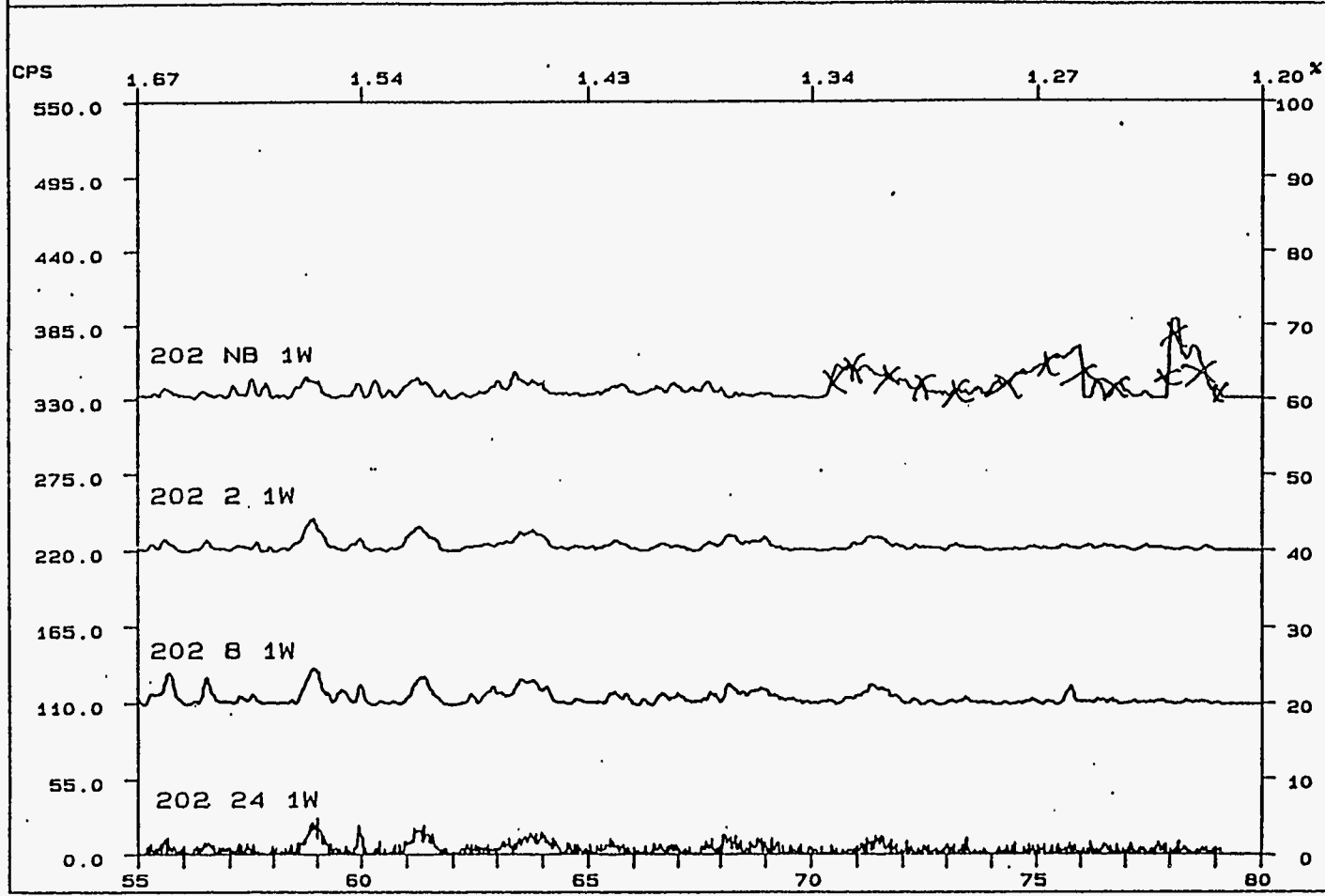
Figure B.36c. Samples 202 24, 202 8, 202 2, and 202 NB, 1-week Data. Expanded 2-theta scale, 55 to 80 degrees. Full intensity scale.
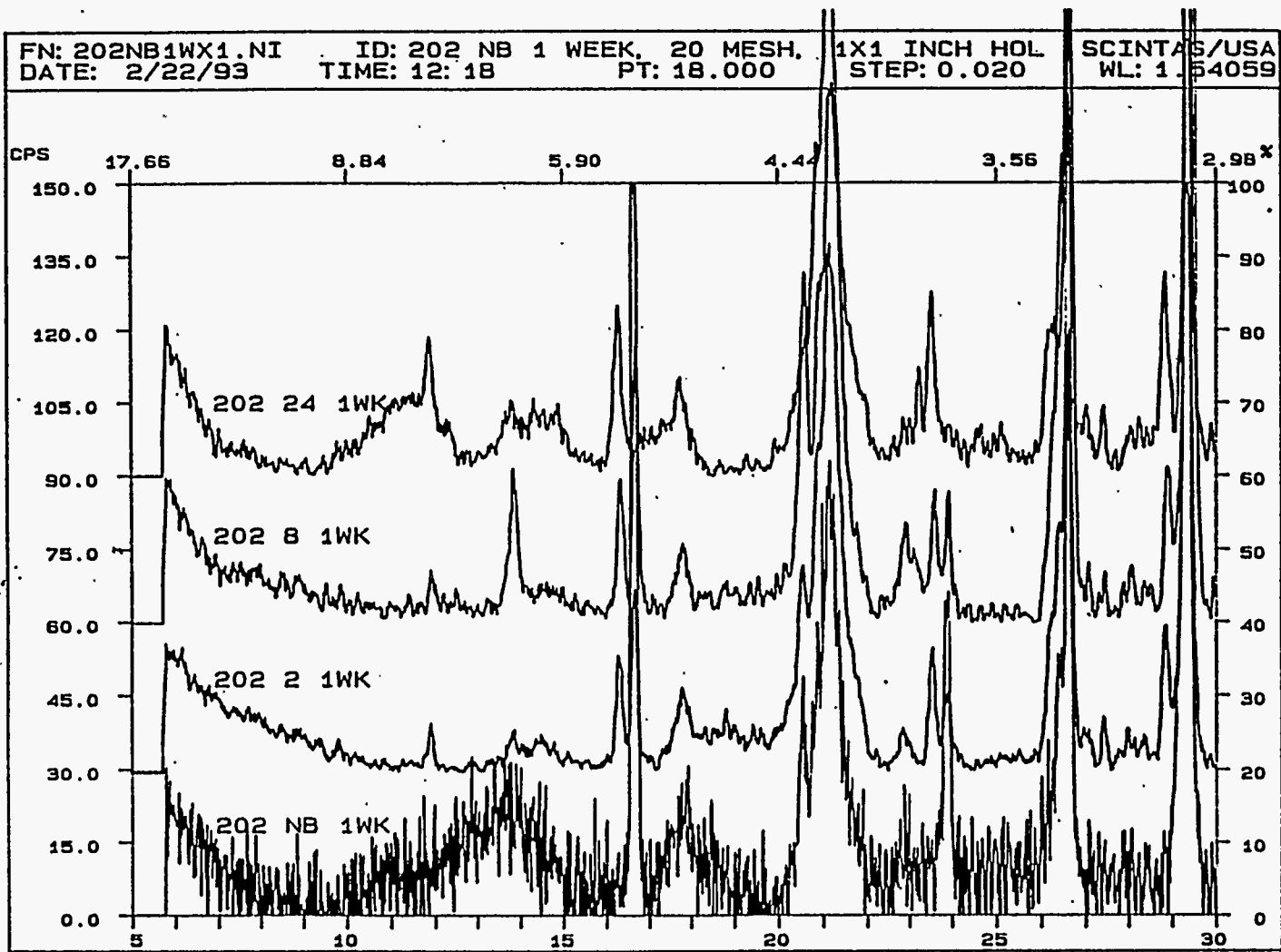
Figure B.37a. Samples 202 24, 202 8, 202 2, and 202 NB, 1-week Data. Expanded 2-theta scale, 5 to 30 degrees. Enhanced intensity scale.
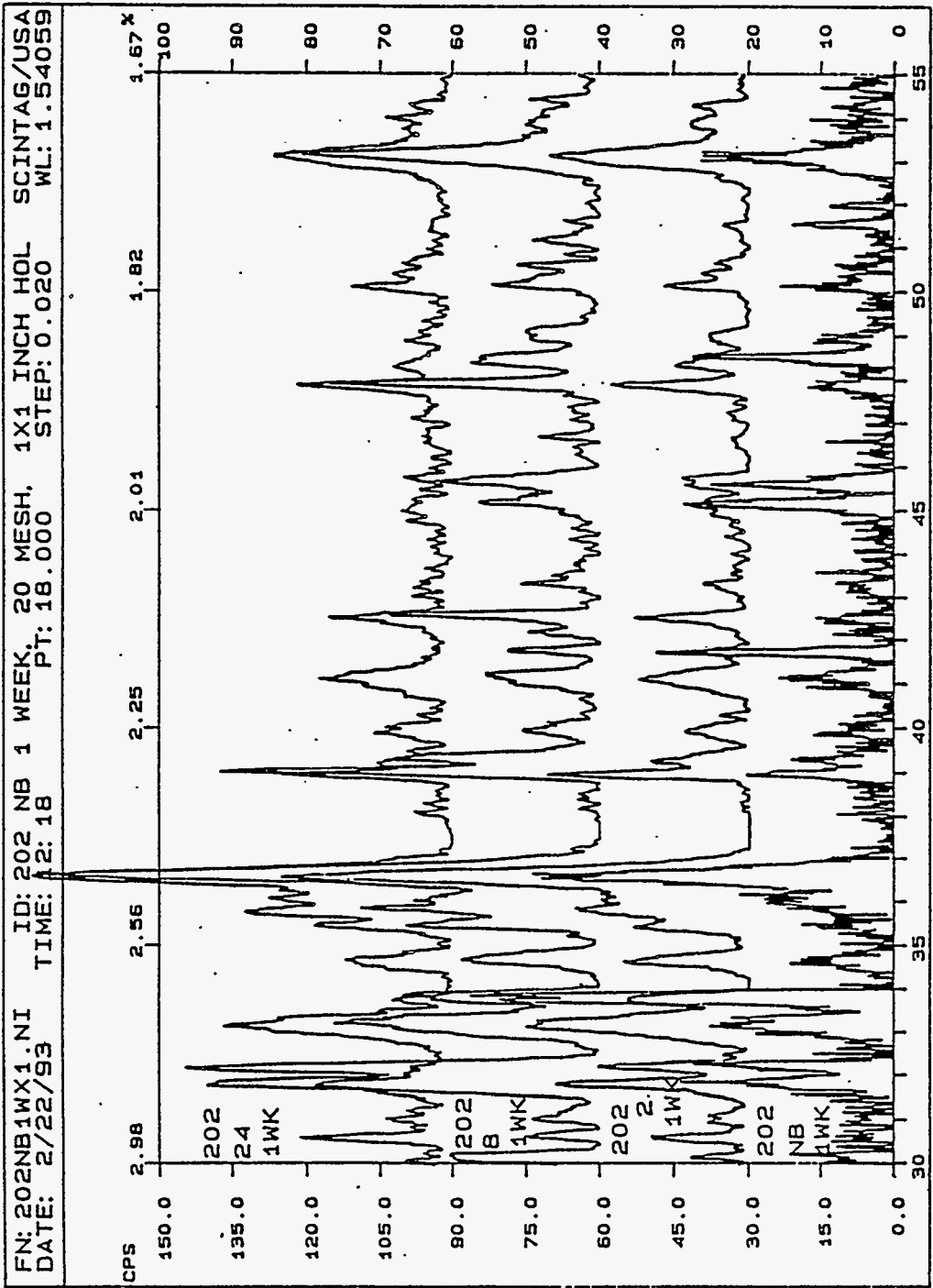
Figure B.37b. Samples 202 24, 202 8, 202 2, and 202 NB, 1-week Data. Expanded 2-theta scale, 30 to 55 degrees. Enhanced intensity scale.
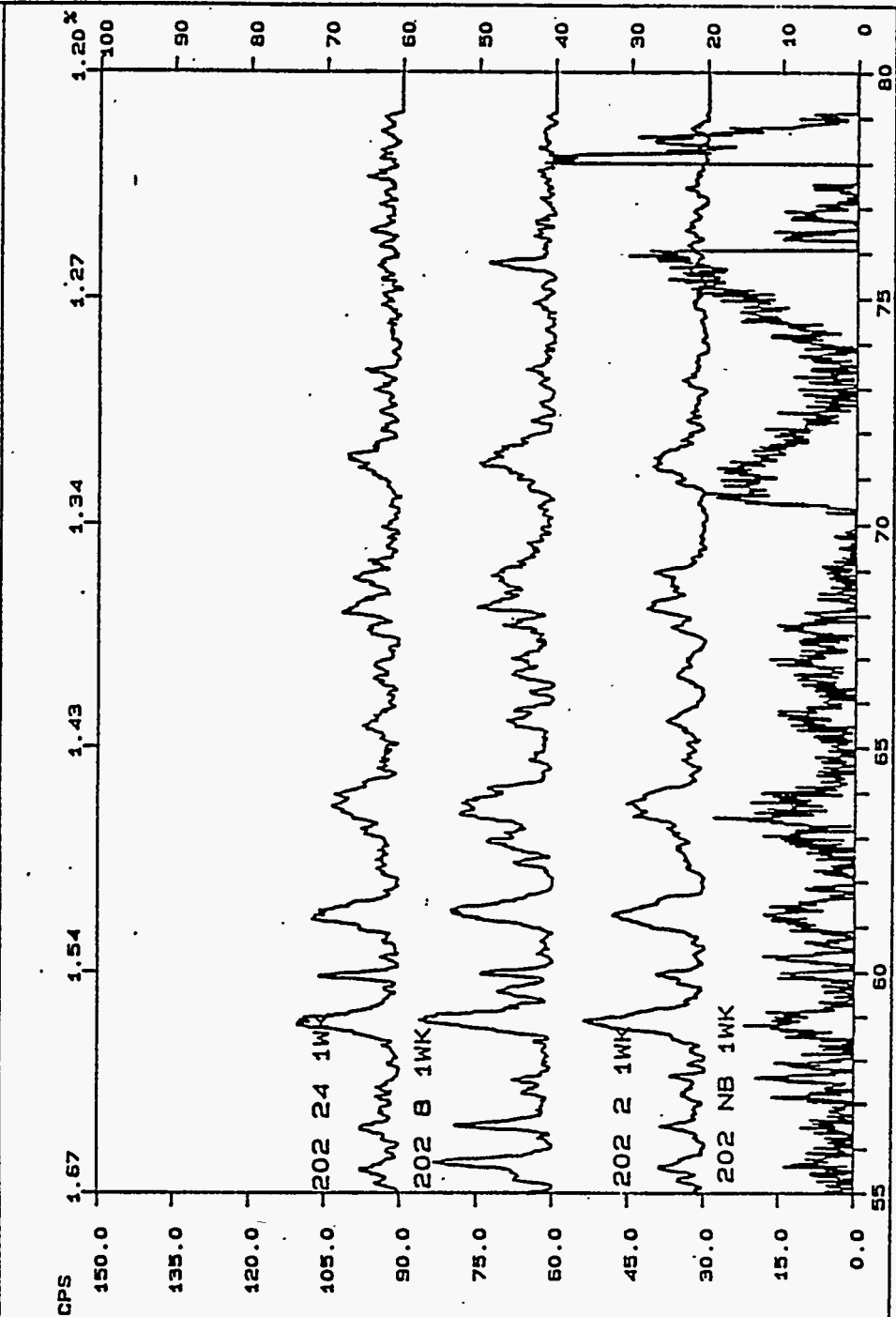
Figure B.37c. Samples 202 24, 202 8, 202 2, and 202 NB, 1-week Data. Expanded 2-theta scale, 55 to 80 degrees. Enhanced intensity scale.
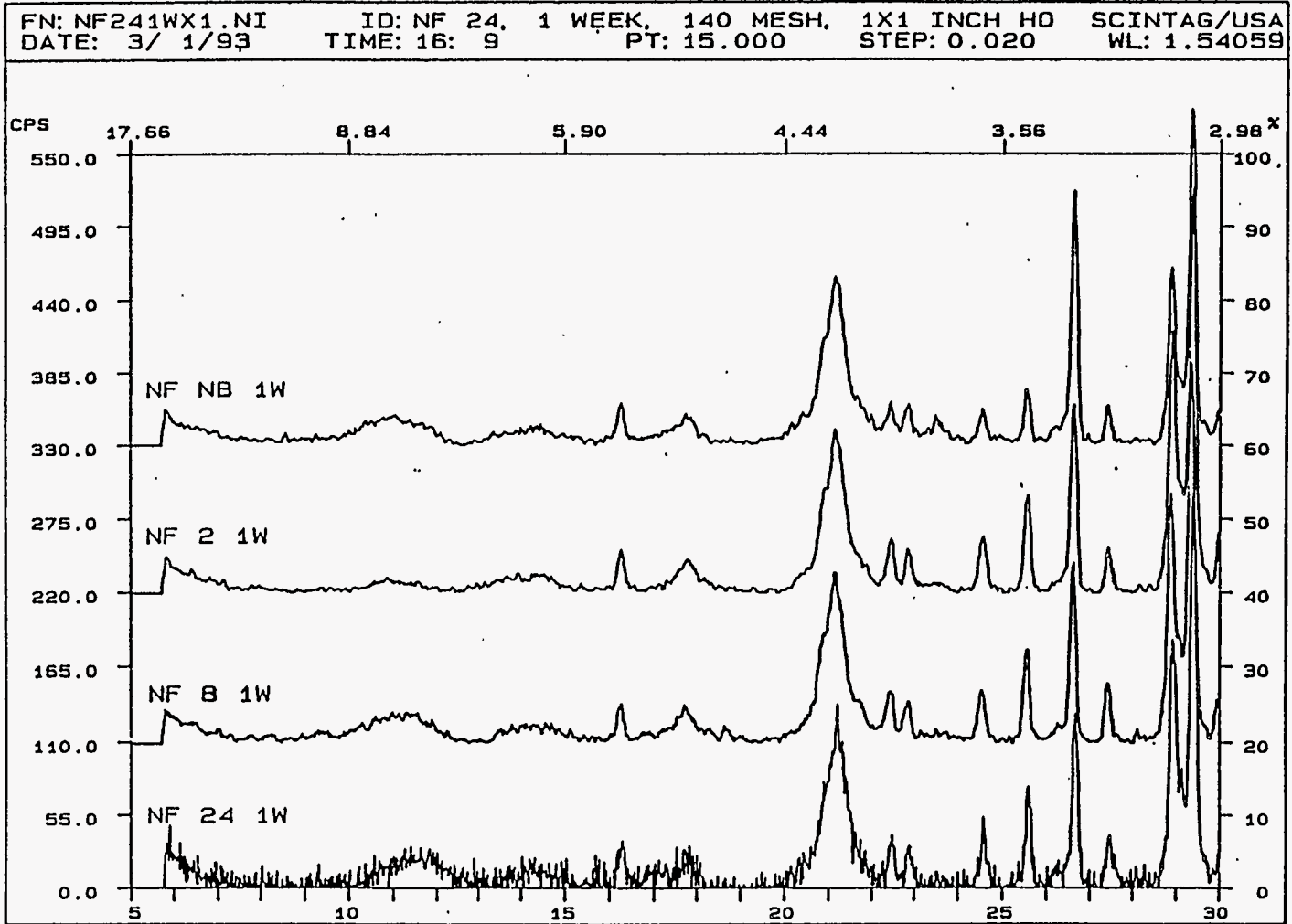
Figure B.38a. Samples NF 24, NF 8, NF 2, and NF NB, 1-week Data. Expanded 2-theta scale, 5 to 30 degrees. Full intensity scale.
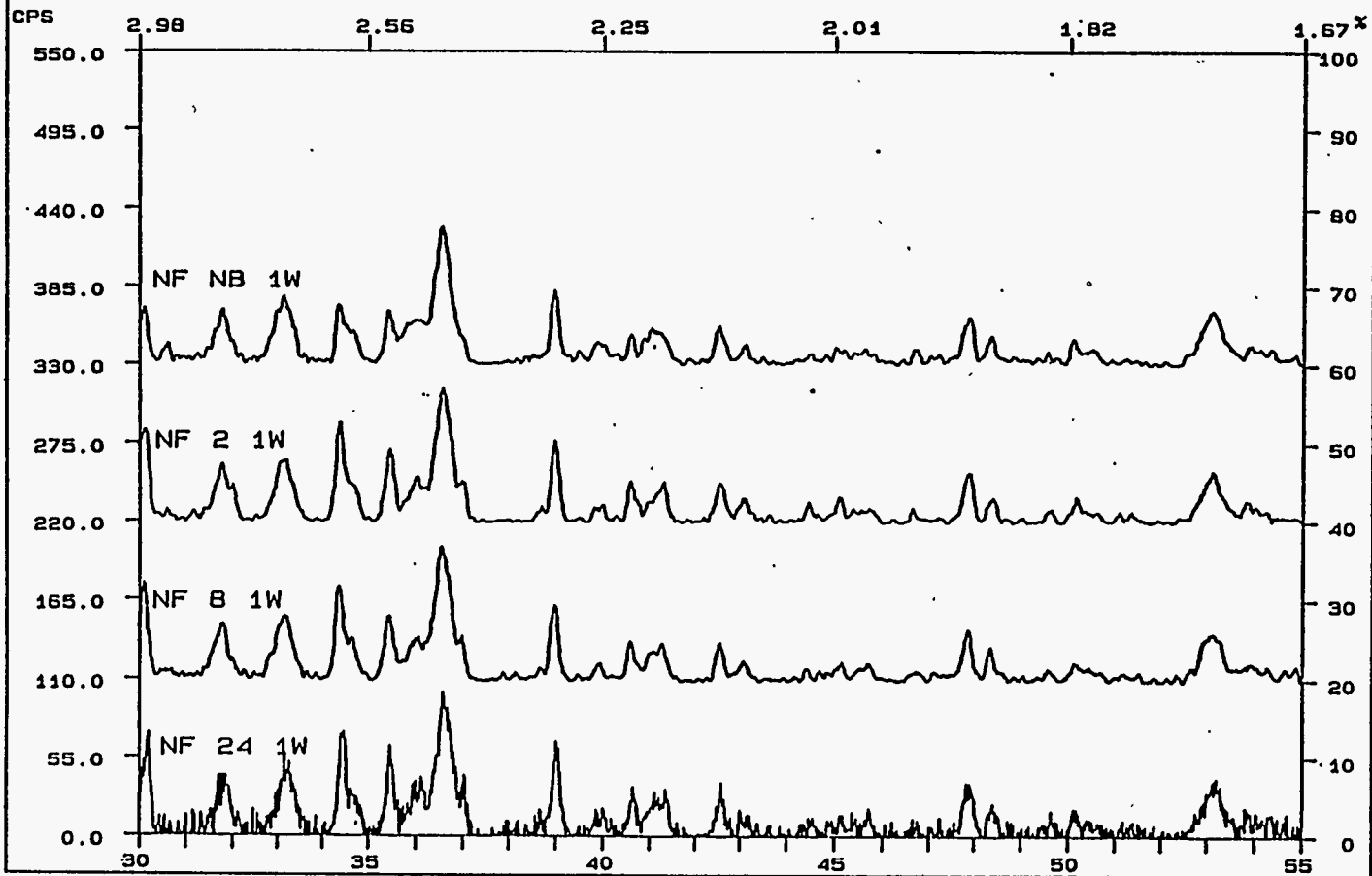
Figure B.38b. Samples NF 24, NF 8, NF 2, and NF NB, 1-week Data. Expanded 2-theta scale, 30 to 55 degrees. Full intensity scale.
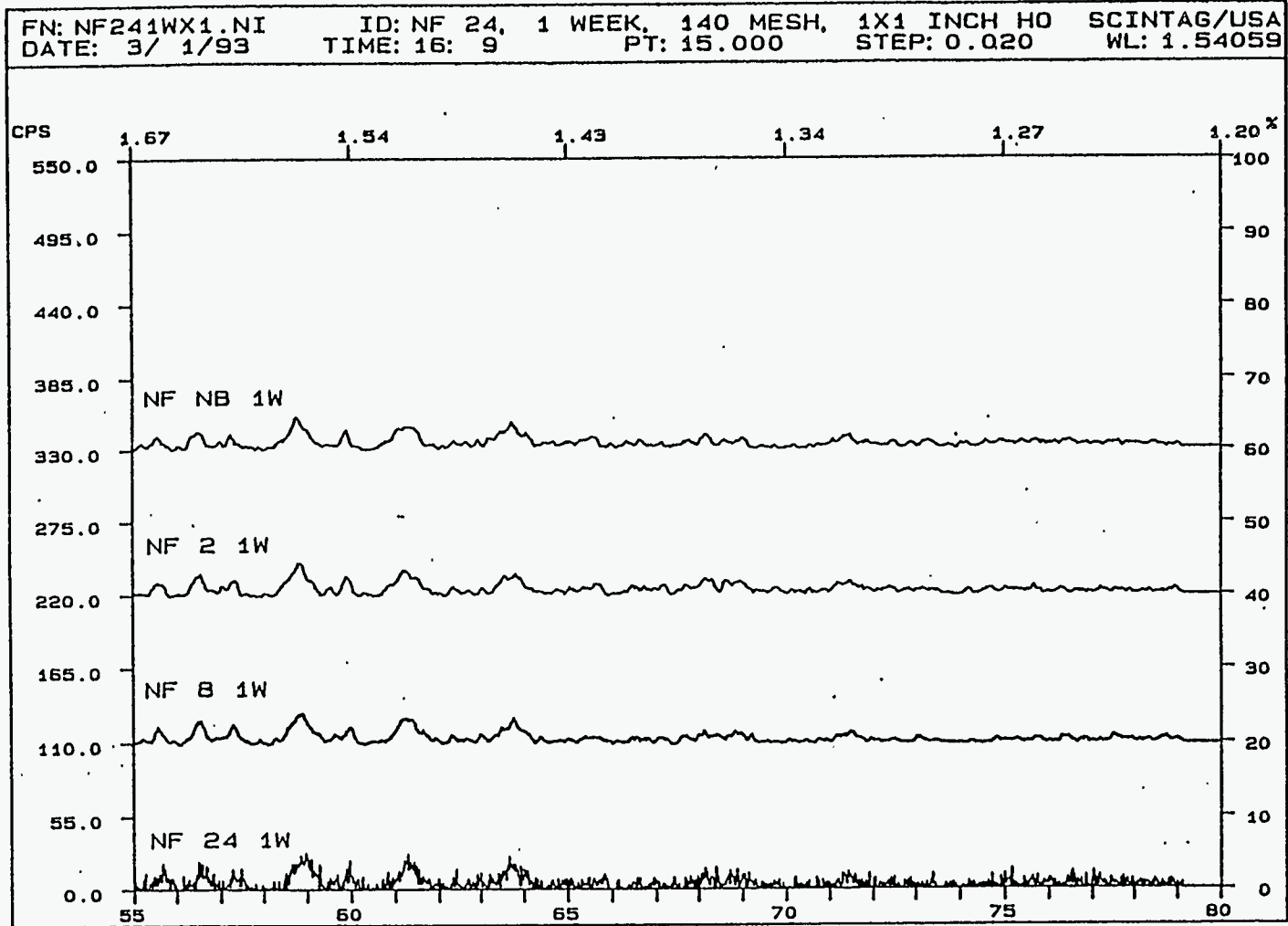
Figure B.38c. Samples NF 24, NF 8, NF 2, and NF NB, 1-week Data. Expanded 2-theta scale, 55 to 80 degrees. Full intensity scale.
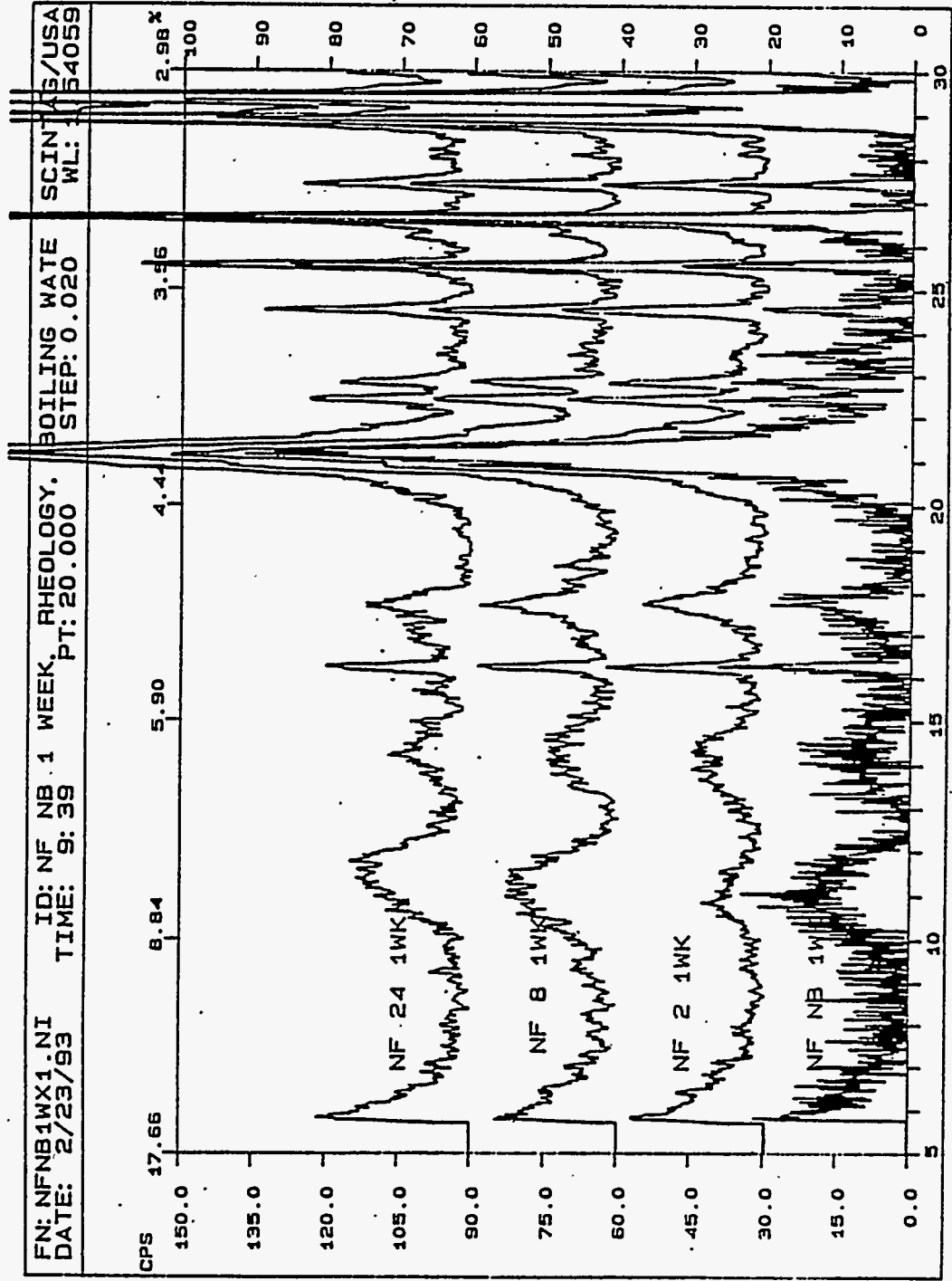
Figure B.39a. Samples NF 24, NF 8, NF 2, and NF NB, 1-week Data. Expanded 2-theta scale, 5 to 30 degrees. Enhanced intensity scale.
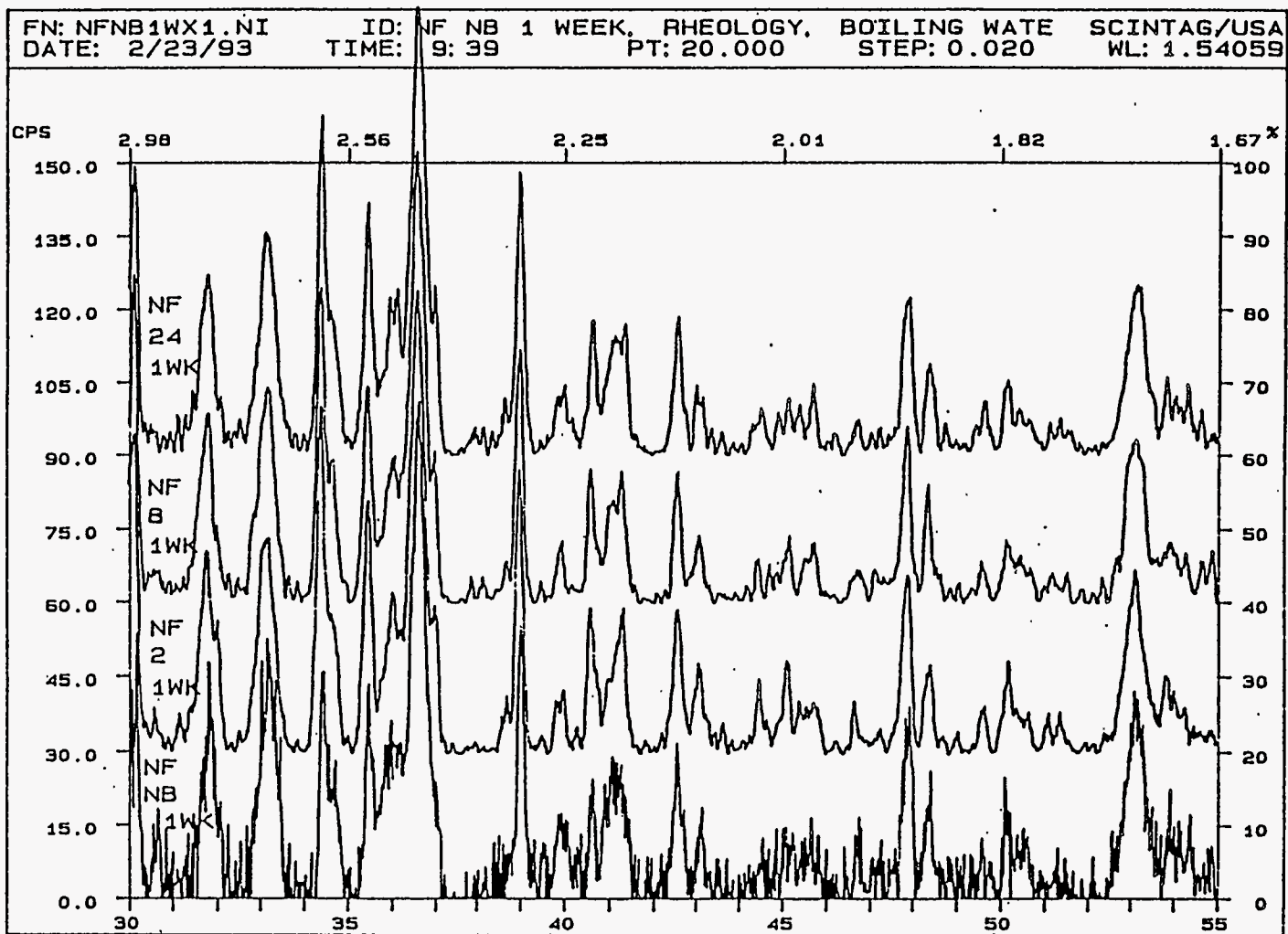
Figure B.39b. Samples NF 24, NF 8, NF 2, and NF NB, 1-week Data. Expanded 2-theta scale, 30 to 55 degrees. Enhanced intensity scale.

B.61

FN: NFNB1WX1.NI   ID: NF NB 1 WEEK, RHEOLOGY, BOILING WATE   SCINTAG/USA
DATE: 2/23/93   TIME: 9: 39   PT: 20.000   STEP: 0.020   WL: 1.54059
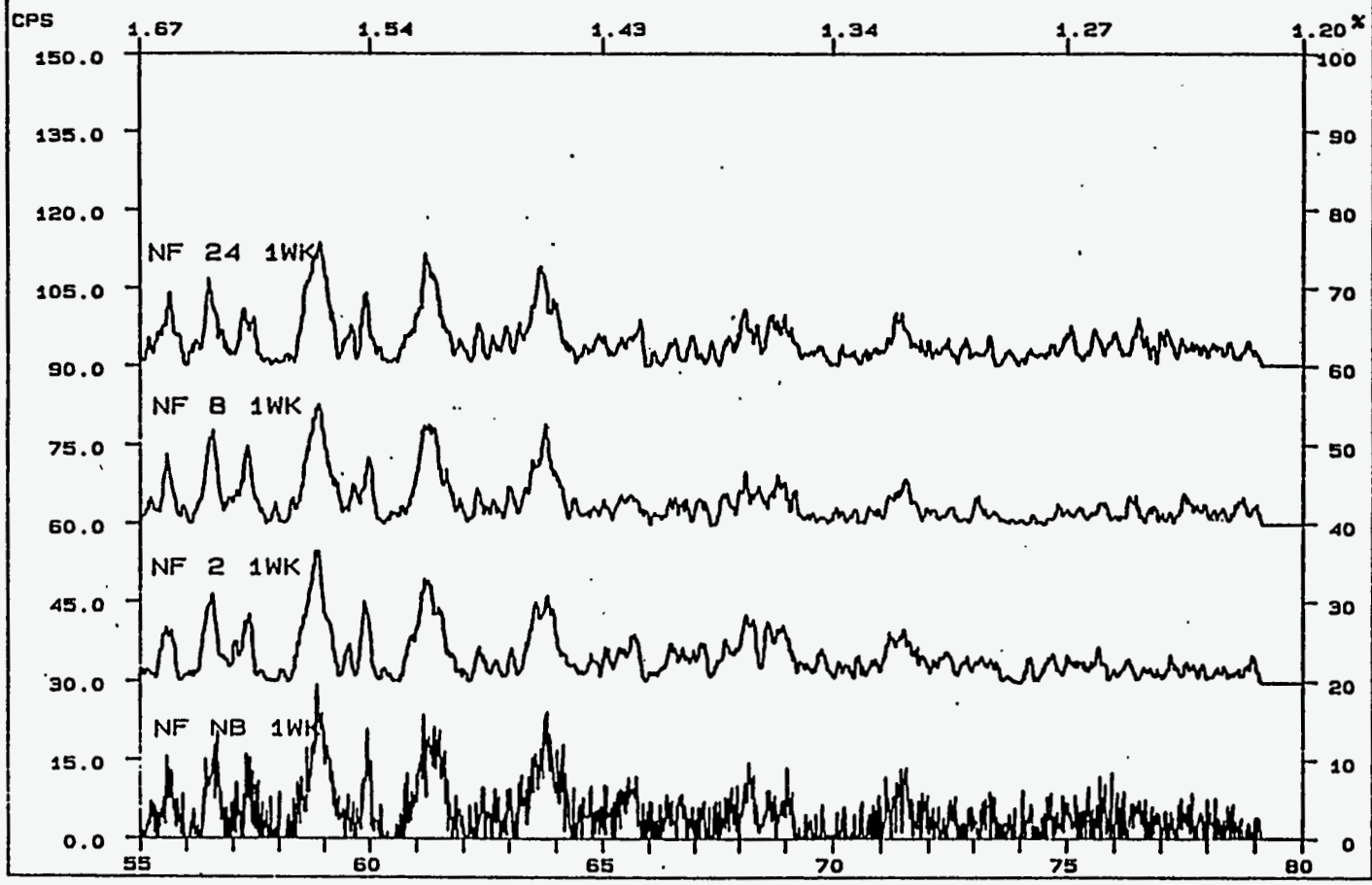
Figure B.39c. Samples NF 24, NF 8, NF 2, and NF NB, 1-week Data. Expanded 2-theta scale, 55 to 80 degrees. Enhanced intensity scale.

Table B.8. Most Intense Lines of Phases found During Rheology Test, 4-week Data, 202 Samples

Phases Identified ICDD Card Number	RELATIVE INTENSITY			
	202 24	202 8	202 2	202 NB
Na NO3/Nitratine 7-271	1.00	1.00	0.95	1.00
Si O2/Silicon Dioxide 33-1161	0.34	0.63	1.00	0.35
FeO OH/ Goethite 29-713	0.21	0.46	0.56	0.31

Table B.9. Most Intense Lines of Phases found During Rheology Test, 4-week Data, NF Samples

Phases Identified ICDD Card Number	RELATIVE INTENSITY			
	NF 24	NF 8	NF 2	NF NB
Na NO3/Nitratine 7-271	0.04	1.00	1.00	1.00
Si O2/Silicon Dioxide 33-1161	1.00	0.28	0.41	0.35
FeO OH/ Goethite 29-713	0.87	0.30	0.34	0.27
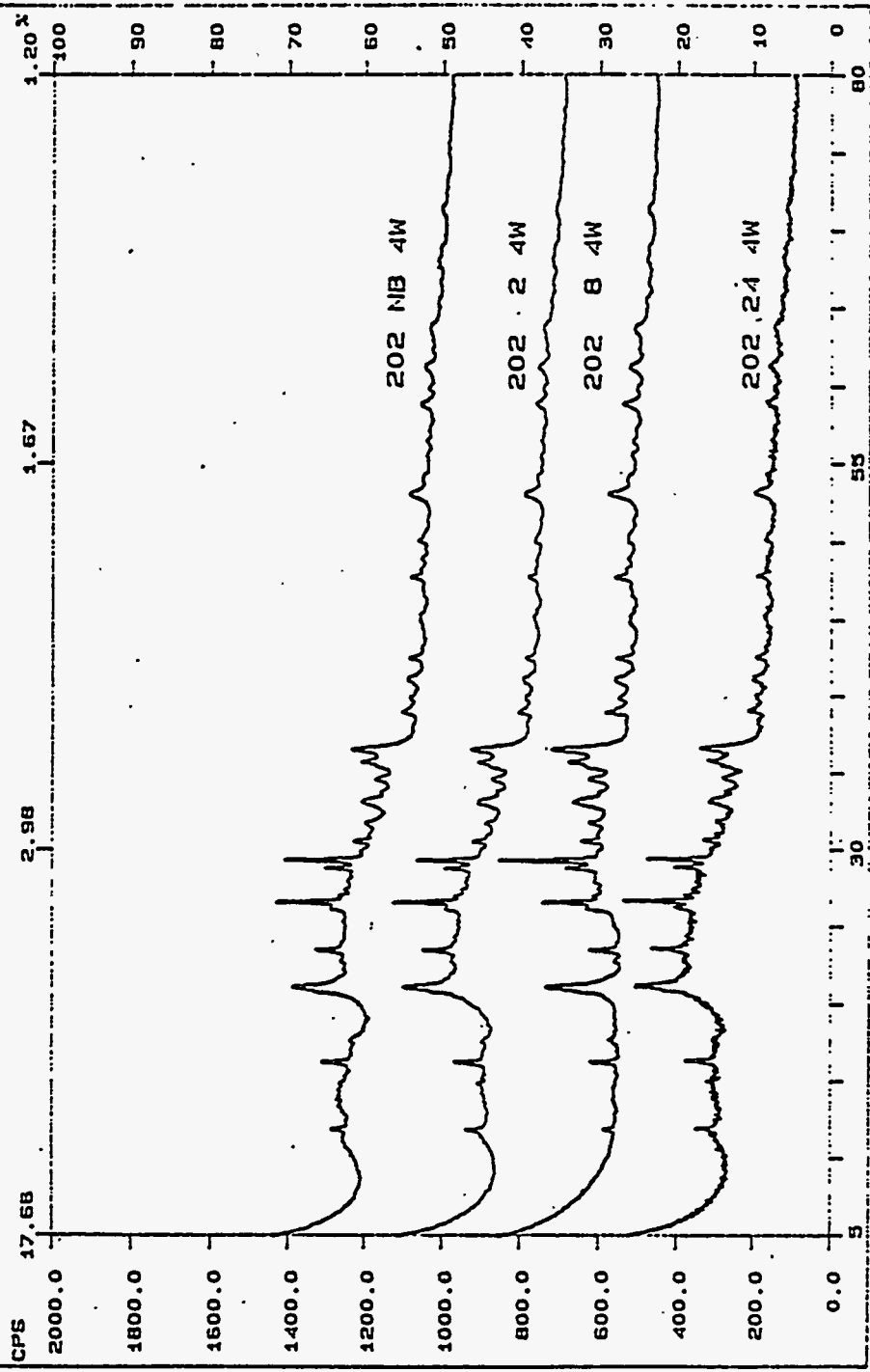
Figure B.40. Samples 202 24, 202 8, 202 2, and 202 NB, 4-week Data. Composite plot of raw data.
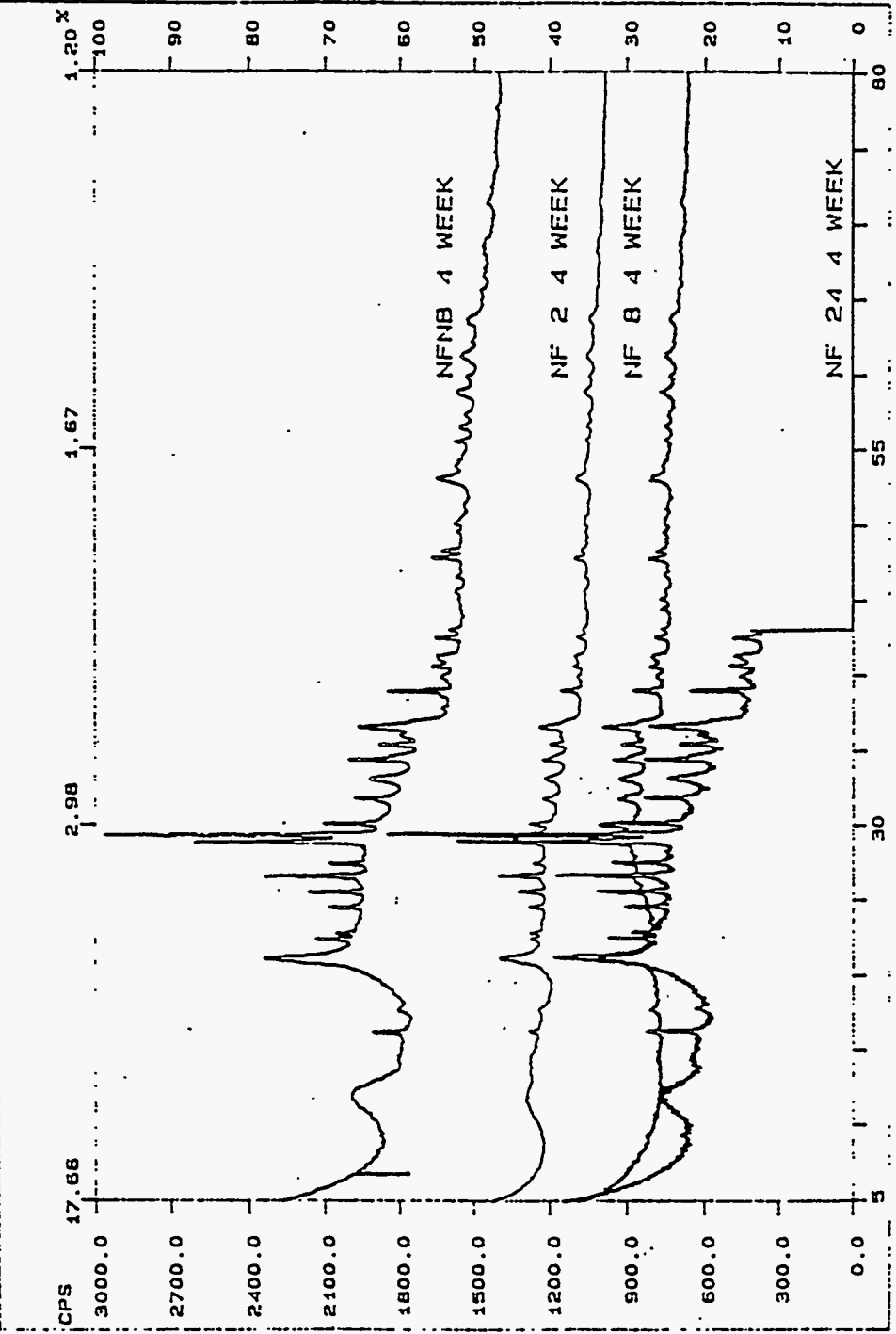
Figure B.41. Samples NF 24, NF 8, NF 2, and NF NB, 4-week Data. Composite plot of raw data.
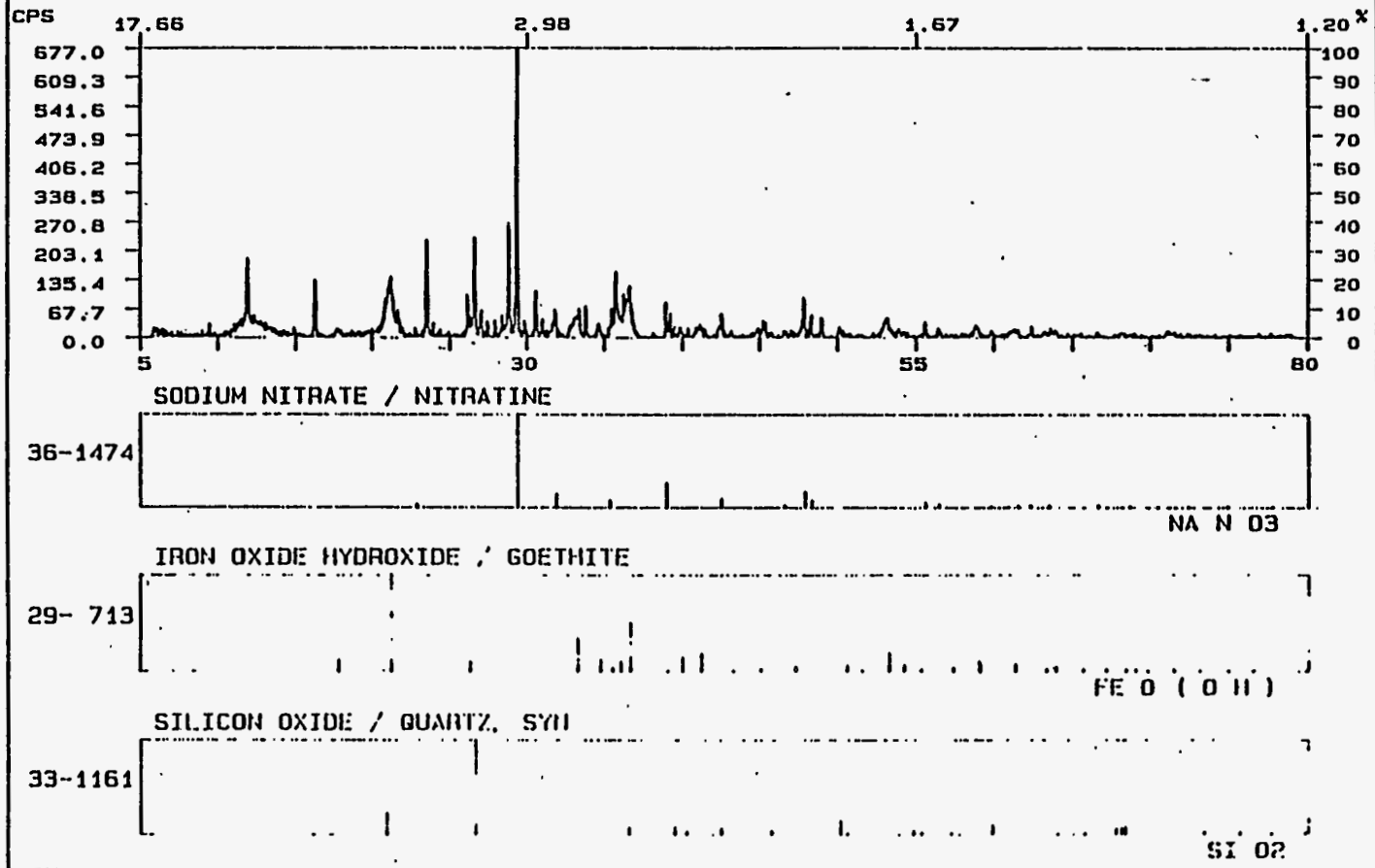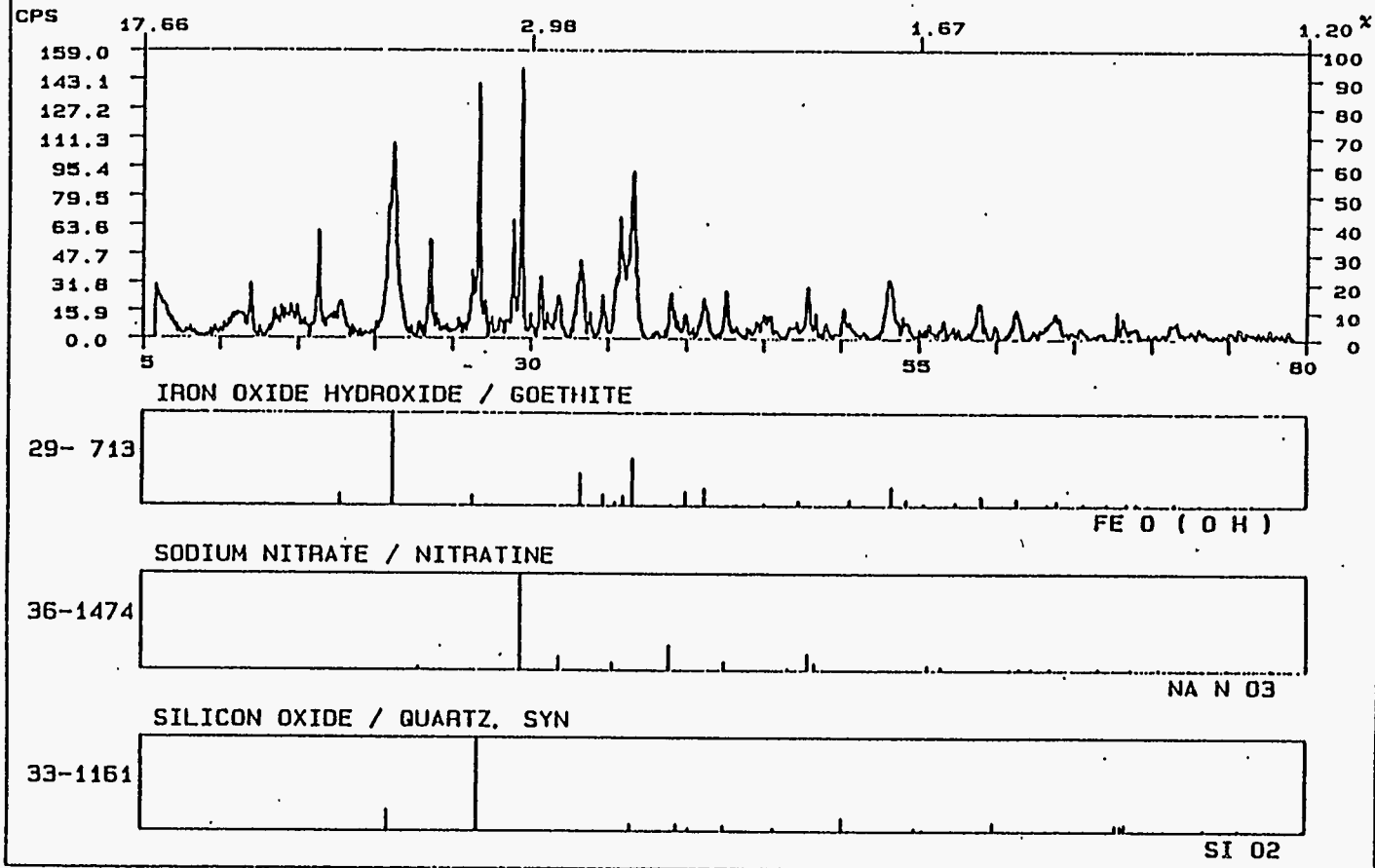
Figure B.42. Sample 202 24, 4-week Data. Net intensity plot with "stick figure" representations of major phases.
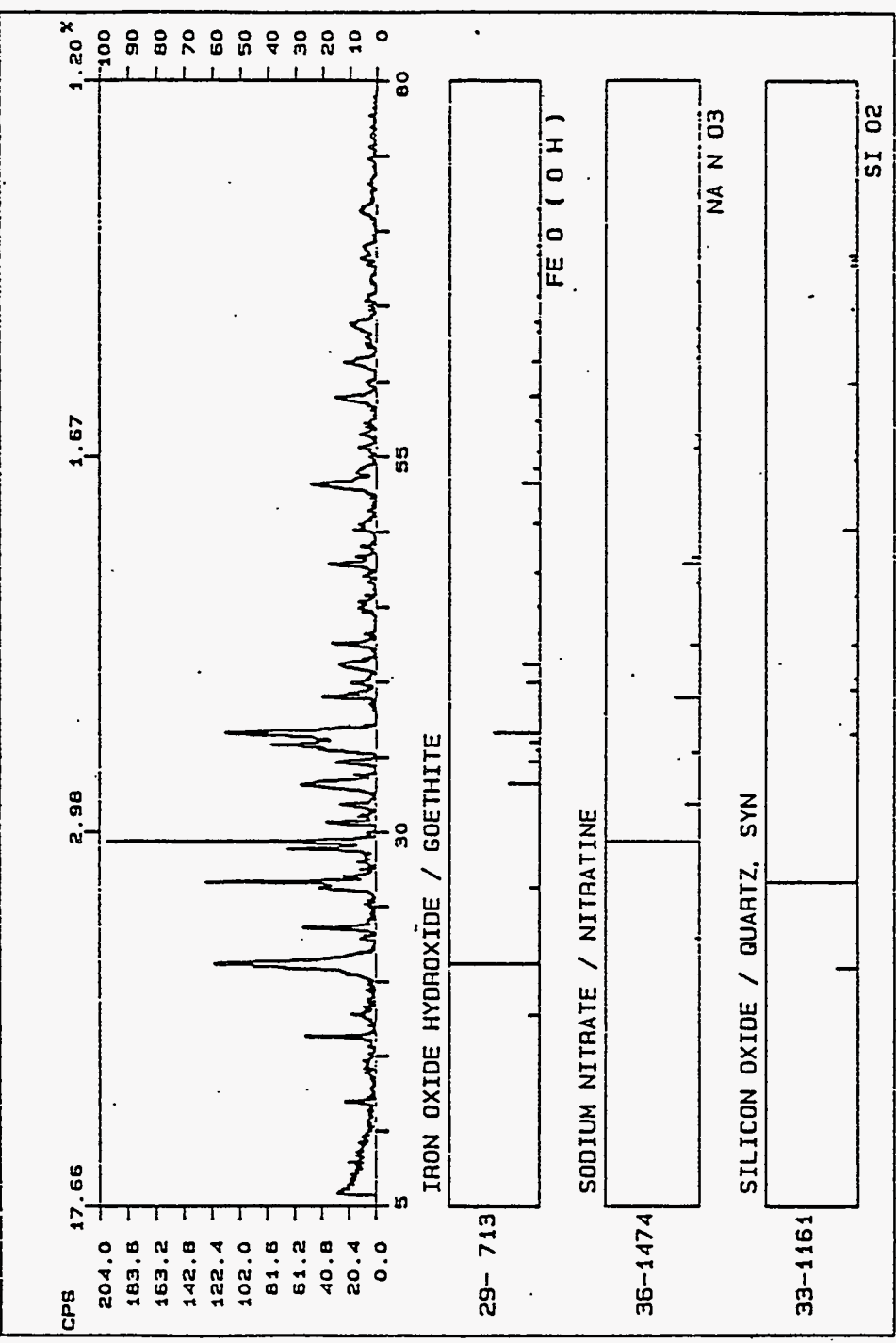
Figure B.43. Sample 202 8, 4-week Data. Net intensity plot with "stick figure" representations of major phases.
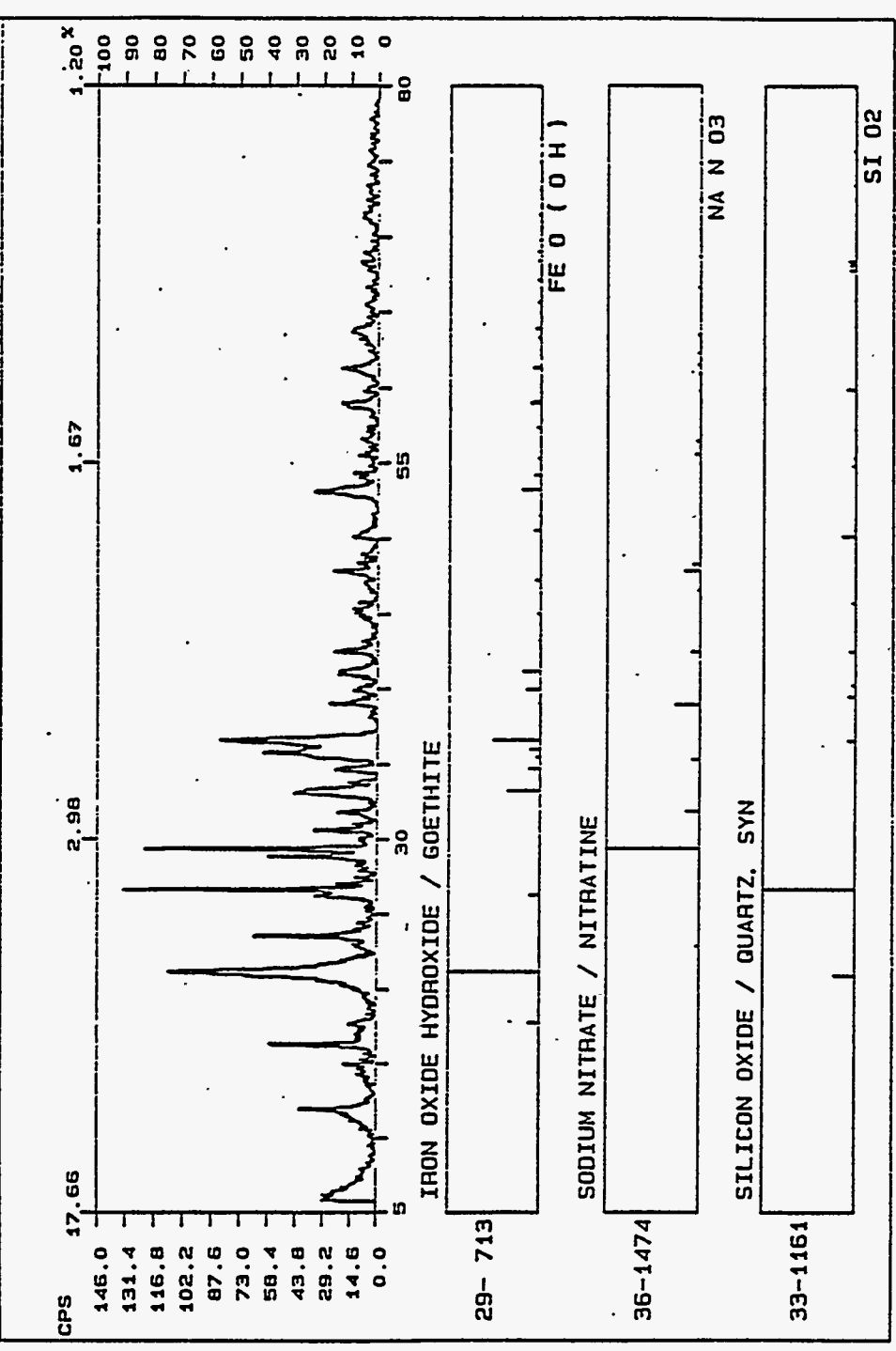
Figure B.44. Sample 202 2, 4-week Data. Net intensity plot with "stick figure" representations of major phases.

Figure B.45. Sample 202 NB, 4-week Data. Net intensity plot with "stick figure" representations of major phases.
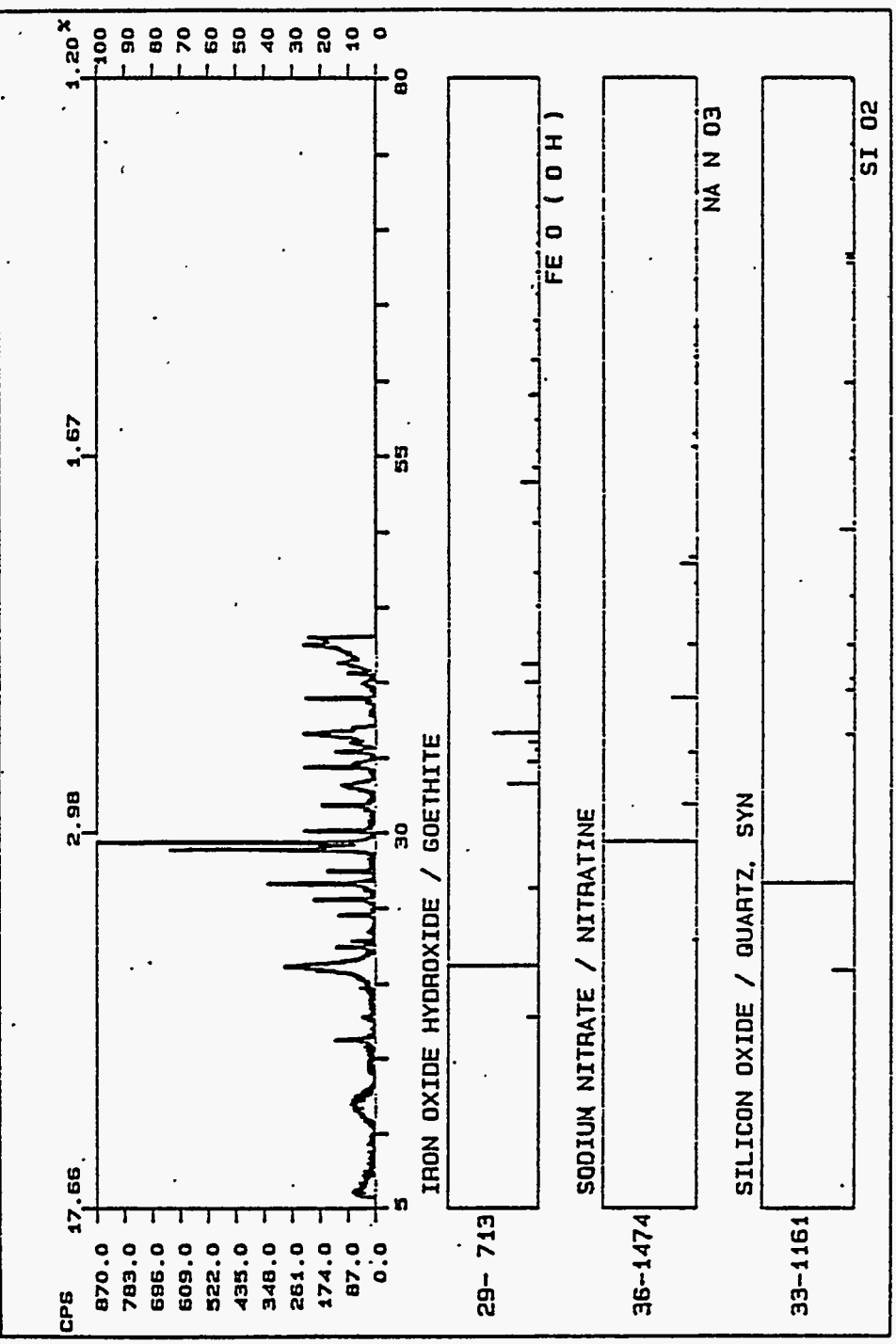
Figure B.46. Sample NF 24, 4-week Data. Net intensity plot with "stick figure" representations of major phases.

B.70
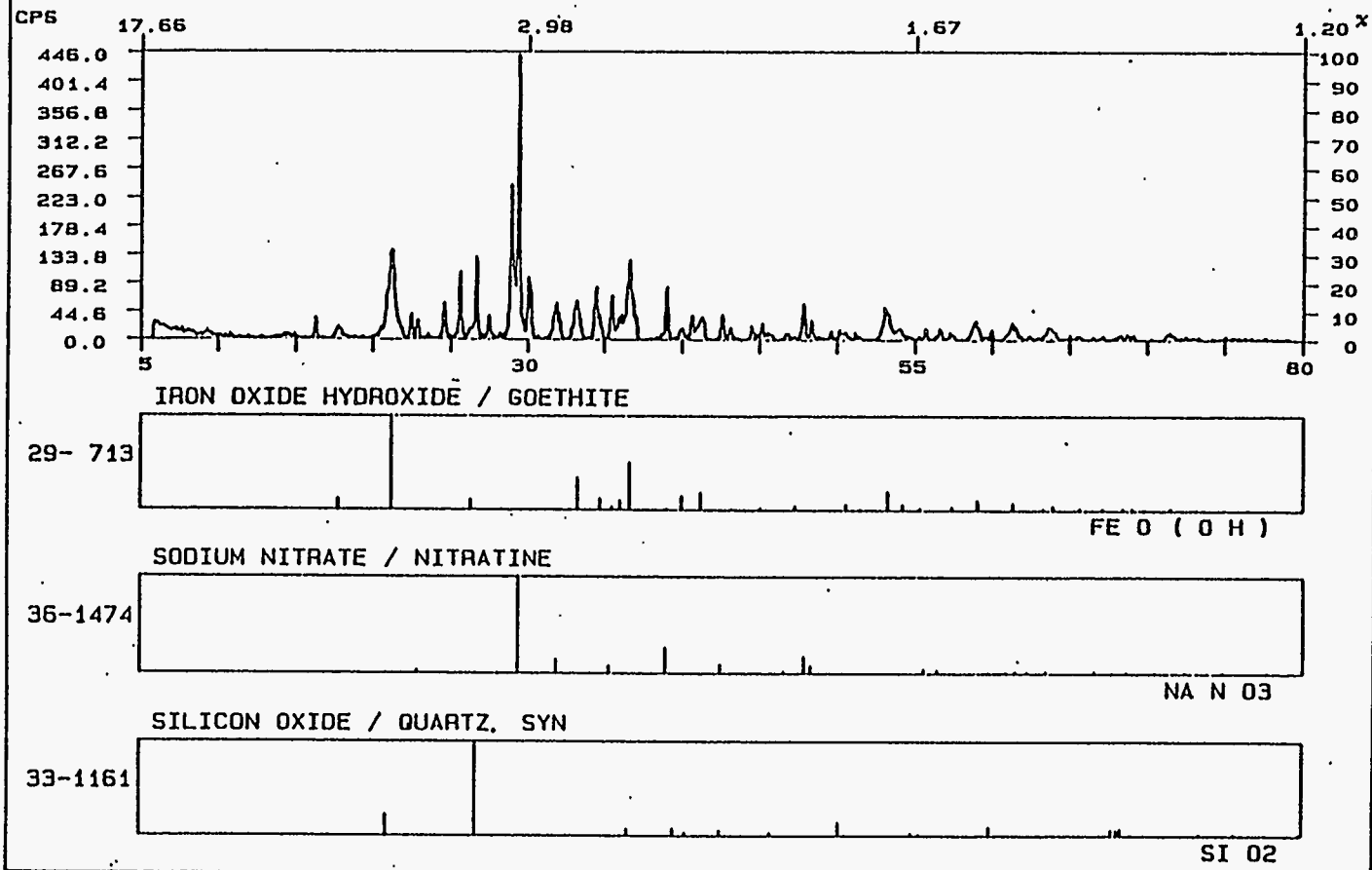
Figure B.47. Sample NF 8, 4-week Data. Net intensity plot with "stick figure" representations of major phases.
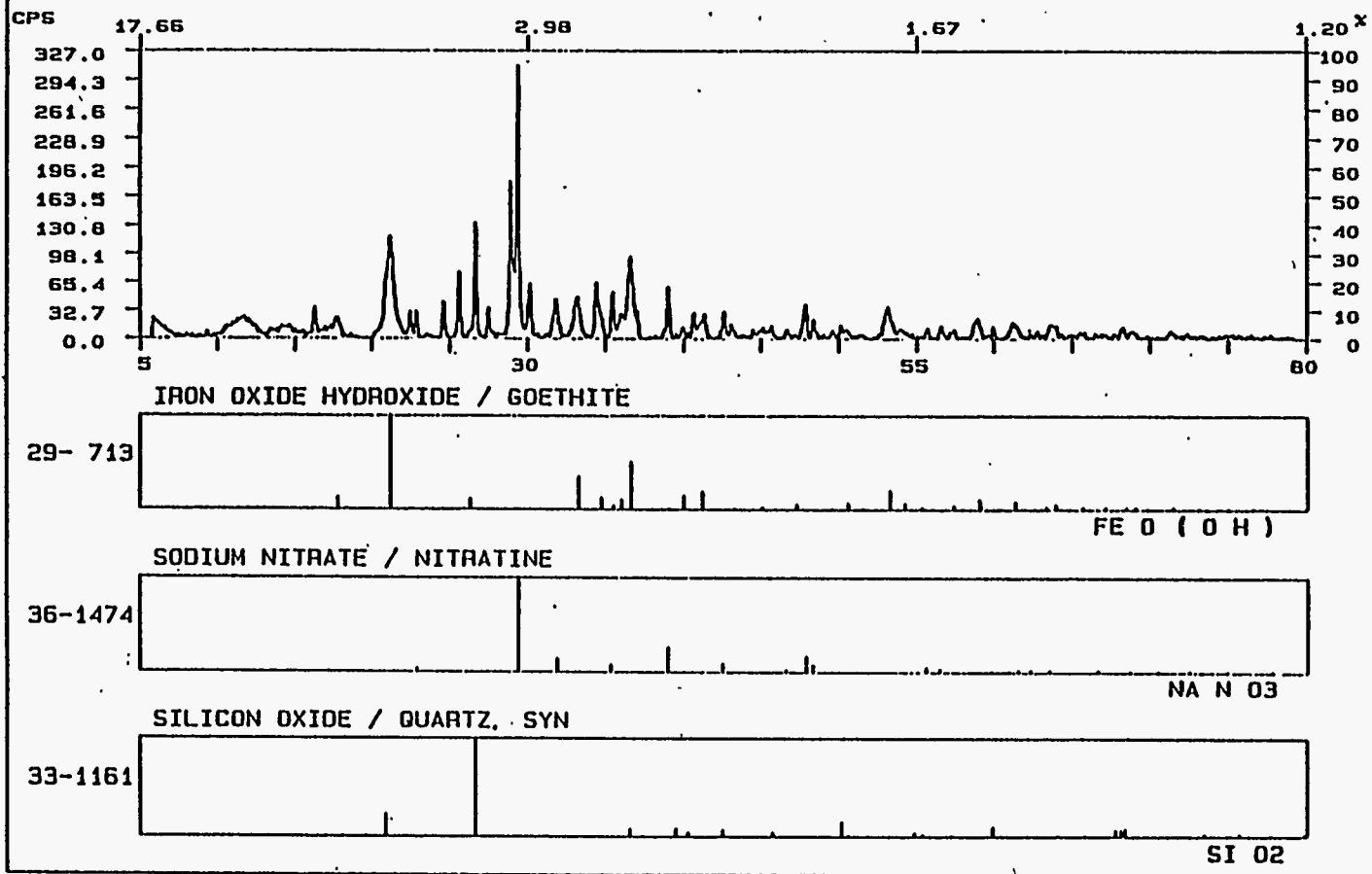
Figure B.48. Sample NF 2, 4-week Data. Net intensity plot with "stick figure" representations of major phases.
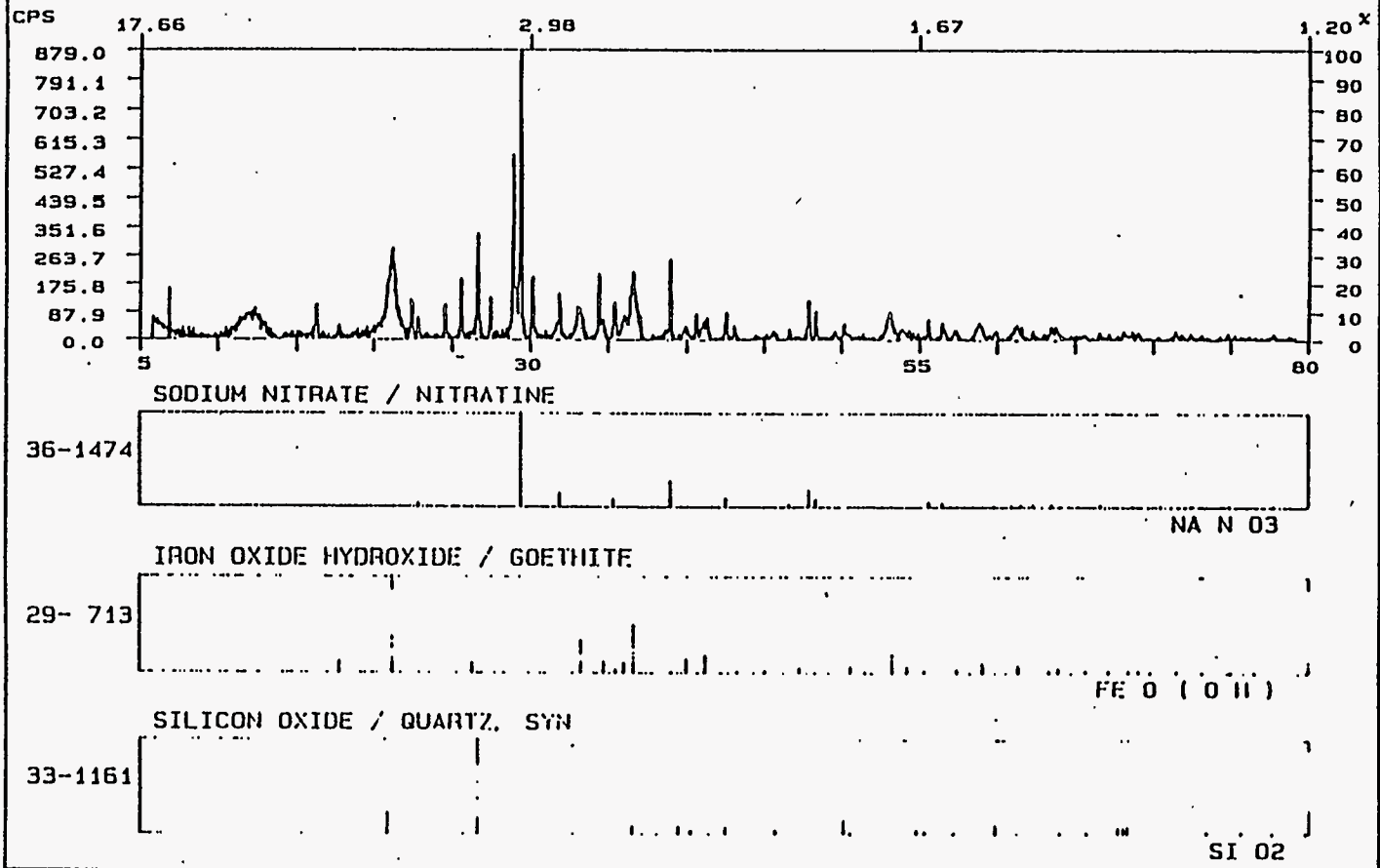
Figure B.49. Sample NF NB, 4-week Data. Net intensity plot with "stick figure" representations of major phases.